RL022574-T-1

MICHIGAN MICROWAVE CANOPY SCATTERING MODEL (MIMICS)

Version 1.0

Fawwaz T. Ulaby
Kamal Sarabandi
Kyle McDonald
Michael Whitt
M. Craig Dobson

Radiation Laboratory
Department of Electrical Engineering and Computer Science
The University of Michigan, Ann Arbor, MI 48109-2122
Tel :(734) 764-0501, Fax:(734) 647-2106
email: ulaby@eecs.umich.edu

ABSTRACT

The Michigan Microwave Canopy Scattering model (MIMICS) is based on a first-order solution of the radiative transfer equation for a tree canopy comprised of a crown layer, a trunk layer, and a rough-surface ground boundary. The crown layer is modeled in terms of distributions of dielectric cylinders (representing needles and/or branches) and disks (representing leaves) and the trunks are treated as vertical dielectric cylinders of uniform diameter. This report describes MIMICS I, which pertains to tree canopies with horizontally continuous (closed) crowns. The model, which is intended for use in the 0.5-10 GHz region at angles greater than 10° from normal incidence, is formulated in terms of a 4x4 Stokes-like transformation matrix from which the backscattering coefficient can be computed for any transmit/receive polarization configuration.

Contents

1 INTRODUCTION 1
1.1 Proposed Model: MIMICS 3
1.2 Approach and Development Plan 5

2 STRUCTURE OF MIMICS I 7

3 NUMERICAL SIMULATIONS 10
3.1 Canopy I — Leaf-Dominated Crown Layer 13
3.2 Canopy II — Branch-Dominated Crown Layer 23
3.3 Canopy III — Crown Layer with Leaves and Branches 33
3.4 Canopy IV — Crown Layer with Needles and Branches 42
3.5 Polarimetric Wave Synthesis 53

REFERENCES 55

A APPENDIX A First-Order Backscattering from a Forest Canopy over a Specular Ground Surface A-1
A.1 Basic Definitions A-1
A.2 Radiative Transfer Equations A-6
A.3 First-Order Solution for Bistatic Scattering A-9
A.4 First-Order Solution for Backscattering A-18

B APPENDIX B Phase and Extinction Matrices of the Crown Layer B-1
B.1 Phase Matrix of the Crown Layer B-2
B.2 Extinction Matrix of the Crown Layer B-5
B.3 Scattering Matrix of a Single Leaf B-9
B.4 Scattering Matrix for a Single Branch B-18
B.5 Scattering Matrix for a Single Needle B-27

C APPENDIX C Phase and Extinction Matrices of the Trunk Layer C-1
C.1 Phase and Extinction Matrices of the Trunk Layer C-1
C.2 Scattering Matrix for a Single Cylinder C-2

D APPENDIX D Surface Scattering Models D-1
D.1 Geometrical Optics Model D-2
D.2 Physical Optics Model D-9
D.3 Small Perturbation Model D-15

E APPENDIX E Dielectric Behavior of the Canopy Constituents E-1
E.1 Dielectric Behavior of Vegetation E-1
E.1.1 Model in Terms of Volumetric Moisture E-1
E.1.2 Model for Leaves E-2
E.2 Dielectric Behavior of the Ground Surface E-3
E.2.1 Soil E-3
E.2.2 Standing Water E-4

F APPENDIX F Relationships Between Canopy Parameters F-1
F.1 Elemental Volume Fractions F-1
F.2 Leaf Area Index F-2
F.3 Biomass Parameters F-3
F.3.1 General Definitions F-3
F.3.2 Constituent Biomasses and Water Contents F-4

G APPENDIX G Wave Synthesis G-1
G.1 Point Target G-1
G.2 Distributed Target G-6
G.3 Polarization Coordinate Systems G-8

H APPENDIX H Numerical Simulations of Selected Canopies H-1
H.1 CANOPY I – Leaf-Dominated Crown Layer H-4
H.2 CANOPY II – Branch-Dominated Crown Layer H-19
H.3 CANOPY III - Crown Layer Consisting of Both Leaves and Branches H-35
H.3 CANOPY IV - Crown Layer Consisting of Needles and Branches . . H-49
H.4 Polarimetric Response Synthesis H-67

List of Tables

1 Development Plan for MIMICS. 7
2 Test Canopy Parameters. 11
E.1 Coefficients of Polynomial Expressions. E-4
F.1 Specific water content and biomasses of the individual canopy constituents. F-5
F.2 Total water content and biomasses of the canopy constituents. . . . F-5
H.1 Test Canopy Parameters. H-3

List of Figures

1 Relevant Canopy Characteristics. 4
2 Backscattering Sources. 6
3 Crown Transmissivity vs. Incidence Angle. Leaf Density = 830 leaves per cubic meter. 15
4 Crown Transmissivity vs. Leaf Density. Incidence Angle = 30°. . . 16
5 Crown Transmissivity vs. Frequency. Incidence Angle = 30°. Leaf Density = 830 leaves per cubic meter. 17
6 Total Like-Polarized Canopy Backscatter vs. Incidence Angle, Canopy I. 18
7 Total Cross-Polarized Canopy Backscatter vs. Incidence Angle, Canopy I. 19
8 L-Band Backscatter Components vs. Incidence Angle, HH Polarization, Canopy I. 20
9 L-Band Backscatter Components vs. Incidence Angle, VV Polarization, Canopy I. 20
10 X-Band Backscatter Components vs. Incidence Angle, HH Polarization, Canopy I. 21
11 X-Band Crown Backscatter Contributions vs. Incidence Angle, HH Polarization, Canopy I. 21
12 Total Canopy Backscatter vs. Frequency. Incidence Angle = 30°, Canopy I 22
13 Aspen Canopy Branch Angle Distribution. 25
14 Crown Transmissivity vs. Incidence Angle. Branch Density = 4.1 branches per cubic meter. 26
15 Crown Transmissivity vs. Frequency. Incidence Angle = 30°, Branch Density = 4.1 branches per cubic meter. 27
16 Total Like-Polarized Canopy Backscatter vs. Incidence Angle, Canopy II. 28
17 Total Cross-Polarized Canopy Backscatter vs. Incidence Angle, Canopy II. 29
18 L-Band Backscatter Components vs. Incidence Angle, HH Polarization, Canopy II. 30
19 L-Band Backscatter Components vs. Incidence Angle, VV Polarization, Canopy II. 30
20 X-Band Backscatter Components vs. Incidence Angle, HH Polarization, Canopy II. 31
21 X-Band Crown Backscatter Contributions vs. Incidence Angle, HH Polarization, Canopy II. 31

22 Total Canopy Backscatter vs. Frequency. Incidence Angle = 30°. Canopy II 32
23 Crown Transmissivity vs. Incidence Angle. Leaf Density = 830 leaves per cubic meter. Branch Density = 4.1 branches per cubic meter. 35
24 Crown Transmissivity vs. Frequency. Incidence Angle = 30°. Leaf Density = 830 leaves per cubic meter. Branch Density = 4.1 branches per cubic meter. 36
25 Total Like-Polarized Canopy Backscatter vs. Incidence Angle, Canopy III. 37
26 Total Cross-Polarized Canopy Backscatter vs. Incidence Angle, Canopy III. 38
27 L-Band Backscatter Components vs. Incidence Angle, HH Polarization, Canopy III. 39
28 L-Band Backscatter Components vs. Incidence Angle, VV Polarization, Canopy III. 39
29 X-Band Backscatter Components vs. Incidence Angle, HH Polarization, Canopy III. 40
30 X-Band Backscatter Components vs. Incidence Angle, HH Polarization, Canopy III. 40
31 Total Canopy Backscatter vs. Frequency. Incidence Angle = 30°, Canopy III. 41
32 White Spruce Canopy Branch Angle Distribution. 44
33 Crown Transmissivity vs. Incidence Angle. Needle Density = 85,000 needles per cubic meter. 45
34 Crown Transmissivity vs. Needle Density. Incidence Angle = 30°. . 46
35 Crown Transmissivity vs. Frequency. Incidence Angle = 30°. Needle Density = 85,000 needles per cubic meter. 47
36 Total Like-Polarized Canopy Backscatter vs. Incidence Angle, Canopy IV. 48
37 Total Cross-Polarized Canopy Backscatter vs. Incidence Angle, Canopy IV. 49
38 L-Band Backscatter Components vs. Incidence Angle, HH Polarization, Canopy IV. 50
39 L-Band Backscatter Components vs. Incidence Angle, VV Polarization, Canopy IV. 50
40 X-Band Backscatter Components vs. Incidence Angle, HH Polarization, Canopy IV. 51
41 X-Band Backscatter Components vs. Incidence Angle, HH Polarization, Canopy IV. 52

42 Total Canopy Backscatter vs. Frequency. Incidence Angle = 30°, Canopy IV. 53
43 C-Band Polarization Response. Incidence Angle = 40°, Canopy III. 55
A.1 Forest Canopy Model A-2
A.2 Problem Geometry A-3
A.3 Scattering Terms for the Bistatic Case A-16
A.4 Scattering Terms for the Backscattering Case A-20
B.1 Coordinate System Geometry. B-3
B.2 Scattering Geometry of a Resistive Sheet. B-10
B.3 Coordinate System Transformations. B-12
B.4 Scattering Geometry of an Arbitrarily Oriented Cylinder. B-19
C.1 Cylinder scattering geometry. C-4
C.2 Specular and forward scattering conditions. C-5
D.1 Rough Surface Geometry. D-3
G.1 Polarization of an Electromagnetic Wave. G-2
G.2 Geometry for the FSA convention. G-9
G.3 Geometry for the BSA convention. G-11
H.1 Total Like-Polarized Canopy Backscatter vs. Incidence Angle, Canopy I H-5
H.2 Total Cross-Polarized Canopy Backscatter vs. Incidence Angle, Canopy I H-6
H.3 L-Band Like-Polarized Canopy Backscatter Components vs. Incidence Angle, Canopy I H-7
H.4 L-Band Like-Polarized Crown Backscatter Components vs. Incidence Angle, Canopy I H-8
H.5 L-Band Cross-Polarized Crown Backscatter Components vs. Incidence Angle, Canopy I H-9
H.6 C-Band Like-Polarized Canopy Backscatter Components vs. Incidence Angle, Canopy I H-10
H.7 C-Band Like-Polarized Crown Backscatter Components vs. Incidence Angle, Canopy I H-11
H.8 C-Band Cross-Polarized Crown Backscatter Components vs. Incidence Angle, Canopy I H-12
H.9 X-Band Like-Polarized Canopy Backscatter Components vs. Incidence Angle, Canopy I H-13
H.10 X-Band Like-Polarized Crown Backscatter Components vs. Incidence Angle, Canopy I H-14
H.11 X-Band Cross-Polarized Crown Backscatter Components vs. Incidence Angle, Canopy I H-15
H.12 Total Canopy Backscatter Components vs. Frequency. Incidence Angle = 30°, Canopy I H-16

H.13 Like-Polarized Crown Backscatter Components vs Frequency Incidence Angle = 30°, Canopy I H-17
H.14 Cross-Polarized Crown Backscatter Components vs. Frequency. Incidence Angle = 30°, Canopy I H-18
H.15 Total Like-Polarized Canopy Backscatter vs. Incidence Angle, Canopy II H-20
H.16 Total Cross-Polarized Canopy Backscatter vs. Incidence Angle, Canopy II H-21
H.17 L-Band Like-Polarized Canopy Backscatter Components vs. Incidence Angle, Canopy II H-22
H.18 L-Band Like-Polarized Crown Backscatter Components vs. Incidence Angle, Canopy II H-23
H.19 L-Band Cross-Polarized Crown Backscatter Components vs. Incidence Angle, Canopy II H-24
H.20 C-Band Like-Polarized Canopy Backscatter Components vs. Incidence Angle, Canopy II H-25
H.21 C-Band Like-Polarized Crown Backscatter Components vs. Incidence Angle, Canopy II H-26
H.22 C-Band Cross-Polarized Crown Backscatter Components vs. Incidence Angle, Canopy II H-27
H.23 X-Band Like-Polarized Canopy Backscatter Components vs. Incidence Angle, Canopy II H-28
H.24 X-Band Like-Polarized Crown Backscatter Components vs. Incidence Angle, Canopy II H-29
H.25 X-Band Cross-Polarized Crown Backscatter Components vs. Incidence Angle, Canopy II H-30
H.26 Total Canopy Backscatter vs. Frequency. Incidence Angle = 30°, Canopy II H-31
H.27 Like-Polarized Canopy Backscatter Components vs. Frequency. Incidence Angle = 30°, Canopy II H-32
H.28 Like-Polarized Crown Backscatter Components vs. Frequency. Incidence Angle = 30°, Canopy II H-33
H.29 Cross-Polarized Crown Backscatter Components vs. Frequency. Incidence Angle = 30°, Canopy II H-34
H.30 Total Like-Polarized Canopy Backscatter vs. Incidence Angle, Canopy III H-36
H.31 Total Cross-Polarized Canopy Backscatter vs. Incidence Angle, Canopy III H-37
H.32 L-Band Like-Polarized Canopy Backscatter Components vs. Incidence Angle, Canopy III H-38

H.33 L-Band Like-Polarized Crown Backscatter Components vs. Incidence Angle, Canopy III H-39
H.34 L-Band Cross-Polarized Crown Backscatter Components vs. Incidence Angle, Canopy III H-40
H.35 C-Band Like-Polarized Canopy Backscatter Components vs. Incidence Angle, Canopy III H-41
H.36 C-Band Like-Polarized Crown Backscatter Components vs. Incidence Angle, Canopy III H-42
H.37 C-Band Cross-Polarized Crown Backscatter Components vs. Incidence Angle, Canopy III H-43
H.38 X-Band Like-Polarized Canopy Backscatter Components vs. Incidence Angle, Canopy III H-44
H.39 X-Band Like-Polarized Crown Backscatter Components vs. Incidence Angle, Canopy III H-45
H.40 X-Band Cross-Polarized Crown Backscatter Components vs. Incidence Angle, Canopy III H-46
H.41 Total Canopy Backscatter vs. Frequency. Incidence Angle = 30°, Canopy III H-47
H.42 Like-Polarized Canopy Backscatter Components vs. Frequency. Incidence Angle = 30°, Canopy III H-48
H.43 Like-Polarized Crown Backscatter Components vs. Frequency. Incidence Angle = 30°, Canopy III H-50
H.44 Cross-Polarized Crown Backscatter Components vs. Frequency. Incidence Angle = 30°, Canopy III H-51
H.45 Total Like-Polarized Canopy Backscatter vs. Incidence Angle, Canopy IV H-52
H.46 Total Cross-Polarized Canopy Backscatter vs. Incidence Angle, Canopy IV H-53
H.47 L-Band Like-Polarized Canopy Backscatter Components vs. Incidence Angle, Canopy IV H-54
H.48 L-Band Like-Polarized Crown Backscatter Components vs. Incidence Angle, Canopy IV H-55
H.49 L-Band Cross-Polarized Crown Backscatter Components vs. Incidence Angle, Canopy IV H-56
H.50 C-Band Like-Polarized Canopy Backscatter Components vs. Incidence Angle, Canopy IV H-57
H.51 C-Band Like-Polarized Crown Backscatter Components vs. Incidence Angle, Canopy IV H-58
H.52 C-Band Cross-Polarized Crown Backscatter Components vs. Incidence Angle, Canopy IV H-59

H.53 X-Band Like-Polarized Canopy Backscatter Components vs. Incidence Angle, Canopy IV H-60
H.54 X-Band Like-Polarized Crown Backscatter Components vs. Incidence Angle, Canopy IV H-61
H.55 X-Band Cross-Polarized Crown Backscatter Components vs. Incidence Angle, Canopy IV H-62
H.56 Total Canopy Backscatter vs. Frequency. Incidence Angle = 30°, Canopy IV H-63
H.57 Like-Polarized Canopy Backscatter Components vs. Frequency. Incidence Angle = 30°, Canopy IV H-64
H.58 Like-Polarized Crown Backscatter Components vs. Frequency. Incidence Angle = 30°, Canopy IV H-65
H.59 Cross-Polarized Crown Backscatter Components vs. Frequency. Incidence Angle = 30°, Canopy IV H-66
H.60 L-Band Polarization Response. Incidence Angle = 40°, Canopy I . . H-68
H.61 C-Band Polarization Response. Incidence Angle = 40°, Canopy I . . H-69
H.62 X-Band Polarization Response. Incidence Angle = 40°, Canopy I . H-70
H.63 L-Band Polarization Response. Incidence Angle = 40°, Canopy II . H-71
H.64 C-Band Polarization Response. Incidence Angle = 40°, Canopy II . H-72
H.65 X-Band Polarization Response. Incidence Angle = 40°, Canopy II . H-73
H.66 L-Band Polarization Response. Incidence Angle = 40°, Canopy III . H-74
H.67 C-Band Polarization Response. Incidence Angle = 40°, Canopy III . H-75
H.68 X-Band Polarization Response. Incidence Angle = 40°, Canopy III . H-76
H.69 L-Band Polarization Response. Incidence Angle = 40°, Canopy IV . H-77
H.70 C-Band Polarization Response. Incidence Angle = 40°, Canopy IV . H-78
H.71 X-Band Polarization Response. Incidence Angle = 40°, Canopy IV . H-79

1 INTRODUCTION

A tree canopy is an inhomogeneous medium comprised of scattering elements with many different sizes, shapes, and orientations. Radar backscattering from a tree canopy may include contributions due to (1) volume scattering in the canopy itself, (2) surface scattering by the underlying ground surface (or understory), and (3) multiple interactions involving both the canopy volume and the ground surface. Because the vegetation elements are somewhat random in terms of their spatial locations and orientations, scattering models usually are formulated in terms of statistical distributions characterizing these and other properties of the canopy scatterers. In addition to considering the statistics associated with the elements of an individual tree, we have to consider the spatial distribution and number density of trees in the canopy, the distribution for the overall shape and dimensions of the trees, and the statistics associated with canopy closure.

Most models for radar scattering from vegetation (Attema and Ulaby, 1978; Fung and Ulaby, 1978; Tsang and Kong, 1981; Lang and Sidhu, 1983; Eom and Fung, 1984; and Richards et al, 1987; Karam and Fung, 1988) treat the canopy as an uniform layer of some specified height containing a random distribution of scatterers. Models based on the field approach (Fung and Ulaby, 1978; Tsang and Kong, 1981) account for the inhomogeneity of the medium through the correlation function characterizing the fluctuating component of the dielectric constant of the medium, and models based on the radiative transfer intensity approach (Eom and Fung, 1984; Ulaby et al., 1986, Chapter 13; Tsang et al., 1985, Chapter 3) account for the inhomogeneity by averaging the Stoke's matrix over the statistical distri-

butions characterizing the sizes, shapes, and orientations of the canopy elements. In general, the field approach is appropriate for weakly scattering media in which the ratio of the fluctuating component of the dielectric constant to the mean value for the medium is small (Lee and Kong, 1985; Ulaby et al.; 1986, pp. 1066-1072). For a medium like vegetation in which the scatterers (leaves, branches, etc.) have discrete configurations and have dielectric constants that are much larger than that of the background (air), the radiative transfer approach is more appropriate.

The major shortcomings of available models are: (1) the canopy is treated as a continuous layer in the horizontal direction, which is valid only for closed canopies, (2) the canopy is treated as having uniform properties in the vertical direction, thereby treating the crown section and the trunk section the same, and (3) usually the scatterers in the crown volume are chosen to be uniform in size, shape, and dielectric constant in order to simplify computations. Because of these shortcomings, available theoretical models are inadequate for relating the radar backscattering coefficient, σ^o, to the physical properties of the canopy. One of the consequences of treating the canopy as uniform in the vertical direction is that bistatic scattering involving the tree trunks and ground surface is totally unaccounted for, whereas experimental evidence (Dobson et al., 1986; Ulaby et al., 1987; Richards et al., 1987) suggests that this scattering mechanism may be the dominant source of scattering at the lower microwave frequencies. Attempts to include the backscatter contribution due to this "corner-reflector" mechanism have been proposed through semi-empirical formulations (Dobson et al., 1986; Richards et al., 1987).

1.1 Proposed Model: MIMICS

The purpose of the present study is to develop a radar scattering model for forest canopies using the generic structure shown in Figure 1. The major attributes of the proposed model, which we shall call "The Michigan Microwave Canopy Scattering" Model—MIMICS—are:

(1) The canopy is divided into three regions: (a) the crown region, (b) the trunk region, and (c) the underlying ground region.

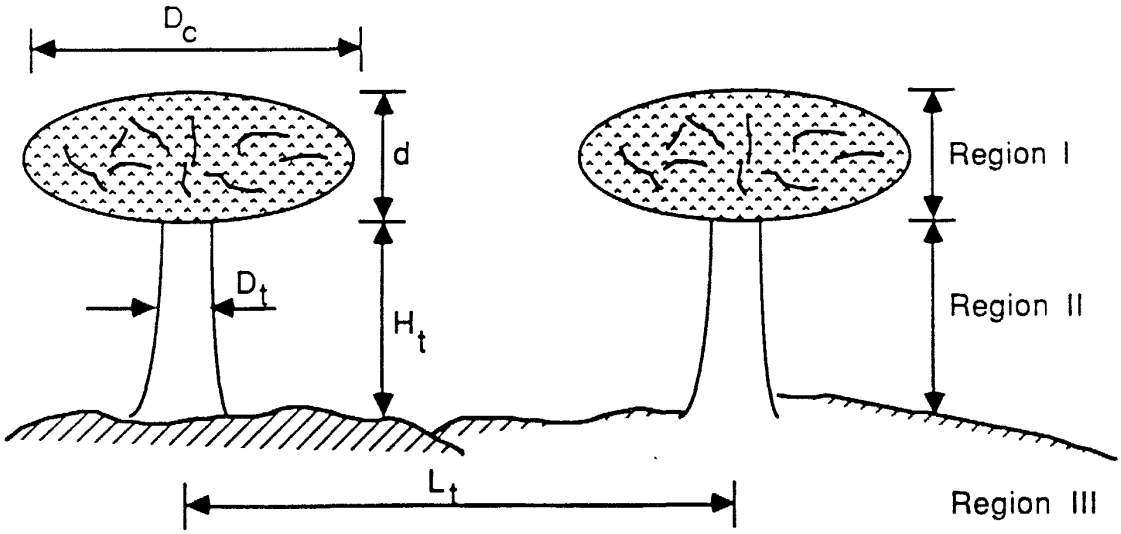
(2) The crown section of an individual tree is assumed to be spheroidal in shape with height d and diameter D_c. For $D_c < d$, the crown is an oblate spheroid and for $D_c > d$, it is a prolate spheroid.

(3) The trunk section is characterized by an average height H_t and average diameter D_t.

(4) The crown section may contain branches and needles, modeled as dielectric cylinders and characterized by a joint probability density function (PDF) $f_c(l; d_c; \theta_c, \phi_c)$, where l is the cylinder length, d_c is its diameter and the angles (θ_c, ϕ_c) define the orientation of its axis.

(5) The crown section may contain leaves, modeled as flat, rectangular discs and characterized by a joint PDF $f_d(a, b; \theta_d, \phi_d)$, where a and b are the dimensions of the leaf surface and the angles (θ_d, ϕ_d) define the orientation of the unit vector normal to the leaf surface.

(6) The number of trees per unit area is defined by the number density N. The trees are assumed to be randomly distributed in location in the horizontal plane.



GEOMETRICAL PARAMETERS

I. Crown Region: d, foliage height
D_c , foliage diameter
Branches and Needles: f_c (l, d_c, θ_c, ϕ_c); cylinder PDF
l = cyl length, d_c = cyl diameter
(θ_c, ϕ_c) = cyl orientation
Leaves: $f_d(a,b,\theta_d,\phi_d)$; disc PDF
a,b = disk surface dimensions
(θ_d, ϕ_d) = orientation of disc surfsce normal

II. Trunk Region: H_t , trunk height
D_t , trunk diameter
L_t , spacing between trunks

III. Ground Region: s , surface rms height
l_s , surface correlation length

DIELECTRIC PARAMETERS

ε_l of leaves
ε_b of branches
ε_t of trunks
ε_s of ground surface
ε_n of needles

Figure 1 Relevant Canopy Characteristics

(7) The roughness of the underlying ground surface is characterized by a roughness correlation function. The ground surface may be soil or water (as in a swamp).

(8) The dielectric constants of the branches (ϵ_b), the needles (ϵ_n), the leaves (ϵ_l), the trunks (ϵ_t), and the ground surface (ϵ_s) are specified by a set of dielectric models in terms of moisture content, microwave frequency f, and physical temperature T.

1.2 Approach and Development Plan

The MIMICS model will be developed in three stages (Table 1). MIMICS I, which has been completed and will be described in detail in this report, applies to the continuous-canopy situation (100 percent closure) and will account for first-order scattering only (which includes scattering mechanisms 1-5 in Figure 2). MIMICS II treats the general case of the non-closed canopy and will include all first-order scattering mechanisms shown in Figure 2. The expectation is that both MIMICS I and II will be valid up to X-band for both like and cross polarization but their validity at higher frequencies is uncertain. MIMICS III will incorporate the following factors, subsequent to investigating each both theoretically and (when possible) experimentally:

(1) Leaf Curvature. Whereas the backscattering from a single curved leaf has been modeled and measured (Sarabandi et al., 1988), the effect of leaf curvature on the scattering phase function for a volume containing a collection of randomly distributed leaves has not yet been evaluated.

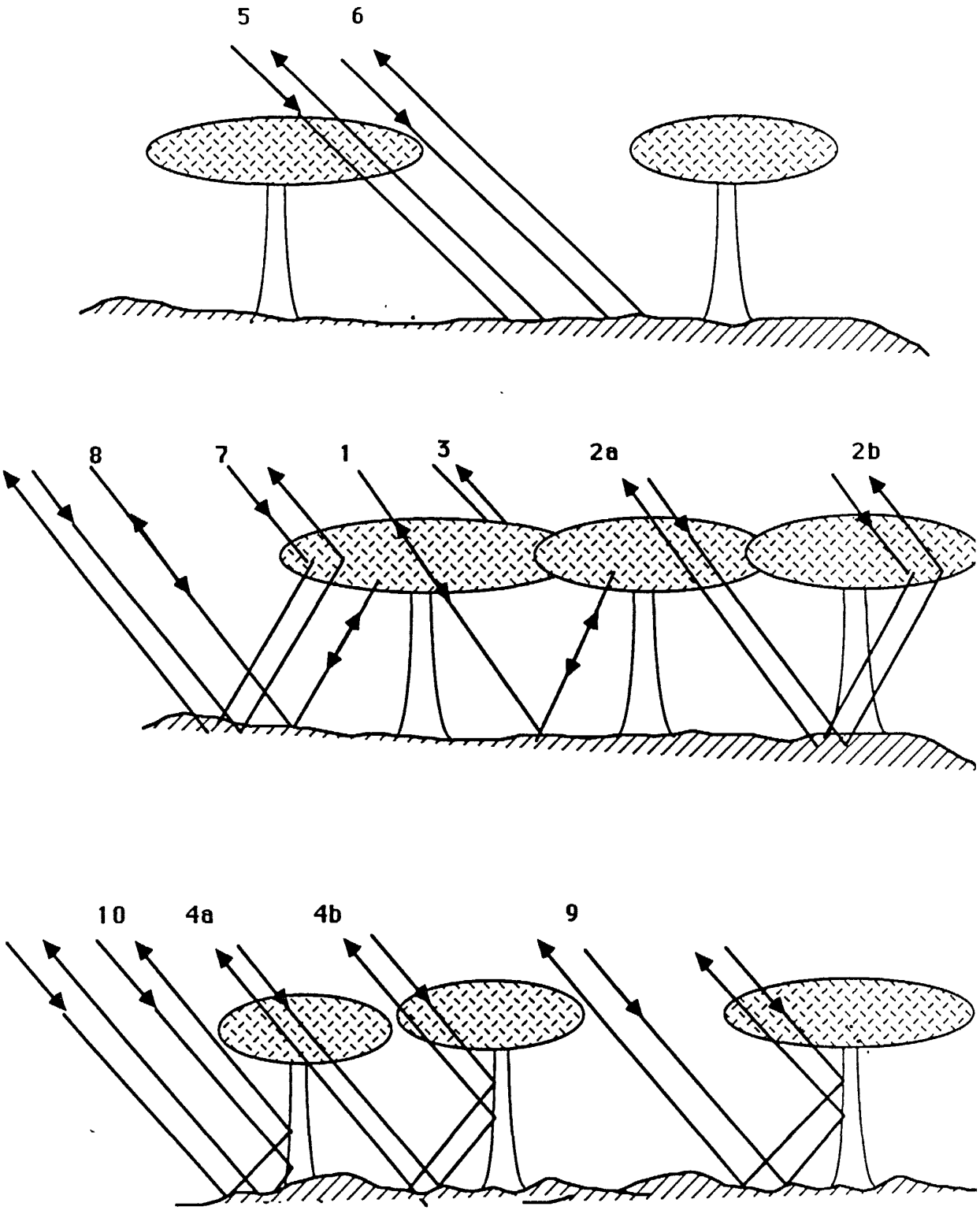


Figure 2. Backscattering Sources

(2) Trunk Surface Roughness. In MIMICS I and II, the trunks are assumed to have smooth surfaces. A model is currently under development to evaluate the effect of the bark roughness on scattering by the tree trunks.

(3) Higher-Order Scattering.

MIMICS I and II will be extended to second—and higher-order scattering to determine the incremental improvement provided by each order versus the resultant increase in model complexity and computational time.

(4) Understory. Approaches will be explored for modeling forest canopies that have an understory of vegetation material on the ground surface.

The succeeding sections of this report are concerned with MIMICS I. Extensions and modifications will be the subject of future reports.

TABLE 1. DEVELOPMENT PLAN FOR MIMICS

	MIMICS I	MIMICS II	MIMICS III
Development Period	1985–1987	1987–1988	1988–1989
Frequency Range	0.5–10 GHz	0.5–10 GHz	0.5–10 GHz or higher
Polarizations	HH,VV,VH,HV	HH,VV,VH,HV	HH,VV,VH,HV
Canopy Crown	Continuous (closed)	Open or closed	Open or closed
Scattering Order	First-order	First-order	Second-or higher order
Status	Operational	Nearing completion	(see Section 1.2)

2 STRUCTURE OF MIMICS I

MIMICS I is a first-order scattering model. The tree canopy is divided into three regions: the crown region, the trunk region and the ground region. By first-order scattering we mean that we will include scattering processes that involve

single scattering by each region and double scattering by pairs of regions Because the trunks are treated as long, vertical cylinders with uniform cross-section and smooth surfaces, they will not backscatter directly except at $\theta_0 = 90°$ (horizontal propagation). Also, unless we include processes involving triple scattering (or higher), we do not get a backscattering contribution involving only the trunk and crown regions.

The backscattering problem is divided into two parts. In the first part, we compute the intensity backscattered from the canopy with the ground surface treated as a specular interface. This is a reasonable assumption because the scattering pattern of the surface usually is dominated by the coherent component pointing in the specular direction. (If the surface is very rough or its mean slope is not zero relative to the vertical direction of the tree trunks, then the specular-surface assumption will not hold). Appendix A contains a derivation for the backscattered intensity vector $\mathbf{I}^s$ based on a first-order solution of the radiative transfer equation. The solution is expressed in the form

$$\mathbf{I}^s(\theta_0, \phi_0) = \mathbf{T}(\theta_0, \phi_0)\mathbf{I}_0 \tag{1}$$

where $\mathbf{I}_0$ is the intensity incident upon the canopy along the direction $(\pi - \theta_0, \phi_0)$ and $\mathbf{T}(\theta_0, \phi_0)$ is a 4x4 transformation matrix given by (A.52).

In the second part of the backscattering problem, we account (partially) for the fact that the ground surface is not specular. We treated the ground surface as specular in Appendix A in order to keep the interactions between the crown/trunk regions and the ground surface reasonably simple. Whereas such an assumption is useful and a valid first-order approximation for computing the backscatter from

the canopy, it totally disregards the contribution due to direct backscatter by the ground surface. This contribution is given by

$$\mathbf{I}_g^s(\theta_0, \phi_0) = \mathbf{T}_g(\theta_0)\mathbf{I}_0, \tag{2}$$

where $\mathbf{T}_g(\theta_0)$ is a transformation matrix that accounts for propagation through the canopy down to the ground surface, backscatter by the ground surface, and propagation again through the canopy back to the radar. The expression for $\mathbf{T}_g(\theta_0)$ is given by

$$\mathbf{T}_g(\theta_0) = e^{-\boldsymbol{\kappa}_c^+ + d\sec\theta_0} e^{-\boldsymbol{\kappa}_t^+ + d\sec\theta_0} \mathbf{G}(\theta_0) e^{-\boldsymbol{\kappa}_t^- - d\sec\theta_0} e^{-\boldsymbol{\kappa}_c^- - d\sec\theta_0} \tag{3}$$

where $\boldsymbol{\kappa}_c^+$ and boldmath κ_c^- are the extinction matrices of the crown layer (see (A.19) to (A.21) for upward propagation in the direction (θ_0, ϕ_0) and downward propagation in the direction $(\pi - \theta_0, \phi_0)$, respectively; similar definitions apply to the trunk extinction matrices $\boldsymbol{\kappa}_t^+$ and $\boldsymbol{\kappa}_t^-$; and $\mathbf{G}(\theta_0)$ is the ground backscattering matrix. Each of the four exponential functions in (3) may be expressed as the product of three 4x4 matrices as discussed in connection with (A.21).

The backscattering matrix $\mathbf{G}(\theta_0)$ is given in Appendix D for three different surface scattering models. The elements of $\mathbf{G}(\theta_0)$ are proportional to the ground backscattering coefficient σ_g°; for example,

$$4\pi \cos\theta_0 \left[\mathbf{G}(\theta_0)\right]_{11} = \sigma_{gvv}^\circ(\theta_0). \tag{4}$$

Upon combining (1) and (2), we obtain an expression for the total backscattered intensity $\mathbf{I}_t^s(\theta_0, \phi_0)$,

$$\mathbf{I}_t^s(\theta_0, \phi_0) \;=\; \left[\mathbf{T}(\theta_0) + \mathbf{T}_g(\theta_0)\right] \mathbf{I}_0 \tag{5}$$

$$= \mathbf{T}_t(\theta_0)\mathbf{I}_0 \tag{6}$$

where $\mathbf{T}_t(\theta_0)$ represents the total backscattering transformation matrix of the forest canopy.

The matrix $T_t(\theta_0)$ can be used to compute the linearly polarized total canopy backscattering coefficients

$$\sigma^\circ_{vv} = 4\pi \cos\theta_0 \left[T_t(\theta_0)\right]_{11},$$

$$\sigma^\circ_{hh} = 4\pi \cos\theta_0 \left[T_t(\theta_0)\right]_{22},$$

$$\sigma^\circ_{hv} = 4\pi \cos\theta_0 \left[T_t(\theta_0)\right]_{21},$$

$$\sigma^\circ_{vh} = 4\pi \cos\theta_0 \left[T_t(\theta_0)\right]_{12},$$

or may be used to compute the backscattering coefficient for any transmit– and receive–polarization combination using the wave synthesis technique described in Appendix G.

3 NUMERICAL SIMULATIONS

This section presents the results of several model simulations. Data are simulated for four forest stands as a function of radar look angle and frequency. Relevant parameters for each of the simulated canopies are listed in Table 2.

TABLE 2. Test Canopy Parameters

Parameter	Canopy I	Canopy II	Canopy III	Canopy IV
Canopy Density (trees per square meter)	0.11	0.11	0.11	0.20
Trunk Height (meters)	8 m	8 m	8 m	16 m
Trunk Diameter (cm)	24 cm	24 cm	24 cm	20.8 cm
Trunk Moisture (gravimetric)	0.5	0.5	0.5	0.6
Crown Thickness (meters)	2 m	2 m	2 m	11.0 m
Leaf/Needle Density (per cubic meter)	830	0	830	85,000
Leaf/Needle Moisture (gravimetric)	0.8	-	0.8	0.8
LAI (single-sided)	5	0	5	11.9
Branch Density (branches per cubic meter)	0	4.1	4.1	3.4
Branch Length (m)	-	0.75 m	0.75 m	2.0 m
Branch Diameter (cm)	-	0.7 cm	0.7 cm	2.0 cm
Branch Moisture (gravimetric)	-	0.4	0.4	0.6
Soil RMS Height	0.45 cm	0.45 cm	0.45 cm	0.45 cm
Soil Correlation Length	18.75 cm	18.75 cm	18.75 cm	18.75 cm
Soil Volumetric Moisture	0.15	0.15	0.15	0.15
Soil % Sand	10	10	10	20
Soil % Silt	30	30	30	70
Soil % Clay	60	60	60	10

The parameters for canopies I, II and III were chosen to represent a trembling aspen stand. Section 3.1 presents an analysis for an aspen canopy whose crown layer consists of leaves only. Section 3.2 presents the results of a simulation performed on a canopy whose crown layer consists of branches only. Section 3.3 discusses a simulation for an aspen canopy whose crown layer consists of both leaves and branches. Except for the presence or absence of leaves and branches, canopy attributes of these three stands remain unchanged so that comparisons may

be made as to the effect of leaves and branches on the radar backscatter

The parameters for canopy IV were chosen to represent a white spruce stand The results of this analysis are presented in Section 3.4. Here, the crown layer consists of both needles and branches.

The data presented include plots of total canopy backscatter as a function of both incidence angle and frequency. Graphs shown as a function of incidence angle were computed for frequencies of 1.62, 4.75 and 10.0 GHz, corresponding to L-, C-, and X-bands, respectively. Graphs shown as a function of frequency were computed using an incidence angle of 30°.

The components of the total backscatter for each canopy are also shown. The total canopy backscatter consists of 1) a ground-trunk interaction component, 2) a total crown backscatter component and 3) a direct ground backscatter component. The total crown backscatter component consists of three contributions resulting from 1) the direct backscatter from the crown, 2) the combination of specular scatter from the ground and forward scatter from the crown layer and 3) the combination of specular scatter from the ground that is scattered directly back to the ground from the crown layer and is again scattered in the specular direction by the ground.

In all cases, the backscatter is shown for the four polarization configurations HH, VV, VH and HV. Since only azimuthally symmetric canopies are considered in this study, the total cross-polarized backscatter consists only of the cross-polarized crown layer contributions. Additional plots of simulated data for each of the four canopy types are included in Appendix H.

Finally, Section 3.5 presents the results of a wave synthesis analysis performed on the simulated data. Several polarimetric signatures are presented for canopies I through IV at a radar look angle of 40°.

3.1 Canopy I — Leaf-Dominated Crown Layer

This section presents the results of an analysis of a trembling aspen stand whose crown layer consists entirely of leaves. Branches are neglected in this example. The leaves are considered to be randomly oriented, 6.18 cm in diameter and 0.1 cm thick. For a 2 meter thick crown layer with 830 leaves per cubic meter, this corresponds to a canopy with a single-sided leaf area index (LAI) of 5.0.

Figure 3 shows the crown transmissivity as a function of incidence angle for both horizontal and vertical polarizations. This represents the fraction of incident radiation that penetrates the crown layer. Figure 4 shows the transmissivity as a function of leaf density. Given the previously stated leaf parameters, a density of 500 leaves/m^3 corresponds to an LAI of 3 and a density of 1500 leaves/m^3 corresponds to an LAI of 9. Figure 5 shows the transmissivity as a function of frequency. In general, transmissivity decreases with increasing incidence angle, leaf density, and frequency.

Figures 6 and 7 show the total canopy backscatter as a function of incidence angle for L-, C- and X-bands. Four linear polarization configurations are represented. Figure 6 shows the two like-polarized configurations and Figure 7 shows the two cross-polarized configurations. The chracteristics of the HH and VV polarized backscatter are very different whereas the VH and HV backscatters are quite similar. Furthermore, for a given polarization, the character of the backscatter

changes somewhat with frequency. The differences between VH and HV polarizations are due in part to computational precision and the fact that the physical optics model used to model the leaves is not reciprocal.

Figures 8 through 11 illustrate the individual contributions to the total canopy backscatter as a function of incidence angle. Figures 8 and 9 show backscatter at L-band for HH and VV polarizations. Figure 10 shows backscatter at X-band for HH polarization. Generally, the ground-trunk interaction mechanism is more of a significant contributor to backscatter at lower frequencies while the scatter from the crown layer is more important at higher frequencies. Furthermore, the direct ground backscatter term decreases very quickly with increasing incidence angle because of the smooth ground surface. Figure 11 illustrates the three mechanisms that contribute to the total crown backscatter for HH polarization at X-band. Here, the direct crown term is the dominant crown scattering mechanism.

Figure 12 shows the total canopy backscatter as a function of frequency for the like and cross polarized cases. The like-polarized cases approach each other as frequency is increased whereas the cross-polarized backscatter decreases.

Additional plots showing the individual scattering components for each of the cases of Figures 6, 7 and 12 are included in Appendix H.

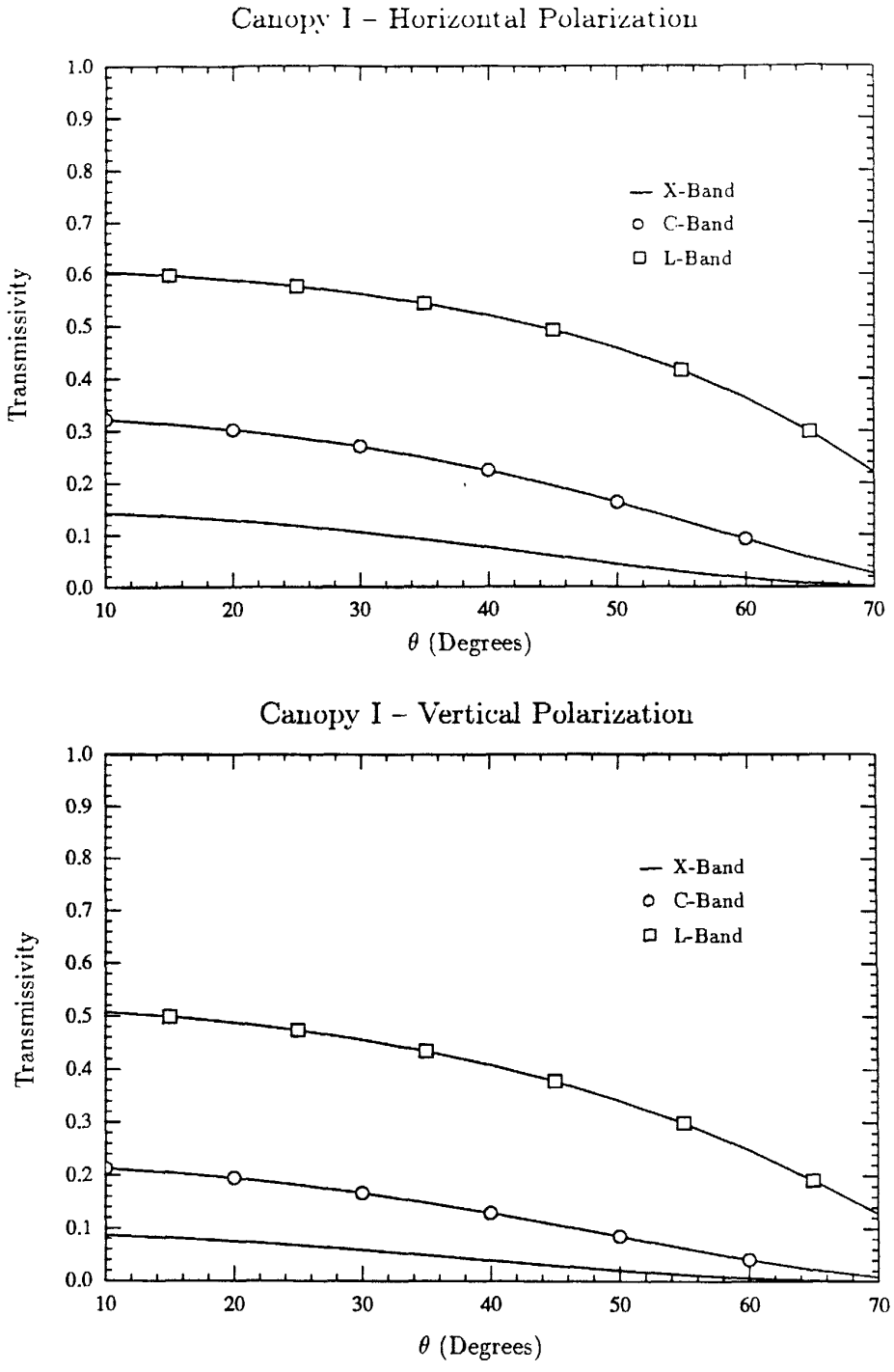


Figure 3 Crown Transmissivity vs. Incidence Angle. Leaf Density = 830 leaves per cubic meter

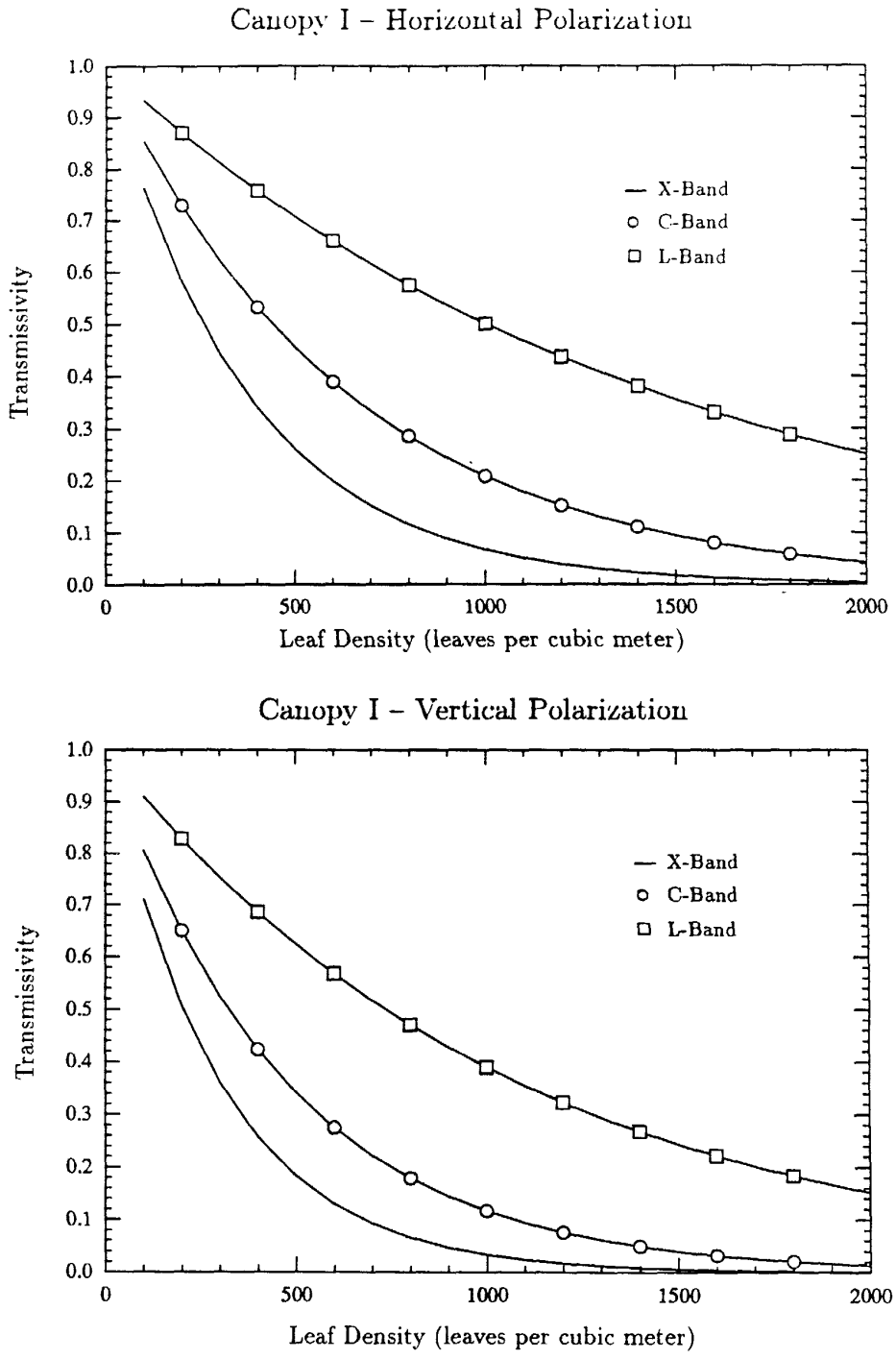


Figure 4· Crown Transmissivity vs. Leaf Density. Incidence Angle = 30°.

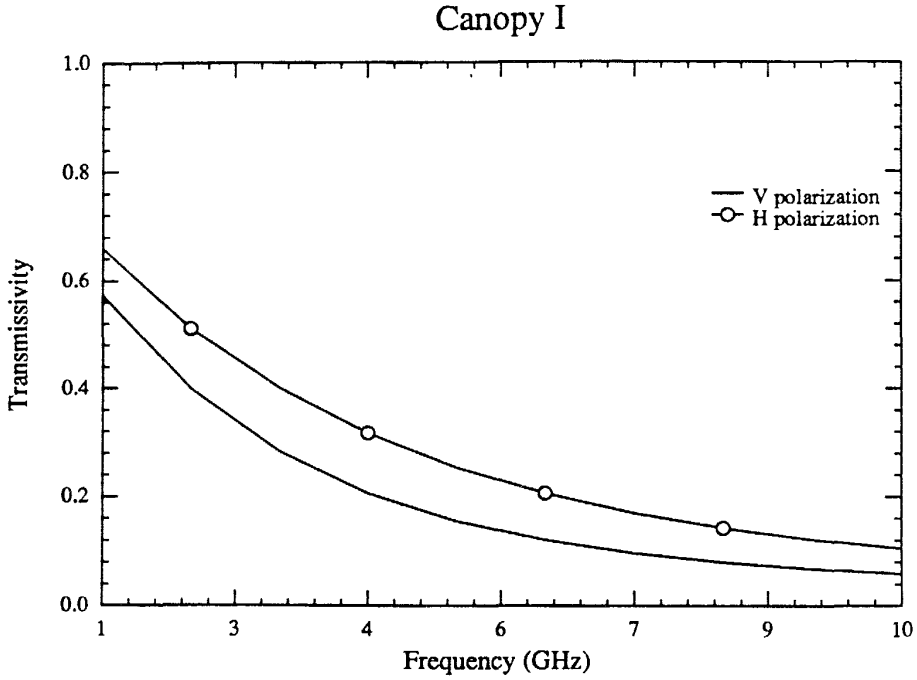


Figure 5: Crown Transmissivity vs. Frequency. Incidence Angle = 30° Leaf Density = 830 leaves per cubic meter.

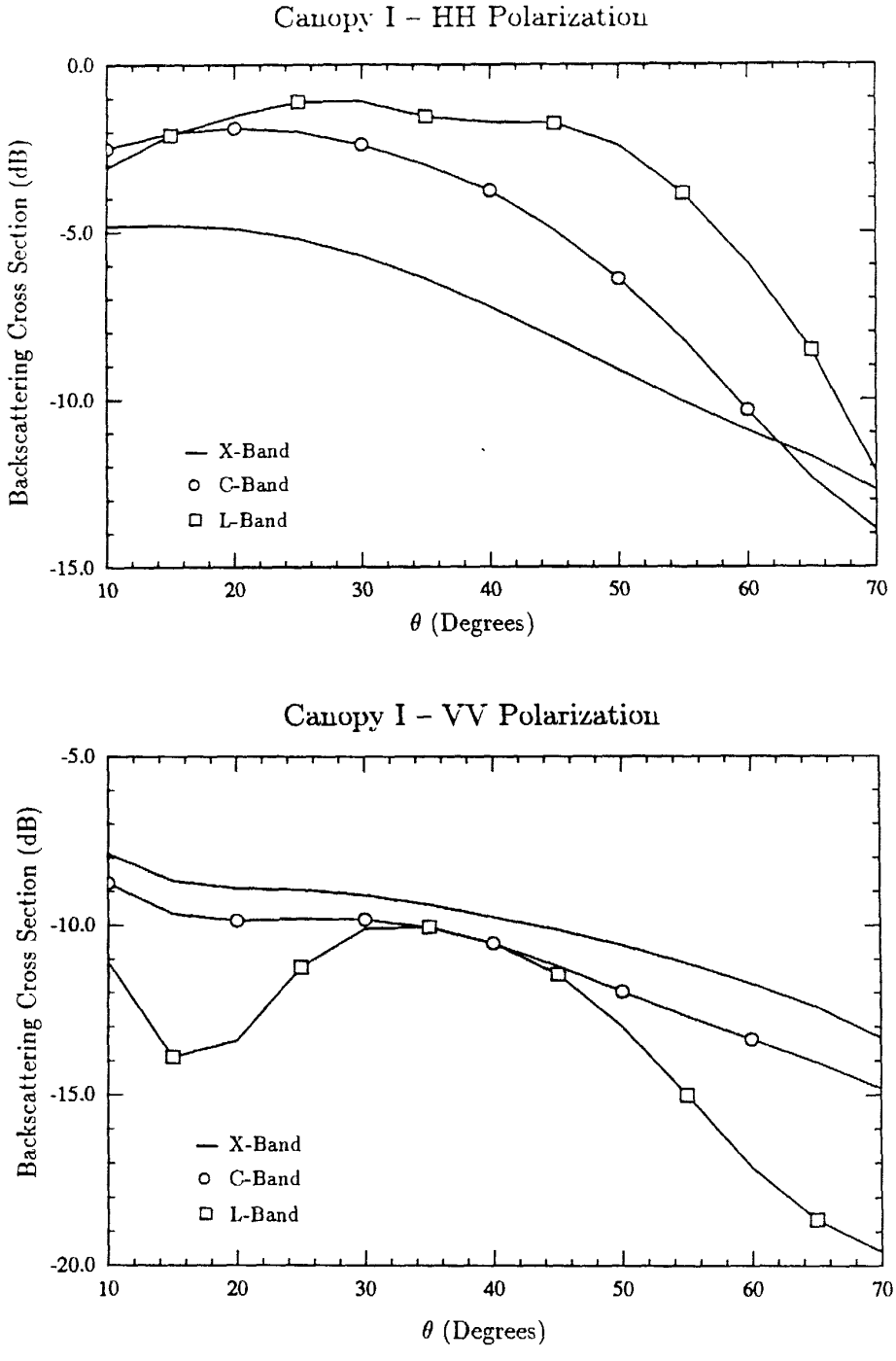


Figure 6: Total Like-Polarized Canopy Backscatter vs. Incidence Angle.

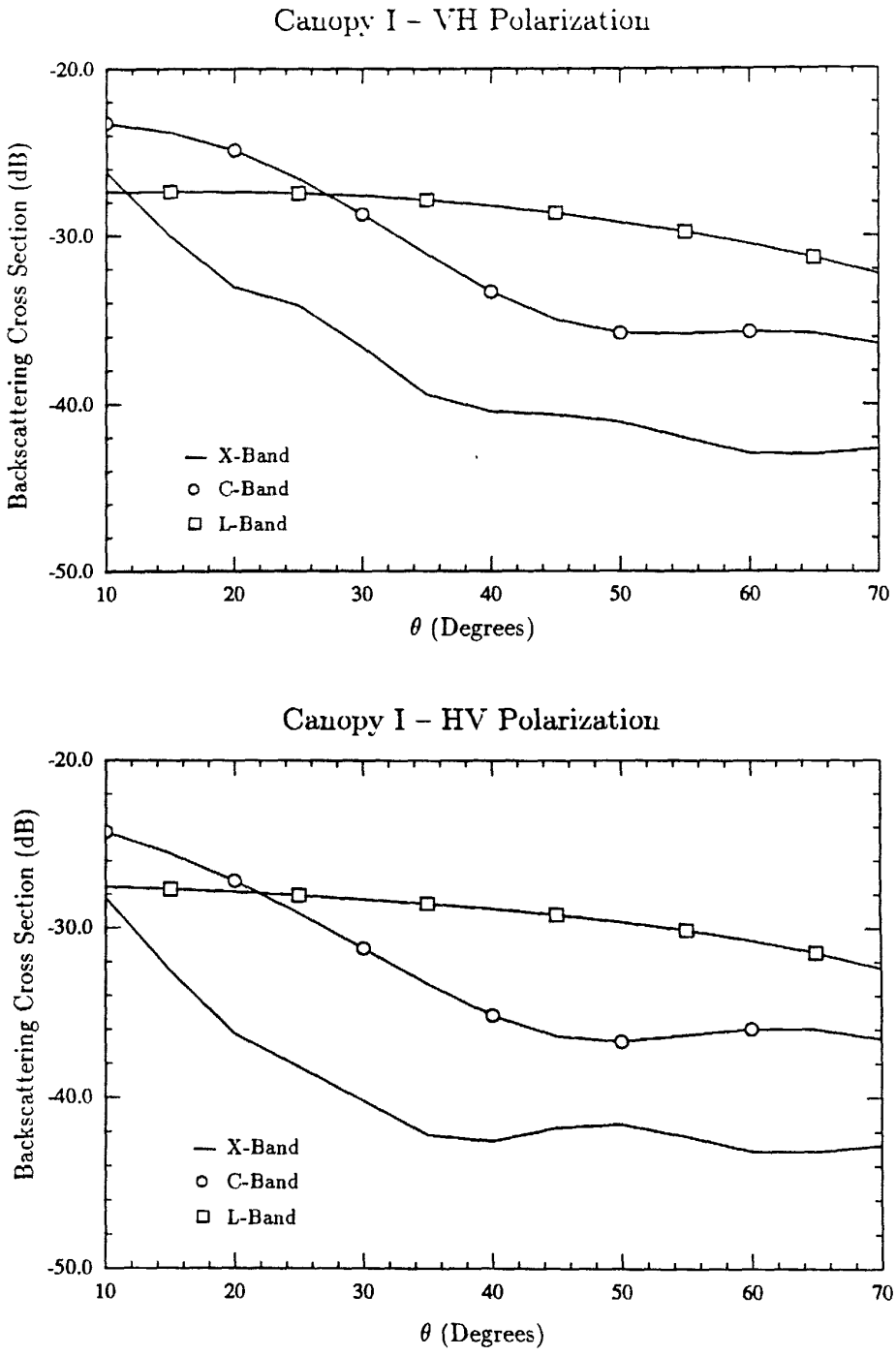


Figure 7: Total Cross-Polarized Canopy Backscatter vs. Incidence Angle.

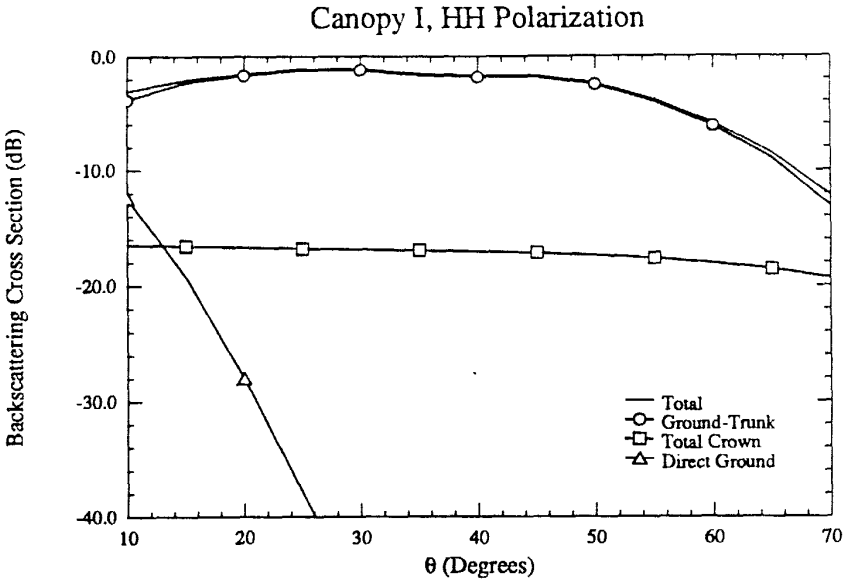


Figure 8: L-Band Backscatter Components vs. Incidence Angle.

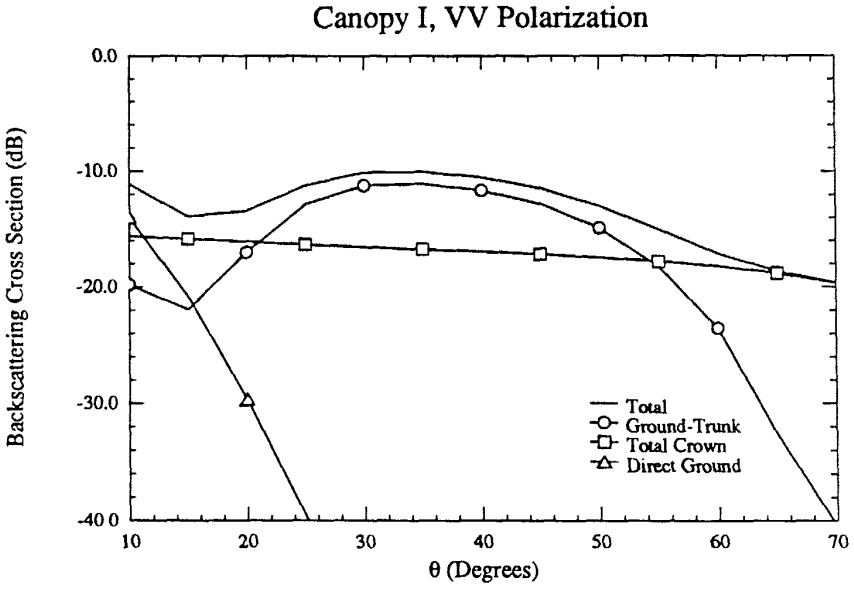


Figure 9: L-Band Backscatter Components vs. Incidence Angle.

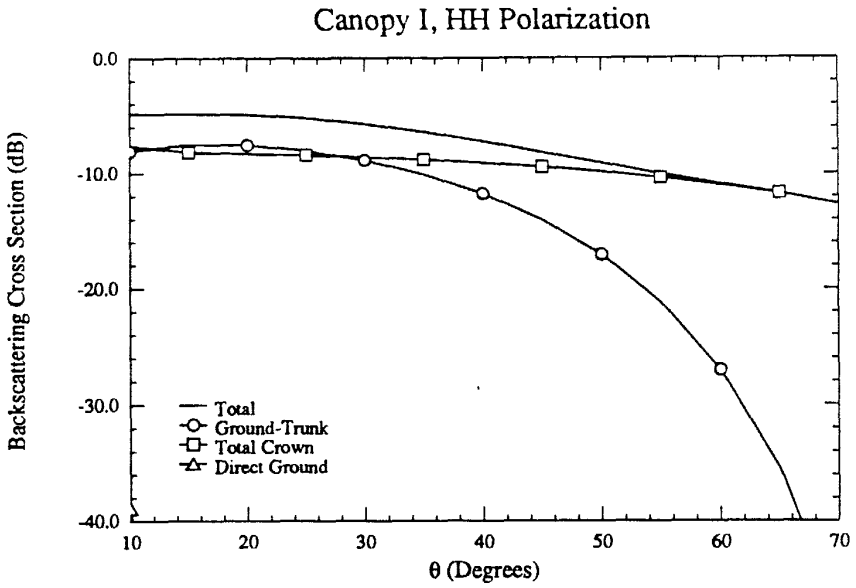


Figure 10: X-Band Backscatter Components vs. Incidence Angle.

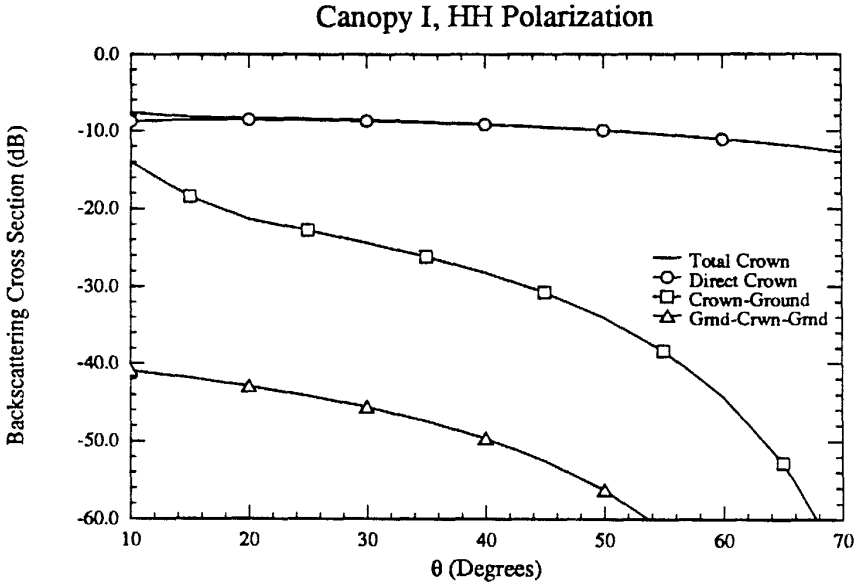


Figure 11: X-Band Crown Backscatter Contributions vs. Incidence Angle

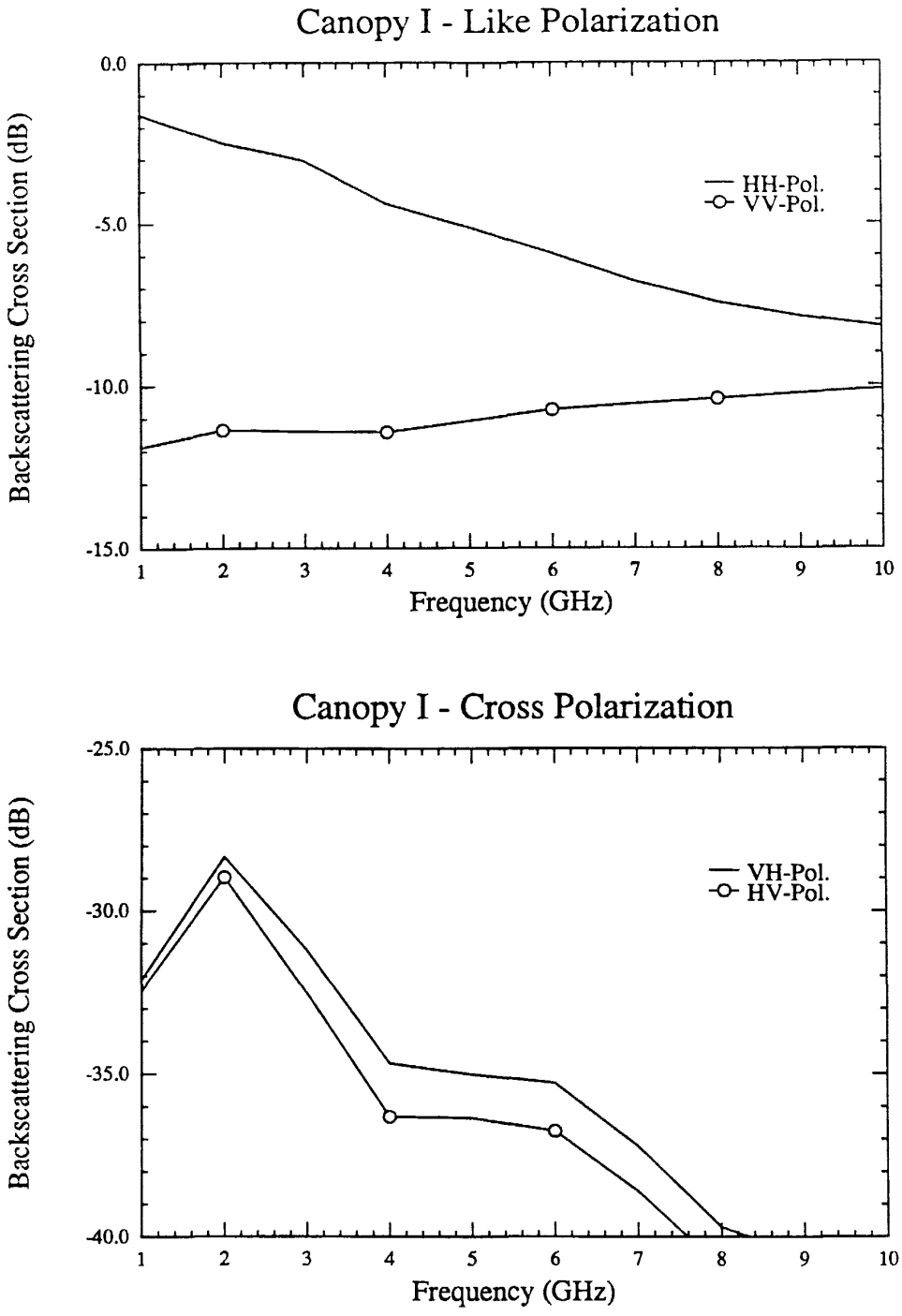


Figure 12: Total Canopy Backscatter vs. Frequency. Incidence Angle = 30°

3.2 Canopy II — Branch-Dominated Crown Layer

This section presents the results of an analysis of a defoliated aspen stand for which the crown layer consists entirely of branches. The branches are 75 cm long with a 0.7 cm diameter and have an orientation uniform in ϕ_c and a PDF in θ_c described by

$$p(\theta_c) = \begin{cases} \frac{\sin^4(2\theta_c)}{\int_0^{\frac{\pi}{2}} \sin^4(2\theta_c')d\theta_c'} & 0 \leq \theta_c \leq \frac{\pi}{2} \\ 0 & \text{otherwise.} \end{cases} \tag{7}$$

This gives an average $\theta_c = 45^o$. These characteristics are based on an analysis of several aspen stands described by Nelson et al.(1981) and Pitts et al.(1985). Figure 13 shows a graph of this PDF along with the measured data from the cited reports.

Crown transmissivity as a function of incidence angle and frequency is shown in Figures 14 and 15. Here, the transmissivity is very close to 1 because of the low volume density of branches.

The total canopy backscatter for each of the four linear polarization configurations is shown in Figures 16 and 17. Here, although the character of HH backscatter is quite different from that of VV, the character of each does not change with frequency.

Figures 18 through 21 illustrate the individual contributions to the total canopy backscatter as a function of incidence angle. Figures 18 and 19 show backscatter at L-band for HH and VV polarizations. Figure 20 shows backscatter at X-band for HH polarization. Because of the absence of leaves, relatively little backscatter is generated by the crown layer. Even at X-band the total canopy backscatter is

dominated by the ground-trunk interaction mechanism.

Figure 21 illustrates the mechanisms that contribute to the total crown backscatter for HH polarization at X-band. In this case, the crown backscatter is dominated by direct crown backscatter at low incidence angles and by the crown-ground interaction at high angles. In either case, the crown backscatter has a negligible effect on total canopy backscatter.

Figure 22 shows the total canopy backscatter as a function of frequency for the like and cross polarized cases. The like-polarized cases monotonically increase with frequency whereas the cross-polarized backscatter approaches a maximum between 6 and 7 GHz and decreases at higher frequencies.

Additional plots showing the individual scattering components for each of the cases of Figures 16, 17 and 22 are included in Appendix H.

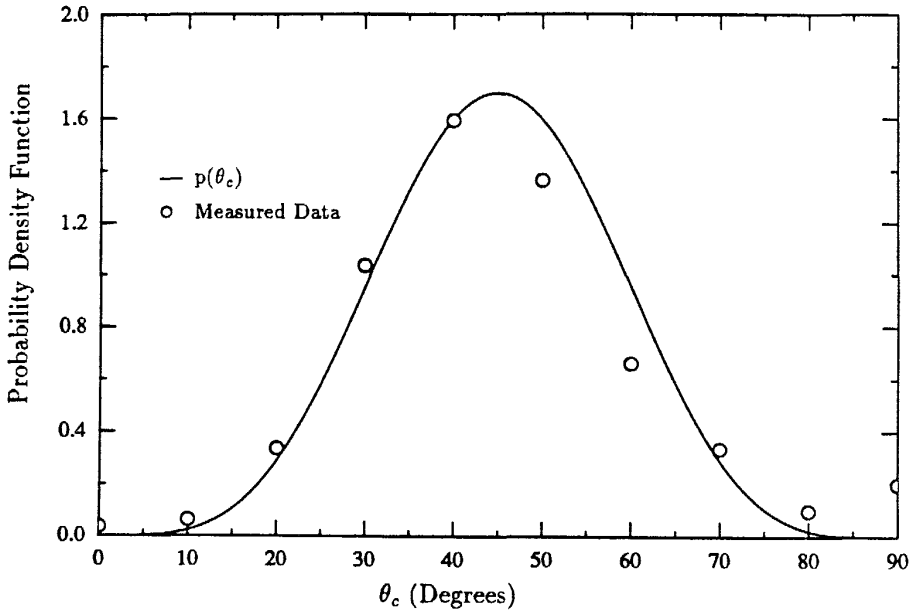


Figure 13: Aspen Canopy Branch Angle Distribution.

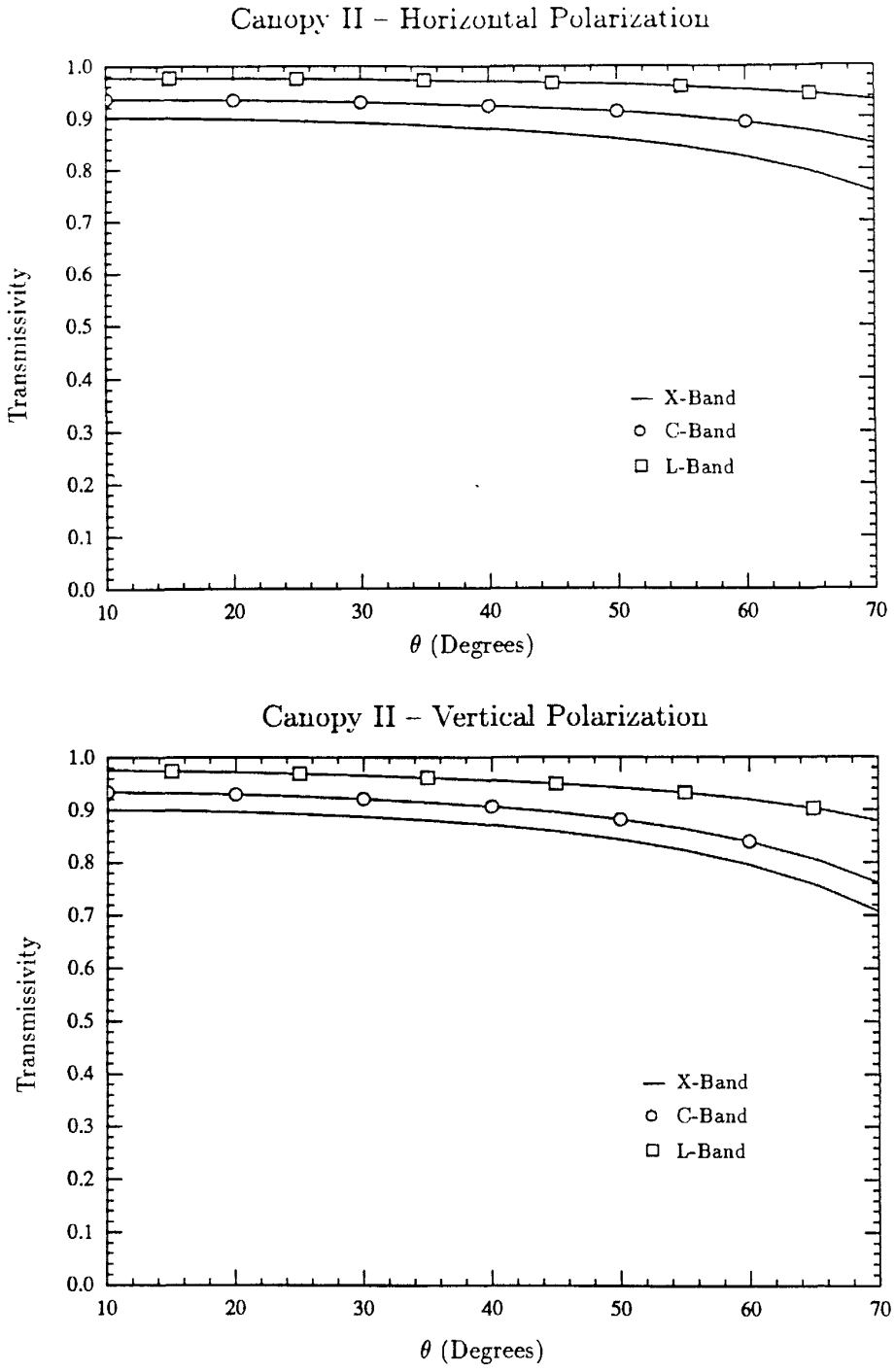


Figure 14. Crown Transmissivity vs. Incidence Angle. Branch Density = 4.1 branches per cubic meter

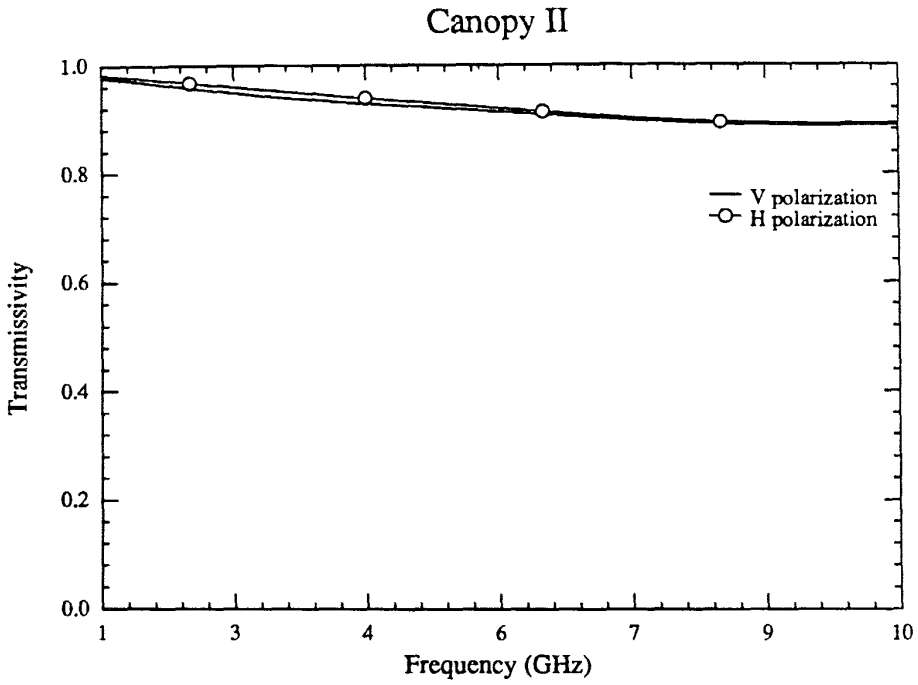


Figure 15: Crown Transmissivity vs. Frequency. Incidence Angle = 30°, Branch Density = 4.1 branches per cubic meter.

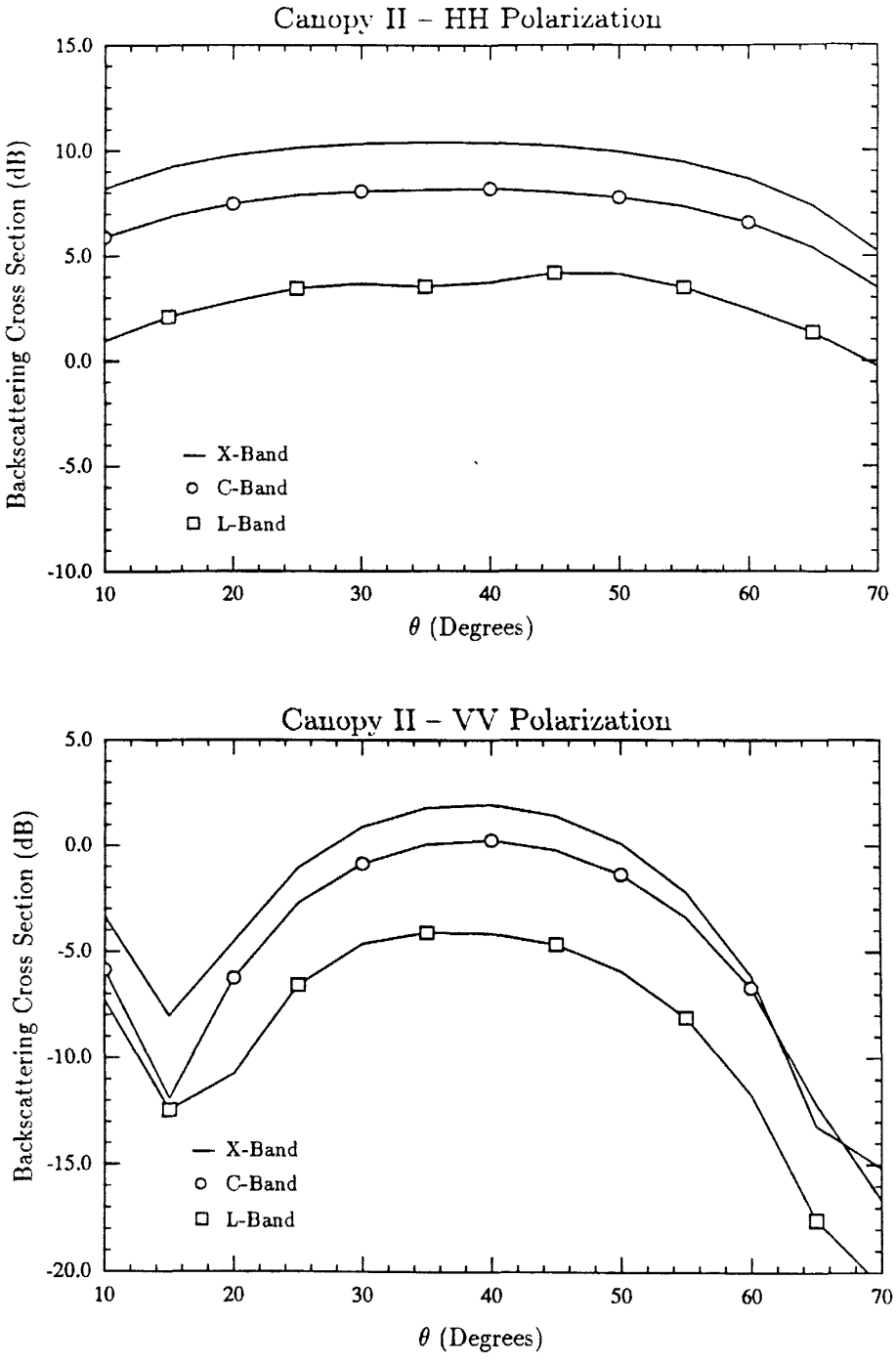


Figure 16: Total Like-Polarized Canopy Backscatter vs. Incidence Angle.

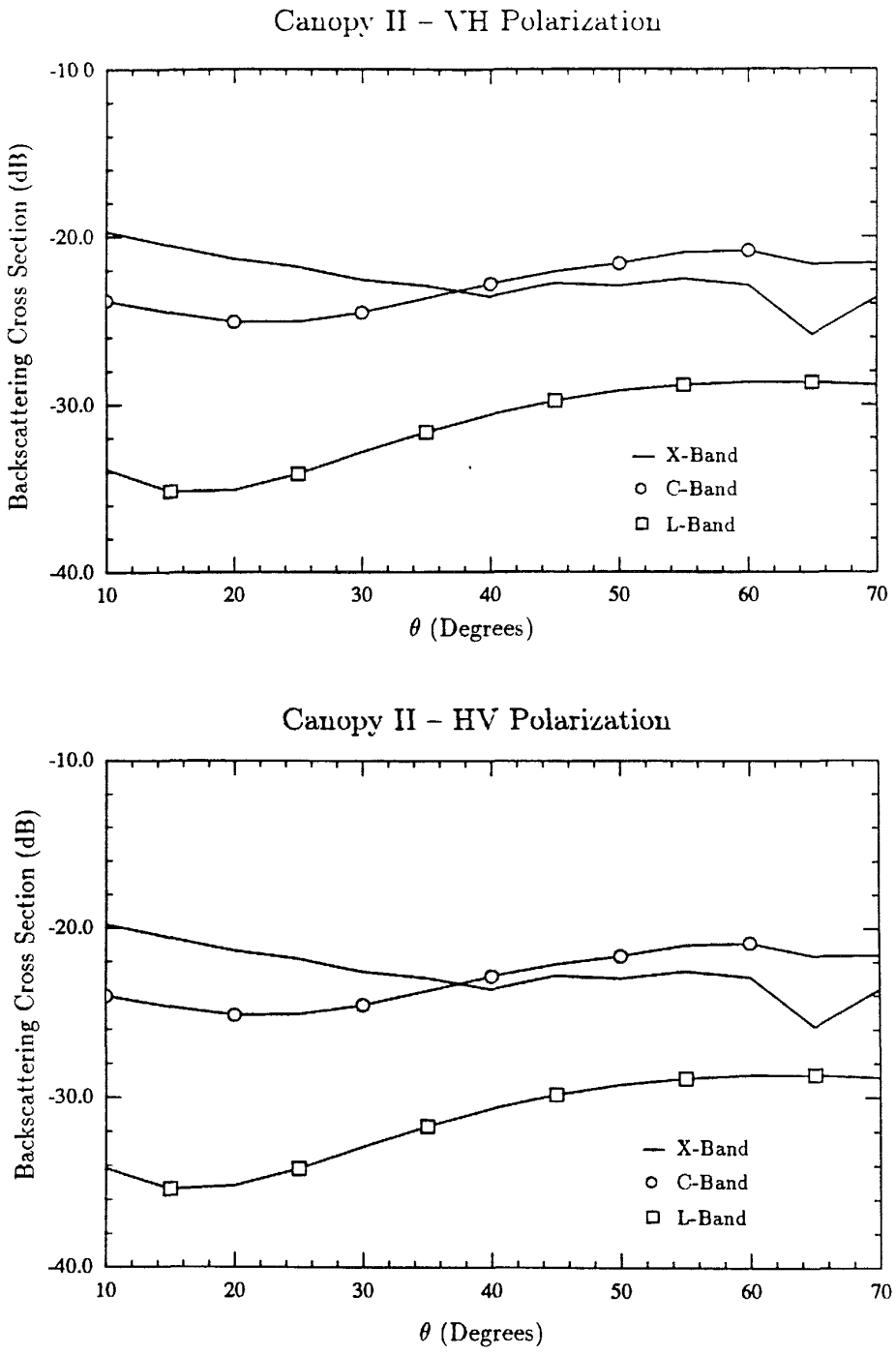


Figure 17: Total Cross-Polarized Canopy Backscatter vs Incidence Angle

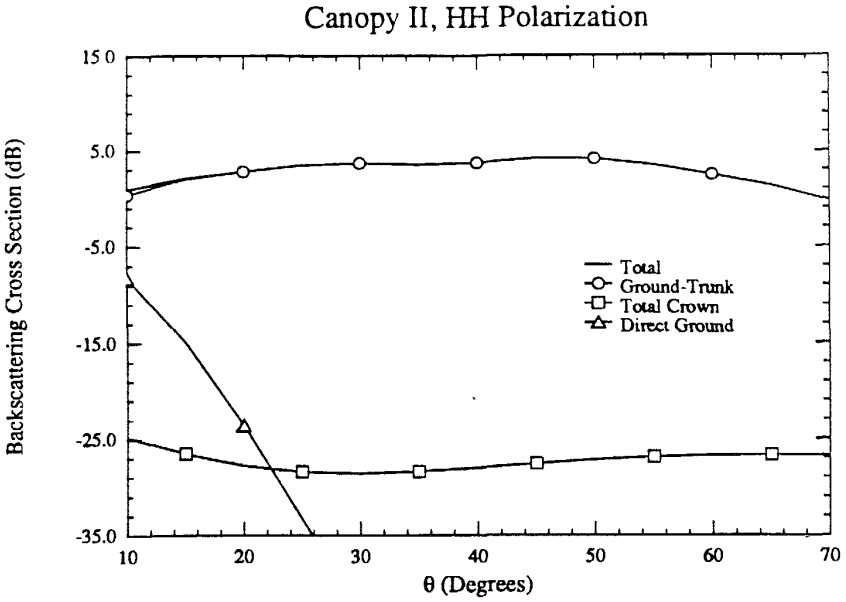


Figure 18: L-Band Backscatter Components vs. Incidence Angle.

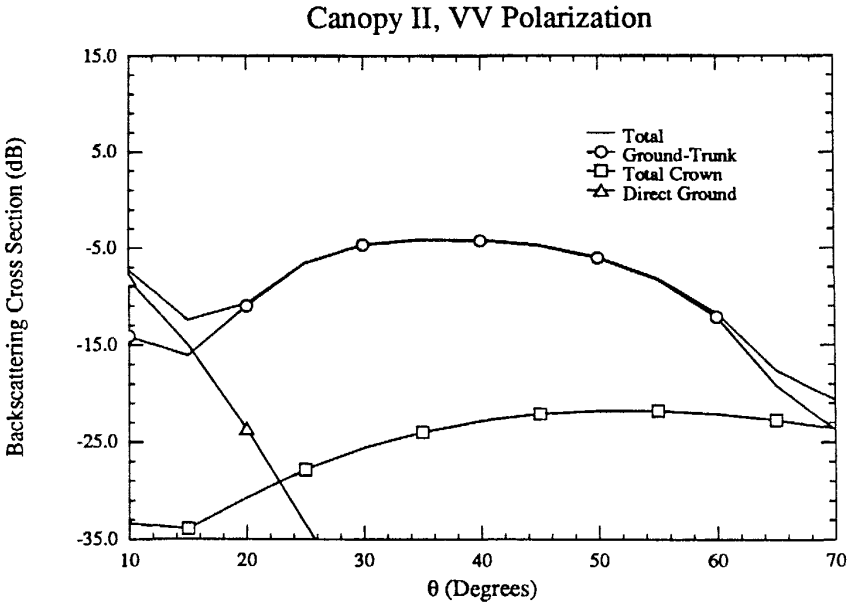


Figure 19: L-Band Backscatter Components vs. Incidence Angle.

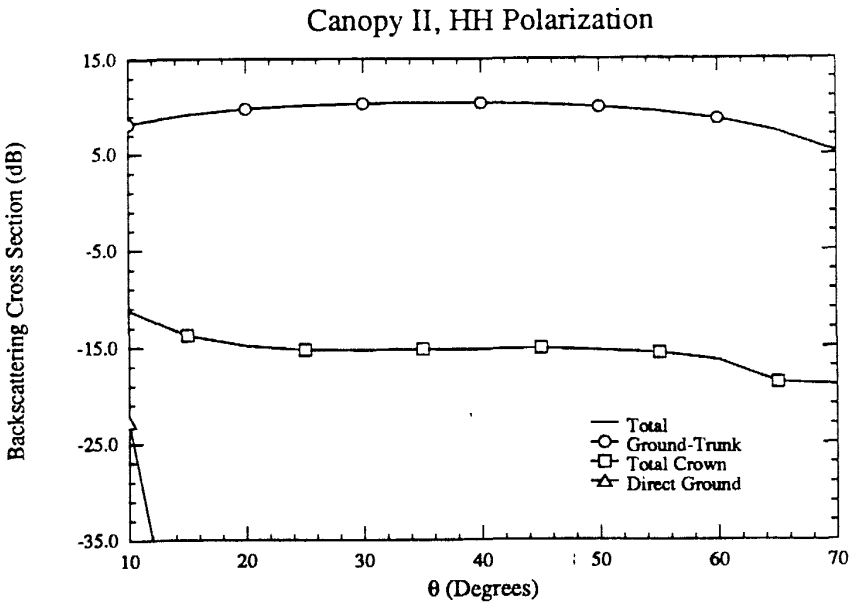


Figure 20: X-Band Backscatter Components vs. Incidence Angle.

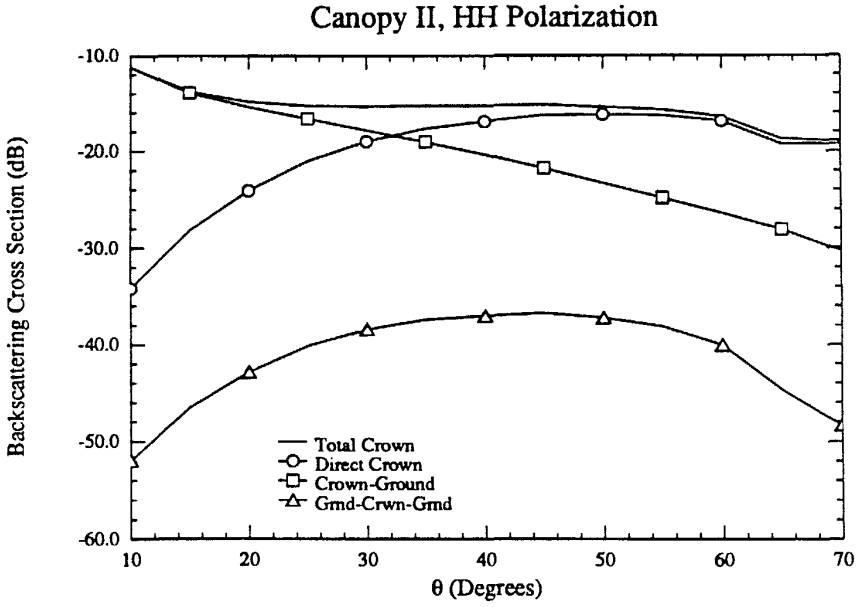


Figure 21: X-Band Crown Backscatter Contributions vs. Incidence Angle.

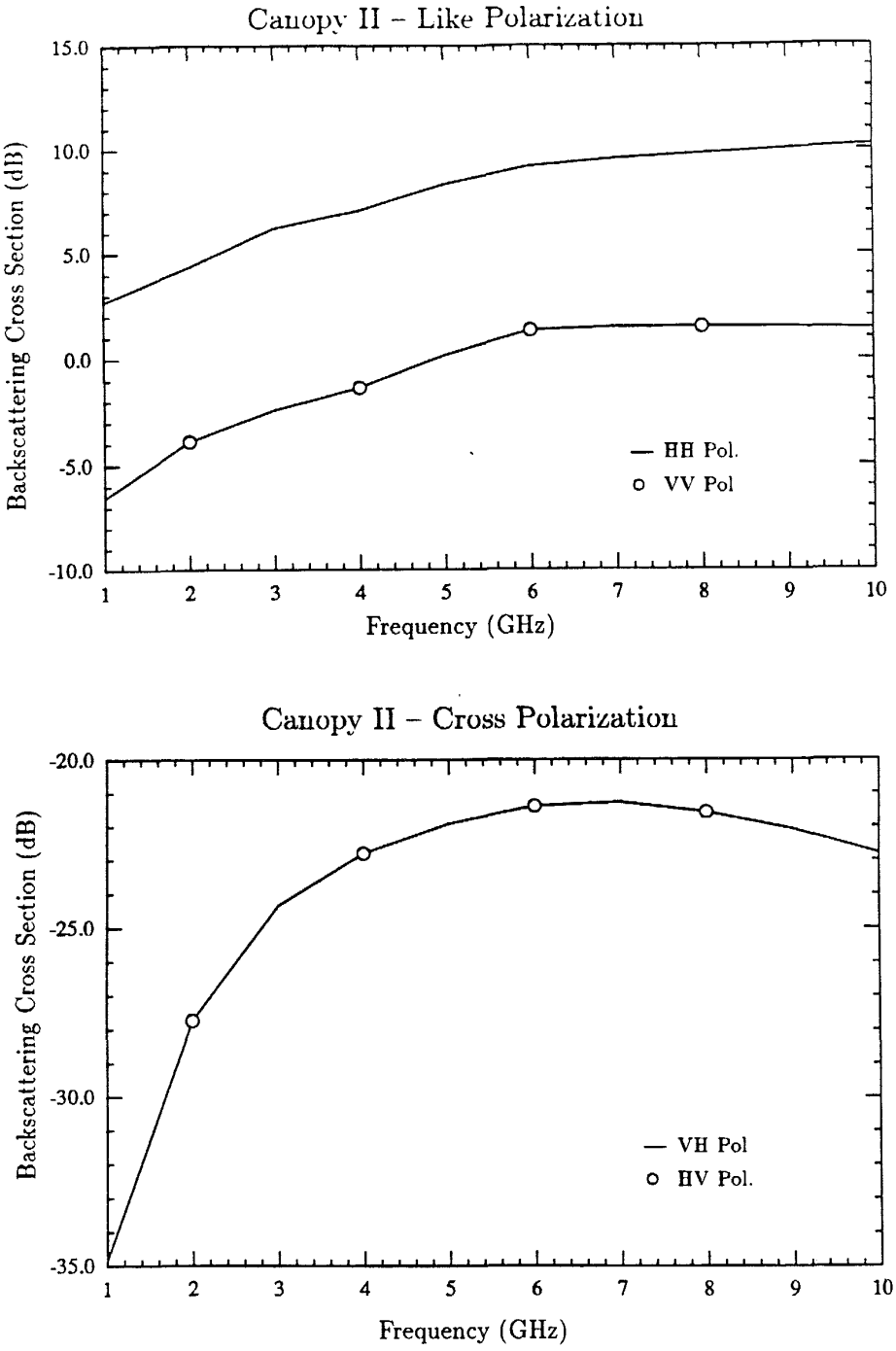


Figure 22: Total Canopy Backscatter vs. Frequency. Incidence Angle = 30°

3.3 Canopy III — Crown Layer with Leaves and Branches

This section presents an analysis of an aspen stand whose crown layer consists of both leaves and branches. The leaf and branch characteristics are identical with those used in Sections 3.1 and 3.2.

Crown transmissivity as a function of incidence angle and frequency is shown in Figures 23 and 24. These figures closely resemble those of the leaf-dominated crown layer.

The total canopy backscatter for each of the four linear polarization configurations is shown in Figures 25 and 26. The like-polarized configurations are almost identical to those found in the leaf-dominated crown layer case of canopy I. The cross-polarized cases, however, increase substantially over the canopy I case for incidence angles greater than 20°. Therefore, the branches have a substantial effect on the cross-polarized canopy backscatter but not on the like-polarized backscatter.

Figures 27 through 30 illustrate the individual contributions to the total canopy backscatter as a function of incidence angle. Figures 27 and 28 show backscatter at L-band for HH and VV polarizations. Figure 29 shows backscatter at X-band for HH polarization. Figure 30 illustrates the mechanisms that contribute to the total crown backscatter for HH polarization at X-band. These plots are almost identical to those presented in the analysis of canopy I.

Figure 31 shows the total canopy backscatter as a function of frequency for the like and cross polarized cases. Whereas the like-polarized backscatter resembles that of canopy I, the cross-polarized backscatter has a completely different character than that of either canopy I or II. In general, more cross-polarized re-

turn is generated here than in the leaf-only case. Also, at high frequencies, more cross-polarized return is generated than in the branch-only case.

Additional plots showing the individual scattering components for each of the cases of Figures 25, 26 and 31 are included in Appendix H.

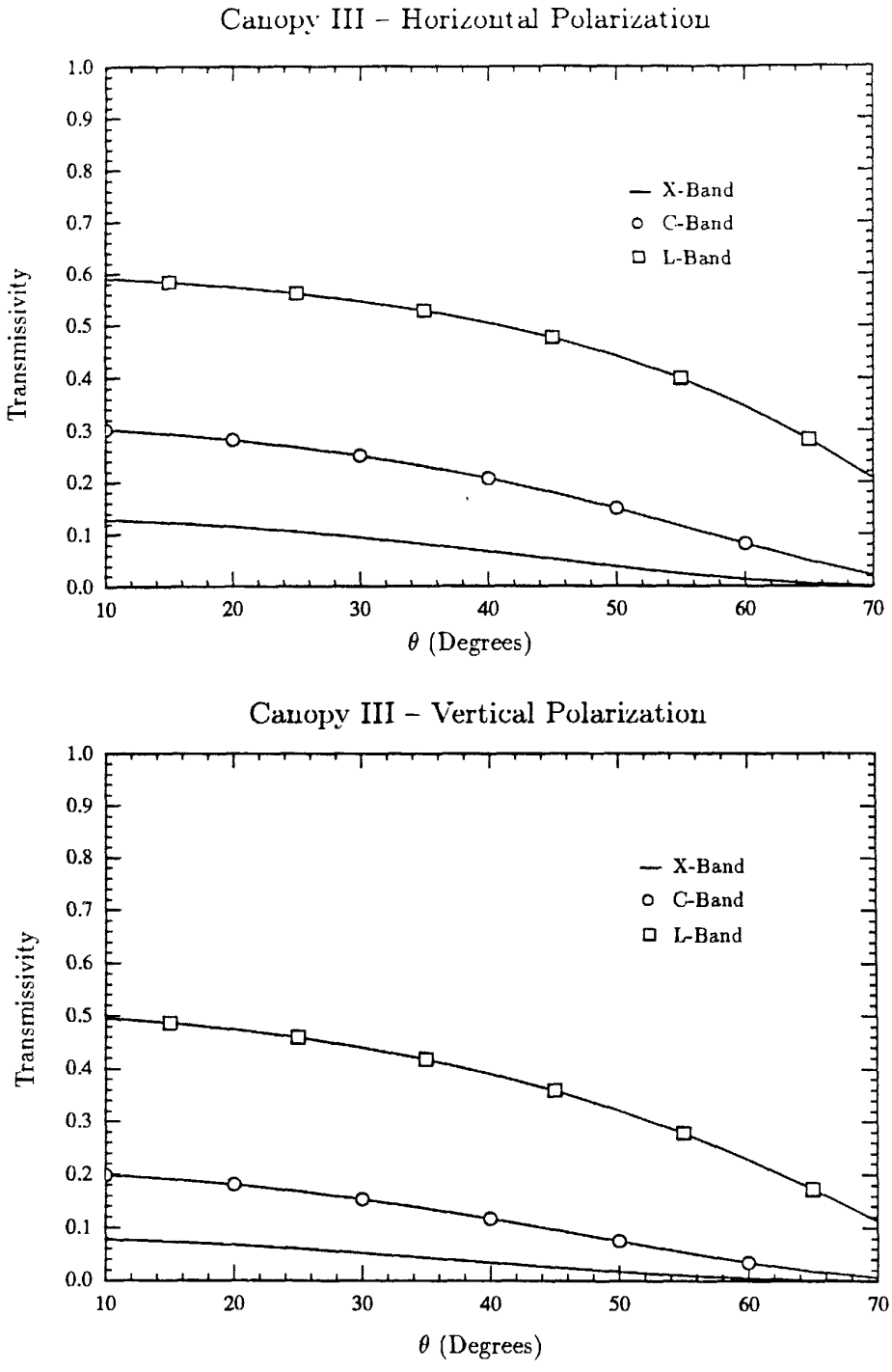


Figure 23: Crown Transmissivity vs. Incidence Angle. Leaf Density = 830 leaves per cubic meter. Branch Density = 4.1 branches per cubic meter.

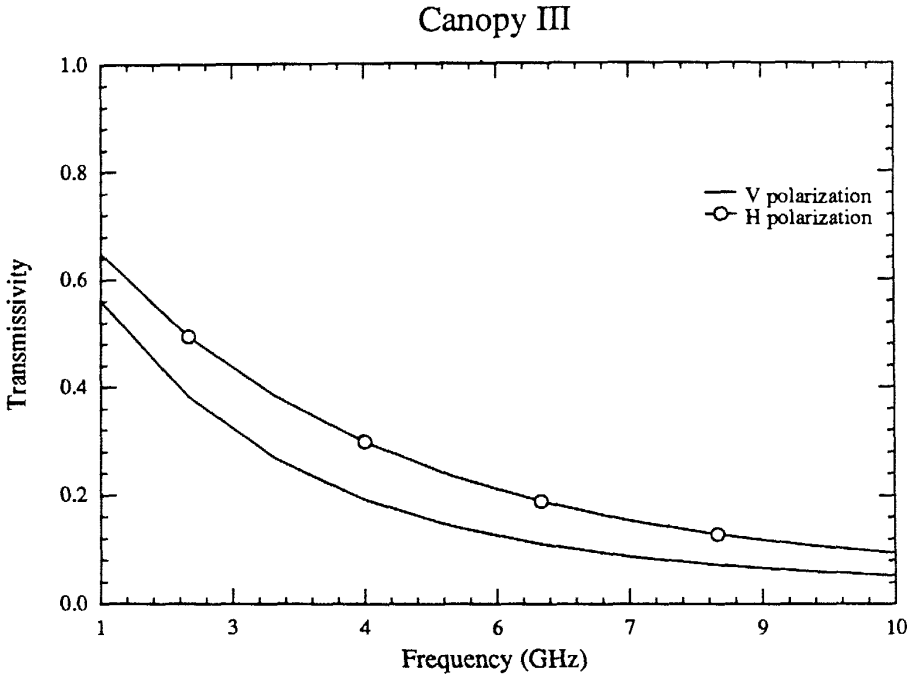


Figure 24: Crown Transmissivity vs. Frequency. Incidence Angle = 30°. Leaf Density = 830 leaves per cubic meter. Branch Density = 4.1 branches per cubic meter.

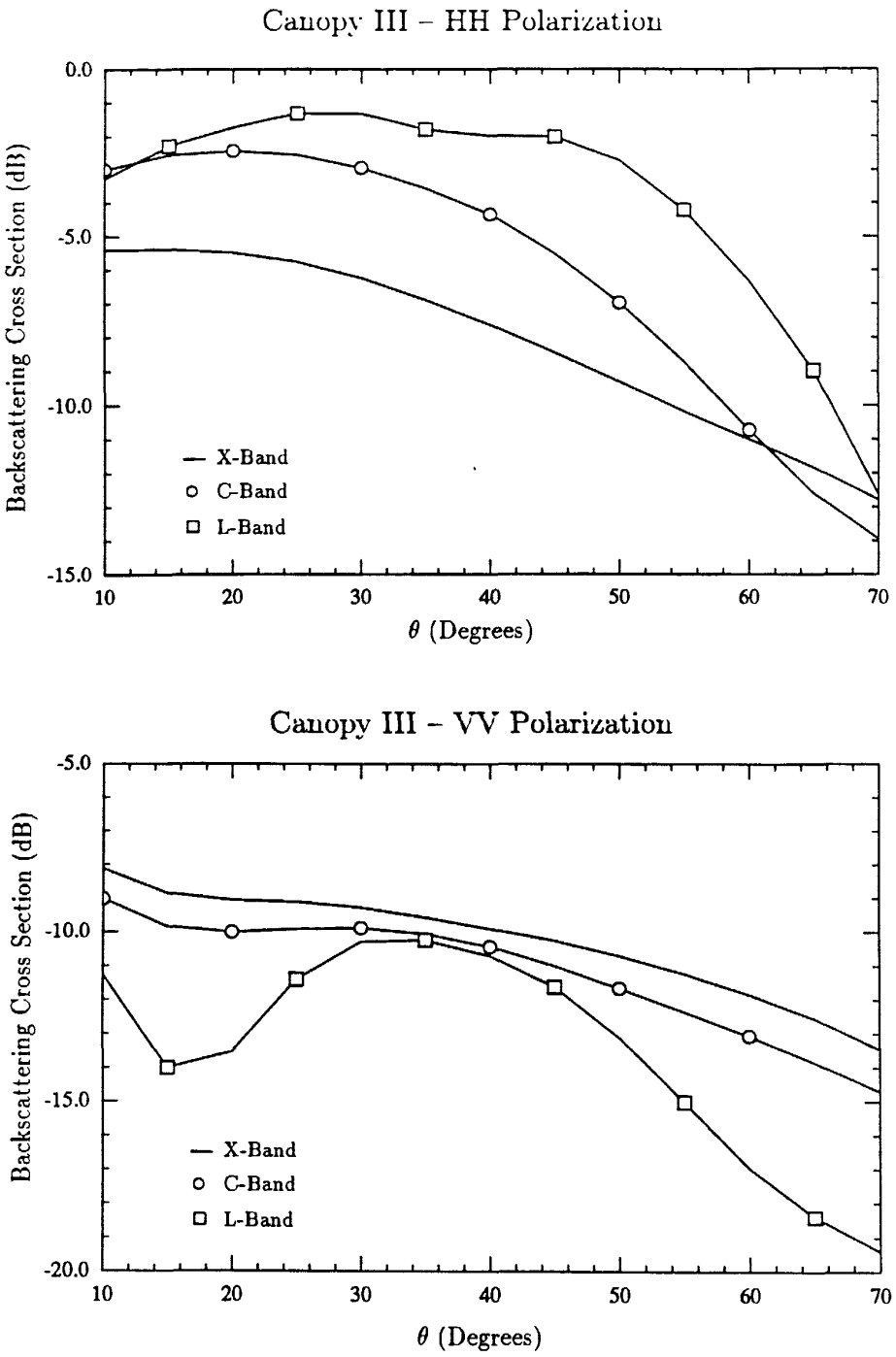


Figure 25: Total Like-Polarized Canopy Backscatter vs. Incidence Angle.

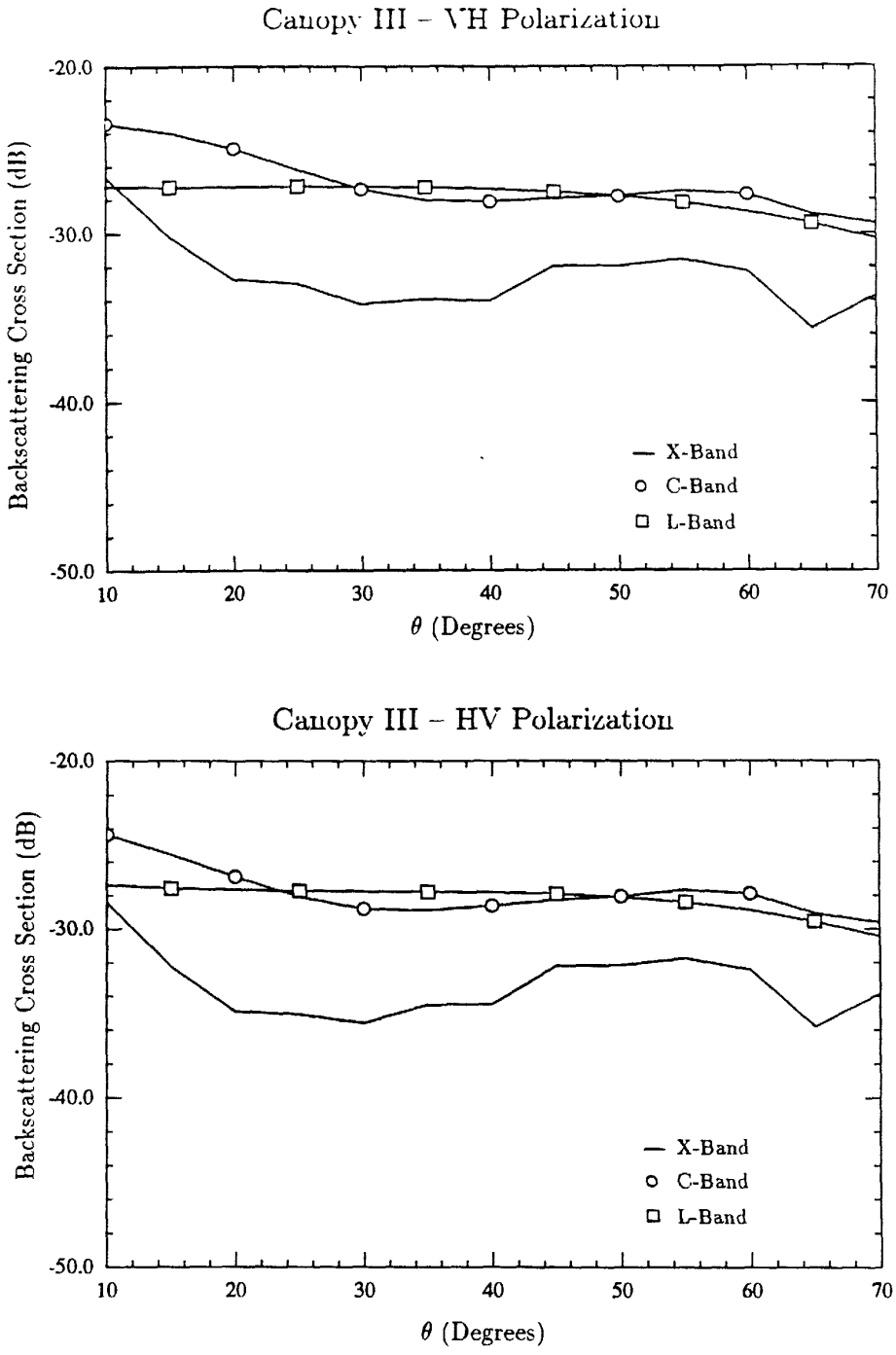


Figure 26: Total Cross-Polarized Canopy Backscatter vs. Incidence Angle.

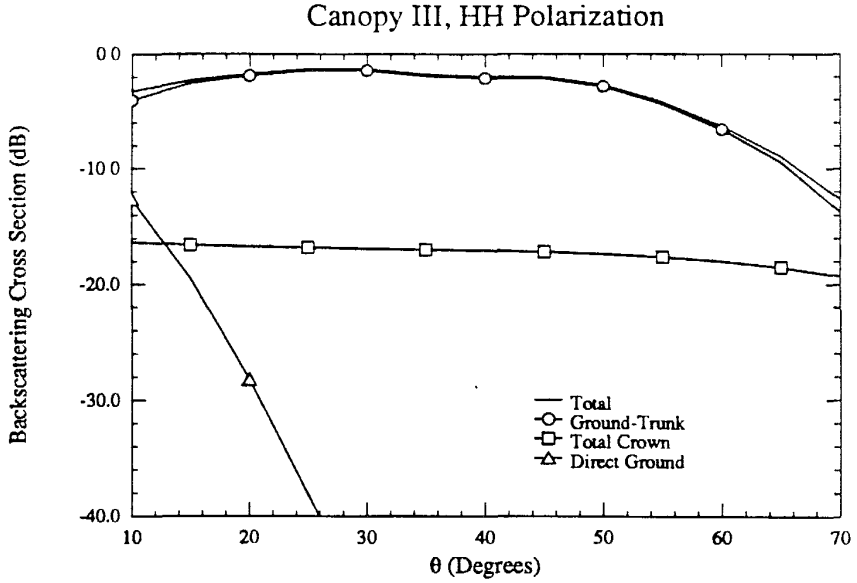


Figure 27: L-Band Backscatter Components vs. Incidence Angle.

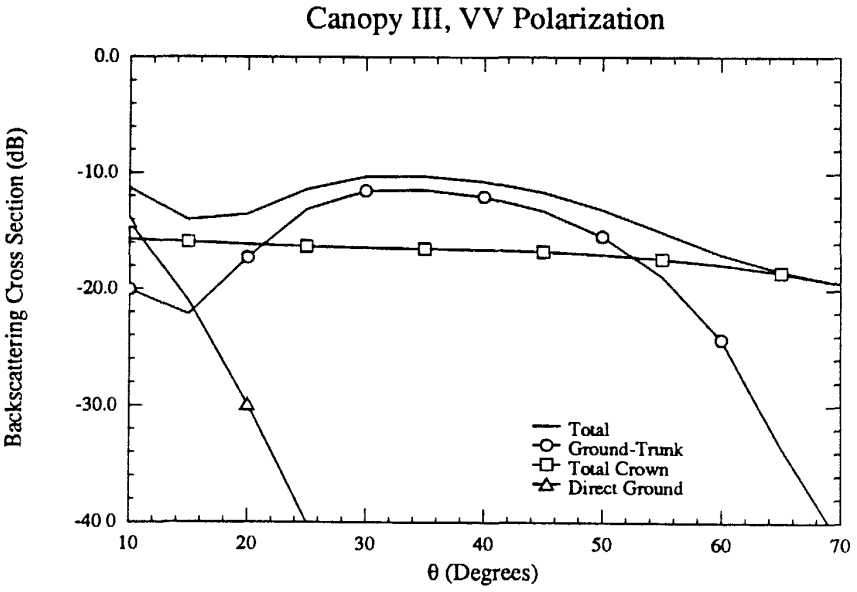


Figure 28: L-Band Backscatter Components vs Incidence Angle

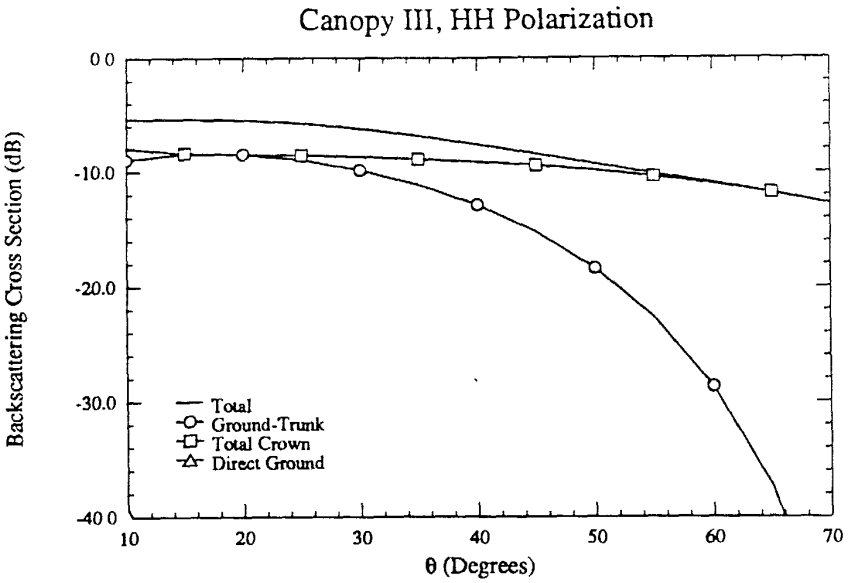


Figure 29: X-Band Backscatter Components vs. Incidence Angle.

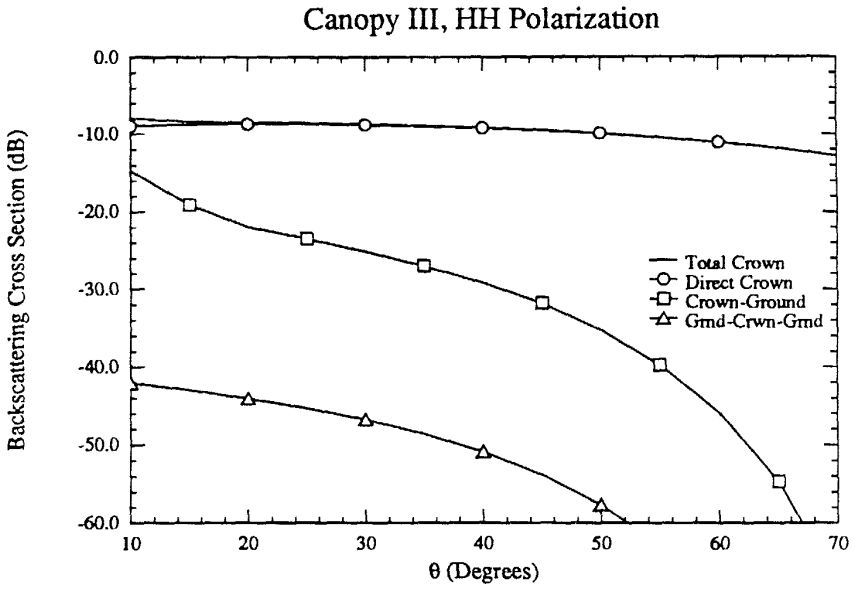


Figure 30. X-Band Backscatter Components vs. Incidence Angle

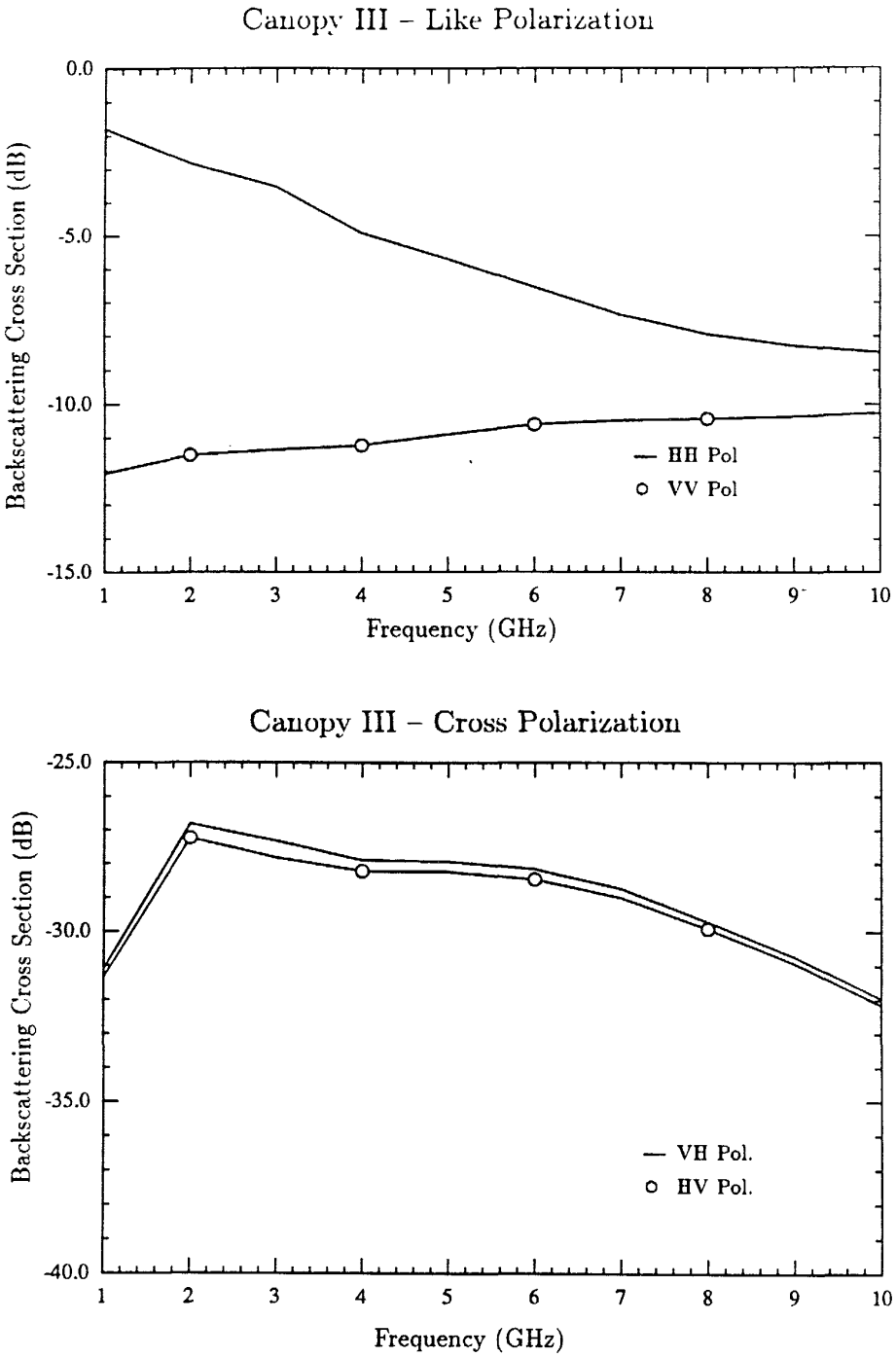


Figure 31: Total Canopy Backscatter vs. Frequency. Incidence Angle = 30°

3.4 Canopy IV — Crown Layer with Needles and Branches

This section presents the results of an analysis performed on a white spruce stand. Here, the crown layer consists of needles and branches. The needles are considered to be randomly oriented, 1.7cm long and 0.1 cm in diameter. For an 11 meter thick crown layer with 85,000 needles per cubic meter, this corresponds to a single-sided LAI of 11.9.

The branches are 2 meters long and 2 cm in diameter with a uniform distribution in ϕ_c and a PDF in θ_c described by

$$p(\theta_c) = \begin{cases} \frac{\sin^2(\theta_c)}{\int_0^\pi \sin^2(\theta_c')d\theta_c'} & 0 \leq \theta_c \leq \pi \\ 0 & \text{otherwise.} \end{cases} \tag{8}$$

This gives an average $\theta_c = 90°$. Figure 32 shows a graph of this PDF. These parameters were determined from an analysis of data presented by Yarie and Van Cleve (1983).

Figure 33 shows the crown transmissivity as a function of incidence angle for both horizontal and vertical polarizations. Figure 34 shows the transmissivity as a function of leaf density. Given the previously stated needle parameters, a density of 25,000 needles/m^3 corresponds to a single-sided LAI of 3.5 and a density of 100,000 needles/m^3 corresponds to a single-sided LAI of 14. Figure 35 shows the transmissivity as a function of frequency. The small values of transmissivity found here are a direct result of the high density of needles used to model the canopy in the 11 meter thick crown layer.

Figures 36 and 37 show the total canopy backscatter as a function of incidence angle for L-, C- and X-bands. Figure 36 shows the two like-polarized configurations

and Figure 37 shows the two cross-polarized configurations. The HH and VV cases are very similar in character as are the VH and HV cases. The small jumps in X- and C-bands are caused by the discretization of the phase matrix integration for the needles and branches. Otherwise, these data would be smoothly varying with θ.

Figures 38 through 41 illustrate the individual contributions to the total canopy backscatter as a function of incidence angle. Figures 38 and 39 show backscatter at L-band for HH and VV polarizations. Figure 40 shows backscatter at X-band for HH polarization. Figure 41 illustrates the three mechanisms that contribute to the total crown backscatter. In all cases, the total backscatter is dominated by the direct crown backscatter component. This is to be expected given the low crown transmissivity.

Figure 42 shows the total canopy backscatter as a function of frequency for the like and cross polarized cases. It is interesting to note the large dip in the cross-polarized backscatter in the neighborhood of C-band.

Additional plots showing the individual scattering components for each of the cases of Figures 36, 37 and 42 are included in Appendix H.

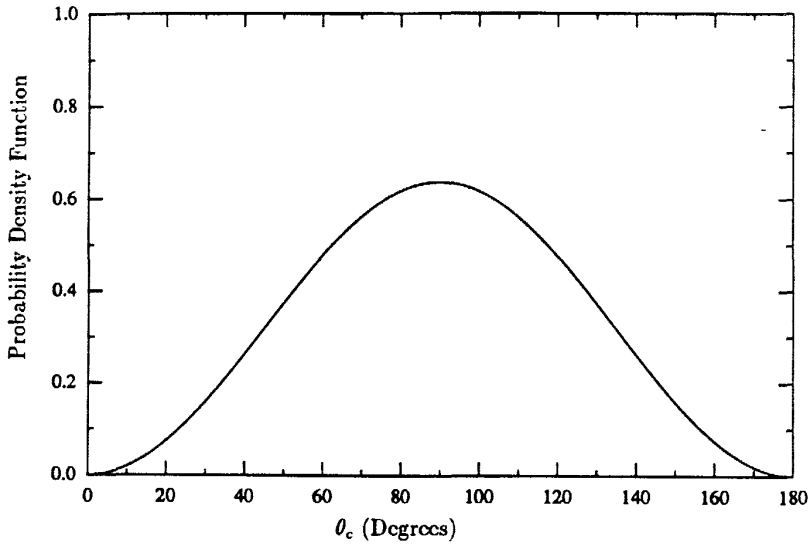


Figure 32: White Spruce Canopy Branch Angle Distribution.

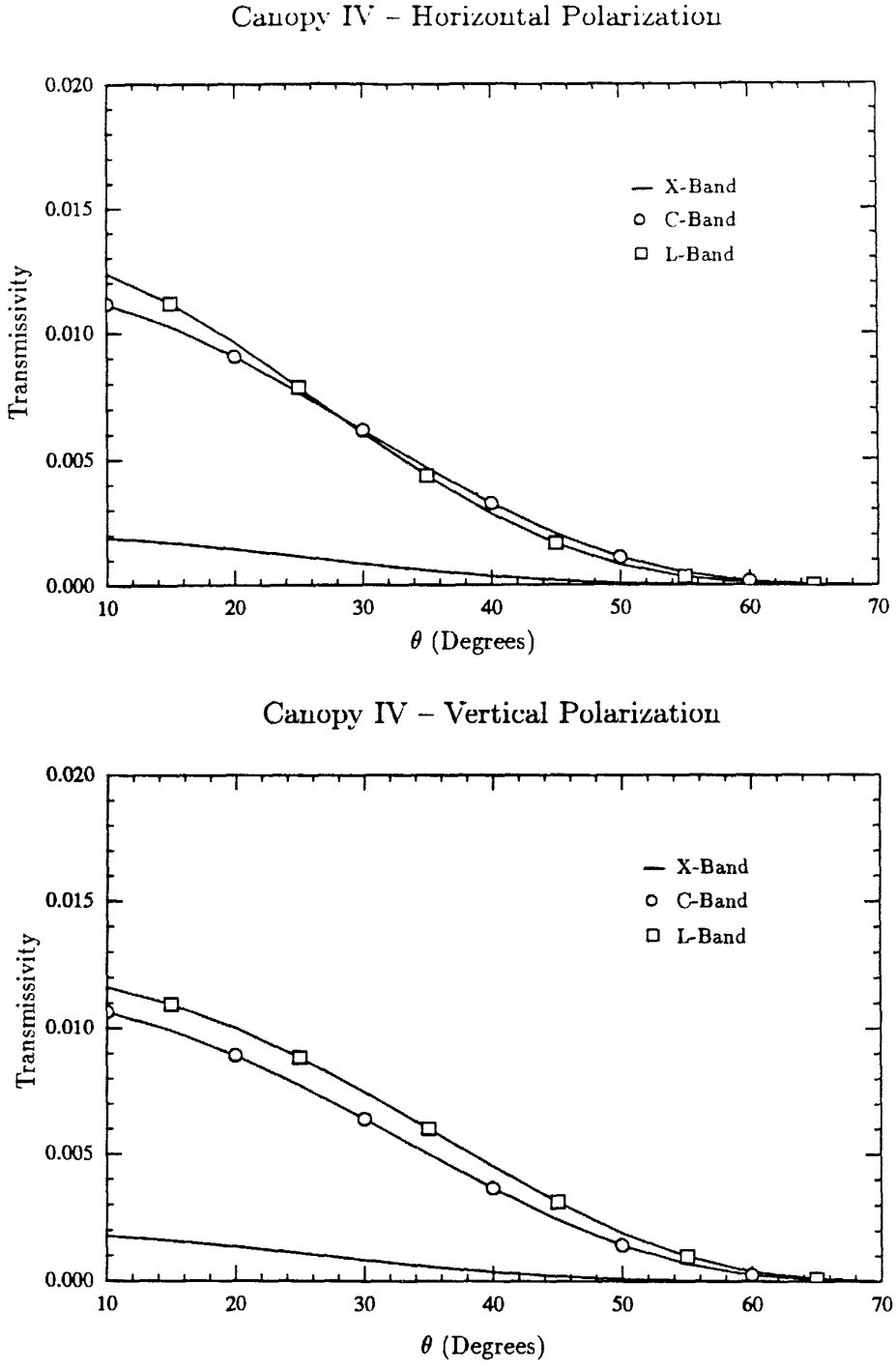


Figure 33: Crown Transmissivity vs Incidence Angle. Needle Density = 85,000 needles per cubic meter.

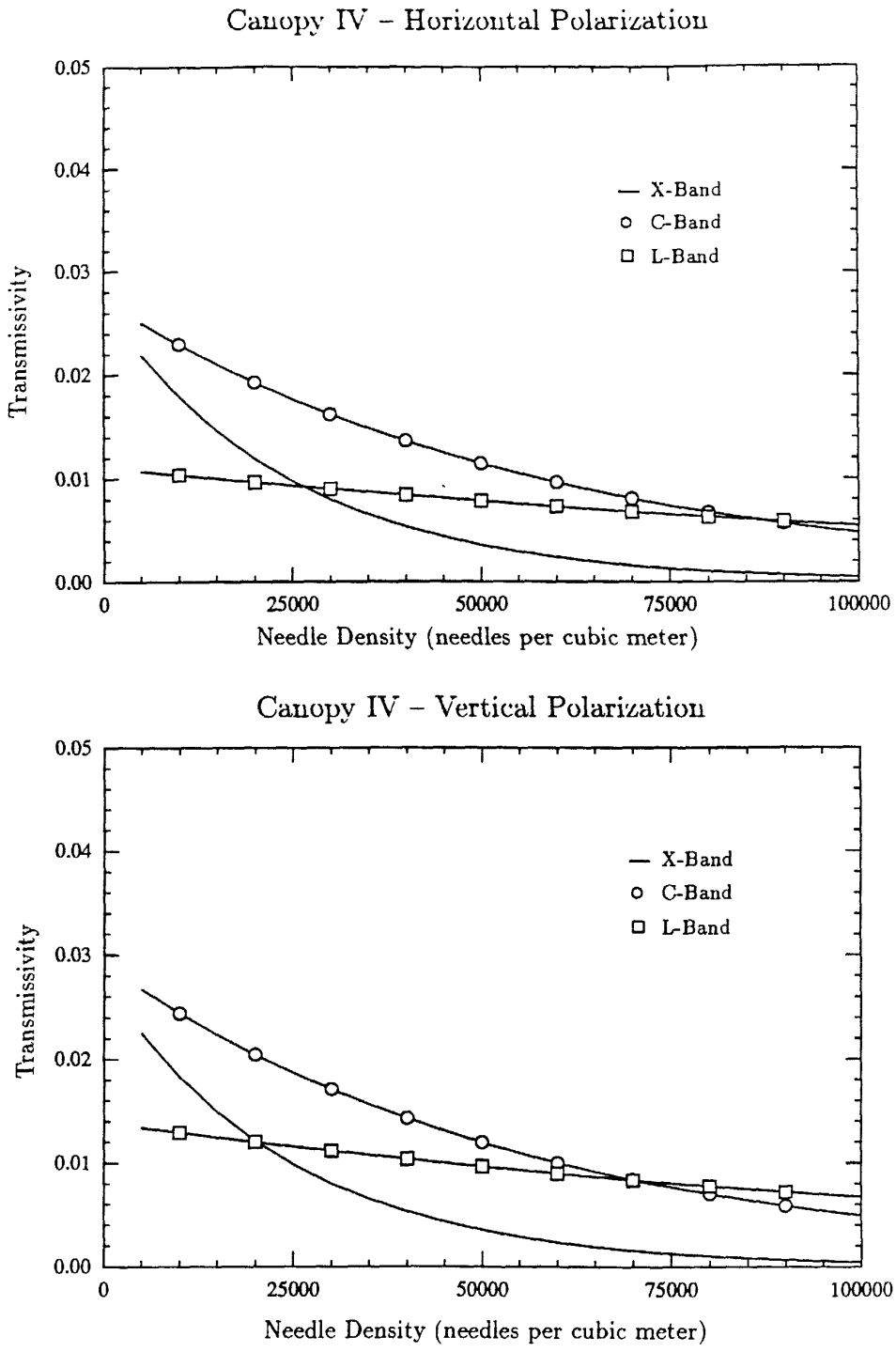


Figure 34: Crown Transmissivity vs. Needle Density. Incidence Angle = 30°.

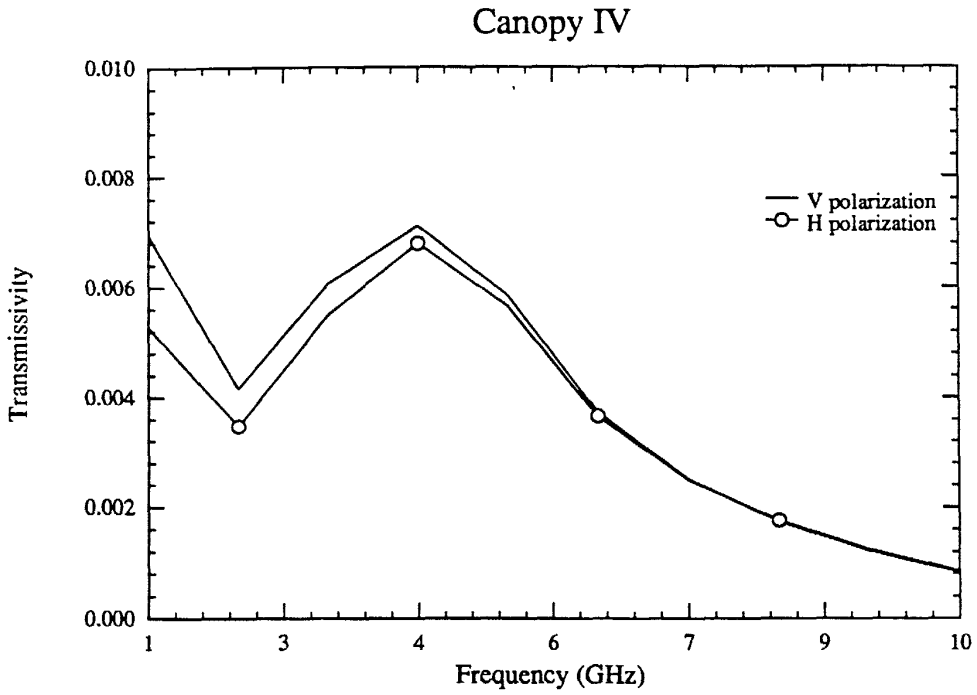


Figure 35: Crown Transmissivity vs. Frequency. Incidence Angle = 30°. Needle Density = 85,000 needles per cubic meter.

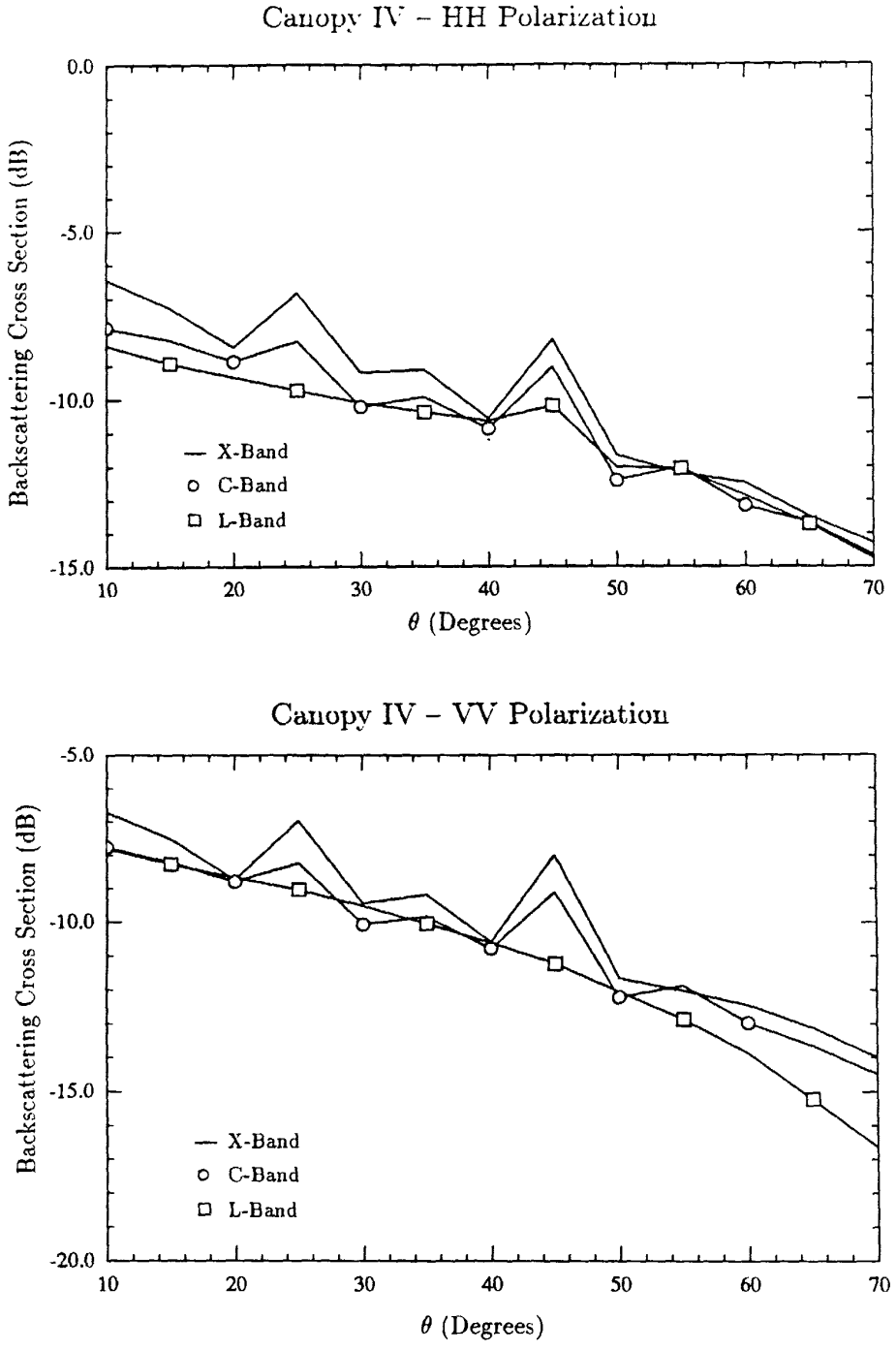


Figure 36. Total Like-Polarized Canopy Backscatter vs. Incidence Angle.

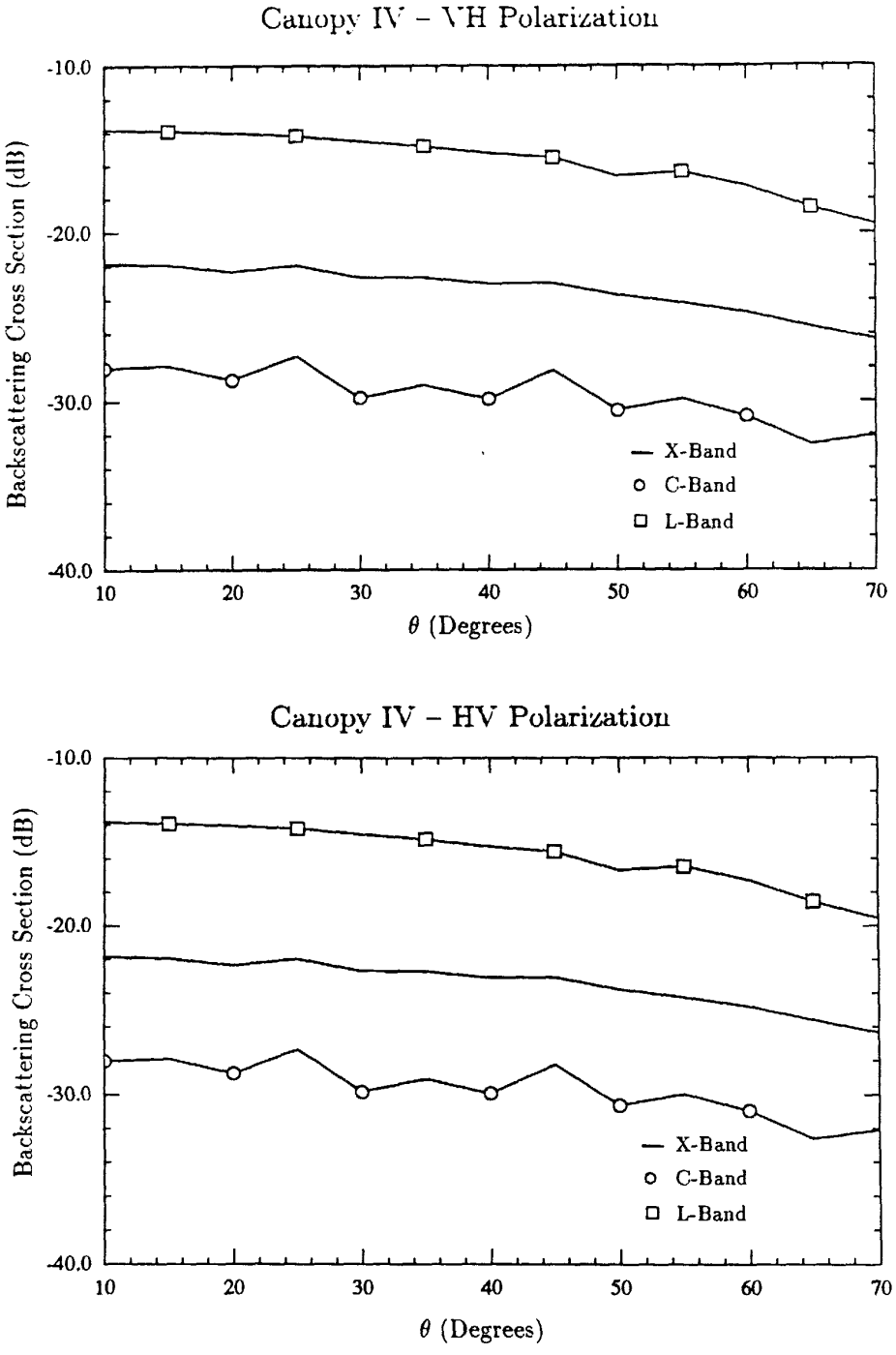


Figure 37: Total Cross-Polarized Canopy Backscatter vs. Incidence Angle.

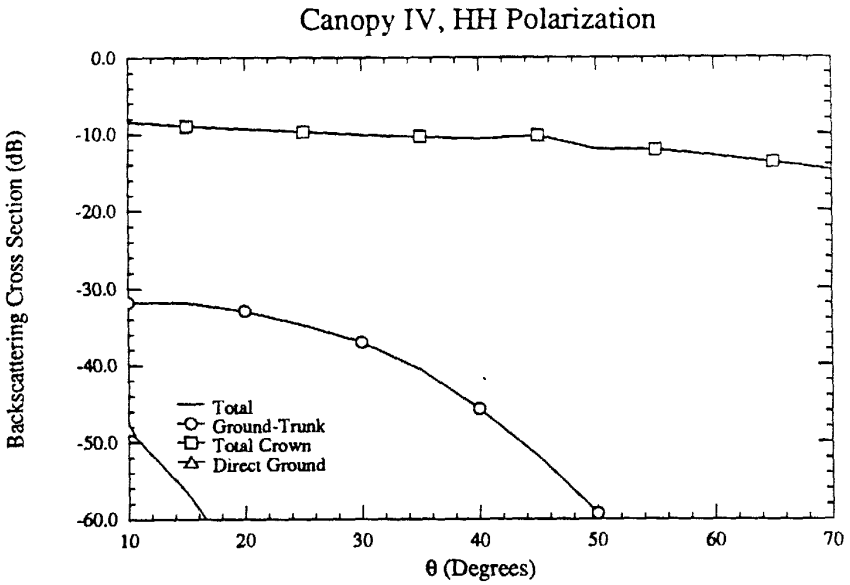


Figure 38: L-Band Backscatter Components vs. Incidence Angle.

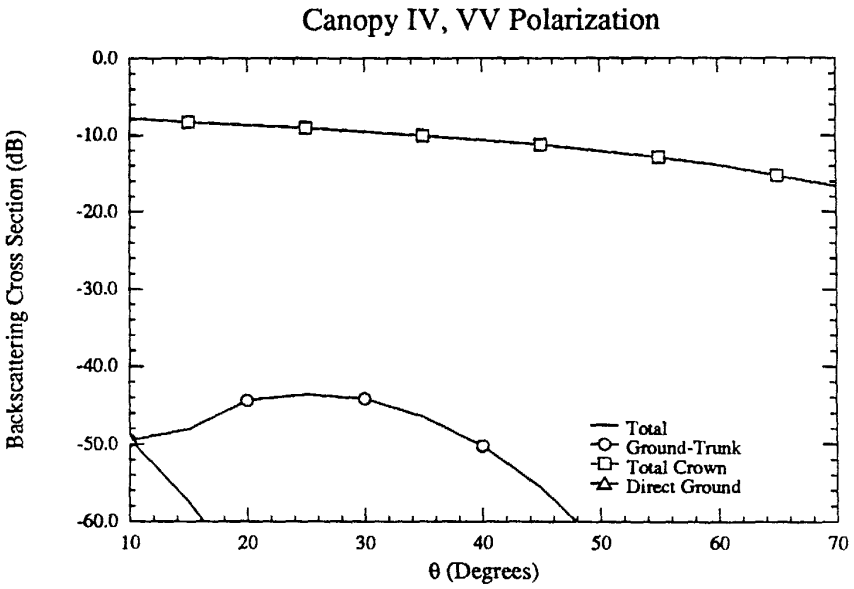


Figure 39: L-Band Backscatter Components vs. Incidence Angle

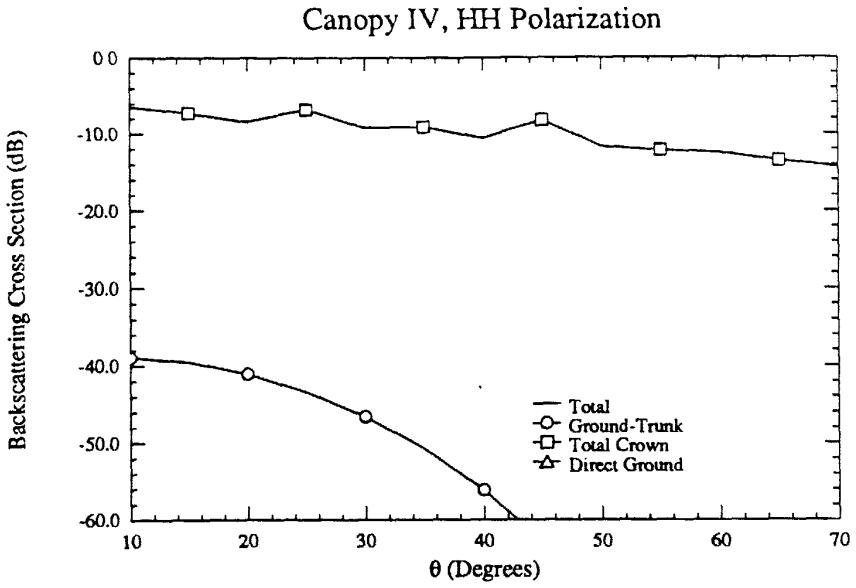


Figure 40: X-Band Backscatter Components vs. Incidence Angle.

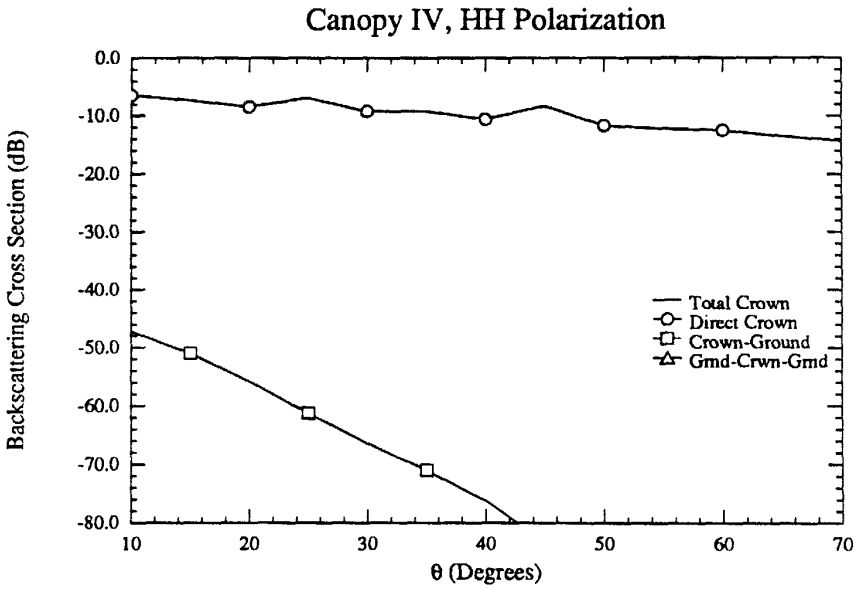


Figure 41: X-Band Backscatter Components vs. Incidence Angle.

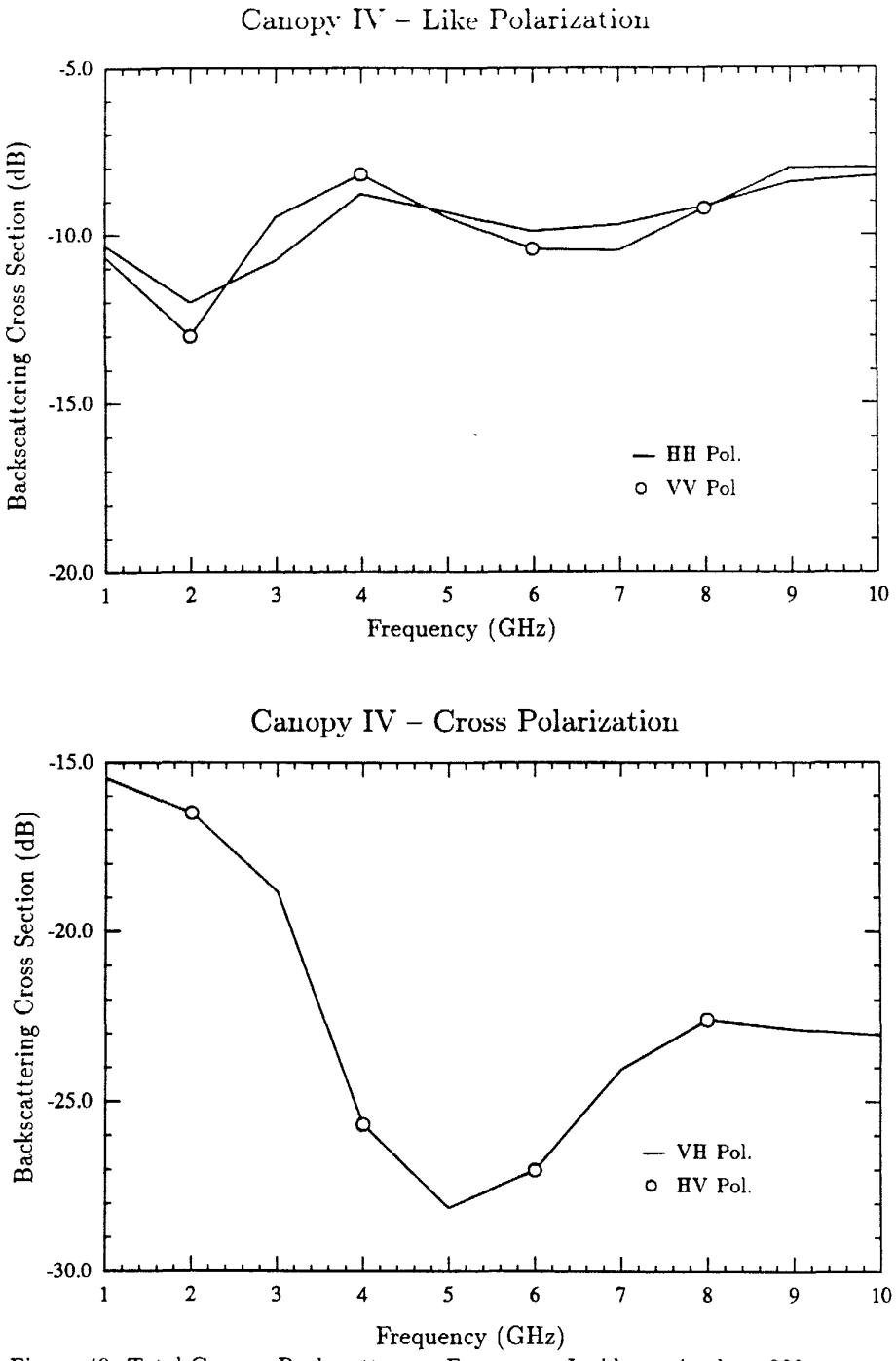


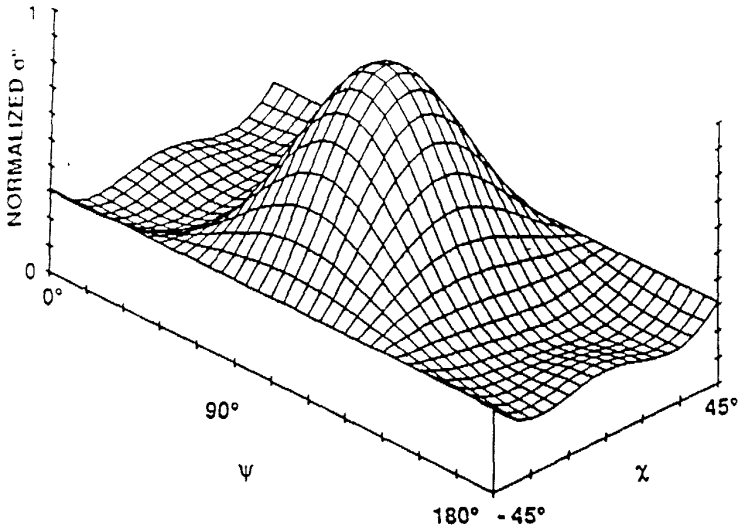
Figure 42: Total Canopy Backscatter vs. Frequency. Incidence Angle = 30°

3.5 Polarimetric Wave Synthesis

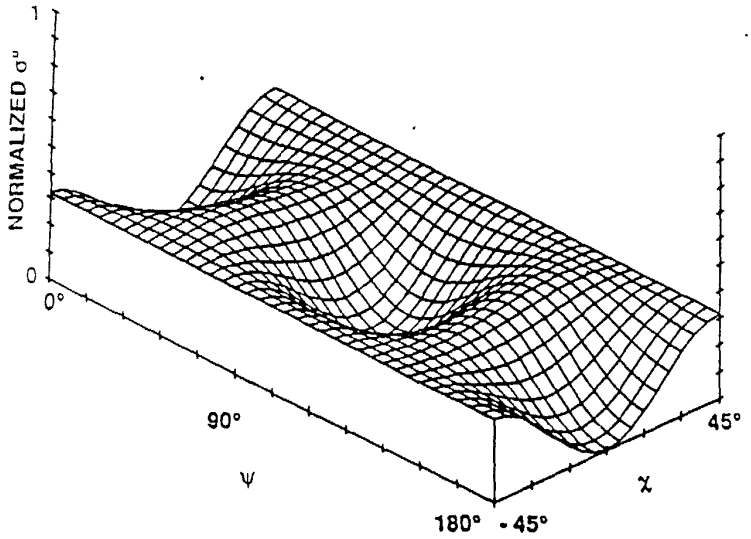
This section presents an example of a polarimetric response synthesis. The backscattering coefficient for any transmit/receive polarization combination can be computed from the total backscattering transformation matrix of the forest canopy using the wave synthesis technique described in Appendix G. The results are presented for a given canopy configuration in the form of a pair of three-dimensional plots called the polarimetric response (or polarization signature) as introduced by van Zyl, et al. (1987) and Zebker, et al. (1987). The like-polarized (cross-polarized) response plots the normalized backscattering coefficient as a function of $\psi = \psi_t = \psi_r$ and $\chi = \chi_t = \chi_r$ ($\psi = \psi_t = 90\,\text{deg} + \psi_r$ and $\chi = \chi_t = -\chi_r$) where the normalization factor is chosen to be the maximum like-polarized backscattering coefficient.

The C-band polarimetric response for the canopy III configuration (leaves and branches) at an incidence angle of $\theta_0 = 40\,\text{deg}$ is given in Figure 43. Since we have chosen the orientation angle ψ with respect to vertical polarization, the polarimetric responses are shifted in ψ by 90 deg with respect to those produced by van Zyl and Zebker. For example, VV polarization now corresponds to $\psi = 0\,\text{deg}$ and $\chi = 0\,\text{deg}$ and HH polarization corresponds to $\psi = 90\,\text{deg}$ and $\chi = 0\,\text{deg}$. A complete set of polarimetric responses for the four canopy types with $\theta_0 = 40\,\text{deg}$ and frequencies at L, C, and X-band are given in Appendix H.

Canopy III



Like Polarized Response.



Cross Polarized Response.

Figure 43: C-Band Polarization Response. Incidence Angle = 40°

References

Attema, E. P. W. and F. T. Ulaby, "Vegetation Modeled as a Water Cloud," *Radio Science*, Vol. 13, No. 2, March–April, 1978, pp. 357–364.

Dobson, M. C. and F. T. Ulaby, "Preliminary Evaluation of the SIR-B Response to Soil Moisture, Surface Roughness, and Crop Canopy Cover," *IEEE Transactions on Geoscience and Remote Sensing*, Vol. GE-24, No. 4, 1986, pp. 517-526.

Eom, H. J. and A. K. Fung, "A Scatter Model for Vegetation up to KU-Band," *Remote Sensing of Environment*, Vol. 15, 1984, pp. 185-200.

Fung, A. K. and F. T. Ulaby, "A Scatter Model for Leafy Vegetation," *IEEE Transactions on Geoscience and Remote Sensing*, Vol. GE-16, No. 4, October 1978, pp. 281–286.

Hallikainen, M. T., F. T. Ulaby, M. C. Dobson, M. A. El-Rayes, and L.-K. Wu, "Microwave Dielectric Behavior of Wet Soil—Part I: Empirical Models and Experimental Observations," *IEEE Transactions on Geoscience and Remote Sensing*, Vol. GE-23, No. 1, 1985, pp. 25–34.

Karam, M. A. and A. K. Fung, "Electromagnetic Scattering from a Layer of Finite Length, Randomly Oriented, Dielectric, Circular Cylinders Over a Rough Interface with Application to Vegetation," *International Journal of Remote Sensing*, Vol. 9, No. 6, June 1988, pp. 1109–1134.

Lang, R. H. and J. S. Sidhu, "Electromagnetic Backscattering From a Layer of Vegetation: A Discrete Approach," *IEEE Transactions on Geoscience and Remote Sensing*, Vol. GE-21, No. 1, January 1983, pp. 62–71.

Lee, J. K. and J. A. Kong, "Active Microwave Remote Sensing of an Anisotropic Random Medium Layer," *IEEE Transactions on Geoscience and Remote Sensing*, Vol. GE-23, 1985, pp. 910–923.

Nelson, N. D., T. Burk, and J. G. Isebrands, "Crown Architecture of Short-Rotation, Intensively Cultured *Populus*. I. Effects of Clone and Spacing on First-Order Branch Characteristics," *Canadian Journal of Forest Research*, Vol. 11, No. 1, 1981, pp. 73–81

Pitts, D. E.*, G. D. Badhwar* and E. Reyna**, "Progress Report on Estimation of Biophysical Properties of Forest Canopies Using Optical And Microwave Data," * NASA Johnson Space Center, Houston TX, ** Lockheed EMSCO, Houston TX, July 15, 1985.

Richards, J. A., G.-Q. Sun, and D. S. Simonett, "L-Band Radar Backscatter Modeling of Forest Stands," *IEEE Transactions on Geoscience and Remote Sensing*, Vol. GE-25, No. 4, July 1987, pp. 487–498.

Ruck, G. T., D. E. Barrick, W. D. Stuart, and C. K. Krichbaum, Radar Cross Section Handbook, Vol. 1, New York, NY: Plenum Press, 1970.

Sarabandi, K., T. B. A. Senior, and F. T. Ulaby, "Effect of Curvature on the Backscattering from Leaves," accepted for publication in *Journal of Electromagnetic Waves and Applications*, July, 1987.

Senior, T. B. A., K. Sarabandi, and F. T. Ulaby, "Measuring and Modeling the Backscattering Cross Section of a Leaf," *Radio Science*, Vol. 22, No. 6, November, 1987, pp. 1109-1116.

Tsang, L. and J. Kong, "Application of Strong Fluctuation Random Medium Theory to Scattering From Vegetation-Like Half Space," *IEEE Transactions on Geoscience and Remote Sensing*, Vol. 19, No. 1, pp. 62–69, 1981.

Tsang, L., J. A. Kong, and R. T. Shin, Theory of Microwave Remote Sensing, New York, NY: John Wiley and Sons, Wiley-Interscience, 1985.

Ulaby, F. T., R. K. Moore, and A. K. Fung, Microwave Remote Sensing: Active and Passive, Vol. II — Radar Remote Sensing, Reading, MA: Addison Wesley, 1982.

Ulaby, F. T., R. K. Moore, and A. K. Fung, Microwave Remote Sensing: Active and Passive, Vol. III—Volume Scattering and Emission Theory, Ad-Advanced Systems and Applications, Dedham, MA: Artech House, Inc., 1986, 1100 pages.

Ulaby, F. T., D. Held, M. C. Dobson, K. McDonald, and T. B. A. Senior, "Relating Polarization Phase Difference of SAR Signals to Scene Properties," *IEEE Transactions on Geoscience and Remote Sensing*, Vol. GE-25, No. 1, 1987, pp. 83–92.

Ulaby, F. T. and M. A. El-Rayes, "Microwave Dielectric Spectrum of Vegetation, Part II:

Dual-Dispersion Model," *IEEE Transactions on Geoscience and Remote Sensing*, Vol. GE-25, 1987, pp. 550–557.

Van de Hulst, H. C., Light Scattering by Small Particles, New York, NY: John Wiley, 1957.

van Zyl, J. J., H. A. Zebker, and C. Elachi, "Imaging Radar Polarization Signatures: Theory and Observations," *Radio Science*, Vol. 22, No. 4, July—August 1987, pp. 529–543.

Yarie, J. and K. Van Cleve. "Biomass and Productivity of White Spruce Stands in Interior Alaska," *Canadian Journal of Forest Research*, Vol. 13. No. 5, 1983, pp. 767–772.

Zebker, H. A., J. J. van Zyl, and D. N. Held, "Imaging Radar Polarimetry from Wave Synthesis," *J. Geophys. Res.*, Vol. 92, No. 81, January 1987, pp. 683–701.

APPENDIX A FIRST-ORDER BACKSCATTERING FROM A FOREST CANOPY OVER A SPECULAR GROUND SURFACE

We seek an expression for the intensity $\mathbf{I}_c^s$ scattered from a forest canopy over a specular ground surface in the form of a first-order solution of the radiative transfer equation. The forest canopy is modeled as two horizontal layers (Fig. A.1), a crown layer of height d above a trunk layer of height H_t. The crown layer, comprised of leaves and branches, is assumed to be continuous in the horizontal direction and statistically homogeneous over the crown volume. The trunk layer is assumed to consist of vertical, homogeneous, dielectric cylinders with smooth outer surfaces. The air-crown interface and the crown-trunk interface are treated as diffuse boundaries, and the interface between the trunk layer and the ground layer is considered a specular surface.

A.1 Basic Definitions

The geometry of the problem is depicted in Fig. A.2. The boundaries at $z = 0$ and $z = -d$ are assumed to be diffuse, and the bottom boundary at $z = -d' = -(d + H_t)$ is treated as a specular surface with a dielectric constant ϵ_g.

The vector radiative transfer problem is formulated in terms of the vector specific intensity $\mathbf{I}$ (Ulaby et al, 1986, pp. 1085-1092). For an elliptically polarized monochromatic plane wave given by

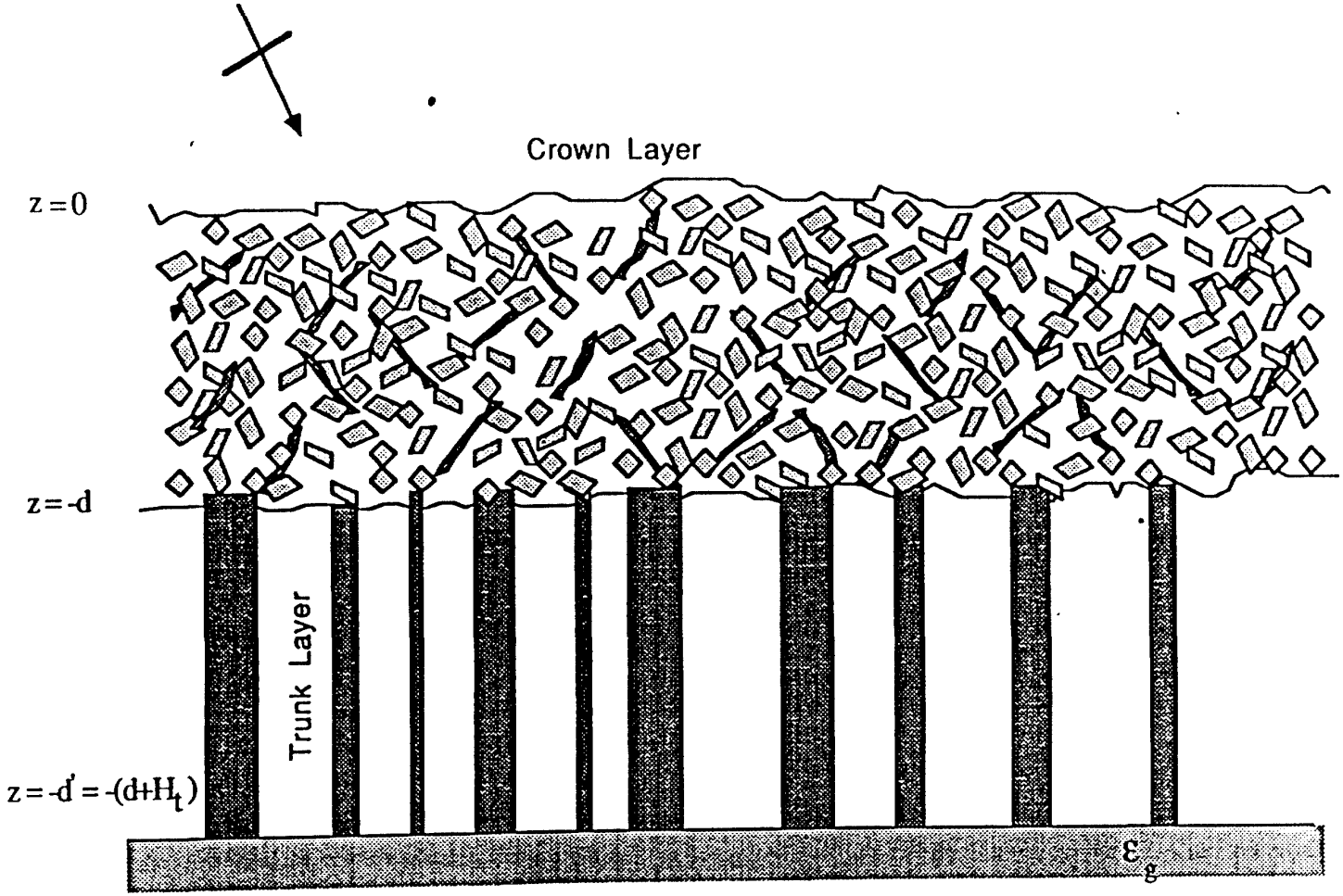


Figure A.1: Forest Canopy Model.

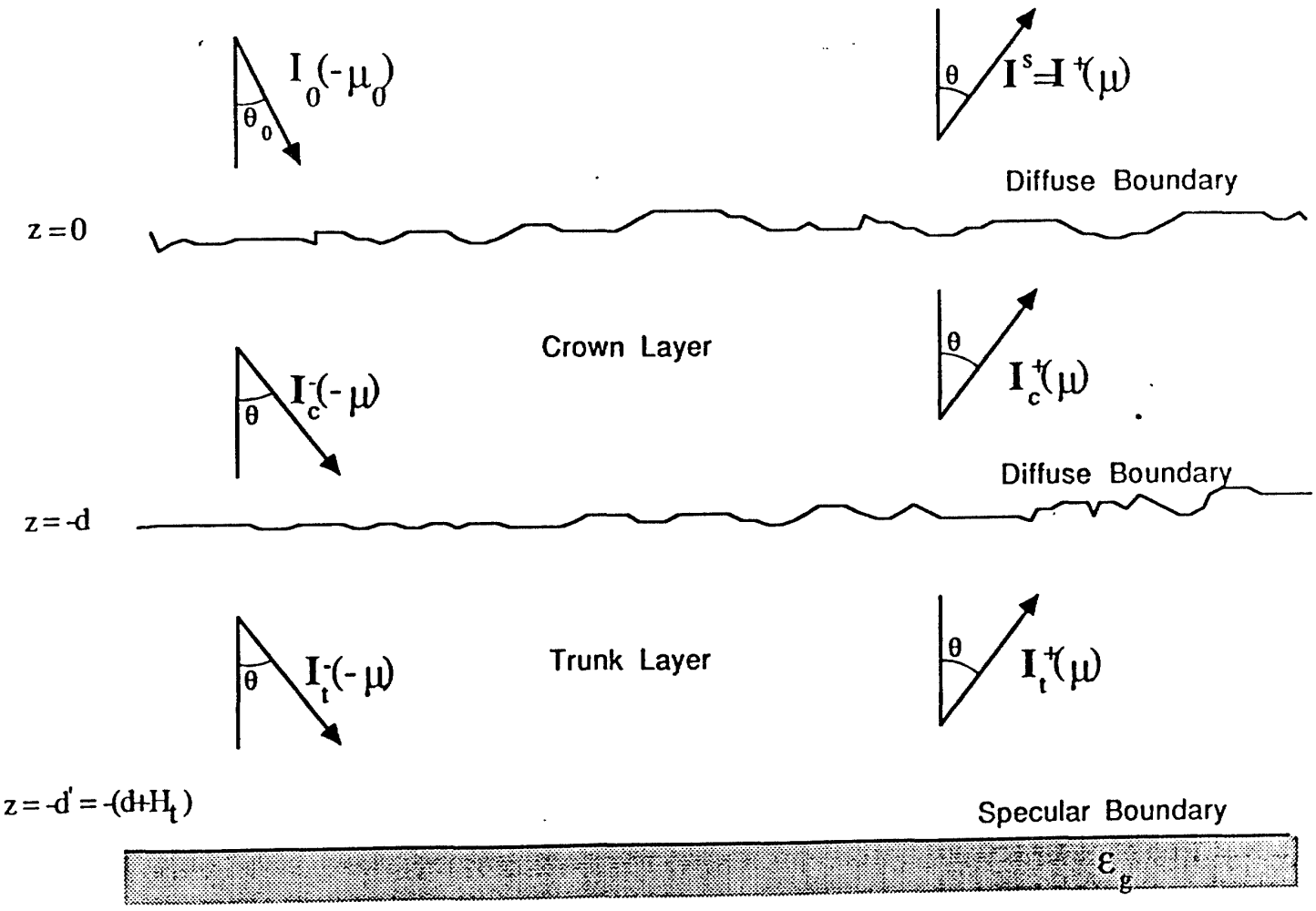


Figure A.2: Problem Geometry.

$$\mathbf{E} = (E_v\hat{\mathrm{v}} + E_h\hat{\mathrm{h}})\epsilon^{ikr}. \tag{A.1}$$

with unit vertical and horizontal polarization vectors $\hat{\mathrm{v}}$ and $\hat{\mathrm{h}}$. $\mathbf{I}$ is defined through the modified Stokes parameters I_v, I_h, U, and V as follows:

$$\mathbf{I} = \begin{bmatrix} I_v \\ I_h \\ U \\ V \end{bmatrix} = \frac{1}{\eta} \begin{bmatrix} |\, E_v \,|^2 \\ |\, E_h \,|^2 \\ 2Re(E_v E_h^*) \\ 2Im(E_v E_h^*) \end{bmatrix}. \tag{A.2}$$

The standard approach used for defining the bistatic scattering coefficient of a distributed target of area A is to compute the field scattered by the target in the direction of interest as a result of illumination by a plane wave. Thus, the incident illumination is a plane wave, whereas the scattered field is a spherical wave. For a spherical wave, the vector specific intensity also is defined in terms of Stokes parameters, but the definition includes normalization by the solid angle $A\cos\theta_s/r^2$, where r is the distance between the distributed target and the observation point and θ_s is the angle between the outward normal to A and the vector defining the direction from the target to the observation point. Hence, the scattered intensity from a random medium is defined as:

$$\mathbf{I^s} = \begin{bmatrix} I_v^s \\ I_h^s \\ U^s \\ V^s \end{bmatrix} = \frac{r^2}{\eta A\cos\theta_s} \begin{bmatrix} \langle |\, E_v^s \,|^2 \rangle \\ \langle |\, E_h^s \,|^2 \rangle \\ 2Re(\langle E_v^s E_h^{s*} \rangle) \\ 2Im(\langle E_v^s E_h^{s*} \rangle) \end{bmatrix} \tag{A.3}$$

where $\langle \quad \rangle$ denotes ensemble average.

The bistatic scattering coefficient $\sigma^{\circ}_{\alpha\beta}$ corresponding to a β-polarized incident plane wave giving rise to α-polarized spherical wave is defined as:

$$\sigma^{\circ}_{\alpha\beta} = \frac{4\pi r^2}{A} \cdot \frac{\langle \mid E^s_\alpha \mid^2 \rangle}{\mid E^i_\beta \mid^2}, \tag{A.4}$$

where $\alpha, \beta = v$ or h polarization. Using (A.1) for $\mid E^i_\beta \mid^2$ and (A.3) for $\langle \mid E^s_\alpha \mid^2 \rangle$, (A.4) can be written as:

$$\sigma^{\circ}_{\alpha\beta}(\pi - \theta_0, \phi_0; \theta, \phi) = \frac{4\pi \cos\theta I^s_\alpha(\theta, \phi)}{I^i_\beta(\pi - \theta_0, \phi_0)} \tag{A.5}$$

where $(\pi - \theta_0, \phi_0)$ denotes the direction of the downward-going incident intensity and (θ, ϕ) denotes the direction of the upward-going scattered intensity.

In the next section we shall consider an intensity

$$\mathbf{I}^i = \mathbf{I_0}\delta(\cos\theta - \cos\theta_0)\delta(\phi - \phi_0) \tag{A.6}$$

incident upon the upper boundary in the direction $(\pi - \theta_0, \phi_0)$ and use the radiative transfer method to derive an expression for the upward-going specific intensity $\mathbf{I}^s(\theta, \phi)$. Then, in section A.3 we shall set $\theta = \theta_0$ and $\phi = \pi + \phi_0$, corresponding to scattering in the backward direction, in order to compute the backscattering coefficient

$$\sigma^{\circ}_{\alpha\beta}(\theta_0) = \frac{4\pi \cos\theta_0 I^s_\alpha(\theta_0, \pi + \phi_0)}{I^i_\beta(\pi - \theta_0, \phi_0)} \tag{A.7}$$

of an azimuthally symmetric canopy.

A.2 Radiative Transfer Equations

When formulating the radiative transfer problem for bounded media, the standard practice is to split the intensity vector into upward-going ($\mathbf{I}^+(\theta,\phi,z)$) and downward-going ($\mathbf{I}^-(\theta,\phi,z)$) components, noting that θ varies between 0 and $\pi/2$ (Ulaby et al., 1986, pp.1090-1092). In the crown layer , the intensity ($\mathbf{I}_c^+(\theta,\phi,z)$) travelling in the upward direction (θ,ϕ) and the intensity ($\mathbf{I}_c^-(\pi-\theta,\phi,z)$) travelling in the downward direction $(\pi-\theta,\phi)$ must satisfy the coupled radiative transfer equations

$$\frac{d}{dz}\mathbf{I}_c^+(\mu,\phi,z) = -\frac{\boldsymbol{\kappa}_c^+}{\mu}\mathbf{I}_c^+(\mu,\phi,z) + \mathbf{F}_c^+(\mu,\phi,z), \qquad -d \le z \le 0 \tag{A.8}$$

$$-\frac{d}{dz}\mathbf{I}_c^-(-\mu,\phi,z) = -\frac{\boldsymbol{\kappa}_c^-}{\mu}\mathbf{I}_c^-(-\mu,\phi,z) + \mathbf{F}_c^-(-\mu,\phi,z), \qquad -d \le z \le 0 \tag{A.9}$$

where $\boldsymbol{\kappa}_c^{\pm}$ is the extinction matrix of the crown layer, $\mu = \cos\theta$, and $-\mu = \cos(\pi-\theta)$. The source functions $\mathbf{F}_c^+(\mu,\phi,z)$ and $\mathbf{F}_c^-(-\mu,\phi,z)$ account for directing the energy incident upon an elemental volume from all directions into the direction (θ,ϕ) and $(\pi-\theta,\phi)$,respectively and are given by

$$\begin{aligned}\mathbf{F}_c^+(\mu,\phi,z) &= \frac{1}{\mu}\Big[\int_0^{2\pi}\int_0^1 \mathbf{P}_c(\mu,\phi;\mu',\phi')\mathbf{I}_c^+(\mu',\phi',z)d\Omega' \\ &\quad + \int_0^{2\pi}\int_0^1 \mathbf{P}_c(\mu,\phi;-\mu',\phi')\mathbf{I}_c^-(-\mu',\phi',z)d\Omega'\Big]\end{aligned} \tag{A.10}$$

$$\begin{aligned}\mathbf{F}_c^-(-\mu,\phi,z) &= \frac{1}{\mu}\Big[\int_0^{2\pi}\int_0^1 \mathbf{P}_c(-\mu,\phi;\mu',\phi')\mathbf{I}_c^+(\mu',\phi',z)d\Omega' \\ &\quad + \int_0^{2\pi}\int_0^1 \mathbf{P}_c(-\mu,\phi;-\mu',\phi')\mathbf{I}_c^-(-\mu',\phi',z)d\Omega'\Big]\end{aligned} \tag{A.11}$$

where $d\Omega' = d\mu' d\phi' = \sin\theta' d\theta' d\phi'$, and $\mathbf{P}_c(\mu,\phi;\mu',\phi')$ is the phase matrix of the crown layer relating the intensity incident (upon a unit volume in the medium) in

the direction (θ', ϕ') to the intensity scattered in the direction (θ, ϕ). The phase matrix of the crown layer is defined in Appendix C where it is related to the shapes, sizes, and orientations of the particles in the crown layer. Equations identical with (A.8) to (A.11) may be written for the trunk layer $(-d' \leq z \leq d)$ upon replacing the subscript c with the subscript t.

The phase matrix of the trunk layer is also given in Appendix C and its dependency on θ has the following form

$$\mathbf{P}_t(\theta_s, \phi_s; \theta_i, \phi_i) \sim \frac{\sin[k_0 H_t(\cos\theta_s - \cos\theta_i)/2]}{k_0 H_t(\cos\theta_s - \cos\theta_i)/2} \tag{A.12}$$

For the forest canopy the height of the trunk layer is assumed to be much larger than the wavelength $(H_t \gg \lambda)$. Thus the following approximation can be employed

$$\frac{\sin[k_0 H_t(\cos\theta_s - \cos\theta_i)/2]}{k_0 H_t(\cos\theta_s - \cos\theta_i)/2} \approx \delta_k(\mu_s - \mu_i) \tag{A.13}$$

where δ_k is the Kronecker delta function and is defined by

$$\delta_k(\mu_s - \mu_i) = \begin{cases} 1; & \mu_s = \mu_i \\ 0; & \text{otherwise} \end{cases} \tag{A.14}$$

As a result of this approximation the cylinders in the trunk layer can only generate upward-going (downward-going) intensity when they are illuminated by an upward-going (downward-going) intensity. Therefore the source functions in the trunk layer are given by

$$\mathbf{F}_t^+(\mu, \phi, z) = \frac{1}{\mu}\int_0^{2\pi} \mathbf{P}_t(\mu, \phi; \mu', \phi')[\int_0^1 \mathbf{I}_t^+(\mu', \phi', z)\delta_k(\mu - \mu')d\mu']d\phi' \tag{A.15}$$

$$\mathbf{F}_t^-(-\mu, \phi, z) = \frac{1}{\mu}\int_0^{2\pi} \mathbf{P}_t(-\mu, \phi; -\mu', \phi')[\int_0^1 \mathbf{I}_t^-(-\mu', \phi', z)\delta_k(\mu - \mu')d\mu']d\phi' \tag{A.16}$$

where the quantity in the bracket is the representation of the specific intensity for a two dimensional problem.

The solution to differential equations (A.8) and (A.9) can formally be expressed as

$$\mathbf{I}_c^+(\mu,\phi,z) = e^{-\boldsymbol{\kappa}_c^+(z+d)/\mu}\mathbf{I}_c^+(\mu,\phi,-d) + \int_{-d}^{z} e^{-\boldsymbol{\kappa}_c^+(z-z')/\mu}\mathbf{F}_c^+(\mu,\phi,z')dz' \quad \text{(A.17)}$$

$$\mathbf{I}_c^-(-\mu,\phi,z) = e^{\boldsymbol{\kappa}_c^- z/\mu}\mathbf{I}_c^-(-\mu,\phi,0) + \int_{z}^{0} e^{\boldsymbol{\kappa}_c^-(z-z')/\mu}\mathbf{F}_c^-(-\mu,\phi,z')dz' \quad \text{(A.18)}$$

where

$$\boldsymbol{\kappa}_c^+ = \boldsymbol{\kappa}_c(\theta,\phi), \quad \text{(A.19)}$$

$$\boldsymbol{\kappa}_c^- = \boldsymbol{\kappa}_c(\pi-\theta,\phi), \quad \text{(A.20)}$$

and the following notation has been adopted

$$e^{-\boldsymbol{\kappa}_c z/\mu} = \mathbf{Q}_c(\mu,\phi)\mathbf{D}_c(\mu,\phi;-z/\mu)\mathbf{Q}_c^{-1}(\mu,\phi) \quad \text{(A.21)}$$

where $\mathbf{Q}_c(\mu,\phi)$ is a matrix whose columns are eigenvectors of the extinction matrix $\boldsymbol{\kappa}_c(\mu,\phi)$, and $\mathbf{D}_c(\mu,\phi;-z/\mu)$ is a diagonal matrix whose diagonal elements are of the following form

$$[\mathbf{D}_c(\mu,\phi;-z/\mu)]_{ii} = e^{-\lambda_i(\mu,\phi)z/\mu} \quad \text{(A.22)}$$

with $\lambda_i(\mu,\phi)$ being the i^{th} eigenvalue of $\boldsymbol{\kappa}_c(\mu,\phi)$.

Similarly the vector specific intensities $\mathbf{I}_t^+$ and $\mathbf{I}_t^-$ in the trunk layer are given by

$$\mathbf{I}_t^+(\mu,\phi,z) = e^{-\boldsymbol{\kappa}_t^+(z+d')/\mu}\mathbf{I}_t^+(\mu,\phi,-d') + \int_{-d'}^{z} e^{-\boldsymbol{\kappa}_t^+(z-z')/\mu}\mathbf{F}_t^+(\mu,\phi,z')dz' \quad \text{(A.23)}$$

$$\mathbf{I}_t^-(-\mu,\phi,z) = e^{\boldsymbol{\kappa}_t^-(z+d)/\mu}\mathbf{I}_t^-(-\mu,\phi,-d) + \int_z^{-d} e^{\boldsymbol{\kappa}_t^-(z-z')/\mu}\mathbf{F}_t^-(-\mu,\phi,z')dz' \quad (A.24)$$

where the subscript t denotes that the propagation and scattering processes are taking place in the trunk layer. If we limit our solution to first-order scattering, the first-order contribution of the trunk layer is observable only on the surface of a cone with generating angle θ_0 which includes the backscattering direction.

A.3 First-Order Solution for Bistatic Scattering

Because there is no reflection at the (diffuse) air-crown boundary ($z = 0$) and the crown-trunk boundary ($z = -d$), the following boundary conditions must be satisfied:

$$\mathbf{I}_c^-(-\mu,\phi,0) = \mathbf{I}_0\delta(\mu-\mu_0)\delta(\phi-\phi_0) \quad (A.25)$$

$$\mathbf{I}_c^+(\mu,\phi,-d) = \mathbf{I}_t^+(\mu,\phi,-d) \quad (A.26)$$

$$\mathbf{I}_t^-(-\mu,\phi,-d) = \mathbf{I}_c^-(-\mu,\phi,-d). \quad (A.27)$$

At the bottom boundary ($z = -d'$), the boundary condition is

$$\mathbf{I}_t^+(\mu,\phi,-d') = \mathbf{R}(\mu)\mathbf{I}_t^-(-\mu,\phi,-d'), \quad (A.28)$$

where $\mathbf{R}(\mu)$ is the reflectivity matrix of the specular surface and is given by (Tsang et al., 1985, p. 242; Ulaby et al., 1986, pp. 1183)

$$\mathbf{R}(\mu) = \begin{bmatrix} |R_v|^2 & 0 & 0 & 0 \\ 0 & |R_h|^2 & 0 & 0 \\ 0 & 0 & Re(R_v R_h^*) & -Im(R_v R_h^*) \\ 0 & 0 & Im(R_v R_h^*) & Re(R_v R_h^*) \end{bmatrix} \tag{A.29}$$

where R_v and R_h are the v-polarized and h-polarized Fresnel reflection coefficients of the specular surface at incidence angle θ.

In order to obtain scattering behavior of the layered media, we need to solve for $\mathbf{I}_c^+(\mu, \phi, z)$ and then evaluate it at $z = 0$.

Upon setting $z = -d$ in (A.18), inserting the result in (A.24), and then evaluating the resultant expression at $z = -d'$, the downward-going intensity at the bottom surface can be obtained. Now the upward-going intensity at the bottom surface ($\mathbf{I}_t^+(\mu, \phi, -d')$) can be found by using the boundary condition (A.28). The expression for $\mathbf{I}_t^+(\mu, \phi, -d')$ can be inserted into equation (A.23) and then the latter can be evaluated at $z = -d$ to obtain an expression for $\mathbf{I}_t^+(\mu, \phi, -d)$. Finally by inserting the resultant expression for $\mathbf{I}_t^+(\mu, \phi, -d)$ into equation (A.17), we end up with the expression

$$\begin{aligned} \mathbf{I}_c^+(\mu, \phi, z) \;=\; & e^{-\boldsymbol{\kappa}_c^+(z+d)/\mu}\mathbf{R}'(\mu, \phi) \cdot [e^{-\boldsymbol{\kappa}_c^- d/\mu}\mathbf{I}_c^-(-\mu, \phi, 0) \\ & + \int_{-d}^{0} e^{-\boldsymbol{\kappa}_c^-(d+z')/\mu}\mathbf{F}_c^-(-\mu, \phi, z')dz'] + \int_{-d}^{z} e^{-\boldsymbol{\kappa}_c^+(z-z')/\mu}\mathbf{F}_c^+(\mu, \phi, z')dz' \\ & e^{-\boldsymbol{\kappa}_c^+(z+d)/\mu}[e^{-\boldsymbol{\kappa}_t^+ H_t/\mu}\mathbf{R}\int_{-d'}^{-d} e^{-\boldsymbol{\kappa}_t^-(z'+d')/\mu}\mathbf{F}_t^-(-\mu, \phi, z')dz' \\ & \int_{-d'}^{-d} e^{-\boldsymbol{\kappa}_t^+(z'+d)/\mu}\mathbf{F}_t^+(\mu, \phi, z')dz'] \end{aligned} \tag{A.30}$$

where

$$\mathbf{R}'(\mu,\phi) = e^{-\boldsymbol{\kappa}_t^+ H_t/\mu} \cdot \mathbf{R}(\mu) \cdot e^{-\boldsymbol{\kappa}_t^- H_t/\mu}. \tag{A.31}$$

The matrix $\mathbf{R}'(\mu,\phi)$ accounts for extinction in the trunk layer and reflection at the specular surface. The above expression is given in terms of the source functions $\mathbf{F}_c^{\pm}$ and $\mathbf{F}_t^{\pm}$ which in turn are given by (A.10),(A.11) and (A.14),(A.15) in terms of $\mathbf{I}_c^{\pm}$ and $\mathbf{I}_t^{\pm}$. Thus we need to solve the coupled integral equations (A.18),(A.23),(A.24), and (A.30) to obtain $\mathbf{I}_c^+(\mu,\phi,0)$. If the scattering albedo of the medium is small, we can solve the integral equations using an iterative approach. We shall start with the zeroth-order solutions, which are obtained by setting $\mathbf{P}_c(\mu,\phi;\mu',\phi') = \mathbf{P}_t(\mu,\phi;\mu',\phi') = 0$ in (A.10),(A.11) and (A.15),(A.16) which renders $\mathbf{F}_c^{\pm}(\mu,\phi,z) = \mathbf{F}_t^{\pm}(-\mu,\phi,z) = 0$. Using the boundary conditions given by (A.26)-(A.28) the zeroth-order specific intensities are given by

$$\mathbf{I}_{c0}^-(-\mu,\phi,z) = e^{\boldsymbol{\kappa}_c^- z/\mu}\mathbf{I_0}\delta(\mu-\mu_0)\delta(\phi-\phi_0) \tag{A.32}$$

$$\mathbf{I}_{t0}^-(-\mu,\phi,z) = e^{\boldsymbol{\kappa}_t^-(z+d)/\mu}e^{-\boldsymbol{\kappa}_c^- d/\mu}\mathbf{I_0}\delta(\mu-\mu_0)\delta(\phi-\phi_0) \tag{A.33}$$

$$\mathbf{I}_{t0}^+(\mu,\phi,z) = e^{-\boldsymbol{\kappa}_t^+(z+d')/\mu}\mathbf{R}e^{-\boldsymbol{\kappa}_t^- H_t/\mu}e^{-\boldsymbol{\kappa}_c^- d/\mu}\mathbf{I_0}\delta(\mu-\mu_0)\delta(\phi-\phi_0) \tag{A.34}$$

$$\mathbf{I}_{c0}^+(\mu,\phi,z) = e^{-\boldsymbol{\kappa}_c^+(z+d)/\mu}e^{-\boldsymbol{\kappa}_t^+ H_t/\mu}\mathbf{R}e^{-\boldsymbol{\kappa}_t^- H_t/\mu}e^{-\boldsymbol{\kappa}_c^- d/\mu}\mathbf{I_0}\delta(\mu-\mu_0)\delta(\phi-\phi_0) \tag{A.35}$$

where the symbols $\mathbf{I}_{c0}^{\pm}$ and $\mathbf{I}_{t0}^{\pm}$ are used to denote the zeroth-order solutions of $\mathbf{I}_c^{\pm}$ and $\mathbf{I}_t^{\pm}$, respectively, and use of (A.25) was made in deriving the expressions.

The zeroth-order solution corresponds to propagation of the coherent wave through the medium with the scattering ignored, except for its contribution to

extinction. To obtain the first-order solution.we first need to use (A.32)-(A.35) in (A.10),(A.11) and (A.15),(A.16) to compute the first-order source functions $\mathbf{F}_{c1}^{\pm}$ and $\mathbf{F}_{t1}^{\pm}$, and then insert the result in (A.30). This process leads to:

$$
\begin{aligned}
\mathbf{I}_1^+(\mu,\phi,z) \;=\; & e^{-\boldsymbol{\kappa}_c^+(z+d)/\mu}\mathbf{R}'(\mu,\phi)e^{-\boldsymbol{\kappa}_c^- d/\mu} \\
& \delta(\mu-\mu_0)\delta(\phi-\phi_0)\mathbf{I}_0 + \frac{1}{\mu}e^{-\boldsymbol{\kappa}_c^+(z+d)/\mu}\mathbf{R}'(\mu,\phi) \\
& \cdot\{\int_{-d}^{0}[e^{-\boldsymbol{\kappa}_c^-(z'+d)/\mu}\mathbf{P}_c(-\mu,\phi;\mu_0,\phi_0)e^{-\boldsymbol{\kappa}_c^+(z'+d)/\mu_0}\mathbf{R}'(\mu_0,\phi_0) \\
& \cdot e^{-\boldsymbol{\kappa}_c^- d/\mu_0} + e^{-\boldsymbol{\kappa}_c^-(z'+d)/\mu}\mathbf{P}_c(-\mu,\phi;-\mu_0,\phi_0)e^{\boldsymbol{\kappa}_c^- z'/\mu_0}]dz'\}\mathbf{I}_0 \\
& +\frac{1}{\mu}\{\int_{-d}^{z}[e^{-\boldsymbol{\kappa}_c^+(z-z')/\mu}\mathbf{P}_c(\mu,\phi;\mu_0,\phi_0)e^{-\boldsymbol{\kappa}_c^+(z'+d)/\mu_0}\mathbf{R}'(\mu_0,\phi_0)e^{-\boldsymbol{\kappa}_c^- d/\mu_0} \\
& +e^{-\boldsymbol{\kappa}_c^+(z-z')/\mu}\mathbf{P}_c(\mu,\phi;-\mu_0,\phi_0)e^{\boldsymbol{\kappa}_c^- z'/\mu_0}]dz'\}\mathbf{I}_0 \\
& +\frac{1}{\mu}e^{-\boldsymbol{\kappa}_c^+(z+d)/\mu}e^{-\boldsymbol{\kappa}_t^+ H_t/\mu}\mathbf{R}\int_{-d'}^{-d}e^{-\boldsymbol{\kappa}_t^-(z'+d')/\mu}\mathbf{P}_t(-\mu,\phi;-\mu,\phi_0)e^{\boldsymbol{\kappa}_t^-(z'+d)/\mu_0}dz' \\
& \cdot e^{-\boldsymbol{\kappa}_c^- d/\mu_0}\delta_k(\mu-\mu_0)\mathbf{I_0} \\
& +\frac{1}{\mu}e^{-\boldsymbol{\kappa}_c^+(z+d)/\mu}\int_{-d'}^{-d}e^{\boldsymbol{\kappa}_t^+(z'+d')/\mu}\mathbf{P}_t(\mu,\phi;\mu,\phi_0)e^{-\boldsymbol{\kappa}_t^+(z'+d')/\mu_0}dz' \\
& \cdot\mathbf{R}e^{-\boldsymbol{\kappa}_t^- H_t/\mu_0}e^{-\boldsymbol{\kappa}_c^- d/\mu_0}\delta_k(\mu-\mu_0)\mathbf{I_0}
\end{aligned}
\tag{A.36}
$$

where it is understood that $\boldsymbol{\kappa}_{c,t}^{\pm}/\mu = \boldsymbol{\kappa}_{c,t}^{\pm}(\mu,\phi)/\mu$ and $\boldsymbol{\kappa}_{c,t}^{\pm}/\mu_0 = \boldsymbol{\kappa}_{c,t}^{\pm}(\mu_0,\phi_0)/\mu_0$. To find an expression for the intensity emerging from the crown layer at $z = 0$, we shall first define the integrals in (A.36) in terms of equivalent matrices. Using the definition given by (A.21)

$$
\begin{aligned}
\mathbf{A}_1(\mu,\phi;\mu_0,\phi_0) \;=\; & \int_{-d}^{0}\mathbf{D}_c(-\mu,\phi;-(z'+d)/\mu)\mathbf{Q}_c^{-1}(-\mu,\phi)\mathbf{P}_c(-\mu,\phi;\mu_0,\phi_0) \\
& \mathbf{Q}_c(\mu_0,\phi_0)\mathbf{D}_c(\mu_0,\phi_0;-(z'+d)/\mu_0)dz',
\end{aligned}
\tag{A.37}
$$

whose $(ij)^{th}$ element is given by

$$[\mathbf{A}_1(\mu,\phi;\mu_0,\phi_0)]_{ij} = \frac{1-\exp[-(\lambda_i(-\mu,\phi)/\mu+\lambda_j(\mu_0,\phi_0)/\mu_0)d]}{\lambda_i(-\mu,\phi)/\mu+\lambda_j(\mu_0,\phi_0)/\mu_0} \cdot[\mathbf{Q}_c^{-1}(-\mu,\phi)\mathbf{P}_c(-\mu,\phi,\mu_0,\phi_0)\mathbf{Q}_c(\mu_0,\phi_0)]_{ij}. \quad (A.38)$$

In a similar manner,

$$\mathbf{A}_2(\mu,\phi;\mu_0,\phi_0) = \int_{-d}^{0}\mathbf{D}_c(-\mu,\phi;-(z'+d)/\mu)\mathbf{Q}_c^{-1}(-\mu,\phi)\mathbf{P}_c(-\mu,\phi;-\mu_0,\phi_0) \mathbf{Q}_c(-\mu_0,\phi_0)\mathbf{D}_c(-\mu_0,\phi_0;z'/\mu_0)dz' \quad (A.39)$$

$$[\mathbf{A}_2(\mu,\phi;\mu_0,\phi_0)]_{ij} = \frac{\exp[-\lambda_i(-\mu,\phi)d/\mu]-\exp[-\lambda_j(-\mu_0,\phi_0)d/\mu_0]}{-\lambda_i(-\mu,\phi)/\mu+\lambda_j(-\mu_0,\phi_0)/\mu_0} \cdot[\mathbf{Q}_c^{-1}(-\mu,\phi)\mathbf{P}_c(-\mu,\phi;-\mu_0,\phi_0)\mathbf{Q}_c(-\mu_0,\phi_0)]_{ij}, \quad (A.40)$$

$$\mathbf{A}_3(\mu,\phi;\mu_0,\phi_0) = \int_{-d}^{0}\mathbf{D}_c(\mu,\phi;z'/\mu)\mathbf{Q}_c^{-1}(\mu,\phi)\mathbf{P}_c(\mu,\phi;\mu_0,\phi_0) \mathbf{Q}_c(\mu_0,\phi_0)\mathbf{D}_c(\mu_0,\phi_0;-(z'+d)/\mu_0)dz' \quad (A.41)$$

$$[\mathbf{A}_3(\mu,\phi;\mu_0,\phi_0)]_{ij} = \frac{\exp[-\lambda_j(\mu_0,\phi_0)d/\mu_0]-\exp[-\lambda_i(\mu,\phi)d/\mu]}{\lambda_i(\mu,\phi)/\mu-\lambda_j(\mu_0,\phi_0)/\mu_0} \cdot[\mathbf{Q}_c^{-1}(\mu,\phi)\mathbf{P}_c(\mu,\phi;\mu_0,\phi_0)\mathbf{Q}_c(\mu_0,\phi_0)]_{ij}, \quad (A.42)$$

and

$$\mathbf{A}_4(\mu,\phi;\mu_0,\phi_0) = \int_{-d}^{0}\mathbf{D}_c(\mu,\phi;z'/\mu)\mathbf{Q}_c^{-1}(\mu,\phi)\mathbf{P}_c(\mu,\phi;-\mu_0,\phi_0) \mathbf{Q}_c(-\mu_0,\phi_0)\mathbf{D}_c(-\mu_0,\phi_0;z'/\mu_0)dz' \quad (A.43)$$

$$[\mathbf{A}_4(\mu,\phi;\mu_0,\phi_0)]_{ij} = \frac{1-\exp[-(\lambda_i(\mu,\phi)/\mu+\lambda_j(-\mu_0,\phi_0)/\mu_0)d]}{\lambda_i(\mu,\phi)/\mu+\lambda_j(-\mu_0,\phi_0)/\mu_0} \cdot[\mathbf{Q}_c^{-1}(\mu,\phi)\mathbf{P}_c(\mu,\phi;-\mu_0,\phi_0)\mathbf{Q}_c(-\mu_0,\phi_0)]_{ij} \quad (A.44)$$

$$\mathbf{A}_5(\mu,\phi;\mu_0,\phi_0) = \int_{-d'}^{-d} \mathbf{D}_t(-\mu,\phi;-(z'+d)/\mu)\mathbf{Q}_t^{-1}(-\mu,\phi)\mathbf{P}_t(-\mu,\phi,-\mu,\phi_0)$$
$$\mathbf{Q}_t(-\mu_0,\phi_0)\mathbf{D}_t(-\mu_0,\phi_0;(z'+d)/\mu_0)dz' \qquad (A.45)$$

$$[\mathbf{A}_5(\mu,\phi;\mu_0,\phi_0)]_{ij} = \frac{\exp[-\lambda_i(-\mu,\phi)H_t/\mu] - \exp[-\lambda_j(-\mu_0,\phi_0)H_t/\mu_0]}{-\lambda_i(-\mu,\phi)/\mu + \lambda_j(-\mu_0,\phi_0)/\mu_0}$$
$$\cdot[\mathbf{Q}_t^{-1}(-\mu,\phi)\mathbf{P}_t(-\mu,\phi;-\mu,\phi_0)\mathbf{Q}_t(-\mu_0,\phi_0)]_{ij}, \qquad (A.46)$$

$$\mathbf{A}_6(\mu,\phi;\mu_0,\phi_0) = \int_{-d'}^{-d} \mathbf{D}_t(\mu,\phi;(z'+d)/\mu)\mathbf{Q}_t^{-1}(\mu,\phi)\mathbf{P}_t(\mu,\phi;\mu,\phi_0)$$
$$\mathbf{Q}_t(\mu_0,\phi_0)\mathbf{D}_t(\mu_0,\phi_0;-(z'+d')/\mu_0)dz' \qquad (A.47)$$

$$[\mathbf{A}_6(\mu,\phi;\mu_0,\phi_0)]_{ij} = \frac{\exp[-\lambda_j(\mu_0,\phi_0)H_t/\mu_0] - \exp[-\lambda_i(\mu,\phi)H_t/\mu]}{\lambda_i(\mu,\phi)/\mu - \lambda_j(\mu_0,\phi_0)/\mu_0}$$
$$\cdot[\mathbf{Q}_t^{-1}(\mu,\phi)\mathbf{P}_t(\mu,\phi;\mu,\phi_0)\mathbf{Q}_t(\mu_0,\phi_0)]_{ij}. \qquad (A.48)$$

In view of these matrices, (A.36) can be evaluated at $z = 0$ and written in the form

$$\begin{aligned}
\mathbf{I}^s(\mu,\phi) &= \mathbf{I}_1^+(\mu,\phi,0) \\
&= e^{-\boldsymbol{\kappa}_c^+ d/\mu}\mathbf{R}'(\mu_0,\phi_0)e^{-\boldsymbol{\kappa}_c^- d/\mu_0}\delta(\mu-\mu_0)\delta(\phi-\phi_0)\mathbf{I}_0 \\
&\quad + \frac{1}{\mu}e^{-\boldsymbol{\kappa}_c^+ d/\mu}\mathbf{R}'(\mu,\phi)\mathbf{Q}_c(-\mu,\phi)\mathbf{A}_1\mathbf{Q}_c^{-1}(\mu_0,\phi_0)\mathbf{R}'(\mu_0,\phi_0)e^{-\boldsymbol{\kappa}_c^- d/\mu_0}\mathbf{I}_0 \\
&\quad + \frac{1}{\mu}e^{-\boldsymbol{\kappa}_c^+ d/\mu}\mathbf{R}'(\mu,\phi)\mathbf{Q}_c(-\mu,\phi)\mathbf{A}_2\mathbf{Q}_c^{-1}(-\mu_0,\phi_0)\mathbf{I}_0 \\
&\quad + \frac{1}{\mu}\mathbf{Q}_c(\mu,\phi)\mathbf{A}_3\mathbf{Q}_c^{-1}(\mu_0,\phi_0)\mathbf{R}'(\mu_0,\phi_0)e^{-\boldsymbol{\kappa}_c^- d/\mu_0}\mathbf{I}_0 \\
&\quad + \frac{1}{\mu}\mathbf{Q}_c(\mu,\phi)\mathbf{A}_4\mathbf{Q}_c^{-1}(-\mu_0,\phi_0)\mathbf{I}_0 \\
&\quad + \frac{1}{\mu}e^{-\boldsymbol{\kappa}_c^+ d/\mu}e^{-\boldsymbol{\kappa}_t^+ H_t/\mu}\mathbf{R}\mathbf{Q}_t(-\mu,\phi)\mathbf{A}_5\mathbf{Q}_t^{-1}(-\mu_0,\phi_0)e^{-\boldsymbol{\kappa}_c^- d/\mu_0}\delta_k(\mu-\mu_0)\mathbf{I}_0 \\
&\quad + \frac{1}{\mu}e^{-\boldsymbol{\kappa}_c^+ d/\mu}\mathbf{Q}_t(\mu,\phi)\mathbf{A}_6\mathbf{Q}_t^{-1}(\mu_0,\phi_0)\mathbf{R}e^{-\boldsymbol{\kappa}_t^- H_t/\mu_0}e^{-\boldsymbol{\kappa}_c^- d/\mu_0}\delta_k(\mu-\mu_0)\mathbf{I}_0
\end{aligned} \qquad (A.49)$$

The seven terms contained in (A.49), which are diagrammed in Fig. A.3, represent:

Term ds This is a coherent reflection term resulting from *direct* propagation of the incident intensity through the layers down to the bottom boundary, followed by *specular* reflection by the bottom boundary, and then followed with direct propagation through the layers to the upper boundary. This term exist only in the specular direction $(\theta, \phi) = (\theta_0, \phi_0)$, and in that case, its magnitude is equal to $\mathbf{I}_0$, reduced by the product of the two-way attenuation and the reflection coefficient.

Term 1 This term represents propagation of the incident intensity through the two layers to the bottom boundary, followed with specular reflection at θ_0, then bistatic scattering by the vegetation material in the crown layer downward in a direction $(\pi - \theta, \phi)$ such that after specular reflection by the lower surface a second time at θ, the reflected intensity propagates upward through the two layers along the direction (θ, ϕ).

Term 2a This term represents propagation of the incident intensity $\mathbf{I}_0$ into the crown layer along the direction (θ_0, ϕ_0), followed with bistatic scattering by the vegetation material downward along the direction $(\pi - \theta, \phi)$, and then followed with specular reflection by the lower boundary upward through the layers along the direction (θ, ϕ).

Term 2b This is the complement of term 2. It represents propagation of the incident intensity $\mathbf{I}_0$ through the layers down to the bottom boundary, spec-

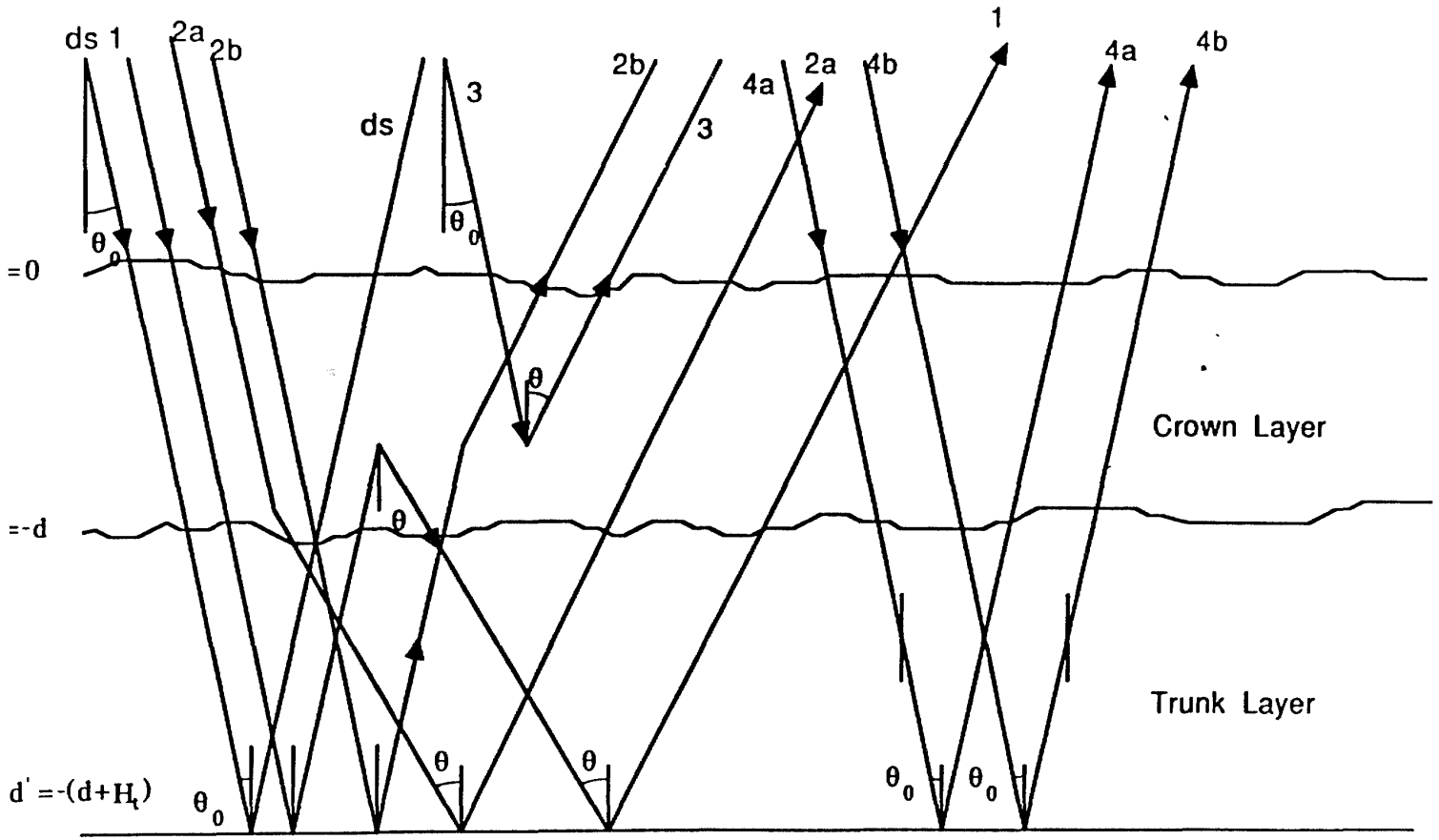


Figure A.3: Scattering Terms for the Bistatic Case.

ular reflection at θ_0, upward propagation at θ_0, then bistatic scattering by the vegetation in the direction (θ, ϕ).

Term 3 This term does not involve reflection by the bottom boundary. It represents incidence at $(\pi - \theta_0, \phi_0)$ followed by bistatic scattering upward along the direction (θ, ϕ). For a semi-infinite layer, the other four term vanish and only this term remains.

Term 4a This term represents the propagation of the incident intensity in the crown layer (i.e. attenuation only but no change in direction), followed by bistatic scattering by the trunks down to the ground surface, followed by bistatic reflection by the surface boundary, and then direct propagation through the trunk and crown layers.

Term 4b This term is the complement of term 5 (same path, but in reverse direction). This term and term 5 will be referred to as *ground-trunk* term. Contribution of these terms is observable only on the surface of a cone with generating angle θ_0.

With $\mathbf{I}_c^s(\mu, \phi)$ given by (A.49), the expression for the bistatic scattering coefficient may now be readily found by inserting (A.49) into (A.5). However, our interest is in the backscattering case, which we shall pursue next.

A.4 First-Order Solution for Backscattering

For the backscattering case, we set $\theta = \theta_0$ and $\phi = \phi_0 + \pi$ in (A.37)-(A.49) For an azimuthally symmetric medium, this condition causes the diagonal components of $\mathbf{A}_2$,$\mathbf{A}_3$ $\mathbf{A}_5$, and $\mathbf{A}_6$ to become indeterminate. Application of L'Hopital's rule, however, leads to

$$\lim_{\mu \to \mu_0} [\mathbf{A}_2(\mu, \phi; \mu_0, \phi_0)]_{ii} = d e^{-\lambda_i(\mu_0) d/\mu_0} \cdot [\mathbf{Q}_c^{-1}(-\mu, \phi) \mathbf{P}_c(-\mu, \phi; -\mu_0, \phi_0) \mathbf{Q}_c(-\mu_0, \phi_0)]_{ii}. \tag{A.50}$$

The same result applies to $\mathbf{A}_3$,$\mathbf{A}_5$, and $\mathbf{A}_6$. The backscattered intensity can be related to the incident intensity through a matrix $\mathbf{T}(\theta_0, \phi_0)$,

$$\mathbf{I}^s = \mathbf{T}(\theta_0, \phi_0) \mathbf{I}_0 \tag{A.51}$$

where

$$\begin{aligned}
\mathbf{T}(\theta_0, \phi_0) \;=\; & \frac{1}{\mu_0} e^{-\boldsymbol{\kappa}_c^+ d/\mu_0} \mathbf{R}'(\mu_0, \phi_0 + \pi) \mathbf{Q}_c(-\mu_0, \phi_0 + \pi) \mathbf{A}_1 \mathbf{Q}_c^{-1}(\mu_0, \phi_0) \mathbf{R}'(\mu_0, \phi_0) e^{-\boldsymbol{\kappa}_c^- d/\mu_0} \\
& + \frac{1}{\mu_0} e^{-\boldsymbol{\kappa}_c^+ d/\mu_0} \mathbf{R}'(\mu_0, \phi_0 + \pi) \mathbf{Q}_c(-\mu_0, \phi_0 + \pi) \mathbf{A}_2 \mathbf{Q}_c^{-1}(-\mu_0, \phi_0) \\
& + \frac{1}{\mu_0} \mathbf{Q}_c(\mu_0, \phi_0 + \pi) \mathbf{A}_3 \mathbf{Q}_c^{-1}(\mu_0, \phi_0) \mathbf{R}'(\mu_0, \phi_0) e^{-\boldsymbol{\kappa}_c^- d/\mu_0} \\
& + \frac{1}{\mu_0} \mathbf{Q}_c(\mu_0, \phi_0 + \pi) \mathbf{A}_4 \mathbf{Q}_c^{-1}(-\mu_0, \phi_0) \\
& + \frac{1}{\mu_0} e^{-\boldsymbol{\kappa}_c^+ d/\mu_0} e^{-\boldsymbol{\kappa}_t^+ H_t/\mu_0} \mathbf{R}(\mu_0) \mathbf{Q}_t(-\mu_0, \phi_0 + \pi) \mathbf{A}_5 \mathbf{Q}_t^{-1}(-\mu_0, \phi_0) e^{-\boldsymbol{\kappa}_c^- d/\mu_0} \\
& + \frac{1}{\mu_0} e^{-\boldsymbol{\kappa}_c^+ d/\mu_0} \mathbf{Q}_t(\mu_0, \phi_0 + \pi) \mathbf{A}_6 \mathbf{Q}_t^{-1}(\mu_0, \phi_0) \mathbf{R}(\mu_0) e^{-\boldsymbol{\kappa}_t^- H_t/\mu_0} e^{-\boldsymbol{\kappa}_c^- d/\mu_0}
\end{aligned} \tag{A.52}$$

The backscattering coefficients, using (A.7) and (A.51), are given by

$$\sigma_{vv}^\circ = 4\pi [\mathbf{T}(\theta_0, \phi_0)]_{11} \cos\theta_0 \tag{A.53}$$

$$\sigma^{\circ}_{hh} = 4\pi[\mathbf{T}(\theta_0, \phi_0)]_{22} \cos\theta_0 \tag{A.54}$$

$$\sigma^{\circ}_{hv} = 4\pi[\mathbf{T}(\theta_0, \phi_0)]_{21} \cos\theta_0 \tag{A.55}$$

$$\sigma^{\circ}_{vh} = 4\pi[\mathbf{T}(\theta_0, \phi_0)]_{12} \cos\theta_0. \tag{A.56}$$

Figure A.4 depicts the scattering mechanisms for the backscattering case.

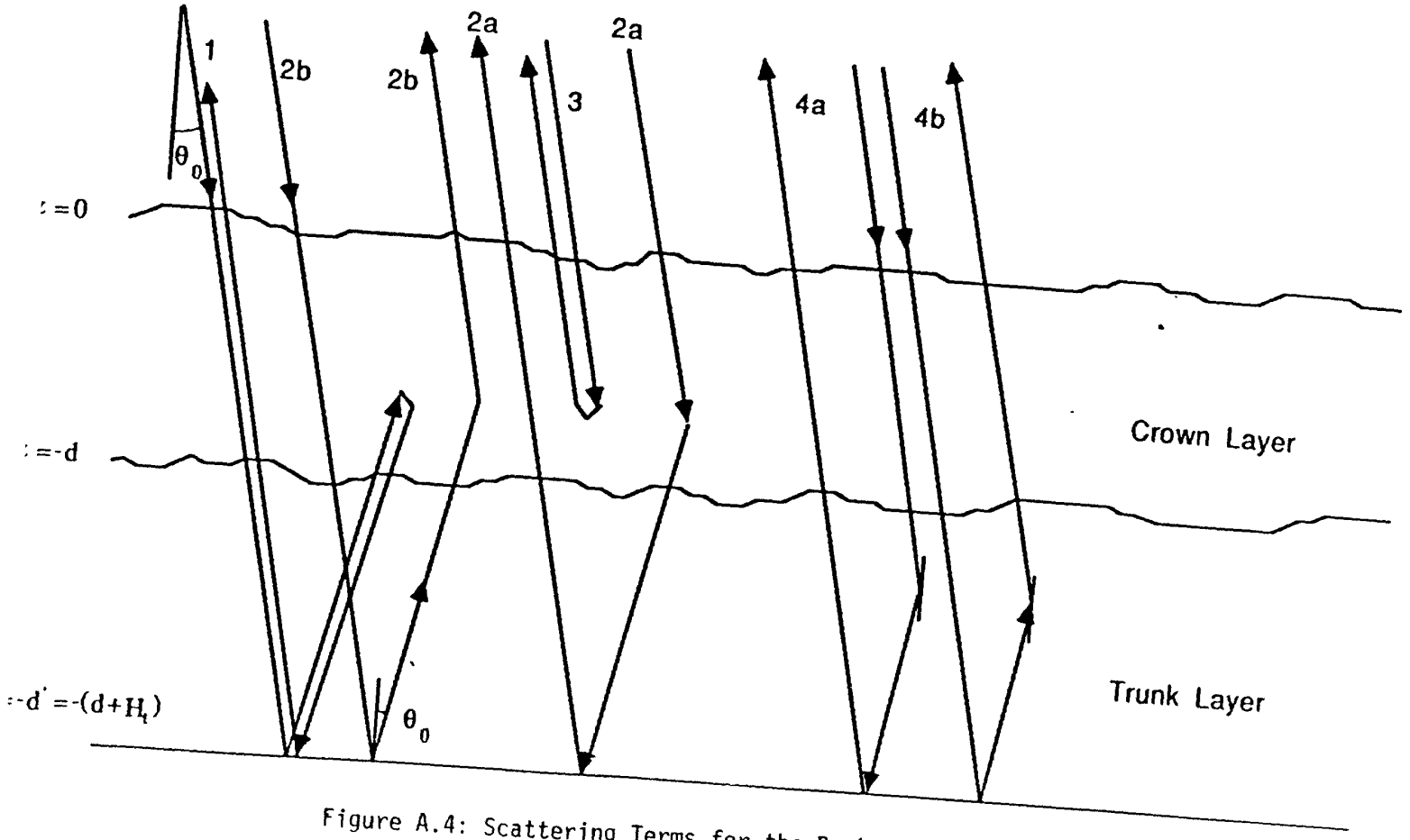


Figure A.4: Scattering Terms for the Backscattering Case.

APPENDIX B PHASE AND EXTINCTION MATRICES OF THE CROWN LAYER

The canopy crown layer is assumed to consist of two types of dielectric particles: discs and cylinders. The discs represent the leaves and the cylinders represent the needles and branches. The discs are modeled as thin, rectangular, flat strips with uniform thickness τ and complex relative dielectric constant ϵ_d. The leaf surface dimensions a and b are treated as random variables characterized by a probability density function (PDF) $f_1(a,b)$, and the leaf orientation is characterized by the PDF $f_2(\theta_d,\phi_d)$ where the orientation angles (θ_d,ϕ_d) define the spherical coordinates of a unit vector normal to the rectangular dielectric with respect to a fixed coordinate system $(\hat{\mathbf{x}},\hat{\mathbf{y}},\hat{\mathbf{z}})$. For convenience, and with negligible loss in computational accuracy (of the scattering cross section), it will be assumed that one side of the rectangular leaf always is parallel to the $x-y$ plane. It is further assumed that the leaf orientation is statistically independent of its size. Hence, the joint PDF $f_d(a,b;\theta_d,\phi_d)$ is given by

$$f_d(a,b;\theta_d,\phi_d) = f_1(a,b)f_2(\theta_d,\phi_d). \tag{B.1}$$

In a similar fashion, the needles and branches are modeled as circular cylinders of diameter d_c and length l, and the orientation of the cylinder axis is defined by the angles (θ_c,ϕ_c). The joint PDF for the cylinders is given by

$$f_c(l,d_c;\theta_c,\phi_c) = f_3(l,d_c)f_4(\theta_c,\phi_c). \tag{B.2}$$

The cylinders may consist of two independent groups, needles with uniform dielectric constant ϵ_n, and branches with uniform dielectric constant ϵ_b. The only

additional parameters required to characterize the crown medium are the volume densities of leaves, needles, and branches: N_d, N_n, and N_b, respectively.

B.1 Phase Matrix of the Crown Layer

In the radiative transfer model given in Appendix A, the formulation is given in terms of the phase function $\mathbf{P}_c(\theta_s, \phi_s; \theta_0, \phi_0)$ relating the intensity scattered by a unit volume of the crown layer into the direction (θ_s, ϕ_s) to the intensity incident upon the unit volume from the direction (θ_0, ϕ_0), with both sets of orientation angles being defined with respect to the reference coordinate system $(\hat{\mathbf{x}}, \hat{\mathbf{y}}, \hat{\mathbf{z}})$. The phase matrix $\mathbf{P}_c$ represents the average Stokes matrix of the particles constituting the unit volume. To relate $\mathbf{P}_c$ to the properties of the crown layer, we start by considering scattering by a single particle. For a plane wave incident upon the particle in the direction $\hat{\mathbf{k}}_i$, its electric field vector may be written in terms of vertical and horizontal polarization components, E_v^i and E_h^i, using the coordinate system $(\hat{\mathbf{v}}_i, \hat{\mathbf{h}}_i, \hat{\mathbf{k}}_i)$ shown in Fig. B.1,

$$\mathbf{E}^i = (E_v^i \hat{\mathbf{v}}_i + E_h^i \hat{\mathbf{h}}_i) e^{ik_0 \hat{\mathbf{k}}_i \cdot \mathbf{r}}, \tag{B.3}$$

where

$$\hat{\mathbf{v}}_i = \cos\theta_i \cos\phi_i \hat{\mathbf{x}} + \cos\theta_i \sin\phi_i \hat{\mathbf{y}} - \sin\theta_i \hat{\mathbf{z}} \tag{B.4}$$

$$\hat{\mathbf{h}}_i = -\sin\phi_i \hat{\mathbf{x}} + \cos\phi_i \hat{\mathbf{y}} \tag{B.5}$$

$$\hat{\mathbf{k}}_i = \sin\theta_i \cos\phi_i \hat{\mathbf{x}} + \sin\theta_i \sin\phi_i \hat{\mathbf{y}} + \cos\theta_i \hat{\mathbf{z}}. \tag{B.6}$$

In (B.3), a time dependence of the form $e^{-i\omega t}$ is assumed and suppressed.

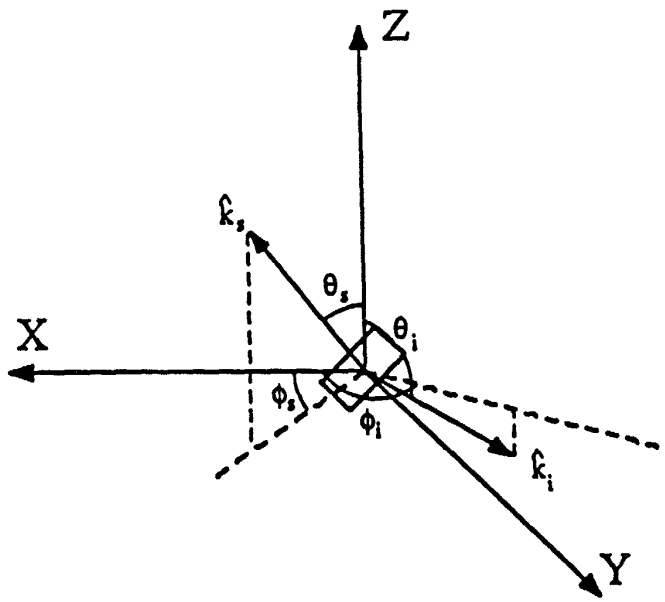


Figure B.1: Coordinate System Geometry.

The far-field wave scattered in the direction $\hat{\mathbf{k}}_s$ is a spherical wave given by

$$\mathbf{E}^s = E_v^s \hat{\mathbf{v}}_s + E_h^s \hat{\mathbf{h}}_s, \tag{B.7}$$

where

$$\hat{\mathbf{v}}_s = \cos\theta_s \cos\phi_s \hat{\mathbf{x}} + \cos\theta_s \sin\phi_s \hat{\mathbf{y}} - \sin\theta_s \hat{\mathbf{z}} \tag{B.8}$$

$$\hat{\mathbf{h}}_s = -\sin\phi_s \hat{\mathbf{x}} + \cos\phi_s \hat{\mathbf{y}} \tag{B.9}$$

$$\hat{\mathbf{k}}_s = \sin\theta_s \cos\phi_s \hat{\mathbf{x}} + \sin\theta_s \sin\phi_s \hat{\mathbf{y}} + \cos\theta_s \hat{\mathbf{z}}. \tag{B.10}$$

The scattering matrix $\mathbf{S}(\theta_s, \phi_s; \theta_i, \phi_i; \theta_j, \phi_j)$ for a particle with orientation angles (θ_j, ϕ_j) relates the incident field components to the components of the scattered field at a range r through

$$\begin{bmatrix} E_v^s \\ E_h^s \end{bmatrix} = \frac{e^{ik_0 r}}{r} \mathbf{S} \begin{bmatrix} E_v^i \\ E_h^i \end{bmatrix} \tag{B.11}$$

and is given by four scattering amplitudes

$$\mathbf{S} = \begin{bmatrix} S_{vv} & S_{vh} \\ S_{hv} & S_{hh} \end{bmatrix}. \tag{B.12}$$

For a disc-shaped particle (i.e., a leaf),(θ_j, ϕ_j) defines the direction of its surface normal, i.e. (θ_d, ϕ_d) and for a cylinder-shaped particle (branch or needle), (θ_j, ϕ_j) defines the direction of the cylinder axis,i.e. (θ_c, ϕ_c).

Noting that the scattered field is a spherical wave, the modified scattered Stokes vector $\mathbf{I}_s$ is related to the modified incident Stokes vector $\mathbf{I}_i$ by [Ulaby et al.,1986,p.1088]

$$\mathbf{I}_s = \frac{1}{r^2} \mathbf{L}(\theta_s, \phi_s; \theta_i, \phi_i; \theta_j, \phi_j) \cdot \mathbf{I}_i \tag{B.13}$$

where $\mathbf{L}(\theta_s, \phi_s; \theta_i, \phi_i; \theta_j, \phi_j)$ is the Stokes matrix and is given by

$$\mathbf{L} = \begin{bmatrix} |S_{vv}|^2 & |S_{vh}|^2 & Re(S_{vh}^* S_{vv}) & -Im(S_{vh}^* S_{vv}) \\ |S_{hv}|^2 & |S_{hh}^*|^2 & Re(S_{hh}^* S_{hv}) & -Im(S_{hh}^* S_{hv}) \\ 2Re(S_{vv} S_{hv}^*) & 2Re(S_{vh} S_{hh}^*) & Re(S_{vv} S_{hh}^* + S_{vh} S_{hv}^*) & -Im(S_{vv} S_{hh}^* - S_{vh} S_{hv}^*) \\ 2Im(S_{vv} S_{hv}^*) & 2Im(S_{vh} S_{hh}^*) & Im(S_{vv} S_{hh}^* + S_{vh} S_{hv}^*) & Re(S_{vv} S_{hh}^* - S_{vh} S_{hv}^*) \end{bmatrix}. \tag{B.14}$$

In radiative transfer theory, the Stokes parameters are added incoherently; therefore, the phase matrix is equal to the Stokes matrix averaged over the particle type, size and orientation distributions. If N_d and N_c are the number of discs and cylinders per unit volume, the phase matrix is given by

$$\mathbf{P}_c(\theta_s, \phi_s; \theta_i, \phi_i) = \mathbf{P}_d(\theta_s, \phi_s; \theta_i, \phi_i) + \mathbf{P}_{cyl}(\theta_s, \phi_s; \theta_i, \phi_i) \tag{B.15}$$

where

$$\mathbf{P}_d(\theta_s, \phi_s; \theta_i, \phi_i) = N_d \iiiint f_d(a, b; \theta_d, \phi_d) \mathbf{L}(\theta_s, \phi_s; \theta_i, \phi_i; \theta_d, \phi_d) da db d\theta_d d\phi_d \tag{B.16}$$

and

$$\mathbf{P}_{cyl}(\theta_s, \phi_s; \theta_i, \phi_i) = N_c \iiiint f_c(l, d_c; \theta_c, \phi_c) \mathbf{L}(\theta_s, \phi_s; \theta_i, \phi_i; \theta_c, \phi_c) dl dd_c d\theta_c d\phi_c \tag{B.17}$$

where f_d and f_c are the PDFs defined earlier. The number density N_c is the sum of N_b (branches) and N_n (needles).

B.2 Extinction Matrix of the Crown Layer

The extinction matrix characterizes the attenuation of the Stokes parameters due to absorption and scattering. For a medium with low concentration of par-

ticles, the attenuation rate can be obtained from the extinction cross section of the individual scatterers. By applying the optical theorem, the extinction cross section, σ_{ext}^{p} ($p = v$ or$h$), is given by

$$\sigma_{ext}^{p} = \frac{4\pi}{k_0} Im[S_{pp}(\theta_i, \phi_i; \theta_i, \phi_i; \theta_j, \phi_j)], \tag{B.18}$$

from which the extinction coefficient can be obtained through

$$\kappa_p = N\langle\sigma_{ext}^{p}\rangle \tag{B.19}$$

where the symbol $\langle \quad \rangle$ denotes the statistical average over the size and orientation angles. To find a better estimate of the coherent field along the propagation direction (θ_i, ϕ_i), Foldy's approximation can be employed. The coupled equations for vertical and horizontal mean field in this approximation is of the following form[Tsang et al., 1985, p.139]

$$\frac{dE_v}{ds} = (ik_0 + M_{vv})E_v + M_{vh}E_h \tag{B.20}$$

$$\frac{dE_h}{ds} = M_{hv}E_v + (ik_0 + M_{hh})E_h \tag{B.21}$$

where s is the distance along the direction of propagation and

$$M_{mn} = \frac{i2\pi N}{k_0}\langle S_{mn}(\theta_i, \phi_i; \theta_i, \phi_i; \theta_j, \phi_j)\rangle \qquad m, n = v, h \tag{B.22}$$

Using the definition of the modified Stokes parameters and (B.20) and (B.21) the following coupled differential equation is found

$$\frac{d}{ds}\mathbf{I} = -\boldsymbol{\kappa}\mathbf{I} \tag{B.23}$$

where $\boldsymbol{\kappa}$ is the extinction matrix and is given by

$$\boldsymbol{\kappa} = \begin{bmatrix} -2Re(M_{vv}) & 0 & -Re(M_{vh}) & -Im(M_{vh}) \\ 0 & -2Re(M_{hh}) & -Re(M_{hv}) & Im(M_{hv}) \\ -2Re(M_{hv}) & -2Re(M_{vh}) & -[Re(M_{vv}) + Re(M_{hh})] & [Im(M_{vv}) - Im(M_{hh})] \\ 2Im(M_{hv}) & -2Im(M_{vh}) & -[Im(M_{vv}) - Im(M_{hh})] & -[Re(M_{vv}) + Re(M_{hh})] \end{bmatrix}. \tag{B.24}$$

The effective propagation constant of the mean field can be obtained from the eigenvalues of the matrix formed by the right hand side coefficients of equations (B.20) and (B.21). The two eigenvalues are given by

$$K_1 = k_0 - \frac{i}{2}[M_{vv} + M_{hh} + r] \tag{B.25}$$

$$K_2 = k_0 - \frac{i}{2}[M_{vv} + M_{hh} - r] \tag{B.26}$$

where

$$r = [(M_{vv} - M_{hh})^2 + 4M_{hv}M_{vh}]^{\frac{1}{2}} \tag{B.27}$$

The eigenvectors corresponding to K_1 and K_2 are denoted by $[1, b_1]$ and $[b_2, 1]$ respectively, and b_1 and b_2 are given by

$$b_1 = \frac{2M_{hv}}{M_{vv} - M_{hh} + r} \tag{B.28}$$

$$b_2 = \frac{2M_{vh}}{-M_{vv} + M_{hh} - r} \tag{B.29}$$

The corresponding effective propagation constant of the coherent Stokes parameters can be obtained from eigenvalue solution of equation (B.23). The eigenvalues

of extinction matrix are given by [Tsang et al., 1985]

$$\boldsymbol{\Lambda}(\theta,\phi) = \begin{bmatrix} \lambda_1 \\ \lambda_2 \\ \lambda_3 \\ \lambda_4 \end{bmatrix} = \begin{bmatrix} 2Im[K_1] \\ iK_2^* - iK_1 \\ iK_1^* - iK_2 \\ 2Im[K_2] \end{bmatrix} \tag{B.30}$$

The eigenmatrix $\mathbf{Q}(\theta,\phi)$ is also defined in such a way that the columns of $\mathbf{Q}(\theta,\phi)$ are the eigenvectors of the extinction matrix and is given by

$$\mathbf{Q}(\theta,\phi) = \begin{bmatrix} 1 & b_2^* & b_2 & \mid b_2 \mid^2 \\ \mid b_1 \mid^2 & b_1 & b_1^* & 1 \\ 2Re[b_1] & 1+b_1b_2^* & 1+b_2b_1^* & 2Re[b_2] \\ -2Im[b_1] & -i(1-b_1b_2^*) & i(1-b_2b_1^*) & 2Im[b_2] \end{bmatrix} \tag{B.31}$$

It is worth noting that at high frequencies or generally for particles with no depolarization where $M_{vh} = M_{hv} = 0$ the eigenmatrix $\mathbf{Q}$ is independent of the particles shape and orientation. In this case the eigenmatrix and its inverse are given by

$$\mathbf{Q} = \begin{bmatrix} 1 & 0 & 0 & 0 \\ 0 & 0 & 0 & 1 \\ 0 & 1 & 1 & 0 \\ 0 & -i & i & 0 \end{bmatrix} \tag{B.32}$$

$$\mathbf{Q}^{-1} = \begin{bmatrix} 1 & 0 & 0 & 0 \\ 0 & 0 & \frac{1}{2} & \frac{i}{2} \\ 0 & 0 & \frac{1}{2} & -\frac{i}{2} \\ 0 & 1 & 0 & 0 \end{bmatrix}. \tag{B.33}$$

B.3 Scattering Matrix of a Single Leaf

To obtain a relatively simple formulation for the scattering matrix of a leaf, the leaf can be regarded as:

1. A homogeneous non-magnetic dielectric material whose complex relative permittivity is $\epsilon = \epsilon' + i\epsilon''$.
2. A thin planar rectangle whose thickness and sides are τ, a and b, respectively.

It has been shown (Senior et al., 1987) that a resistive sheet model in conjunction with the physical optics approximation accurately predicts the backscattering cross section of a leaf at almost all angles of incidence. In this model the sheet is simply an electric current sheet characterized by a complex resistivity R where

$$R = \frac{iZ_0}{k_0\tau(\epsilon - 1)}. \tag{B.34}$$

Here, k_0 and Z_0 are the propagation constant and intrinsic impedance, respectively, of free space. Further, for use in connection with the physical optics approximation, the total current supported by an infinitely extended resistive sheet when illuminated by a plane wave is needed.

To derive the induced physical-optics current on the resistive sheet, consider the geometry depicted in Fig. B.2. In this geometry the direction of the unit vector normal to the leaf ($\hat{\boldsymbol{\xi}}'$) is characterized by spherical coordinates (θ_j, ϕ_j). The leaf coordinate system $(\hat{\boldsymbol{\zeta}}', \hat{\boldsymbol{\eta}}', \hat{\boldsymbol{\xi}}')$ is defined such that $\hat{\boldsymbol{\eta}}'$ is in the plane of the leaf and parallel to the x-y plane. The rectangular leaf occupies the region $-a/2 \leq \eta' \leq a/2$,

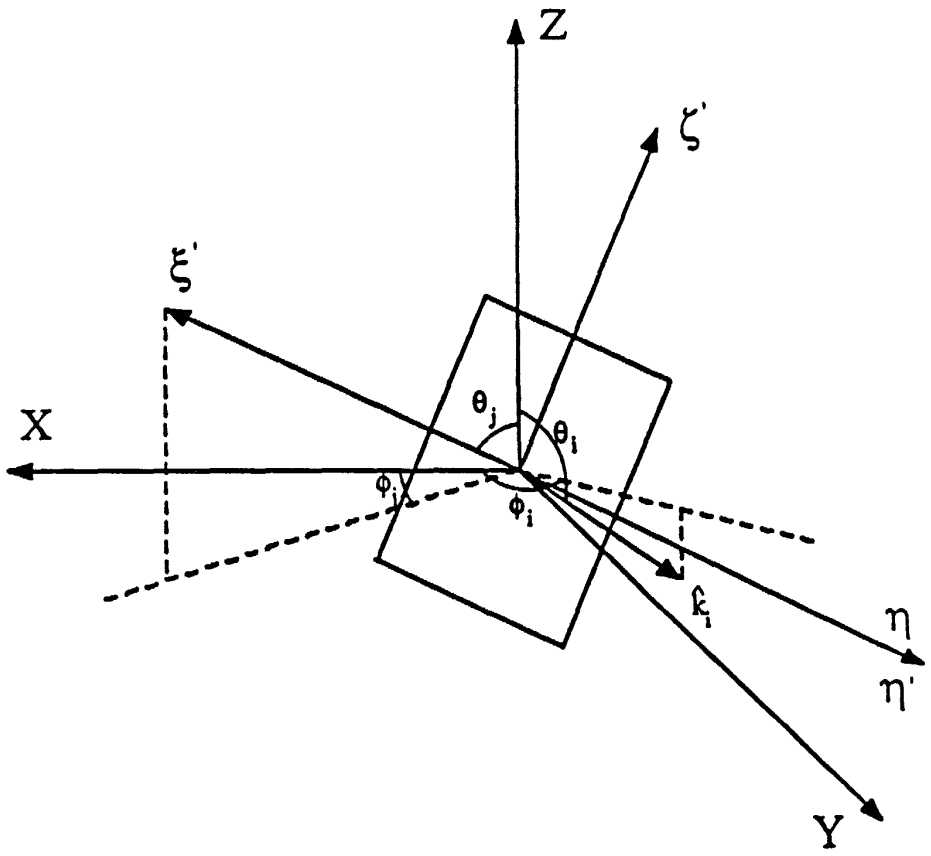


Figure B.2: Scattering Geometry of a Resistive Sheet.

$-b/2 \leq \zeta' \leq b/2$ and the directions of the incident wave and observation point are described by (B.4)-(B.6) and (B.8)-(B.10). The transformation relationship between the leaf coordinate system and the $(\hat{\mathbf{x}}, \hat{\mathbf{y}}, \hat{\mathbf{z}})$ coordinate system is of the following form

$$\hat{\boldsymbol{\xi}}' = \sin\theta_j \cos\phi_j \hat{\mathbf{x}} + \sin\theta_j \sin\phi_j \hat{\mathbf{y}} + \cos\theta_j \hat{\mathbf{z}} \tag{B.35}$$

$$\hat{\boldsymbol{\eta}}' = -\sin\phi_j \hat{\mathbf{x}} + \cos\phi_j \hat{\mathbf{y}} \tag{B.36}$$

$$\hat{\boldsymbol{\zeta}}' = -\cos\theta_j \cos\phi_j \hat{\mathbf{x}} - \cos\theta_j \sin\phi_j \hat{\mathbf{y}} + \sin\theta_j \hat{\mathbf{z}}. \tag{B.37}$$

It should be noted that the direction of the vector normal to the leaf plane is chosen such that the angle between the normal $(\hat{\boldsymbol{\xi}}')$ and the direction of incidence $(\hat{\mathrm{k}}_i)$ is obtuse, i.e.,

$$\cos\phi_1 = -(\hat{\mathrm{k}}_i \cdot \hat{\boldsymbol{\xi}}') = -[\sin\theta_j \sin\theta_i \cos(\phi_j - \phi_i) + \cos\theta_i \cos\theta_j] \geq 0. \tag{B.38}$$

A new coordinate system $(\hat{\boldsymbol{\xi}}, \hat{\boldsymbol{\eta}}, \hat{\boldsymbol{\zeta}})$ is also defined so that $\hat{\boldsymbol{\eta}}$ is parallel to $\hat{\boldsymbol{\eta}}'$ and $\hat{\boldsymbol{\zeta}}$ is normal to $\hat{\boldsymbol{\eta}}'$ and $\hat{\mathrm{k}}_i$. Figure B.3 depicts the relationship between the leaf coordinate system $(\hat{\boldsymbol{\xi}}', \hat{\boldsymbol{\eta}}', \hat{\boldsymbol{\zeta}}')$ and the coordinate system $(\hat{\boldsymbol{\xi}}, \hat{\boldsymbol{\eta}}, \hat{\boldsymbol{\zeta}})$. The coordinate transformation from $(\hat{\boldsymbol{\xi}}, \hat{\boldsymbol{\eta}}, \hat{\boldsymbol{\zeta}})$ to $(\hat{\mathbf{x}}, \hat{\mathbf{y}}, \hat{\mathbf{z}})$ is given by

$$\hat{\boldsymbol{\xi}} = -q[\sin\theta_i \cos\phi_j \cos(\phi_j - \phi_i)\hat{\mathbf{x}} + \sin\theta_i \sin\phi_j \cos(\phi_j - \phi_i)\hat{\mathbf{y}} + \cos\theta_i \hat{\mathbf{z}}] \tag{B.39}$$

$$\hat{\boldsymbol{\eta}} = -\sin\phi_j \hat{\mathbf{x}} + \cos\phi_j \hat{\mathbf{y}} \tag{B.40}$$

$$\hat{\boldsymbol{\zeta}} = q[\cos\theta_i \cos\phi_j \hat{\mathbf{x}} + \cos\theta_i \sin\phi_j \hat{\mathbf{y}} - \sin\theta_i \cos(\phi_j - \phi_i)\hat{\mathbf{z}}]. \tag{B.41}$$

where q is a constant and given by

$$q = [1 - \sin^2\theta_i \sin^2(\phi_j - \phi_i)]^{-1/2} \tag{B.42}$$

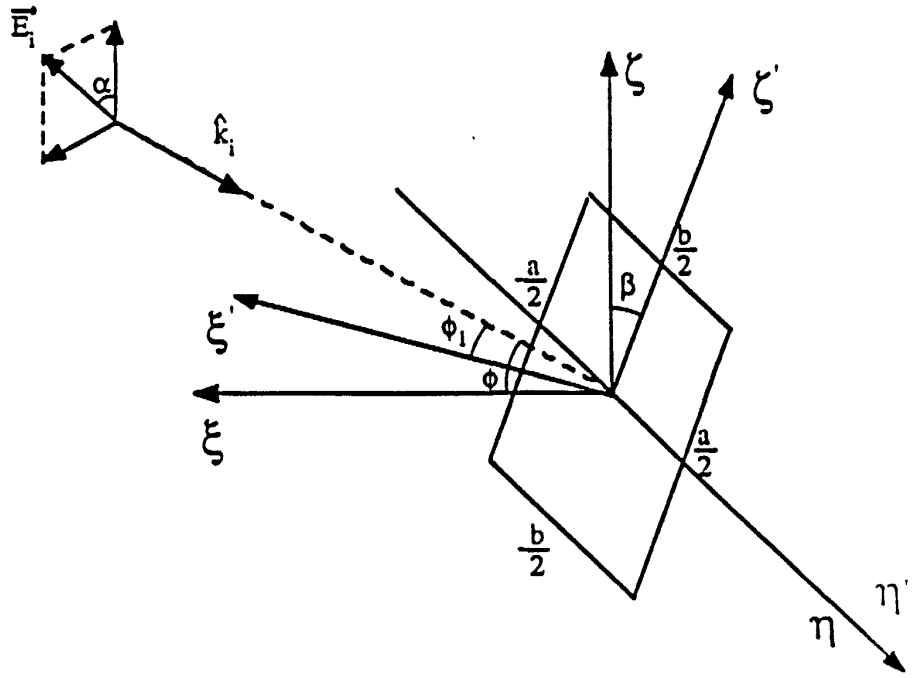


Figure B.3: Coordinate System Transformations.

If the angle between $\hat{\boldsymbol{\xi}}$ and $-\hat{\mathbf{k}}_i$ is denoted by ϕ and the angle between $\mathbf{E}^i$ and $\hat{\boldsymbol{\zeta}}$ by α_p ($p = v$ or h), then the incident electric field in $(\hat{\boldsymbol{\xi}}, \hat{\boldsymbol{\eta}}, \hat{\boldsymbol{\zeta}})$ coordinate system is given by

$$\mathbf{E}^i = (\hat{\boldsymbol{\xi}} \sin\alpha_p \sin\phi + \hat{\boldsymbol{\eta}} \sin\alpha_p \cos\phi + \hat{\boldsymbol{\zeta}} \cos\alpha_p) e^{-ik_0(\xi\cos\phi - \eta\sin\phi)}, \tag{B.43}$$

where the expressions for sine and cosine of the angles α_p and ϕ are as follows:

$$\cos\alpha_p = \begin{cases} q\cos(\phi_i - \phi_j); & \text{p=v} \\ -q\cos\theta_i \sin(\phi_i - \phi_j); & \text{p=h} \end{cases} \tag{B.44}$$

$$\sin\alpha_p = \begin{cases} q\cos\theta_i \sin(\phi_i - \phi_j); & \text{p=v} \\ -q\cos(\phi_i - \phi_j); & \text{p=h} \end{cases} \tag{B.45}$$

and

$$\cos\phi = [1 - \sin^2\theta_i \sin^2(\phi_i - \phi_j)]^{1/2} \qquad , \sin\phi = \sin\theta_i \sin(\phi_i - \phi_j). \tag{B.46}$$

The angle β shown in Fig. B.3 is the angle between the unit vectors $\hat{\boldsymbol{\zeta}}$ and $\hat{\boldsymbol{\zeta}}'$ and the expressions for $\cos\beta$ and $\sin\beta$ are given by

$$\cos\beta = -q[\cos\theta_i \cos\theta_j + \sin\theta_i \sin\theta_j \cos(\phi_i - \phi_j)] \tag{B.47}$$

$$\sin\beta = q[\cos\theta_i \sin\theta_j - \sin\theta_i \cos\theta_j \cos(\phi_i - \phi_j)]. \tag{B.48}$$

Now the induced current on a resistive sheet occupying $\eta' - \zeta'$ plane can easily be obtained by applying the resistive sheet boundary condition and has the following form [Sarabandi et al., 1988]

$$\mathbf{J}(\eta', \zeta') = \mathbf{J}_0 e^{ik_0(\eta'\sin\phi + \zeta'\sin\beta\cos\phi)} \tag{B.49}$$

where

$$\mathbf{J}_0 = \frac{2P}{Z_0}\{\sin\alpha_p\cos\beta\sin\phi + \cos\alpha_p\sin\beta)\Gamma_H(\phi_1)\hat{\boldsymbol{\eta}}_1$$
$$-(\sin\alpha_p\sin\beta - \cos\alpha_p\cos\beta\sin\phi)\cos\beta\cos\phi\Gamma_E(\phi_1)\hat{\boldsymbol{\zeta}}_1\}. \quad \text{(B.50)}$$

Here $\hat{\boldsymbol{\eta}}_1$ and $\hat{\boldsymbol{\zeta}}_1$ are unit vectors in and perpendicular to the plane of incidence, lying in the $\eta' - \zeta'$ plane and are given by

$$\hat{\boldsymbol{\eta}}_1 = P[-\hat{\boldsymbol{\xi}}\sin^2\beta\cos\phi + \hat{\boldsymbol{\eta}}\sin\phi + \hat{\boldsymbol{\zeta}}\sin\beta\cos\beta\cos\phi], \quad \text{(B.51)}$$

$$\hat{\boldsymbol{\zeta}}_1 = P[-\hat{\boldsymbol{\xi}}\sin\beta\sin\phi - \hat{\boldsymbol{\eta}}\sin\beta\cos\phi + \hat{\boldsymbol{\zeta}}\cos\beta\sin\phi] \quad \text{(B.52)}$$

where

$$P = (1 - \cos^2\beta\cos^2\phi)^{-1/2}. \quad \text{(B.53)}$$

Moreover, $\Gamma_H(\phi_1)$ and $-\Gamma_E(\phi_1)$ in expression (B.41) respectively are the plane wave reflection coefficients for H polarization when the magnetic vector is perpendicular to the plane of incidence and for E polarization when the electric vector is similarly inclined, and are given by

$$\Gamma_H(\phi_1) = (1 + \frac{2R}{Z_0}\sec\phi_1)^{-1} \quad \text{(B.54)}$$

$$\Gamma_E(\phi_1) = (1 + \frac{2R}{Z_0}\cos\phi_1)^{-1} \quad \text{(B.55)}$$

Using the coordinate transformation (B.30)-(B.32) and the equations (B.42)-(B.43), the expression (B.41) can be written as

$$\mathbf{J}_0 = \frac{2P^2}{Z_0}\{-\cos\phi(\cos\theta_j\cos\phi_j\hat{\mathbf{x}} + \cos\theta_j\sin\phi_j\hat{\mathbf{y}} - \sin\theta_j\hat{\mathbf{z}})$$
$$\cdot[\cos\beta(\sin\beta\sin\phi\sin\alpha_p - \cos\beta\cos\alpha_p)(\Gamma_H - \Gamma_E) + \cos\alpha_p(\Gamma_H - \cos^2\beta\cos^2\phi\Gamma_E)]$$
$$+(-\sin\phi_j\hat{\mathbf{x}} + \cos\phi_j\hat{\mathbf{y}})$$

$$\cdot[-\cos^2\phi\sin\alpha_p\cos\beta(\Gamma_H-\Gamma_E)+(\sin\alpha_p\cos\beta+\cos\alpha_p\sin\beta\sin\phi)$$

$$\cdot(\Gamma_H-\cos^2\beta\cos^2\phi\Gamma_E)]\}. \tag{B.56}$$

The above equation can now be expressed in terms of incident and leaf coordinate angles using equations (B.35) through (B.39); i.e.,

$$\sin\beta\sin\phi\sin\alpha_p-\cos\beta\cos\alpha_p=\begin{cases}\sin\theta_i\sin\theta_j+\cos\theta_i\cos\theta_j\cos(\phi_i-\phi_j); & \text{p=v}\\ -\cos\theta_j\sin(\phi_i-\phi_j); & \text{p=h}\end{cases} \tag{B.57}$$

$$\cos\phi\cos\alpha_p=\begin{cases}\cos(\phi_i-\phi_j); & \text{p=v}\\ -\cos\theta_i\sin(\phi_i-\phi_j); & \text{p=h}\end{cases} \tag{B.58}$$

and

$$\sin\alpha_p\cos\beta+\cos\alpha_p\sin\beta\sin\phi=\begin{cases}-\cos\theta_j\sin(\phi_i-\phi_j); & \text{p=v}\\ -[\sin\theta_i\sin\theta_j+\cos\theta_i\cos\theta_j\cos(\phi_i-\phi_j)]; & \text{p=h}\end{cases} \tag{B.59}$$

$$\cos\phi\sin\alpha_p=\begin{cases}\cos\theta_i\sin(\phi_i-\phi_j); & \text{p=v}\\ \cos(\phi_i-\phi_j); & \text{p=h}\end{cases} \tag{B.60}$$

We are now in a position to evaluate the bistatic scattered field by applying the physical optics approximation. The Hertz vector potential in the scattering direction is given by

$$\boldsymbol{\Pi}(\mathrm{r})=\frac{e^{ik_0r}}{r}\cdot\frac{iZ_0}{4\pi k_0}\int_{-a/2}^{a/2}\int_{-b/2}^{b/2}\mathbf{J}(\eta',\zeta')e^{-ik_0(\mathbf{r}'\cdot\hat{\mathrm{k}}_s)}d\eta'd\zeta' \tag{B.61}$$

where $\mathbf{r}=r\hat{\mathrm{k}}_s$ and $\mathbf{r}'=\eta'\hat{\boldsymbol{\eta}}'+\zeta'\hat{\boldsymbol{\zeta}}'$. From equations(B.8)-(B.10) and (B.26)-(B.28) we obtain

$$\hat{\boldsymbol{\eta}}'\cdot\hat{\mathrm{k}}_s=\sin\theta_s\sin(\phi_s-\phi_j) \tag{B.62}$$

$$\hat{\boldsymbol{\zeta}}'\cdot\hat{\mathrm{k}}_s=\cos\theta_s\sin\theta_j-\sin\theta_s\cos\theta_j\cos(\phi_s-\phi_j) \tag{B.63}$$

To arrive at a short expression for the scattered field, the following equations are defined in a manner analogous to (B.37) and (B.38)-(B.39),

$$\cos\phi' = (1 - \sin^2\theta_s \sin^2(\phi_s - \phi_j))^{1/2} \tag{B.64}$$

$$\sin\phi' = \sin\theta_s \sin(\phi_s - \phi_j) \tag{B.65}$$

and

$$\sin\beta' = \frac{\cos\theta_s \sin\theta_j - \cos\theta_j \sin\theta_s \cos(\phi_s - \phi_j)}{\sqrt{1 - \sin^2\theta_s \sin^2(\phi_s - \phi_j)}} \tag{B.66}$$

Using equations (B.40) and (B.53) through (B.57) into (B.52), the Hertz vector potential can be written as

$$\begin{aligned} \boldsymbol{\Pi}(\mathbf{r}) &= \frac{e^{ik_0 r}}{r} \cdot \frac{iZ_0}{4\pi k_0} \mathbf{J}_0 \int_{-a/2}^{a/2} \int_{-b/2}^{b/2} e^{ik_0[(\sin\phi - \sin\phi')\eta' + (\sin\beta\cos\phi - \sin\beta'\cos\phi')\zeta']} d\eta' d\zeta' \\ &= \frac{e^{ik_0 r}}{r} \cdot \frac{iZ_0 ab}{4\pi k_0} \mathbf{J}_0 \frac{\sin U}{U} \cdot \frac{\sin V}{V} \end{aligned} \tag{B.67}$$

where

$$U = \frac{k_0 a}{2}(\sin\phi - \sin\phi'), \tag{B.68}$$

$$V = \frac{k_0 b}{2}(\sin\beta\cos\phi - \sin\beta'\cos\phi'). \tag{B.69}$$

The scattered electric field and its far-field approximation are obtained by

$$\mathbf{E}^s(\mathbf{r}) = \nabla \times \nabla \times \boldsymbol{\Pi}(\mathbf{r}) \cong (ik_0 \hat{\mathbf{k}}_s) \times [(ik_0 \hat{\mathbf{k}}_s) \times \boldsymbol{\Pi}(\mathbf{r})] \tag{B.70}$$

and the far-field amplitude ($\mathbf{S}$) is defined in terms of

$$\mathbf{E}^s(\mathbf{r}) = \frac{e^{ik_0 r}}{r} \mathbf{S}. \tag{B.71}$$

Therefore the far field amplitude, using (B.58) and (B.61), has the following form

$$\mathbf{S} = \frac{iZ_0 ab}{4\pi} \cdot k_0 \frac{\sin U}{U} \cdot \frac{\sin V}{V} [\mathbf{J}_0 - (\hat{\mathbf{k}}_s \cdot \mathbf{J}_0)\hat{\mathbf{k}}_s]. \tag{B.72}$$

The scattered electric field can be decomposed into vertical (parallel to $\hat{\mathbf{v}}_s$) and horizontal (parallel to $\hat{\mathbf{h}}_s$) components from which, and together with the definition (B.11), the scattering matrix can be obtained. After some algebraic manipulations the following entries of the scattering matrix are obtained

$$\begin{aligned}
S_{vv} &= \frac{-iab}{\lambda}\frac{\sin U}{U}\frac{\sin V}{V}P^2\{\cos\phi\cos\beta[(\sin\theta_i\sin\theta_j+\cos\theta_i\cos\theta_j\cos(\phi_i-\phi_j))\\
&\cdot(\sin\theta_s\sin\theta_j+\cos\theta_s\cos\theta_j\cos(\phi_s-\phi_j))+\cos\theta_i\sin(\phi_i-\phi_j)\cos\theta_s\sin(\phi_s-\phi_j)]\\
&\cdot(\Gamma_H-\Gamma_E)\\
&+[\cos(\phi_i-\phi_j)(\sin\theta_s\sin\theta_j+\cos\theta_s\cos\theta_j\cos(\phi_s-\phi_j))+\cos\theta_j\sin(\phi_i-\phi_j)\\
&\cdot\cos\theta_s\sin(\phi_s-\phi_j)]\cdot(\Gamma_H-\cos^2\beta\cos^2\phi\Gamma_E)\} \qquad \text{(B.73)}
\end{aligned}$$

$$\begin{aligned}
S_{vh} &= \frac{-iab}{\lambda}\frac{\sin U}{U}\frac{\sin V}{V}P^2\{\cos\phi\cos\beta[-\cos\theta_j\sin(\phi_i-\phi_j)\\
&\cdot(\sin\theta_s\sin\theta_j+\cos\theta_s\cos\theta_j\cos(\phi_s-\phi_j))+\cos(\phi_i-\phi_j)\cos\theta_s\sin(\phi_s-\phi_j)]\\
&\cdot(\Gamma_H-\Gamma_E)+[-\cos\theta_i\sin(\phi_i-\phi_j)(\sin\theta_s\sin\theta_j+\cos\theta_s\cos\theta_j\cos(\phi_s-\phi_j))\\
&+(\sin\theta_i\sin\theta_j+\cos\theta_i\cos\theta_j\cos(\phi_i-\phi_j))\\
&\cdot\cos\theta_s\sin(\phi_s-\phi_j)]\cdot(\Gamma_H-\cos^2\beta\cos^2\phi\Gamma_E)\} \qquad \text{(B.74)}
\end{aligned}$$

$$\begin{aligned}
S_{hv} &= \frac{-iab}{\lambda}\frac{\sin U}{U}\frac{\sin V}{V}P^2\{\cos\phi\cos\beta[(\sin\theta_i\sin\theta_j+\cos\theta_i\cos\theta_j\cos(\phi_i-\phi_j))\\
&\cdot\cos\theta_j\sin(\phi_j-\phi_s)+\cos\theta_i\sin(\phi_i-\phi_j)\cos(\phi_s-\phi_j)](\Gamma_H-\Gamma_E)\\
&+[\cos(\phi_i-\phi_j)\cos\theta_j\sin(\phi_j-\phi_s)+\cos\theta_j\sin(\phi_i-\phi_j)\cos(\phi_s-\phi_j)]\\
&\cdot(\Gamma_H-\cos^2\beta\cos^2\phi\Gamma_E)\} \qquad \text{(B.75)}
\end{aligned}$$

$$\begin{aligned}
S_{hh} &= \frac{-iab}{\lambda}\frac{\sin U}{U}\frac{\sin V}{V}P^2\{\cos\phi\cos\beta[-\cos\phi_j\sin(\phi_i-\phi_j)\cos\theta_j\sin(\phi_j-\phi_s)\\
&+\cos(\phi_i-\phi_j)\cos(\phi_s-\phi_j)](\Gamma_H-\Gamma_E)+[-\cos\theta_i\sin(\phi_i-\phi_j)\cos\theta_j\sin(\phi_j-\phi_s)
\end{aligned}$$

$$+(\sin\theta_i \sin\theta_j + \cos\theta_i \cos\theta_j \cos(\phi_i - \phi_j)) \cos(\phi_s - \phi_j)]$$

$$\cdot(\Gamma_H - \cos^2\beta \cos^2\phi \Gamma_E)\} \tag{B.76}$$

B.4 Scattering Matrix for a Single Branch

Figure B.4 shows the scattering geometry for an arbitrarily oriented cylinder. The unprimed coordinates represent the canopy coordinate system while the primed coordinate system represents the coordinates local to the cylinder. The cylinder z' axis forms an angle θ_c to the zenith direction z and the cylinder rotation angle is given by ϕ_c. $\hat{\mathbf{k}}_i$ is the unit vector pointing in the direction of propagation of the incident plane wave while $\hat{\mathbf{k}}_s$ points in the direction of the scattered wave.

The primed unit vectors are, in terms of the unprimed coordinates,

$$\hat{\mathbf{x}}' = \cos\theta_c \cos\phi_c \hat{\mathbf{x}} + \cos\theta_c \sin\phi_c \hat{\mathbf{y}} - \sin\theta_c \hat{\mathbf{z}} \tag{B.77}$$

$$\hat{\mathbf{y}}' = -\sin\phi_c \hat{\mathbf{x}} + \cos\phi_c \hat{\mathbf{y}} \tag{B.78}$$

$$\hat{\mathbf{z}}' = \sin\theta_c \cos\phi_c \hat{\mathbf{x}} + \sin\theta_c \sin\phi_c \hat{\mathbf{y}} + \cos\theta_c \hat{\mathbf{z}} \tag{B.79}$$

and the cylindrical coordinate unit vectors for the scattered wave are

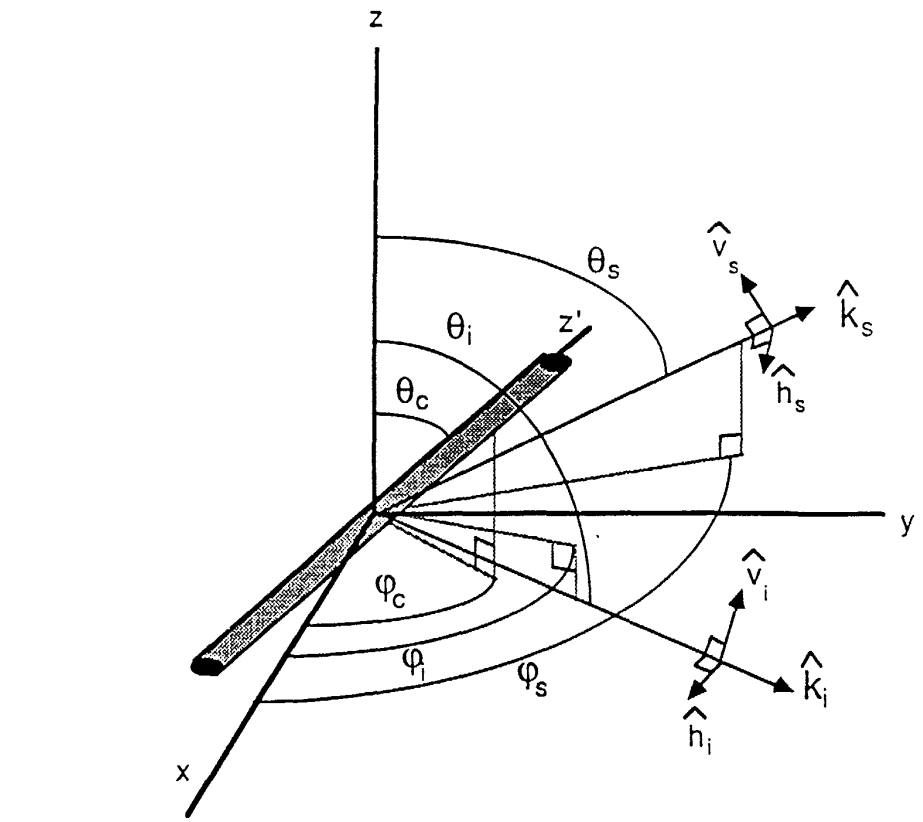
$$\hat{\mathbf{z}}_c = \hat{\mathbf{z}}' \tag{B.80}$$

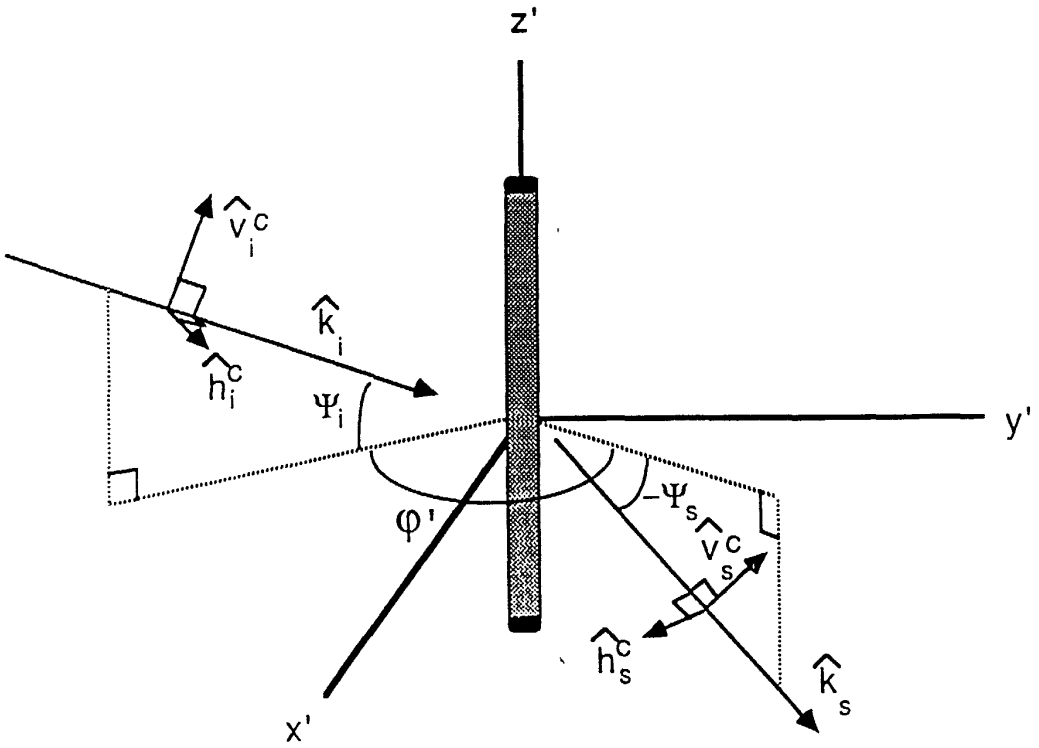
$$\hat{\mathbf{r}}_c = \frac{\hat{\mathbf{k}}_s - \left(\hat{\mathbf{z}}_c \cdot \hat{\mathbf{k}}_s\right) \hat{\mathbf{z}}_c}{\left|\hat{\mathbf{k}}_s - \left(\hat{\mathbf{z}}_c \cdot \hat{\mathbf{k}}_s\right) \hat{\mathbf{z}}_c\right|} \tag{B.81}$$

$$\hat{\boldsymbol{\phi}}_c = \hat{\mathbf{z}}_c \times \hat{\mathbf{r}}_c. \tag{B.82}$$

An arbitrary wave incident on the cylinder may be expressed as

$$\mathbf{E}^i = \left(E_v^i \hat{\mathbf{v}}_i + E_h^i \hat{\mathbf{h}}_i\right) e^{ik_0 \hat{\mathbf{k}}_i \cdot \mathbf{r}} \tag{B.83}$$


z
θs
θi
z'
θc
y
φc
φi
φs
x
$\hat{v}_s$
$\hat{k}_s$
$\hat{h}_s$
$\hat{v}_i$
$\hat{k}_i$
$\hat{h}_i$


z'
$\hat{v}_i^c$
$\hat{k}_i$
$\hat{h}_i^c$
Ψi
y'
φ'
-Ψs
$\hat{v}_s^c$
$\hat{h}_s^c$
$\hat{k}_s$
x'

where $\hat{\mathbf{v}}_i$ and $\hat{\mathbf{h}}_i$ are the vertical and horizontal polarization unit vectors in the unprimed coordinate system for the incident field. Similarly, the scattered field may be written as

$$\mathbf{E}^s = \left(E_v^s \hat{\mathbf{v}}_s + E_h^s \hat{\mathbf{h}}_s\right) e^{ik_0 \hat{\mathbf{k}}_s \cdot \mathbf{r}} \tag{B.84}$$

where $\hat{\mathbf{v}}_s$ and $\hat{\mathbf{h}}_s$ are the vertical and horizontal polarization unit vectors in the unprimed coordinate system for the scattered field.

The polarization vectors $\hat{\mathbf{v}}_i^c$ and $\hat{\mathbf{h}}_i^c$ incident on the cylinder are given by

$$\hat{\mathbf{h}}_i^c = \frac{\hat{\mathbf{k}}_i \times \hat{\mathbf{z}}'}{\left|\hat{\mathbf{k}}_i \times \hat{\mathbf{z}}'\right|} \tag{B.85}$$

$$\hat{\mathbf{v}}_i^c = \frac{\hat{\mathbf{h}}_i^c \times \hat{\mathbf{k}}_i}{\left|\hat{\mathbf{h}}_i^c \times \hat{\mathbf{k}}_i\right|}. \tag{B.86}$$

Similarly, the polarization vectors for the scattered field local to the cylinder coordinates are

$$\hat{\mathbf{h}}_s^c = \frac{\hat{\mathbf{k}}_s \times \hat{\mathbf{z}}'}{\left|\hat{\mathbf{k}}_s \times \hat{\mathbf{z}}'\right|} \tag{B.87}$$

$$\hat{\mathbf{v}}_s^c = \frac{\hat{\mathbf{h}}_s^c \times \hat{\mathbf{k}}_s}{\left|\hat{\mathbf{h}}_s^c \times \hat{\mathbf{k}}_s\right|}. \tag{B.88}$$

The transformation of the incident field from the unprimed reference frame to the reference frame of the cylinder is

$$E_i^{TM} \hat{\mathbf{v}}_i^c = \left[E_v^i \left(\hat{\mathbf{v}}_i \cdot \hat{\mathbf{v}}_i^c\right) + E_h^i \left(\hat{\mathbf{h}}_i \cdot \hat{\mathbf{v}}_i^c\right)\right] \hat{\mathbf{v}}_i^c \tag{B.89}$$

$$E_i^{TE} \hat{\mathbf{h}}_i^c = \left[E_v^i \left(\hat{\mathbf{v}}_i \cdot \hat{\mathbf{h}}_i^c\right) + E_h^i \left(\hat{\mathbf{h}}_i \cdot \hat{\mathbf{h}}_i^c\right)\right] \hat{\mathbf{h}}^c \tag{B.90}$$

so that the incident field on the cylinder may be expressed as

$$\mathbf{E}_i = \left(E_i^{TM} \hat{\mathbf{v}}_i^c + E_i^{TE} \hat{\mathbf{h}}_i^c\right) e^{k_0 \hat{\mathbf{k}}_i \cdot \mathbf{r}} \tag{B.91}$$

where E_i^{TM} is the component of the incident electric field that lies along the vertically polarized direction relative to the cylinder and E_i^{TE} is the component that lies along the horizontally polarized direction. Here, a time dependence $e^{-i\omega t}$ has been assumed and suppressed.

The TE incident magnetic field is given by

$$H_i^{TE} = -\frac{1}{\eta_0} E_i^{TE} \tag{B.92}$$

where η_0 is the intrinsic impedance of free space. The z' components of the incident field on the cylinder are then

$$E_{z,i}^{TM} = E_i^{TM} \cos\psi_i \exp\left[ik_0\left(-z\sin\psi_i - x\cos\psi_i\right)\right] \tag{B.93}$$

and

$$H_{z,i}^{TE} = H_i^{TE} \cos\psi_i \exp\left[ik_0\left(-z\sin\psi_i - x\cos\psi_i\right)\right] \tag{B.94}$$

where the angle of incidence ψ_i is

$$\psi_i = \frac{\pi}{2} - \cos^{-1}\left(-\hat{\mathbf{z}}' \cdot \hat{\mathbf{k}}_i\right). \tag{B.95}$$

The scattering plane is defined by the angle

$$\phi' = \cos^{-1}\left(-\hat{\mathbf{a}} \cdot \hat{\mathbf{b}}\right) \tag{B.96}$$

where

$$\hat{\mathbf{a}} = \frac{\hat{\mathbf{k}}_i - \left(\hat{\mathbf{k}}_i \cdot \hat{\mathbf{z}}'\right)\hat{\mathbf{z}}'}{\left|\hat{\mathbf{k}}_i - \left(\hat{\mathbf{k}}_i \cdot \hat{\mathbf{z}}'\right)\hat{\mathbf{z}}'\right|} \tag{B.97}$$

$$\hat{\mathbf{b}} = \frac{\hat{\mathbf{k}}_s - \left(\hat{\mathbf{k}}_s \cdot \hat{\mathbf{z}}'\right)\hat{\mathbf{z}}'}{\left|\hat{\mathbf{k}}_s - \left(\hat{\mathbf{k}}_s \cdot \hat{\mathbf{z}}'\right)\hat{\mathbf{z}}'\right|}. \tag{B.98}$$

In the far-field, the electric field scattered from an infinitely long cylinder for the TM incident case is given by Ruck et al, 1970, as

$$E_z^{s,TM} = \sqrt{\frac{2}{\pi}} \frac{E_i^{TM} \sqrt{\cos\psi_i} \exp\left[i\left(-k_0 z \sin_i \psi + k_0 r \cos\psi_i - \frac{\pi}{4}\right)\right]}{\sqrt{k_0 r}} \sum_{n=-\infty}^{\infty} (-1)^n C_n^{TM} e^{in\phi'} \tag{B.99}$$

$$E_\phi^{s,TM} = \sqrt{\frac{2}{\pi}} \frac{E_i^{TM} \exp\left[i\left(-k_0 z \sin\psi_i + k_0 r \cos\psi_i - \frac{\pi}{4}\right)\right]}{\sqrt{k_0 r \cos\psi_i}} \sum_{n=-\infty}^{\infty} (-1)^n \bar{C}_n e^{in\phi'} \tag{B.100}$$

$$E_r^{s,TM} = E_z^{s,TM} \tan\psi_i. \tag{B.101}$$

and the scattered magnetic field for the TE incident case is

$$H_z^{s,TE} = \sqrt{\frac{2}{\pi}} \frac{H_i^{TE} \sqrt{\cos\psi_i} \exp\left[i\left(-k_0 z \sin\psi_i + k_0 r \cos\psi_i - \frac{\pi}{4}\right)\right]}{\sqrt{k_0 r}} \sum_{n=-\infty}^{\infty} (-1)^n C_n^{TE} e^{in\phi'} \tag{B.102}$$

$$H_\phi^{s,TE} = \sqrt{\frac{2}{\pi}} \frac{H_i^{TE} \exp\left[i\left(-k_0 z \sin\psi_i + k_0 r \cos\psi - \frac{\pi}{4}\right)\right]}{\sqrt{k_0 r \cos\psi_i}} \sum_{n=-\infty}^{\infty} (-1)^n \bar{C}_n e^{in\phi'} \tag{B.103}$$

$$H_r^{s,TE} = H_z^{s,TE} \tan\psi_i \tag{B.104}$$

so that the scattered electric field for this case is

$$E_z^{s,TE} = -\sqrt{\frac{2}{\pi}} \frac{\eta_0 H_i^{TE} \sqrt{\cos\psi_i} \exp\left[i\left(-k_0 z \sin\psi_i + k_0 r \cos\psi_i - \frac{\pi}{4}\right)\right]}{\sqrt{k_0 r}} \sum_{n=-\infty}^{\infty} (-1)^n \bar{C}_n e^{in\phi'} \tag{B.105}$$

$$= \sqrt{\frac{2}{\pi}} \frac{E_i^{TE} \sqrt{\cos\psi_i} \exp\left[i\left(-k_0 z \sin\psi_i + k_0 r \cos\psi_i - \frac{\pi}{4}\right)\right]}{\sqrt{k_0 r}} \sum_{n=-\infty}^{\infty} (-1)^n \bar{C}_n e^{in\phi'} \tag{B.106}$$

$$E_\phi^{s,TE} = \sqrt{\frac{2}{\pi}} \frac{\eta_0 H_i^{TE} \exp\left[i\left(-k_0 z \sin\psi_i + k_0 r \cos\psi_i - \frac{\pi}{4}\right)\right]}{\sqrt{k_0 r \cos\psi_i}} \sum_{n=-\infty}^{\infty} (-1)^n C_n^{TE} e^{in\phi'} \tag{B.107}$$

$$= -\sqrt{\frac{2}{\pi}} \frac{E_i^{TE} \exp\left[i\left(-k_0 z \sin\psi_i + k_0 r \cos\psi_i - \frac{\pi}{4}\right)\right]}{\sqrt{k_0 r \cos\psi_i}} \sum_{n=-\infty}^{\infty} (-1)^n C_n^{TE} e^{in\phi'} \tag{B.108}$$

$$E_r^{s,TE} = E_z^{s,TE} \tan\psi_i. \tag{B.109}$$

The summation coefficients in (B.99) through (B.109) for a homogeneous cylinder with relative dielectric constant ϵ_r and diameter d are:

$$C_n^{TM} = -\frac{V_n P_n - q_n^2 J_n(x_0) H_n^{(1)}(x_0) J_n^2(x_1)}{P_n N_n - \left[q_n H_n^{(1)}(x_0) J_n(x_1)\right]^2} \tag{B.110}$$

$$C_n^{TE} = -\frac{M_n N_n - q_n^2 J_n(x_0) H_n^{(1)}(x_0) J_n^2(x_1)}{P_n N_n - \left[q_n H_n^{(1)}(x_0) J_n(x_1)\right]^2} \tag{B.111}$$

$$\tilde{C}_n = i\frac{2}{\pi x_0}\left[\frac{s_0 q_n J_n^2(x_1)}{P_n N_n - \left[q_n H_n^{(1)}(x_0) J_n(x_1)\right]^2}\right] \tag{B.112}$$

where

$$x_0 = \frac{k_0 d \cos\psi_i}{2} \tag{B.113}$$

$$x_1 = \frac{k_0 d}{2}\sqrt{\epsilon_r - \sin^2\psi_i} \tag{B.114}$$

$$q_n = \frac{n \sin\psi_i}{\frac{k_0 d}{2}}\left(\frac{1}{\epsilon_r - \sin^2\psi_i} - \frac{1}{\cos^2\psi_i}\right) \tag{B.115}$$

$$V_n = s_1 J_n(x_0) J_n'(x_1) - s_0 J_n'(x_0) J_n(x_1) \tag{B.116}$$

$$P_n = r_1 H_n^{(1)}(x_0) J_n'(x_1) - s_0 H_n'^{(1)}(x_0) J_n(x_1) \tag{B.117}$$

$$N_n = s_1 H_n^{(1)}(x_0) J_n'(x_1) - s_0 H_n'^{(1)}(x_0) J_n(x_1) \tag{B.118}$$

$$M_n = r_1 J_n(x_0) J_n'(x_1) - s_0 J_n'(x_0) J_n(x_1) \tag{B.119}$$

and

$$s_0 = \frac{1}{\cos\psi_i}\ , \quad s_1 = \frac{\epsilon_r}{\sqrt{\epsilon_r - \sin^2\psi_i}}\ , \quad r_1 = \frac{1}{\sqrt{\epsilon_r - \sin^2\psi_i}}. \tag{B.120}$$

Here, $J_n(\ )$ and $J_n'(\ )$ represent the Bessel functions of the first kind of order n and their derivatives and $H_n^{(1)}(\ )$ and $H_n'^{(1)}(\ )$ represent the Hankel functions of the first kind of order n and their derivatives.

The total scattered field from the infinite cylinder is

$$\mathbf{E}^{s,inf} = \mathbf{E}^{s,TM} + \mathbf{E}^{s,TE} \tag{B.121}$$

where the contributions from each of the polarizations are themselves composed of

three terms

$$\mathbf{E}^{s,p} = E_z^{s,p}\hat{\mathbf{z}}_c + E_\phi^{s,p}\hat{\boldsymbol{\phi}}_c + E_r^{s,p}\hat{\mathbf{r}}_c, \quad p = TE \text{ or } TM. \tag{B.122}$$

It follows that the total scattered electric field in the cylindrical coordinate system is

$$\begin{aligned}\mathbf{E}^{s,inf} &= \left(E_z^{s,TM} + E_z^{s,TE}\right)\hat{\mathbf{z}}_c + \left(E_\phi^{s,TM} + E_\phi^{s,TE}\right)\hat{\boldsymbol{\phi}}_c \\ &\quad + \left(E_r^{s,TM} + E_r^{s,TE}\right)\hat{\mathbf{r}}_c\end{aligned} \tag{B.123}$$

which yields

$$\begin{aligned}\mathbf{E}^{s,inf} &= A\Bigg\{\cos\psi_i\left[\sum_{n=-\infty}^{\infty}(-1)^n\left(E_i^{TM}C_n^{TM} + E_i^{TE}\bar{C}_n\right)e^{in\phi'}\right]\hat{\mathbf{z}}_c \\ &\quad + \left[\sum_{n=-\infty}^{\infty}(-1)^n\left(E_i^{TM}\bar{C}_n - E_i^{TE}C_n^{TE}\right)e^{in\phi'}\right]\hat{\boldsymbol{\phi}}_c \\ &\quad + \sin\psi_i\left[\sum_{n=-\infty}^{\infty}(-1)^n\left(E_i^{TM}C_n^{TM} + E_i^{TE}\bar{C}_n\right)e^{in\phi'}\right]\hat{\mathbf{r}}_c\Bigg\}\end{aligned} \tag{B.124}$$

where

$$A = \sqrt{\frac{2}{\pi}}\frac{\exp\left[i\left(-k_0 z\sin\psi_i + k_0 r\cos\psi_i - \frac{\pi}{4}\right)\right]}{\sqrt{k_0 r\cos\psi_i}}. \tag{B.125}$$

In the far-field, (B.124) may be written in terms of the scattered field polarization vectors as

$$\begin{aligned}\mathbf{E}^{s,inf} &= A\Bigg\{\left[\sum_{n=-\infty}^{\infty}(-1)^n\left(E_i^{TM}C_n^{TM} + E_i^{TE}\bar{C}_n\right)e^{in\phi'}\right]\hat{\mathbf{v}}_s^{c,inf} \\ &\quad - \left[\sum_{n=-\infty}^{\infty}(-1)^n\left(E_i^{TM}\bar{C}_n - E_i^{TE}C_n^{TE}\right)e^{in\phi'}\right]\hat{\mathbf{h}}_s^{c,inf}\Bigg\}\end{aligned} \tag{B.126}$$

where the polarizartion vectors $\hat{\mathbf{v}}_s^{c,inf}$ and $\hat{\mathbf{h}}_s^{c,inf}$ define the direction of propagation of the field scattered by the infinitely long cylinder such that

$$\hat{\mathbf{v}}_s^{c,inf} \times \hat{\mathbf{h}}_s^{c,inf} = \hat{\mathbf{k}}_s^{inf}. \tag{B.127}$$

All power scattered from the infinite cylinder propagates in the cone which forms the angle $\psi_s^{inf} = -\psi_i$ with respect to the $x' - y'$ plane. For the finite cylinder, however, scattered power propagates at an arbitrary ψ_s given by

$$\psi_s = \frac{\pi}{2} - \cos^{-1}\left(\hat{\mathbf{z}}' \cdot \hat{\mathbf{k}}_s\right). \tag{B.128}$$

In order to account for the difference in propagation direction between the infinite and the finite cylinders, the scattered field polarization vectors for the finite cylinder given in (B.84) must be related to the scattered field polarization vectors of the infinite cylinder. The direction of propagation in the specular cone of the infinite cylinder is

$$\hat{\mathbf{k}}_s^{inf} = \hat{\mathbf{b}} \cos\psi_s^{inf} + \hat{\mathbf{z}}' \sin\psi_s^{inf} \tag{B.129}$$

$$= \hat{\mathbf{b}} \cos\psi_i - \hat{\mathbf{z}}' \sin\psi_i. \tag{B.130}$$

The horizontal polarization vector local to the cylinder for the field scattered by the infinite cylinder is

$$\hat{\mathbf{h}}_s^{c,inf} = \hat{\mathbf{h}}_s^c \tag{B.131}$$

where $\hat{\mathbf{h}}_s^c$ is given by (B.87). The vertical polarization vector local to the cylinder in the specular cone is determined from

$$\hat{\mathbf{v}}_s^{c,inf} = \frac{\hat{\mathbf{k}}_s^{inf} \times \hat{\mathbf{h}}_s^{c,inf}}{\left|\hat{\mathbf{k}}_s^{inf} \times \hat{\mathbf{h}}_s^{c,inf}\right|}. \tag{B.132}$$

The relationships

$$\hat{\mathbf{h}}_s^{inf} = \left(\hat{\mathbf{h}}_s \cdot \hat{\mathbf{h}}_s^c\right) \hat{\mathbf{h}}_s^{c,inf} + \left(\hat{\mathbf{h}}_s \cdot \hat{\mathbf{v}}_s^c\right) \hat{\mathbf{v}}_s^{c,inf} \tag{B.133}$$

$$\hat{\mathbf{v}}_s^{inf} = \left(\hat{\mathbf{v}}_s \cdot \hat{\mathbf{h}}_s^c\right) \hat{\mathbf{h}}_s^{c,inf} + \left(\hat{\mathbf{v}}_s \cdot \hat{\mathbf{v}}_s^c\right) \hat{\mathbf{v}}_s^{c,inf}. \tag{B.134}$$

are applied to transform the scattered electric field for the infinite cylinder into the unprimed reference frame.

The scattered field from the infinite cylinder may now be written in terms of the matrix equation

$$\begin{bmatrix} E_v^{s,inf} \\ E_h^{s,inf} \end{bmatrix} = A \cdot \begin{bmatrix} T_{vv} & T_{vh} \\ T_{hv} & T_{hh} \end{bmatrix} \cdot \begin{bmatrix} E_v^i \\ E_h^i \end{bmatrix} \tag{B.135}$$

where

$$\begin{bmatrix} T_{vv} & T_{vh} \\ T_{hv} & T_{hh} \end{bmatrix} = \begin{bmatrix} \left(\hat{\mathbf{v}}_s^{c,inf} \cdot \hat{\mathbf{v}}_s^{inf}\right) & \left(\hat{\mathbf{h}}_s^{c,inf} \cdot \hat{\mathbf{v}}_s^{inf}\right) \\ \left(\hat{\mathbf{v}}_s^{c,inf} \cdot \hat{\mathbf{h}}_s^{inf}\right) & \left(\hat{\mathbf{h}}_s^{c,inf} \cdot \hat{\mathbf{h}}_s^{inf}\right) \end{bmatrix} \cdot \begin{bmatrix} T'_{vv} & T'_{vh} \\ T'_{hv} & T'_{hh} \end{bmatrix} \cdot \begin{bmatrix} (\hat{\mathbf{v}}_i \cdot \hat{\mathbf{v}}_i^c) & \left(\hat{\mathbf{h}}_i \cdot \hat{\mathbf{v}}_i^c\right) \\ \left(\hat{\mathbf{v}}_i \cdot \hat{\mathbf{h}}_i^c\right) & \left(\hat{\mathbf{h}}_i \cdot \hat{\mathbf{h}}_i^c\right) \end{bmatrix} \tag{B.136}$$

with

$$T'_{vv} = \sum_{n=-\infty}^{\infty} (-1)^n C_n^{TM} e^{in\phi'} \tag{B.137}$$

$$T'_{vh} = \sum_{n=-\infty}^{\infty} (-1)^n \bar{C}_n e^{in\phi'} \tag{B.138}$$

$$T'_{hv} = -\sum_{n=-\infty}^{\infty} (-1)^n \bar{C}_n e^{in\phi'} \tag{B.139}$$

$$T'_{hh} = \sum_{n=-\infty}^{\infty} (-1)^n C_n^{TE} e^{in\phi'}. \tag{B.140}$$

In order to transform (B.135) to the finite cylinder case, it is assumed that the length l_c of the cylinder is such that $l_c >> \lambda$ or that the cylinder dimensions are such that the relations $0.5 < k_0\frac{d}{2} < 10$ and $l_c >> \frac{d}{2}$ hold. In this case, Van de hulst, 1957, approximated the scattered field for the finite cylinder. In matrix

notation, the scattered field is

$$\begin{bmatrix} E_v^s \\ E_h^s \end{bmatrix} = \frac{e^{ikr}}{r} \left[Q\left(\psi_i, \psi_s\right) \right] \begin{bmatrix} T_{vv}\left(\psi_s, \psi_i, \phi'\right) & T_{vh}\left(\psi_s, \psi_i, \phi'\right) \\ T_{hv}\left(\psi_s, \psi_i, \phi'\right) & T_{hh}\left(\psi_s, \psi_i, \phi'\right) \end{bmatrix} \cdot \begin{bmatrix} E_v^i \\ E_h^i \end{bmatrix} \quad \text{(B.141)}$$

where

$$Q\left(\psi_i, \psi_s\right) = \frac{-il_c \cos\psi_s}{\pi \cos\psi_i} \left\{ \frac{\sin\left[k_0\left(\sin\psi_i + \sin\psi_s\right)\frac{l_c}{2}\right]}{\left[k_0\left(\sin\psi_i + \sin\psi_s\right)\frac{l_c}{2}\right]} \right\}. \quad \text{(B.142)}$$

so that the scattering matrix for the arbitrarily oriented cylinder is

$$\mathbf{S} = Q \begin{bmatrix} \left(\hat{\mathbf{v}}_s^c \cdot \hat{\mathbf{v}}_s\right) & \left(\hat{\mathbf{h}}_s^c \cdot \hat{\mathbf{v}}_s\right) \\ \left(\hat{\mathbf{v}}_s^c \cdot \hat{\mathbf{h}}_s\right) & \left(\hat{\mathbf{h}}_s^c \cdot \hat{\mathbf{h}}_s\right) \end{bmatrix} \cdot \begin{bmatrix} T'_{vv} & T'_{vh} \\ T'_{hv} & T'_{hh} \end{bmatrix} \cdot \begin{bmatrix} \left(\hat{\mathbf{v}}_i \cdot \hat{\mathbf{v}}_i^c\right) & \left(\hat{\mathbf{h}}_i \cdot \hat{\mathbf{v}}_i^c\right) \\ \left(\hat{\mathbf{v}}_i \cdot \hat{\mathbf{h}}_i^c\right) & \left(\hat{\mathbf{h}}_i \cdot \hat{\mathbf{h}}_i^c\right) \end{bmatrix} \quad \text{(B.143)}$$

Given the previously stated constraints on the cylinder dimensions, the only region of error for (B.143) is at angles of incidence at or near end-on ($\psi_i \simeq \frac{\pi}{2}$).

B.5 Scattering Matrix for a Single Needle

The scattering geometry of an arbitrarily oriented needle may also be represented by the cylinder geometry shown in Figure B.4. In this case, the scattering matrix in unprimed canopy coordinates may be related to the scattering matrix in primed coordinates by

$$\mathbf{S} = \begin{bmatrix} \left(\hat{\mathbf{v}}_s^c \cdot \hat{\mathbf{v}}_s\right) & \left(\hat{\mathbf{h}}_s^c \cdot \hat{\mathbf{v}}_s\right) \\ \left(\hat{\mathbf{v}}_s^c \cdot \hat{\mathbf{h}}_s\right) & \left(\hat{\mathbf{h}}_s^c \cdot \hat{\mathbf{h}}_s\right) \end{bmatrix} \cdot \begin{bmatrix} S'_{vv} & S'_{vh} \\ S'_{hv} & S'_{hh} \end{bmatrix} \cdot \begin{bmatrix} \left(\hat{\mathbf{v}}_i \cdot \hat{\mathbf{v}}_i^c\right) & \left(\hat{\mathbf{h}}_i \cdot \hat{\mathbf{v}}_i^c\right) \\ \left(\hat{\mathbf{v}}_i \cdot \hat{\mathbf{h}}_i^c\right) & \left(\hat{\mathbf{h}}_i \cdot \hat{\mathbf{h}}_i^c\right) \end{bmatrix} \quad \text{(B.144)}$$

where the polarization vectors are those illustrated in Figure B.4.

If the needle is assumed to have a diameter d_c that is much less than the radar wavelength ($d_c \ll \lambda$) and a length l such that $l > d_c$ and $l \ll \lambda$ then it may be modeled as a prolate spheroid [Tsang et al., 1985, p.160] with semi-axes a_e, b_e and

c_e given by

$$a_e = \frac{1}{2}\left(\frac{3}{2}\right)^{\frac{1}{3}} d_c \tag{B.145}$$

$$b_e = a_e \tag{B.146}$$

$$c_e = \frac{1}{2}\left(\frac{3}{2}\right)^{\frac{1}{3}} l. \tag{B.147}$$

The scattering matrix elements of a prolate spheroid relative dielectric $\epsilon_n = \epsilon_r' + i\epsilon_r''$ are

$$S'_{vv} = \frac{k_0^2}{4\pi} V_0 (\epsilon_n - 1) \frac{1}{1 + V_d A_a} \tag{B.148}$$

$$S'_{vh} = 0 \tag{B.149}$$

$$S'_{hv} = 0 \tag{B.150}$$

$$S'_{hh} = \frac{k_0^2}{4\pi} V_0 (\epsilon_n - 1) \frac{1}{1 + V_d A_c} \tag{B.151}$$

where

$$V_0 = \frac{4\pi}{3} a_e b_e c_e \tag{B.152}$$

$$V_d = \frac{a_e b_e c_e}{2} (\epsilon_n - 1) \tag{B.153}$$

$$A_c = -\frac{1}{c_e^3 e^3}\left[2e + \ln\frac{1-e}{1+e}\right] \tag{B.154}$$

$$A_a = \frac{1}{2}\left(\frac{2}{a_e b_e c_e} - A_c\right) \tag{B.155}$$

$$\tag{B.156}$$

with $e = \sqrt{1 - a_e^2/c_e^2}$.

The incident field polarization vectors are defined by Equations (B.4), (B.5), (B.85) and (B.86). The scattered field polarization vectors are defined by Equations (B.8), (B.9), (B.87) and (B.88).

APPENDIX C PHASE AND EXTINCTION MATRICES OF THE TRUNK LAYER

This appendix provides the formulations for computing the phase and extinction matrices of the trunk layer. The trunks are modeled as identical finite-length vertically-oriented homogeneous dielectric cylinders. Section C.1 gives the form of these matrices in terms of the elements of the scattering matrix. Section C.2 gives the scattering matrix for a finite length vertically-oriented cylinder. This development may easily be extended to account for trunks of differing sizes that are distributed in the neighborhood of the vertical direction by applying the techniques discussed in Appendix B for and arbitrarily oriented cylinder.

C.1 Phase and Extinction Matrices of the Trunk Layer

Two types of scattering are considered within the trunk layer. These are forward scattering from the trunks that gives rise to extinction of the forward propagating field and specular scattering from the trunks that gives rise to a ground-trunk interaction contribution to the field backscattered from the canopy. In both cases, the depolarized components of the scattered field vanish.

The general form of the Stokes matrix for the trunk layer is given in terms of the scattering matrix elements by (B.14). When considering cases in which the

cross-polarized scattered field vanishes, (B.14) reduces to

$$\mathbf{L} = \begin{bmatrix} |S_{vv}|^2 & 0 & 0 & 0 \\ 0 & |S_{hh}^*|^2 & 0 & 0 \\ 0 & 0 & Re(S_{vv}S_{hh}^*) & -Im(S_{vv}S_{hh}^*) \\ 0 & 0 & Im(S_{vv}S_{hh}^*) & Re(S_{vv}S_{hh}^*) \end{bmatrix}. \tag{C.1}$$

The phase matrix for a trunk layer of height H_t and density N_t trunks per square meter is then

$$\mathbf{P}_d(\theta_s, \phi_s; \theta_i, \phi_i) = \frac{N_t}{H_t}\mathbf{L}(\theta_s, \phi_s; \theta_i, \phi_i) \tag{C.2}$$

where (θ_i, ϕ_i) and (θ_s, ϕ_s) are the angles of incidence and scattering, respectively.

The form of the extinction matrix $\boldsymbol{\kappa}$ is given by (B.24). For cases in which the cross-polarized scattered field vanishes the extinction matrix reduces to

$$\boldsymbol{\kappa} = \begin{bmatrix} -2Re(M_{vv}) & 0 & 0 & 0 \\ 0 & -2Re(M_{hh}) & 0 & 0 \\ 0 & 0 & -[Re(M_{vv}) + Re(M_{hh})] & [Im(M_{vv}) - Im(M_{hh})] \\ 0 & 0 & -[Im(M_{vv}) - Im(M_{hh})] & -[Re(M_{vv}) + Re(M_{hh})] \end{bmatrix} \tag{C.3}$$

where

$$M_{pp} = \frac{i2\pi\left(\frac{N_t}{H_t}\right)}{k_0} S_{pp}. \tag{C.4}$$

C.2 Scattering Matrix for a Single Cylinder

Figure C.1 illustrates the geometry of the cylinder scattering problem. Here, $\hat{\mathbf{k}}_o^i$ and $\hat{\mathbf{k}}_o^s$ are the unit vectors pointing in the directions of propagation of the incident

and scattered waves, respectively. The vector $\hat{\mathbf{k}}_o^i$ lies in the $x-z$ plane and forms an angle ψ_i with respect to the $x-y$ plane. The vector $\hat{\mathbf{k}}_o^s$ forms an angle ϕ' with respect to the $x-z$ plane and an angle ψ_s with respect to the $x-y$ plane. When considering the geometry shown in Figure C.2, $\psi_i = \frac{\pi}{2} - \theta_0$ where θ_0 is the radar pointing angle from nadir. Specular scattering from the cylinder occurs at $\phi' = 0$ and $\psi_s = -\psi_i$ whereas forward scattering occurs at $\phi' = \pi$ and $\psi_s = -\psi_i$.

The TM polarized wave is defined as a wave whose electric-field vector is in the $x-z$ plane of the cylinder. This wave is also described as having parallel or vertical (v) polarization. The TE polarized wave is a wave whose electric-field vector is orthogonal to the $x-z$ plane. This wave may also be described as having perpendicular or horizontal (h) polarization.

The fields scattered from an infinitely long cylinder in the far-field are given by Ruck et al. (1970) and may be expressed in terms of a scattering matrix as

$$\begin{bmatrix} E_v^{s,inf} \\ E_h^{s,inf} \end{bmatrix} = \sqrt{\frac{2}{\pi}} \frac{e^{i(-k_0 z \sin\psi_i + k_0 r \cos\psi_i - \frac{\pi}{4})}}{\sqrt{k_0 r \cos\psi_i}} \begin{bmatrix} T_{vv}(\psi_i, \phi') & T_{vh}(\psi_i, \phi') \\ T_{hv}(\psi_i, \phi') & T_{hh}(\psi_i, \phi') \end{bmatrix} \cdot \begin{bmatrix} E_v^i \\ E_h^i \end{bmatrix} \quad \text{(C.5)}$$

where

$$T_{vv} = \sum_{n=-\infty}^{\infty} (-1)^n C_n^{TM} e^{in\phi'} \quad \text{(C.6)}$$

$$T_{vh} = \sum_{n=-\infty}^{\infty} (-1)^n \bar{C}_n e^{in\phi'} \quad \text{(C.7)}$$

$$T_{hv} = -\sum_{n=-\infty}^{\infty} (-1)^n \bar{C}_n e^{in\phi'} \quad \text{(C.8)}$$

$$T_{hh} = \sum_{n=-\infty}^{\infty} (-1)^n C_n^{TE} e^{in\phi'}. \quad \text{(C.9)}$$

Those quantities with TE superscripts designate values associated with TE or h-polarized incident waves and those with TM superscripts designate values asso-

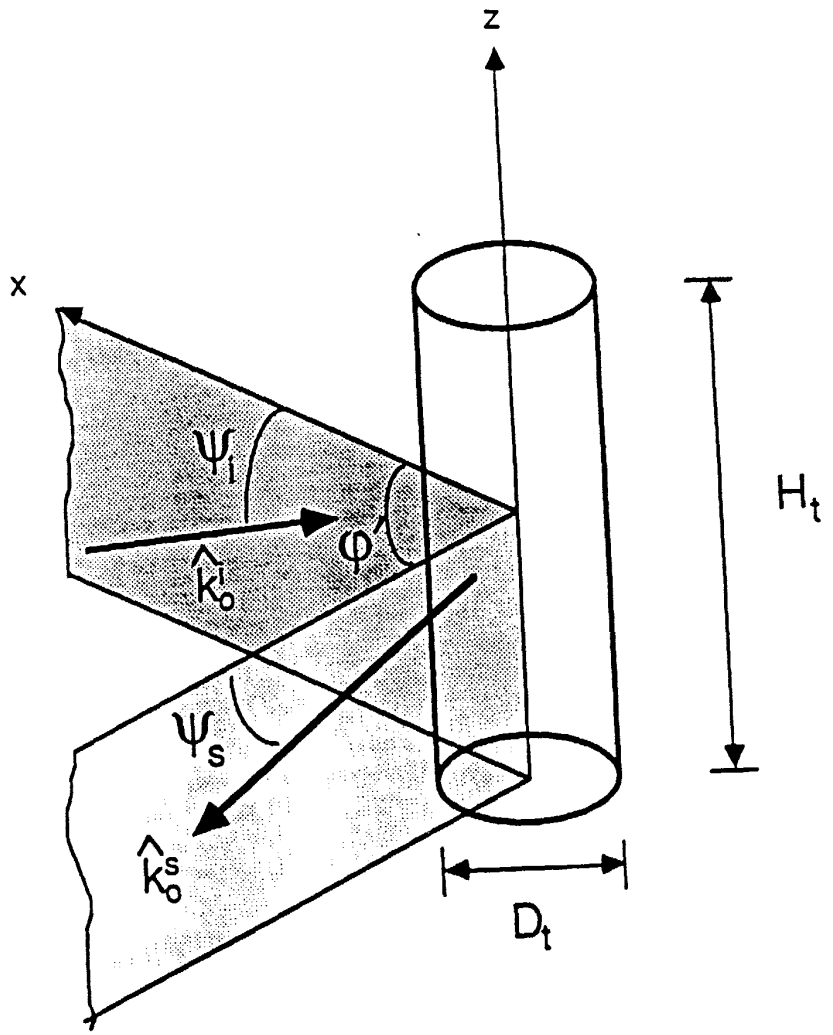


Figure C.1· Cylinder scattering geometry.

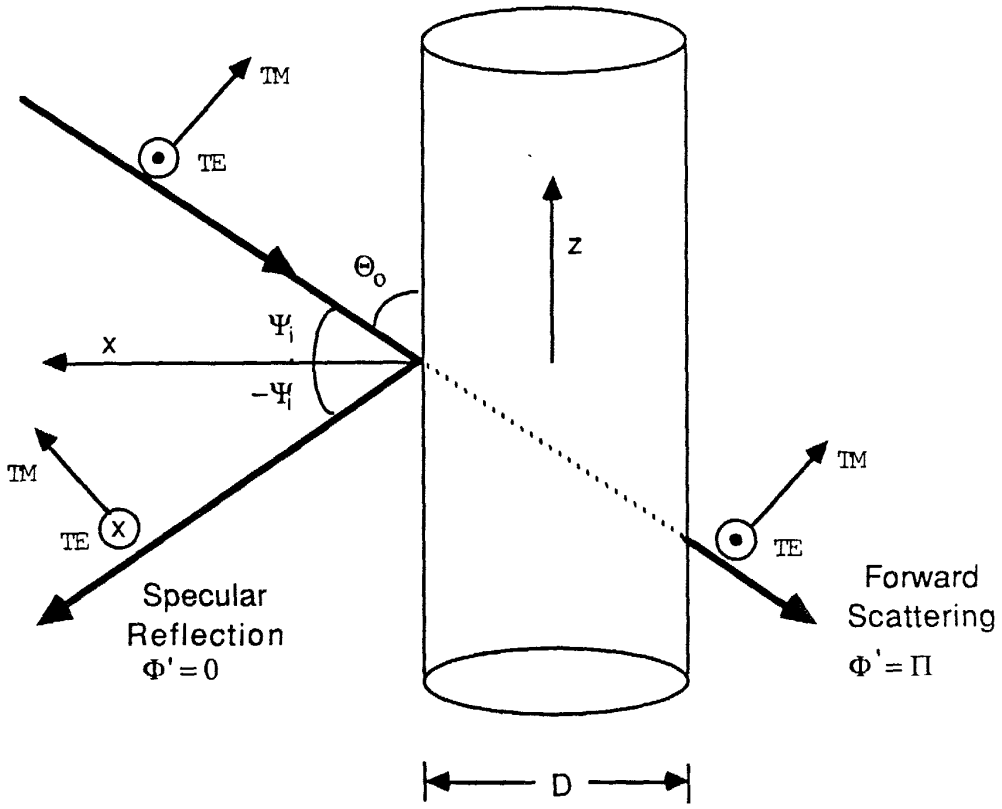


Figure C.2: Specular and forward scattering conditions.

ciated with TM or v-polarized incident waves. For a cylinder with a homogeneous relative dielectric constant ϵ_r, the summation coefficients are:

$$C_n^v = -\frac{V_n P_n - q_n^2 J_n(x_0) H_n^{(1)}(x_0) J_n^2(x_1)}{P_n N_n - \left[q_n H_n^{(1)}(x_0) J_n(x_1)\right]^2} \tag{C.10}$$

$$C_n^h = -\frac{M_n N_n - q_n^2 J_n(x_0) H_n^{(1)}(x_0) J_n^2(x_1)}{P_n N_n - \left[q_n H_n^{(1)}(x_0) J_n(x_1)\right]^2} \tag{C.11}$$

$$\bar{C}_n = i\frac{2}{\pi x_0}\left[\frac{s_0 q_n J_n^2(x_1)}{P_n N_n - \left[q_n H_n^{(1)}(x_0) J_n(x_1)\right]^2}\right] \tag{C.12}$$

where

$$x_0 = \frac{k_0 D_t \cos\psi_i}{2} \tag{C.13}$$

$$x_1 = \frac{k_0 D_t}{2}\sqrt{\epsilon_r - \sin^2\psi_i} \tag{C.14}$$

$$q_n = \frac{n \sin\psi_i}{\frac{k_0 D_t}{2}}\left(\frac{1}{\epsilon_r - \sin^2\psi_i} - \frac{1}{\cos^2\psi_i}\right) \tag{C.15}$$

$$V_n = s_1 J_n(x_0) J_n'(x_1) - s_0 J_n'(x_0) J_n(x_1) \tag{C.16}$$

$$P_n = r_1 H_n^{(1)}(x_0) J_n'(x_1) - s_0 H_n'^{(1)}(x_0) J_n(x_1) \tag{C.17}$$

$$N_n = s_1 H_n^{(1)}(x_0) J_n'(x_1) - s_0 H_n'^{(1)}(x_0) J_n(x_1) \tag{C.18}$$

$$M_n = r_1 J_n(x_0) J_n'(x_1) - s_0 J_n'(x_0) J_n(x_1) \tag{C.19}$$

and

$$s_0 = \frac{1}{\cos\psi_i}\ , \quad s_1 = \frac{\epsilon_r}{\sqrt{\epsilon_r - \sin^2\psi_i}}\ , \quad r_1 = \frac{1}{\sqrt{\epsilon_r - \sin^2\psi_i}}. \tag{C.20}$$

$J_n(\ )$ and $J_n'(\ )$ represent the Bessel functions of the first kind of order n and their derivatives. $H_n^{(1)}(\ )$ and $H_n'^{(1)}(\ )$ represent the Hankel functions of the first kind of order n and their derivatives. These expressions have assumed an $e^{-i\omega t}$ time dependence. All power scattered from the infinite cylinder propagates in the

cone which forms an angle $-\psi_i$ with respect to the $x-y$ plane.

In order to transform (C.5) to the finite cylinder case, it is assumed that the length H_t of the cylinder is such that $H_t >> \lambda$ or that the cylinder dimensions are such that the relations $0.5 < k_0\frac{D_t}{2} < 10$ and $H_t >> \frac{D_t}{2}$ hold. In this case, we use the approximate expressions given by Van de hulst (1957) and Ruck et al. (1970) for the field scattered by a finite cylinder. In terms of the scattering matrix, the scattered field far from the cylinder is

$$\begin{bmatrix} E_v^s \\ E_h^s \end{bmatrix} = \frac{e^{ik_0 r}}{r} \begin{bmatrix} S_{vv}(\psi_s, \psi_i, \phi') & S_{vh}(\psi_s, \psi_i, \phi') \\ S_{hv}(\psi_s, \psi_i, \phi') & S_{hh}(\psi_s, \psi_i, \phi') \end{bmatrix} \cdot \begin{bmatrix} E_v^i \\ E_h^i \end{bmatrix} \tag{C.21}$$

where

$$S_{rt}(\psi_s, \psi_i, \phi') = Q(\psi_i, \psi_s) \cdot T_{rt}(\psi_i, \phi') \tag{C.22}$$

with

$$Q(\psi_i, \psi_s) = \frac{-iH_t \cos\psi_s}{\pi \cos\psi_i} \left\{ \frac{\sin\left[k_0(\sin\psi_i + \sin\psi_s)\frac{H_t}{2}\right]}{\left[k_0(\sin\psi_i + \sin\psi_s)\frac{H_t}{2}\right]} \right\}. \tag{C.23}$$

Given the previously stated constraints on the cylinder dimensions, the only region of error for (C.21) is at angles of incidence at or near end-on ($\theta_0 \simeq 0$).

In both the forward and specular scattering cases, the depolarized field components vanish. Furthermore, in the forward scattering case, $\psi_s = -\psi_i$ and $\phi' = \pi$, so that the scattering matrix reduces to

$$\mathbf{S}(-\psi_i, \psi_i, \pi) = \begin{bmatrix} S_{vv}(-\psi_i, \psi_i, \pi) & 0 \\ 0 & S_{hh}(-\psi_i, \psi_i, \pi) \end{bmatrix} \tag{C.24}$$

$$= \begin{bmatrix} \frac{-iH_t}{\pi}\sum_{n=-\infty}^{\infty} C_n^{TM} & 0 \\ 0 & \frac{-iH_t}{\pi}\sum_{n=-\infty}^{\infty} C_n^{TE} \end{bmatrix} \tag{C.25}$$

and in the specular scattering case, $\psi_s = -\psi_i$ and $\phi' = 0$ so that

$$\mathbf{S}(-\psi_i, \psi_i, 0) = \begin{bmatrix} S_{vv}(-\psi_i, \psi_i, 0) & 0 \\ 0 & S_{hh}(-\psi_i, \psi_i, 0) \end{bmatrix} \tag{C.26}$$

$$= \begin{bmatrix} \frac{-iH_t}{\pi} \sum_{n=-\infty}^{\infty} (-1)^n C_n^{TM} & 0 \\ 0 & \frac{-iH_t}{\pi} \sum_{n=-\infty}^{\infty} (-1)^n C_n^{TE} \end{bmatrix} \tag{C.27}$$

APPENDIX D SURFACE SCATTERING MODELS

The roughness of a random surface can be characterized in terms of the rms surface height s and the surface correlation function $\rho(\xi)$. If the form of $\rho(\xi)$ is specified, its surface correlation length l_s may then be used to represent the horizontal character of the surface, just as s is used to represent the vertical character of the surface.

Most theoretical models for scattering from a random surface are formulated in terms of $\rho(\xi)$ or its Fourier transform. The backscattering coefficient of a randomly rough surface may be computed exactly using numerical techniques, such as the method of moments. However, numerical techniques are computationally prohibitive and, therefore, they are used only in evaluating the accuracy and range of validity of approximate models (Chen and Fung, 1988).

In the microwave region, the models most commonly used for computing the backscattering from a natural surface are (1) the Kirchhoff model under the stationary phase approximation (also known as the geometrical optics model), (2) the Kirchhoff model under the scalar approximation (also known as the physical optics model), and (3) the small perturbation model. Loosely speaking, the geometrical optics model is best suited for very rough surfaces, the physical optics model is suitable for surfaces with intermediate scales of roughness, and the small perturbation model is suitable for surfaces with short correlation lengths. Based on an evaluation of (a) the analytical conditions for the range of validity of the models

as reported in the literature, (b) the range of validity of the models as reported by Chen and Fung (1988) on the basis of comparison with numerical computations, and (c) the level of agreement experienced in the past between model calculations and experimental measurements, the following forms of the models and associated validity conditions are recommended.

D.1 Geometrical Optics Model

Consider the rough surface geometry shown in Figure D.1 with the unit vectors $\hat{\mathbf{n}}_i$ and $\hat{\mathbf{n}}_s$ representing the incident and scattered directions, respectively. Let $\hat{\mathbf{v}}_i$ and $\hat{\mathbf{h}}_i$ be unit polarization vectors for the vertical and horizontal components of the incident field, and let $\hat{\mathbf{v}}_s$ and $\hat{\mathbf{h}}_s$ be unit polarization vectors for the scattered field. These unit vectors are given in terms of the angles (θ_i, ϕ_i) and (θ_s, ϕ_s) for the incident and scattered fields by the following relations:

$$\hat{\mathbf{n}}_i = \hat{\mathbf{x}} \sin\theta_i \cos\phi_i + \hat{\mathbf{y}} \sin\theta_i \sin\phi_i + \hat{\mathbf{z}} \cos\theta_i \tag{D.1}$$

$$\hat{\mathbf{h}}_i = -\hat{\mathbf{x}} \sin\phi_i + \hat{\mathbf{y}} \cos\phi_i \tag{D.2}$$

$$\hat{\mathbf{v}}_i = \hat{\mathbf{h}}_i \times \hat{\mathbf{n}}_i = \hat{\mathbf{x}} \cos\theta_i \cos\phi_i + \hat{\mathbf{y}} \cos\theta_i \sin\phi_i - \hat{\mathbf{z}} \sin\theta_i \tag{D.3}$$

$$\hat{\mathbf{n}}_s = \hat{\mathbf{x}} \sin\theta_s \cos\phi_s + \hat{\mathbf{y}} \sin\theta_s \sin\phi_s + \hat{\mathbf{z}} \cos\theta_s \tag{D.4}$$

$$\hat{\mathbf{h}}_s = -\hat{\mathbf{x}} \sin\phi_s + \hat{\mathbf{y}} \cos\phi_s \tag{D.5}$$

$$\hat{\mathbf{v}}_s = \hat{\mathbf{h}}_s \times \hat{\mathbf{n}}_s = \hat{\mathbf{x}} \cos\theta_s \cos\phi_s + \hat{\mathbf{y}} \cos\theta_s \sin\phi_s - \hat{\mathbf{z}} \sin\theta_s. \tag{D.6}$$

The scattered field in medium one under the Kirchhoff and stationary-phase approximations is given in (Ulaby, et al., 1982, p. 931). Consider an incident field

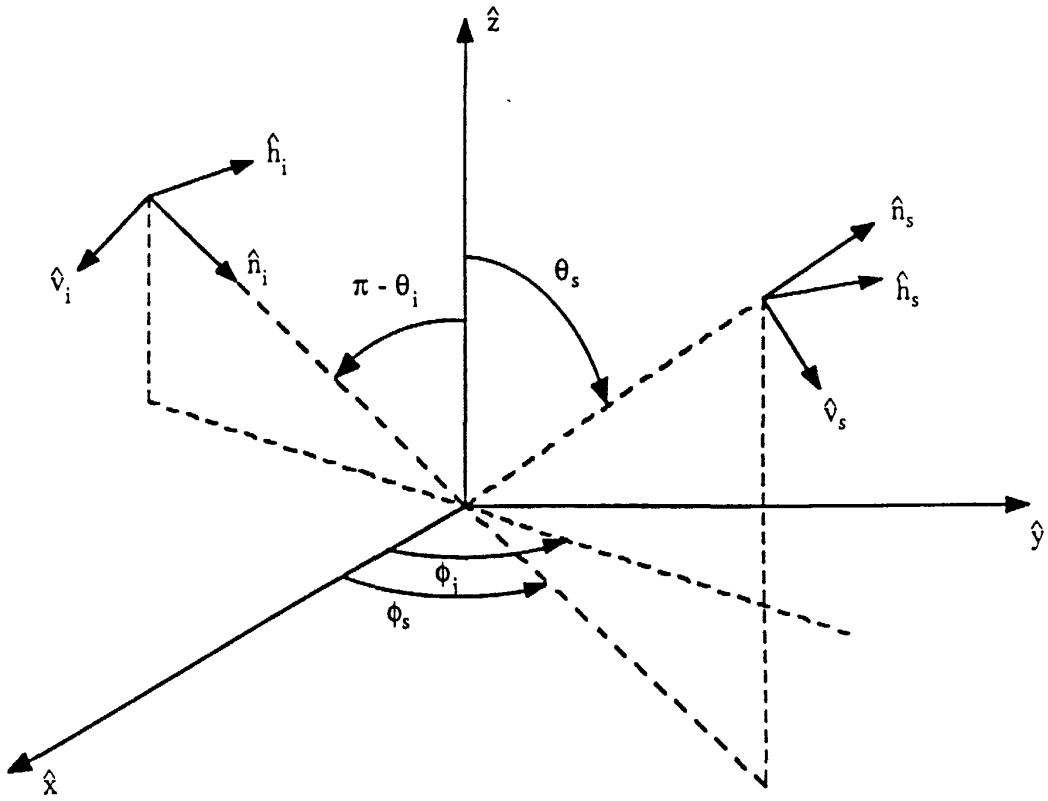


Figure D.1: Rough Surface Geometry.

of the form

$$\mathbf{E}^i = \hat{\mathbf{a}} E_0 e^{ik_1 \hat{\mathbf{n}}_i \cdot \mathbf{r}} \tag{D.7}$$

where $\hat{\mathbf{a}} \in \{\hat{\mathbf{h}}_i, \hat{\mathbf{v}}_i\}$, k_1 is the wave number in medium one, and an $e^{-i\omega t}$ time dependence has been assumed and suppressed. When $\hat{\mathbf{a}} = \hat{\mathbf{h}}_i$, the horizontal and vertical components of the scattered field are

$$\begin{aligned} E^s_{hh} &= \hat{\mathbf{h}}_s \cdot \mathbf{E}^s = KE_0 I_1 U_{hh} \\ &= -M_1[R_\perp(\hat{\mathbf{v}}_s \cdot \hat{\mathbf{n}}_i)(\hat{\mathbf{v}}_i \cdot \hat{\mathbf{n}}_s) + R_\parallel(\hat{\mathbf{h}}_s \cdot \hat{\mathbf{n}}_i)(\hat{\mathbf{h}}_i \cdot \hat{\mathbf{n}}_s)] \qquad \text{(D.8)} \\ E^s_{vh} &= \hat{\mathbf{v}}_s \cdot \mathbf{E}^s = KE_0 I_1 U_{vh} \\ &= M_1[R_\perp(\hat{\mathbf{h}}_s \cdot \hat{\mathbf{n}}_i)(\hat{\mathbf{v}}_i \cdot \hat{\mathbf{n}}_s) - R_\parallel(\hat{\mathbf{v}}_s \cdot \hat{\mathbf{n}}_i)(\hat{\mathbf{h}}_i \cdot \hat{\mathbf{n}}_s)], \qquad \text{(D.9)} \end{aligned}$$

and when $\hat{\mathbf{a}} = \hat{\mathbf{v}}_i$ the vertical and horizontal components of the scattered field are

$$\begin{aligned} E^s_{vv} &= \hat{\mathbf{v}}_s \cdot \mathbf{E}^s = KE_0 I_1 U_{vv} \\ &= -M_1[R_\perp(\hat{\mathbf{h}}_s \cdot \hat{\mathbf{n}}_i)(\hat{\mathbf{h}}_i \cdot \hat{\mathbf{n}}_s) + R_\parallel(\hat{\mathbf{v}}_s \cdot \hat{\mathbf{n}}_i)(\hat{\mathbf{v}}_i \cdot \hat{\mathbf{n}}_s)] \qquad \text{(D.10)} \\ E^s_{hv} &= \hat{\mathbf{h}}_s \cdot \mathbf{E}^s = KE_0 I_1 U_{hv} \\ &= M_1[R_\perp(\hat{\mathbf{v}}_s \cdot \hat{\mathbf{n}}_i)(\hat{\mathbf{h}}_i \cdot \hat{\mathbf{n}}_s) - R_\parallel(\hat{\mathbf{h}}_s \cdot \hat{\mathbf{n}}_i)(\hat{\mathbf{v}}_i \cdot \hat{\mathbf{n}}_s)] \qquad \text{(D.11)} \end{aligned}$$

where

$$R_\perp = \frac{\eta_2 \cos\theta_{il} - \eta_1 \cos\theta_{tl}}{\eta_2 \cos\theta_{il} + \eta_1 \cos\theta_{tl}} \tag{D.12}$$

$$R_\parallel = \frac{\eta_1 \cos\theta_{il} - \eta_2 \cos\theta_{tl}}{\eta_1 \cos\theta_{il} + \eta_2 \cos\theta_{tl}} \tag{D.13}$$

$$M_1 = \frac{KI_1 E_0 q |q_z|}{k_1 q_z[(\hat{\mathbf{n}}_i \cdot \hat{\mathbf{h}}_s)^2 + (\hat{\mathbf{n}}_i \cdot \hat{\mathbf{v}}_s)^2]} \tag{D.14}$$

$$K = \frac{ik_1}{4\pi R_0} e^{ik_1 R_0} \tag{D.15}$$

$$I_1 = \int e^{-ik_1(\hat{\mathbf{n}}_s - \hat{\mathbf{n}}_i)\cdot\mathbf{r}'} dS' \quad \text{(D 16)}$$

$$q_x = k_1(\sin\theta_i \cos\phi_i - \sin\theta_s \cos\phi_s) \quad \text{(D.17)}$$

$$q_y = k_1(\sin\theta_i \sin\phi_i - \sin\theta_s \sin\phi_s) \quad \text{(D.18)}$$

$$q_z = k_1(\cos\theta_i - \cos\theta_s) \quad \text{(D.19)}$$

$$q^2 = q_x^2 + q_y^2 + q_z^2 \quad \text{(D.20)}$$

R_0 = Range from center of illuminated area to the point of observation

θ_{il} = The local angle of incidence with respect to specular points

θ_{tl} = The local angle of transmission with respect to specular points

$k_1,\ k_2$ = wave numbers in media 1 and 2, respectively

$\eta_1,\ \eta_2$ = intrinsic impedances in media 1 and 2, respectively.

The angles θ_{il} and θ_{tl} are given in terms of the incidence and scattering angles by the relations

$$\cos\theta_{il} = -\frac{q|q_z|}{2k_1 q_z} \quad \text{(D.21)}$$

$$\sin\theta_{tl} = \frac{k_1}{k_2}\sin\theta_{il}. \quad \text{(D.22)}$$

The form of the solution used here differs slightly from that in (Ulaby, et al., 1982) to reflect an $e^{-i\omega t}$ time dependence and a different definition of θ_i. Here, we measure θ_i from the positive z axis to remain consistent with other sections of this document. The unit polarization vectors $(\hat{\mathbf{h}}_i, \hat{\mathbf{v}}_i, \hat{\mathbf{h}}_s, \hat{\mathbf{v}}_s)$ used here were chosen such that $\hat{\mathbf{v}}_i = \hat{\mathbf{v}}_s$ and $\hat{\mathbf{h}}_i = \hat{\mathbf{h}}_s$ for forward scatter.

To compute the average modified Mueller matrix (see Appendix G) characterizing the rough surface, the term $\langle E^s_{pq} E^{s*}_{mn} \rangle$ must first be determined. The subscripts

$p, q, m, n \in \{h, v\}$, and $\langle \ldots \rangle$ denotes the ensemble average. Since the only non-deterministic quantity in E^s_{pq} is I_1, the problem reduces to computing $\langle |I_1|^2 \rangle$. The result is (Ulaby, et al., 1982, p. 935)

$$\langle |I_1|^2 \rangle = \frac{2\pi A q^2}{q_z^4 m^2} \exp\left[-\frac{q_x^2 + q_y^2}{2 q_z^2 m^2}\right] \tag{D.23}$$

where A is the illuminated area, m is the surface rms slope, and the following assumptions have been made:

1. The surface is Gaussian-distributed with surface-height distribution

$$p(z) = \frac{1}{\sqrt{2\pi s^2}} \exp\left[-\frac{z^2}{2s^2}\right], \tag{D.24}$$

   and s^2 is the variance of surface heights.

2. The surface roughness is isotropic with Gaussian correlation coefficient

$$\rho(\xi) = \exp\left[-\frac{\xi^2}{l_s^2}\right], \tag{D.25}$$

   and l_s is the surface correlation length.

3. $(q_z s)^2$ is large.

The surface rms slope m for a surface characterized by a Gaussian correlation coefficient is related to the rms height s and the surface correlation length l_s by the relation

$$m = \sqrt{2}\frac{s}{l_s}. \tag{D.26}$$

Using (D.8) through (D.11), the intensity $\langle E^s_{pq} E^{s*}_{mn} \rangle$ is given by

$$\langle E^s_{pq} E^{s*}_{mn} \rangle = \frac{|k_1 E_0|^2}{(4\pi R_0)^2} U_{pq} U^*_{mn} \langle |I_1|^2 \rangle \tag{D.27}$$

with $\langle |I_1|^2 \rangle$ as given in (D.23). Defining the scattering matrix $\mathbf{S}$ such that

$$\mathbf{E}^s = \frac{e^{ik_1 R_0}}{R_0}\mathbf{S}\mathbf{E}^i \quad \text{or} \quad \begin{bmatrix} E_v^s \\ E_h^s \end{bmatrix} = \frac{e^{ik_1 R_0}}{R_0}\begin{bmatrix} S_{vv} & S_{vh} \\ S_{hv} & S_{hh} \end{bmatrix}\begin{bmatrix} E_v^i \\ E_h^i \end{bmatrix}, \tag{D.28}$$

we have the relation

$$\langle S_{pq} S_{mn}^* \rangle = \frac{R_0^2}{|E_0|^2}\langle E_{pq}^s E_{mn}^{s*} \rangle = \frac{|k_1|^2}{(4\pi)^2} U_{pq} U_{mn}^* \langle |I_1|^2 \rangle. \tag{D.29}$$

¿From the results of Appendix G, equation (D.29) can be used to obtain the average modified Mueller matrix representation $\overline{\mathbf{M}}_m$ for the rough surface. The resulting expression is

$$\overline{\mathbf{M}}_m = U_0 \widetilde{\mathbf{V}}^{-1} \begin{bmatrix} U_{vv}U_{vv}^* & U_{vh}U_{vh}^* & U_{vv}U_{vh}^* & U_{vh}U_{vv}^* \\ U_{hv}U_{hv}^* & U_{hh}U_{hh}^* & U_{hv}U_{hh}^* & U_{hh}U_{hv}^* \\ U_{vv}U_{hv}^* & U_{vh}U_{hh}^* & U_{vv}U_{hh}^* & U_{vh}U_{hv}^* \\ U_{hv}U_{vv}^* & U_{hh}U_{vh}^* & U_{hv}U_{vh}^* & U_{hh}U_{vv}^* \end{bmatrix} \mathbf{V}^{-1} \tag{D.30}$$

where $\mathbf{V}$ is given in Appendix G and

$$U_0 = \frac{|k_1|^2 A q^2}{8\pi q_z^4 m^2} \exp\left[-\frac{q_x^2 + q_y^2}{2q_z^2 m^2}\right]. \tag{D.31}$$

Again using Appendix G, the bistatic scattering coefficient is

$$\sigma_{rt}^0(\psi_r, \chi_r, \psi_t, \chi_t) = \frac{4\pi}{A}\mathbf{Y}_m^r \mathbf{I}_p \overline{\mathbf{M}}_m \mathbf{Y}_m^t, \tag{D.32}$$

where $\mathbf{Y}_m^t$ and $\mathbf{Y}_m^r$ are the *normalized* modified Stokes vectors for the transmitter and receiver polarizations t and r, respectively. As shown in Appendix G, the matrix $\mathbf{I}_p$ must be added to convert the Mueller matrix in terms of the FSA convention to the traditional Mueller matrix (van Zyl, et al., 1987; Zebker, et al., 1987) in

terms of the BSA convention. Defining the incident and scattered intensities as

$$\mathbf{I}^i = \frac{1}{\eta_1}\begin{bmatrix} \langle|E_v^i|^2\rangle \\ \langle|E_h^i|^2\rangle \\ 2\mathrm{Re}\langle E_v^i E_h^{i*}\rangle \\ 2\mathrm{Im}\langle E_v^i E_h^{i*}\rangle \end{bmatrix} \quad \text{and} \quad \mathbf{I}^s = \frac{R_0^2}{\eta_1 A\cos\theta_s}\begin{bmatrix} \langle|E_v^s|^2\rangle \\ \langle|E_h^s|^2\rangle \\ 2\mathrm{Re}\langle E_v^s E_h^{s*}\rangle \\ 2\mathrm{Im}\langle E_v^s E_h^{s*}\rangle \end{bmatrix} \tag{D.33}$$

where η_1 is the intrinsic impedance of medium 1, a relationship can be given between the incident and scattered intensities (see Appendix G). For the general bistatic case,

$$\mathbf{I}^s = \mathbf{G}\mathbf{I}^i \tag{D.34}$$

where $\mathbf{G}$ is given by

$$\mathbf{G} = \frac{1}{A\cos\theta_s}\mathbf{V}\widetilde{\mathbf{V}}\overline{\mathbf{M}}_m. \tag{D.35}$$

For backscatter from the rough surface, $\theta_s = \pi - \theta_i = \theta_0$, $\phi_s = \pi$, and $\phi_i = 0$. Substituting these angles into (D.29), we find that $U_{vv} = U_{hh}$, $U_{hv} = U_{vh} = 0$, and

$$\langle S_{pq}S_{mn}^*\rangle = \begin{cases} \frac{A|R(0)|^2}{8\pi m^2\cos^4\theta_0}\exp\left[-\frac{\tan^2\theta_0}{2m^2}\right] & p = q \text{ and } m = n \\ 0 & p \neq q \text{ or } m \neq n \end{cases} \tag{D.36}$$

where $R(0)$ is the Fresnel reflection coefficient evaluated at normal incidence. Thus, the average modified Mueller matrix for backscatter from the rough surface is

$$\overline{\mathbf{M}}_m^b = U_0^b\widetilde{\mathbf{V}}^{-1}\mathbf{I}_4\mathbf{V}^{-1} = U_0^b(\mathbf{V}\widetilde{\mathbf{V}})^{-1} \tag{D.37}$$

where $\mathbf{I}_4$ is the 4×4 identity matrix and U_0^b is given by

$$U_0^b = \frac{A|R(0)|^2}{8\pi m^2\cos^4\theta_0}\exp\left[-\frac{\tan^2\theta_0}{2m^2}\right]. \tag{D.38}$$

The backscattering coefficient for transmit and receive polarizations t and r can now be written as

$$\sigma^b_{rt}(\psi_r, \chi_r, \psi_t, \chi_t) = \frac{4\pi}{A}\mathbf{Y}^r_m \mathbf{I}_p \overline{\mathbf{M}}^b_m \mathbf{Y}^t_m, \tag{D.39}$$

and the matrix $\mathbf{G}^b$ relating the incident and backscattered intensities is

$$\mathbf{G}^b = \frac{1}{A\cos\theta_0}\mathbf{V}\widetilde{\mathbf{V}}\overline{\mathbf{M}}^b_m = \frac{U^b_0}{A\cos\theta_0}\mathbf{I}_4. \tag{D.40}$$

Validity Conditions: $s \gtrsim \frac{\lambda}{3}$

$l_s \gtrsim \lambda$

$l_s^2 > 2.76\, s\lambda$

Recommended Conditions: $0.4 \leq m \leq 0.7$

D.2 Physical Optics Model

The scattered field $\mathbf{E}^s_{pq}$ under the Kirchhoff and scalar approximations is given by the following expression (Ulaby, et al., 1982, p. 937) where the notation of Section D.1 has been used;

$$\mathbf{E}^s_{pq} = KE_0 \int \overline{U}_{pq} \exp\left[-ik_1(\hat{\mathbf{n}}_s - \hat{\mathbf{n}}_i)\cdot \mathbf{r}'\right] dS' \tag{D.41}$$

where

$$\overline{U}_{pq} = a_{pq} + b_{pq}Z_x + c_{pq}Z_y \tag{D.42}$$

$$a_{pq} = \begin{cases} R_{\perp 0}(\cos\theta_i - \cos\theta_s)\cos(\phi_s - \phi_i) & pq = hh \\ -R_{\perp 0}(1 - \cos\theta_i\cos\theta_s)\sin(\phi_s - \phi_i) & pq = vh \\ R_{\|0}(1 - \cos\theta_i\cos\theta_s)\sin(\phi_s - \phi_i) & pq = hv \\ R_{\|0}(\cos\theta_i - \cos\theta_s)\cos(\phi_s - \phi_i) & pq = vv \end{cases} \tag{D.43}$$

$$b_{pq} = \begin{cases} Z_{hh}\cos\phi_i & pq = hh \\ Z_{vh}\cos\phi_i & pq = vh \\ Z_{hv}\cos\phi_i & pq = hv \\ Z_{vv}\cos\phi_i & pq = vv \end{cases} \tag{D.44}$$

$$c_{pq} = \begin{cases} Z_{hh}\sin\phi_i & pq = hh \\ Z_{vh}\sin\phi_i & pq = vh \\ Z_{hv}\sin\phi_i & pq = hv \\ Z_{vv}\sin\phi_i & pq = vv \end{cases} \tag{D.45}$$

$$Z_{hh} = R_{\perp 0}[\sin\theta_s - \sin\theta_i\cos(\phi_s - \phi_i)] + R_{\perp 1}(\cos\theta_i - \cos\theta_s)\cos(\phi_s - \phi_i) \tag{D.46}$$

$$Z_{vh} = -\sin(\phi_s - \phi_i)[R_{\perp 0}\sin\theta_i\cos\theta_s + R_{\perp 1}(1 - \cos\theta_i\cos\theta_s)] \tag{D.47}$$

$$Z_{hv} = \sin(\phi_s - \phi_i)[R_{\|0}\sin\theta_i\cos\theta_s + R_{\|1}(1 - \cos\theta_i\cos\theta_s)] \tag{D.48}$$

$$Z_{vv} = R_{\|0}[\sin\theta_s - \sin\theta_i\cos(\phi_s - \phi_i)] + R_{\|1}(\cos\theta_i - \cos\theta_s)\cos(\phi_s - \phi_i) \tag{D.49}$$

$$R_{\perp 0} = \frac{\eta_2\cos\theta_i + \eta_1\cos\theta_t}{\eta_2\cos\theta_i - \eta_1\cos\theta_t} \tag{D.50}$$

$$R_{\perp 1} = R_{\perp 0}\frac{\eta_2\sin\theta_i + \eta_1\sin\theta_t}{\eta_2\cos\theta_i - \eta_1\cos\theta_t} \tag{D.51}$$

$$R_{\|0} = \frac{\eta_1\cos\theta_i + \eta_2\cos\theta_t}{\eta_1\cos\theta_i - \eta_2\cos\theta_t} \tag{D.52}$$

$$R_{\|1} = -\frac{[\eta_1 \sin\theta_i - \eta_2 \sin\theta_t - R_{\|0}(\eta_1 \sin\theta_i + \eta_2 \sin\theta_t)]}{\eta_1 \cos\theta_i - \eta_2 \cos\theta_t} \quad \text{(D.53)}$$

$$Z_x = \text{Surface slope along the x-axis} \quad \text{(D.54)}$$

$$Z_y = \text{Surface slope along the y-axis.} \quad \text{(D.55)}$$

The angles θ_i, θ_s, and θ_t are the incident, scattered, and transmitted angles with respect to the mean surface, respectively. The angles θ_i and θ_s are user specified, and θ_t is given by

$$k_1 \sin\theta_i = k_2 \sin\theta_t. \quad \text{(D.56)}$$

In the development, it was assumed that both the surface rms slope and the change in $R_\perp$ and $R_\|$ are small.

Keeping only terms up to first order in surface slope, the intensity $\langle \mathbf{E}^s_{pq} \mathbf{E}^{s*}_{mn} \rangle$ can be written as the sum of three terms;

$$\langle \mathbf{E}^s_{pq} \mathbf{E}^{s*}_{mn} \rangle = |KE_0|^2 I_{pqmn} = |KE_0|^2 (I_c + I_n + I_s). \quad \text{(D.57)}$$

The first term represents coherent scattering from the surface and is present only in the specular direction with respect to the mean surface. The second term represents noncoherent scattering, and the third term represents noncoherent scattering due to the surface slope. The surface slope term can be further written as the sum of slope terms along the x and y axes ($I_s = I_{sx} + I_{sy}$). For an illuminated area much larger than the correlation length of the surface, these terms can be written as (Ulaby, et al., 1982, pp. 937-940)

$$I_c = (2\pi A)^2 a_{pq} a^*_{mn} \delta(q_x)\delta(q_y) e^{-q_z^2 s^2} \quad \text{(D.58)}$$

$$I_n = 2\pi A a_{pq} a^*_{mn} e^{-q_z^2 s^2} \sum_{n=1}^{\infty} \frac{(q_z s)^{2n}}{n!} \int_0^\infty \rho(\xi)^n J_0(q_t \xi) \xi \, d\xi \quad \text{(D.59)}$$

$$I_{sx} = 2\pi A K_1 e^{-q_z^2 s^2} \int_0^\infty \frac{q_x}{q_t} \frac{d\rho(\xi)}{d\xi} J_1(q_t\xi) e^{q_z^2 s^2 \rho(\xi)} \xi d\xi \quad \text{(D.60)}$$

$$I_{sy} = 2\pi A K_2 e^{-q_z^2 s^2} \int_0^\infty \frac{q_y}{q_t} \frac{d\rho(\xi)}{d\xi} J_1(q_t\xi) e^{q_z^2 s^2 \rho(\xi)} \xi d\xi \quad \text{(D.61)}$$

where the correlation coefficient ρ has been assumed to be isotropic, and

$$K_1 = q_z s^2 (b_{pq} a^*_{mn} + a_{pq} b^*_{mn}) \quad \text{(D.62)}$$

$$K_2 = q_z s^2 (c_{pq} a^*_{mn} + a_{pq} c^*_{mn}) \quad \text{(D.63)}$$

$$q_t = \sqrt{q_x^2 + q_y^2} \quad \text{(D.64)}$$

$$J_0(\ldots) = \text{zeroth order Bessel function} \quad \text{(D.65)}$$

$$J_1(\ldots) = \text{first order Bessel function.} \quad \text{(D.66)}$$

The product of the delta functions in (D.58) is given by

$$\delta(q_x)\delta(q_y) = \begin{cases} \frac{A^2}{(2\pi)^2} & q_x = q_y = 0 \\ 0 & \text{otherwise} \end{cases}. \quad \text{(D.67)}$$

The average modified Mueller matrix $\overline{\mathbf{M}}_m$ can now be computed from the relation

$$\langle \mathbf{S}_{pq} \mathbf{S}^*_{mn} \rangle = \frac{R_0^2}{|E_0|^2} \langle \mathbf{E}^s_{pq} \mathbf{E}^{s*}_{mn} \rangle = \frac{|k_1|^2}{(4\pi)^2} I_{pqmn} \quad \text{(D.68)}$$

in the same manner as in Section D.1;

$$\overline{\mathbf{M}}_m = \frac{|k_1|^2}{(4\pi)^2} \widetilde{\mathbf{V}}^{-1} \begin{bmatrix} I_{vvvv} & I_{vhvh} & I_{vvvh} & I_{vhvv} \\ I_{hvhv} & I_{hhhh} & I_{hvhh} & I_{hhhv} \\ I_{vvhv} & I_{vhhh} & I_{vvhh} & I_{vhhv} \\ I_{hvvv} & I_{hhvh} & I_{hvvh} & I_{hhvv} \end{bmatrix} \mathbf{V}^{-1}. \quad \text{(D.69)}$$

Given $\overline{\mathbf{M}}_m$, the bistatic scattering coefficient is given by

$$\sigma^0_{rt}(\psi_r, \chi_r, \psi_t, \chi_t) = \frac{4\pi}{A} \mathbf{Y}^r_m \mathbf{I}_p \overline{\mathbf{M}}_m \mathbf{Y}^t_m, \quad \text{(D.70)}$$

and the incident and scattered intensities as defined by (D.33) are related by the expression

$$\mathbf{I}^s = \mathbf{G}\mathbf{I}^i \tag{D.71}$$

where $\mathbf{G}$ is given by

$$\mathbf{G} = \frac{1}{A\cos\theta_s}\mathbf{V}\widetilde{\mathbf{V}}\overline{\mathbf{M}}_m. \tag{D.72}$$

For backscatter from the rough surface ($\phi_i = 0$, $\phi_s = \pi$, and $\theta_s = \pi - \theta_i = \theta_0$), the factor $c_{pq} = 0$ for $p, q \in \{h, v\}$, and the factors a_{pq} and b_{pq} become

$$a^b_{pq} = \begin{cases} 2R_{\perp 0}\cos\theta_0 & pq = hh \\ 2R_{\|0}\cos\theta_0 & pq = vv \\ 0 & pq = hv, vh \end{cases} \tag{D.73}$$

$$b^b_{pq} = \begin{cases} 2R_{\perp 0}\sin\theta_0 + 2R_{\perp 1}\cos\theta_0 & pq = hh \\ 2R_{\|0}\sin\theta_0 + 2R_{\|1}\cos\theta_0 & pq = vv \\ 0 & pq = hv, vh \end{cases} . \tag{D.74}$$

Using these results in (D.58) through (D.61), the factor I_{pqmn} for backscatter can be written as

$$I^b_{pqmn} = I^b_n + I^b_s \tag{D.75}$$

where we have ignored the coherent component which is present only at normal incidence, and

$$I^b_n = 2\pi A a^b_{pq} a^{b*}_{mn} e^{-K_0^2} \sum_{n=1}^{\infty} \frac{K_0^{2n}}{n!} \int_0^{\infty} \rho(\xi)^n J_0(2k_1\xi\sin\theta_0)\xi d\xi \tag{D.76}$$

$$I^b_s = 2\pi A K_1 e^{-K_0^2} \int_0^{\infty} \frac{d\rho(\xi)}{d\xi} J_1(2k_1\xi\sin\theta_0) e^{K_0^2\rho(\xi)}\xi d\xi \tag{D.77}$$

with

$$K_0 = 2k_1 s \cos\theta_0. \tag{D.78}$$

Using (D.75) instead of I_{pqmn} in (D.69), the average modified Mueller matrix for backscatter from the rough surface is given by

$$\overline{\mathbf{M}}_m^b = \frac{|k_1|^2}{(4\pi)^2}\widetilde{\mathbf{V}}^{-1}\begin{bmatrix} I_{vvvv}^b & I_{vhvh}^b & I_{vvvh}^b & I_{vhvv}^b \\ I_{hvhv}^b & I_{hhhh}^b & I_{hvhh}^b & I_{hhhv}^b \\ I_{vvhv}^b & I_{vhhh}^b & I_{vvhh}^b & I_{vhhv}^b \\ I_{hvvv}^b & I_{hhvh}^b & I_{hvvh}^b & I_{hhvv}^b \end{bmatrix}\mathbf{V}^{-1}. \tag{D.79}$$

Further, the backscattering coefficient is given by

$$\sigma_{rt}^b(\psi_r, \chi_r, \psi_t, \chi_t) = \frac{4\pi}{A}\mathbf{Y}_m^r \mathbf{I}_p \overline{\mathbf{M}}_m^b \mathbf{Y}_m^t, \tag{D.80}$$

and the matrix $\mathbf{G}^b$ relating the incident and backscattered intensities is

$$\mathbf{G}^b = \frac{1}{A\cos\theta_0}\mathbf{V}\widetilde{\mathbf{V}}\overline{\mathbf{M}}_m^b. \tag{D.81}$$

Validity Conditions: $0.05\lambda \lesssim s \lesssim 0.15\lambda$

$l_s \gtrsim \lambda$

$m \lesssim 0.25$

Recommended Correlation Function: $\rho(\xi) = \exp\left[-\dfrac{\xi^2}{(l^4 + \xi^2 l_s^2)^{\frac{1}{2}}}\right]$

where l and l_s are small-scale and large-scale correlation lengths of the

surface.

Recommended Conditions: $l \simeq \frac{\lambda}{6}$

$$l_s \geq 6\, l$$

$$0.05\,\lambda \lesssim s \lesssim 0.15\,\lambda$$

D.3 Small Perturbation Model

For an incident field with amplitude E_0, the scattered intensity from the rough surface using the small perturbation method can be written as (Tsang, et al., 1985)

$$\langle E^s_{pq} E^{s*}_{mn} \rangle = |E_0|^2 \int f_{pq} f^*_{mn} W(|\mathbf{k}_\perp - \mathbf{k}_{\perp i}|) d\mathbf{k}_\perp \tag{D.82}$$

where an $e^{-i\omega t}$ time dependence has been assumed, and

$$d\mathbf{k}_\perp = dk_x dk_y \tag{D.83}$$

$$\mathbf{k}_\perp = \hat{\mathbf{x}} k_x + \hat{\mathbf{y}} k_y \tag{D.84}$$

$$\mathbf{k}_{\perp i} = \hat{\mathbf{x}} k_{xi} + \hat{\mathbf{y}} k_{yi} \tag{D.85}$$

$$k_x = k_1 \sin\theta_s \cos\phi_s \tag{D.86}$$

$$k_y = k_1 \sin\theta_s \sin\phi_s \tag{D.87}$$

$$k_{xi} = k_1 \sin\theta'_i \cos\phi_i \tag{D.88}$$

$$k_{yi} = k_1 \sin\theta'_i \sin\phi_i \tag{D.89}$$

$$k_{1z} = k_1 \cos\theta_s \tag{D.90}$$

$$k_{1zi} = k_1 \cos\theta'_i \tag{D.91}$$

$$k_{2z} = \sqrt{k_2^2 - k_1^2 \sin^2\theta_s} \tag{D.92}$$

$$k_{2zi} = \sqrt{k_2^2 - k_1^2 \sin^2\theta_i'} \tag{D.93}$$

$$k_\rho = k_x^2 + k_y^2 = k_1 \sin\theta_s \tag{D.94}$$

$$k_{\rho i} = k_{xi}^2 + k_{yi}^2 = k_1 \sin\theta_i' \tag{D.95}$$

$$\theta_i' = \pi - \theta_i. \tag{D.96}$$

Using the polarization unit vectors as defined in (D.1) to (D.6), the polarization dependent factors f_{pq} are

$$f_{hh} = -\frac{2k_{1zi}(k_2^2 - k_1^2)}{(k_{1z} + k_{2z})(k_{1zi} + k_{2zi})} K_1 \tag{D.97}$$

$$f_{vh} = -\frac{2k_1 k_{2z} k_{1zi}(k_2^2 - k_1^2)}{(k_2^2 k_{1z} + k_1^2 k_{2z})(k_{1zi} + k_{2zi})} K_2 \tag{D.98}$$

$$f_{hv} = \frac{2k_1 k_{2zi} k_{1zi}(k_2^2 - k_1^2)}{(k_{1z} + k_{2z})(k_2^2 k_{1zi} + k_1^2 k_{2zi})} K_2 \tag{D.99}$$

$$f_{vv} = \frac{2k_2^2 k_{1zi}(k_2^2 - k_1^2)}{(k_2^2 k_{1z} + k_1^2 k_{2z})(k_2^2 k_{1zi} + k_1^2 k_{2zi})} \left[-k_\rho k_{\rho i} + \frac{k_1^2}{k_2^2} k_{2z} k_{2zi} K_1 \right] \tag{D.100}$$

with

$$K_1 = \frac{k_x k_{xi} + k_y k_{yi}}{k_\rho k_{\rho i}} \tag{D.101}$$

$$K_2 = \frac{k_y k_{xi} - k_x k_{yi}}{k_\rho k_{\rho i}}. \tag{D.102}$$

The function $W(|\mathbf{k}_\perp - \mathbf{k}_{\perp i}|)$ is the spectral density of the rough surface, or simply the Fourier transform of the correlation function $\rho(\mathbf{r}_\perp)$;

$$W(\mathbf{k}_\perp) = \frac{s^2}{(2\pi)^2} \int \rho(\mathbf{r}_\perp) e^{i\mathbf{k}_\perp \cdot \mathbf{r}_\perp} d\mathbf{r}_\perp \tag{D.103}$$

where s is the standard deviation of the surface heights, and

$$\mathbf{r}_\perp = \hat{\mathbf{x}} x + \hat{\mathbf{y}} y \tag{D.104}$$

$$d\mathbf{r}_\perp = dx dy. \tag{D.105}$$

For a surface with a Gaussian correlation function ($\rho(\xi) = e^{-\xi^2/l_s^2}$), the spectral density is

$$W(|\mathrm{k}_\perp - \mathrm{k}_{\perp i}|) = \frac{(sl_s)^2}{4\pi} \exp\left[-\frac{l_s^2}{4}|\mathrm{k}_\perp - \mathrm{k}_{\perp i}|^2\right] \tag{D.106}$$

where

$$|\mathrm{k}_\perp - \mathrm{k}_{\perp i}|^2 = k_1^2\left[\sin^2\theta_s + \sin^2\theta_i' - 2\sin\theta_s \sin\theta_i' \cos(\phi_s - \phi_i)\right]. \tag{D.107}$$

¿From (D.82), we have an expression of the form

$$\langle E_{pq}^s E_{mn}^{s*}\rangle = |E_0|^2 \int f(k_x, k_y) d\mathrm{k}_\perp = |E_0|^2 \int k_1^2 \cos\theta_s f(k_x, k_y) d\Omega_s \tag{D.108}$$

where

$$f(k_x, k_y) = |E_0|^2 f_{pq} f_{mn}^* W(|\mathrm{k}_\perp - \mathrm{k}_{\perp i}|). \tag{D.109}$$

Denoting $\Delta\langle E_{pq}^s E_{mn}^{s*}\rangle$ as the intensity within the narrow spectral bands $\Delta k_x \Delta k_y$ centered at k_x and k_y, we obtain (Ulaby, et al., 1982, Appendix 12H)

$$\Delta\langle E_{pq}^s E_{mn}^{s*}\rangle \approx |E_0|^2 f(k_x, k_y)\Delta k_x \Delta k_y = |E_0|^2 k_1^2 \cos\theta_s f(k_x, k_y)\Delta\Omega_s. \tag{D.110}$$

Thus, the average intensity per unit solid angle is

$$\frac{\Delta\langle E_{pq}^s E_{mn}^{s*}\rangle}{\Delta\Omega_s} = |E_0|^2 k_1^2 \cos\theta_s f(k_x, k_y). \tag{D.111}$$

The average intensity P at a receiver located at a distance R_0 from the illuminated area A is equal to the average intensity per unit solid angle times the solid angle subtended by the receiver, or equivalently

$$P = \frac{\Delta\langle E_{pq}^s E_{mn}^{s*}\rangle}{\Delta\Omega_s}\left(\frac{A\cos\theta_s}{R_0^2}\right) = \frac{|E_0|^2}{R_0^2} A k_1^2 \cos^2\theta_s f(k_x, k_y). \tag{D.112}$$

The factor $\langle S_{pq} S^*_{mn} \rangle$ (which is used with Appendix G to compute the average modified Mueller matrix characterizing the surface) is thus given by

$$\langle S_{pq} S^*_{mn} \rangle = \frac{R_0^2}{|E_0|^2} P = A k_1^2 \cos^2 \theta_s f_{pq} f^*_{mn} W(|\mathbf{k}_\perp - \mathbf{k}_{\perp i}|). \tag{D.113}$$

Using Appendix G, the average modified Mueller matrix is

$$\overline{\mathbf{M}}_m = U_0 \widetilde{\mathbf{V}}^{-1} \begin{bmatrix} f_{vv} f^*_{vv} & f_{vh} f^*_{vh} & f_{vv} f^*_{vh} & f_{vh} f^*_{vv} \\ f_{hv} f^*_{hv} & f_{hh} f^*_{hh} & f_{hv} f^*_{hh} & f_{hh} f^*_{hv} \\ f_{vv} f^*_{hv} & f_{vh} f^*_{hh} & f_{vv} f^*_{hh} & f_{vh} f^*_{hv} \\ f_{hv} f^*_{vv} & f_{hh} f^*_{vh} & f_{hv} f^*_{vh} & f_{hh} f^*_{vv} \end{bmatrix} \mathbf{V}^{-1} \tag{D.114}$$

where

$$U_0 = A k_1^2 \cos^2 \theta_s W(|\mathbf{k}_\perp - \mathbf{k}_{\perp i}|). \tag{D.115}$$

Given $\overline{\mathbf{M}}_m$, the bistatic scattering coefficient is given by

$$\sigma^0_{rt}(\psi_r, \chi_r, \psi_t, \chi_t) = \frac{4\pi}{A} \mathbf{Y}^r_m \mathbf{I}_p \overline{\mathbf{M}}_m \mathbf{Y}^t_m, \tag{D.116}$$

and the incident and scattered intensities are related by the expression

$$\mathbf{I}^s = \mathbf{G}\mathbf{I}^i \tag{D.117}$$

where G is given by

$$\mathbf{G} = \frac{1}{A \cos \theta_s} \mathbf{V} \widetilde{\mathbf{V}} \overline{\mathbf{M}}_m. \tag{D.118}$$

A case of special interest is backscatter from a surface with $\mu_r = 1$. For backscatter, $\phi_s - \phi_i = \pi$, $\theta_s = \theta'_i = \theta_0$, $f_{vh} = f_{hv} = 0$, and

$$f_{hh} = -\frac{2k_1 \cos \theta_0 (\epsilon_r - 1)}{[\cos \theta_0 + \sqrt{\epsilon_r - \sin^2 \theta_0}]^2} \tag{D.119}$$

$$f_{vv} = 2k_1 \cos \theta_0 (\epsilon_r - 1) \frac{\sin^2 \theta_0 - \epsilon_r (1 + \sin^2 \theta_0)}{\epsilon_r \cos \theta_0 + \sqrt{\epsilon_r - \sin^2 \theta_0}]^2}. \tag{D.120}$$

Using these results, the average modified Mueller matrix becomes

$$\overline{\mathbf{M}}_m^b = U_0^b \widetilde{\mathbf{V}}^{-1} \begin{bmatrix} f_{vv} f_{vv}^* & 0 & 0 & 0 \\ 0 & f_{hh} f_{hh}^* & 0 & 0 \\ 0 & 0 & f_{vv} f_{hh}^* & 0 \\ 0 & 0 & 0 & f_{hh} f_{vv}^* \end{bmatrix} \mathbf{V}^{-1} \tag{D.121}$$

where

$$U_0^b = A k_1^2 \cos^2 \theta_s W(2k_1 \sin \theta_0). \tag{D.122}$$

The backscattering coefficient can now be written as

$$\sigma_{rt}^b(\psi_r, \chi_r, \psi_t, \chi_t) = \frac{4\pi}{A} \mathbf{Y}_m^r \mathbf{I}_p \overline{\mathbf{M}}_m^b \mathbf{Y}_m^t, \tag{D.123}$$

and the matrix $\mathbf{G}^b$ relating the incident and backscattered intensities is

$$\mathbf{G}^b = \frac{1}{A \cos \theta_0} \mathbf{V} \widetilde{\mathbf{V}} \overline{\mathbf{M}}_m^b. \tag{D.124}$$

For a surface with a Gaussian correlation function,

$$W(2k \sin \theta_0) = \frac{(s l_s)^2}{2} \exp\left[-(k l_s \sin \theta_0)^2\right]. \tag{D.125}$$

Validity Conditions: $s \leq 0.05\lambda$

$m \leq 0.3$

$l_s \leq 0.5\lambda$

Recommended Conditions: $l_s \leq 0.25\,\lambda$

$s \leq 0.05\lambda.$

APPENDIX E DIELECTRIC BEHAVIOR OF THE CANOPY CONSTITUENTS

This appendix describes the relationships of the dielectric constants of the various canopy constituents to their respective moisture contents. Section E.1 discusses the variation of vegetation dielectric with gravimetric water content. The same dielectric model is used for all vegetation material, including leaves, trunks and branches. The dielectric behavior is governed by the gravimetric moisture content m_g and the bulk density ρ, which together define the volumetric moisture content m_v. The model used to relate the dielectric constant of soil to its volumetric water content is given in Section E.2. This section also provides expressions for the dielectric constant of standing water. In all cases, the dielectric constants are assumed to have the form $\epsilon = \epsilon' - j\epsilon''$.

E.1 Dielectric Behavior of Vegetation

E.1.1 Model in Terms of Volumetric Moisture

Ulaby and El-Rayes (1987) have shown that the dielectric constant of vegetation material may be modeled by a Debye-Cole dual-dispersion model. This model consists of a free water component that accounts for the volume of the vegetation occupied by water in free form and a bound water component that accounts for the volume of the vegetation occupied by water molecules bound to bulk vegetation molecules. Based on this model, the dielectric constant for vegetation is given by:

$$\epsilon = A + B\left(4.9 + \frac{\epsilon_s - \epsilon_\infty}{1 + j\frac{f(\text{Hz})}{f_o}} - j\frac{22.74}{f(\text{GHz})}\right) + C\left(2.9 + \frac{55}{1 + \sqrt{j\frac{f(\text{GHz})}{0.18}}}\right) \quad \text{(E.1)}$$

where f(Hz) is frequency in Hz, f(GHz) is frequency in GHz, and

$$\epsilon_\infty = 4.9 \tag{E.2}$$

$$\epsilon_s = 88.045 - 0.4147T + 6.295 \times 10^{-4}T^2 + 1.075 \times 10^{-5}T^3 \tag{E.3}$$

$$f_o = (2\pi\tau)^{-1} \tag{E.4}$$

$$(2\pi\tau) = 1.1109 \times 10^{-10} - 3.824 \times 10^{-12}T + 6.938 \times 10^{-14}T^2 - 5.096 \times 10^{-16}T^3. \tag{E.5}$$

where T is temperature in °C and (E.4) gives f_o in Hz. Given the gravimetric moisture content m_g and the bulk density of the dry vegetation material ρ, the volumetric water content m_v of the vegetation material may be found from

$$m_v = \frac{m_g \rho}{1 - m_g(1 - \rho)}. \tag{E.6}$$

The constants A,B and C are then computed using

$$A = 1.7 + 3.2m_v + 6.5m_v^2 \tag{E.7}$$

$$B = m_v(0.82m_v + 0.166) \tag{E.8}$$

$$C = \frac{31.4m_v^2}{59.5m_v^2 + 1}. \tag{E.9}$$

E.1.2 Model for Leaves

For leafy vegetation, A, B and C in (E.1) may be computed directly from the moisture gravimetric fraction. The constants become

$$A = 1.7 - 0.74m_g + 6.16m_g^2 \tag{E.10}$$

$$B = m_g(0.55m_g - 0.076) \tag{E.11}$$

$$C = \frac{4.64m_g^2}{7.36m_g^2 + 1}. \tag{E.12}$$

The dielectric model given by (E.1) has been found to give excellent agreement with experimental data over a wide range of moisture conditions and over a frequency range extending from 0.2 to 20 GHz. It is used together with (E.6) through (E.9) to model the dielectric constants of trunks and branches and with (E.10) through (E.12) to model the dielectric constant of leaves.

E.2 Dielectric Behavior of the Ground Surface

In this section, the dielectric properties for two types of ground surfaces are considered. The first is a soil surface consisting of a mixture of sand, silt and clay. The second is a standing water surface. The dielectric constant for the soil surface is determined using an empirical model whereas a semi-analytic model is used to predict the dielectric of a standing water surface.

E.2.1 Soil

Hallikainen et al. (1985) expressed the dielectric constant of soil consisting of a mixture of sand, silt and clay as

$$\epsilon_s = \epsilon_s' - j\epsilon_s'' \tag{E.13}$$

where the real and imaginary parts each fit a polynomial of the form

$$\epsilon = (a_0 + a_1 S + a_2 C) + (b_0 + b_1 S + b_2 C)\, m_v + (c_0 + c_1 S + c_2 C)\, m_v^2, \tag{E.14}$$

$$\epsilon = \epsilon_s' \text{ or } \epsilon_s''.$$

Here, m_v is the soil volumetric moisture content while S and C are the sand and clay textural components of the soil in percent by weight. The polynomial

coefficients are listed in Table E.1 and the prediction accuracy of the model is given by Hallikainen et al. (1985).

Table E.1.

Coefficients of Polynomial Expressions

	Frequency (GHz)	a_0	a_1	a_2	b_0	b_1	b_2	c_0	c_1	c_2
ϵ_s'	1.4	2.862	-0.012	0.001	3.803	0.462	-0.341	119.006	-0.500	0 633
	4	2.927	-0.012	-0.001	5.505	0.371	0.062	114.826	-0.389	-0.547
	6	1.993	0.002	0.015	38.086	-0.176	-0.633	10.720	1.256	1 522
	8	1.997	0.002	0.018	25.579	-0.017	-0 412	39.793	0.723	0 941
	10	2.502	-0.003	-0.003	10.101	0.221	-0.004	77.482	-0.061	-0 135
	12	2.200	-0.001	0.012	26.473	0.013	-0.523	34.333	0.284	1 062
	14	2.301	0.001	0.009	17.918	0.084	-0.282	50.149	0.012	0.387
	16	2.237	0.002	0.009	15.505	0.076	-0.217	48.260	0.168	0.289
	18	1.912	0.007	0.021	29.123	-0.190	-0.545	6.960	0.822	1.195
ϵ_s''	1.4	0.356	-0.003	-0.008	5.507	0.044	-0.002	17.753	-0.313	0.206
	4	0.004	0.001	0.002	0.951	0.005	-0.010	16.759	0.192	0.290
	6	-0.123	0.002	0.003	7.502	-0.058	-0.116	2.942	0.452	0.543
	8	-0.201	0.003	0.003	11.266	-0.085	-0.155	0.194	0.584	0.581
	10	-0.070	0.000	0.001	6.620	0.015	-0.081	21.578	0.293	0.332
	12	-0.142	0.001	0.003	11.868	-0.059	-0.225	7.817	0.570	0.801
	14	-0.096	0.001	0.002	8.583	-0.005	-0.153	28.707	0.297	0.357
	16	-0.027	-0.001	0.003	6.179	0.074	-0.086	34.126	0.143	0.206
	18	-0.071	0.000	0.003	6.938	0.029	-0.128	29.945	0.275	0.377

This model is independent of soil temperature. In general, the dielectric constant of soil changes very little with temperature for soil that is not frozen. For soil temperatures below freezing, however, the temperature dependence becomes more important. Variations in the real and imaginary parts of ϵ_s as a function of temperature and moisture content are shown in Ulaby et al. (1986, p. 2099).

E.2.2 Standing Water

The dielectric constant of standing water is, in general, a function of the water salinity S. At frequencies above 5 GHz, however, salinity exercises a negligible influence on ϵ and, therefore, S may be set to zero in the expressions below (Ulaby

et al., 1986, pp. 2020-2025):

$$\epsilon_{sw} = \epsilon'_{sw} - j\epsilon''_{sw} \tag{E.15}$$

$$\epsilon'_{sw} = \epsilon_{sw\infty} + \frac{\epsilon_{sw0} - \epsilon_{sw\infty}}{1 + (2\pi f \tau_{sw})^2} \tag{E.16}$$

$$\epsilon''_{sw} = \frac{2\pi f \tau_{sw} (\epsilon_{sw0} - \epsilon_{sw\infty})}{1 + (2\pi f \tau_{sw})^2} + \frac{\sigma_i}{2\pi \epsilon_0 f} \tag{E.17}$$

where ϵ_0 is the permittivity of free space, $\epsilon_{sw\infty} = 4.9$ and f is frequency in Hz.

In general, ϵ_{sw0} varies with salinity S (parts per thousand) and temperature T (°C) as

$$\epsilon_{sw0}(T,S) = \epsilon_{sw0}(T,0) \cdot a(T,S) \tag{E.18}$$

where

$$\epsilon_{sw0}(T,0) = 87.134 - 0.1949T - 0.01276T^2 + 2.491 \times 10^{-4}T^3 \tag{E.19}$$

$$a(T,S) = 1.0 + 1.613 \times 10^{-5}TS - 3.656 \times 10^{-3}S + 3.210 \times 10^{-5}S^2 - 4.232 \times 10^{-7}S^3. \tag{E.20}$$

These expressions are based on data generated for salinities in the range $4 < S < 35$.

Similarly, the relaxation time τ_{sw} may be expressed as

$$\tau_{sw}(T,S) = \tau_{sw}(T,0) \cdot b(T,S) \tag{E.21}$$

where

$$\tau_{sw}(T,0) = \left(\frac{1}{2\pi}\right)(1.1109 \times 10^{-10} - 3.824 \times 10^{-12}T + 6.938 \times 10^{-14}T^2 - 5.096 \times 10{-}16T^3) \tag{E.22}$$

$$b(T,S) = 1.0 + 2.282 \times 10^{-5}TS - 7.38 \times 10^{-4}S$$

$$-7.760 \times 10^{-6} S^2 + 1.105 \times 10^{-8} S^3. \qquad \text{(E.23)}$$

This expression is based on data for $0 \leq T \leq 40^o$C and $0 \leq S \leq 157$ for a solution of NaCl.

Finally, the ionic conductivity σ_i is

$$\sigma_i(T, S) = \sigma_i(25, S)\, e^{-\phi} \qquad \text{(E.24)}$$

where

$$\begin{aligned} \sigma_i(25, S) &= S\big[0.18252 - 1.4619 \times 10^{-3} S \\ &\quad + 2.093 \times 10^{-5} S^2 - 1.282 \times 10^{-7} S^3\big] \qquad \text{(E.25)} \\ \phi &= \Delta\big[2.033 \times 10^{-2} + 1.266 \times 10^{-4} \Delta + 2.464 \times 10^{-6} \Delta^2 \\ &\quad - S(1.849 \times 10^{-5} - 2.551 \times 10^{-7} \Delta \\ &\quad + 2.551 \times 10^{-8} \Delta^2)\big] \qquad \text{(E.26)} \end{aligned}$$

with $\Delta = 25 - T$. These expressions are valid for $0 \leq S \leq 40$.

APPENDIX F RELATIONSHIPS BETWEEN CANOPY PARAMETERS

This appendix discusses some connecting models that relate fundamental canopy parameters to the parameters that drive MIMICS. Section F.1 defines the volume fractions of leaves, branches and trunks in a canopy, section F.2 defines the leaf area index of a canopy and section F.3 defines the specific and total water densities and biomasses of the canopy constituents. All three sections relate their defined parameters to MIMICS inputs.

F.1 Elemental Volume Fractions

The volume fraction of particles with an average volume $\bar{V}_p$ (cubic meters) distributed with a density N_p (particles per cubic meter) is

$$v_p = N_p \bar{V}_p. \tag{F.1}$$

Therefore, the volume fraction of leaves within the crown layer is given by

$$v_l = N_l \tau \iint ab f_d(a,b)\, da\, db \tag{F.2}$$

where N_l is the number density of leaves within the crown volume, τ is the leaf thickness, a and b are the dimensions of the equivalent flat plates that model the leaves and $f_d(a,b)$ is the probability distribution function (PDF) of leaf sizes. Here, the leaf thickness is assumed to be constant for all of the leaves.

Similarly, the volume fraction of branches within the crown layer is given by

$$v_b = \frac{\pi N_b}{4} \iint l_c d_c^2 f_c(l_c, d_c)\, dl_c\, dd_c \tag{F.3}$$

where N_b is the number density of branches within the volume, l_c is the branch length, d_c is the branch diameter and $f_c(l_c, d_c)$ is the PDF of branch sizes.

Finally, the volume fraction of boles within the trunk layer is

$$v_t = \frac{\pi N_t}{4\bar{H}_t} \iint H_t d_t^2 f_c(H_t, d_t)\, dH_t\, dd_t \tag{F.4}$$

where N_t is the area density of trunks over the appropriate landscape patch, $\bar{H}_t$ is the average height of the trunk layer, H_t and d_t are the bole height and diameter, respectively, and $f_c(H_t, d_t)$ is the PDF that describes the distribution of bole size. Here, a landscape patch is defined as a section of land that consists of some identifiable stand that is homogeneous with respect to the spatial distribution of the canopy elements.

F.2 Leaf Area Index

The leaf area index (LAI) is defined by Ulaby et al. (1986, p. 1563) as the total single-side surface area of all the leaves contained in the canopy over a unit area of ground. This quantity is given by

$$LAI = \frac{d\, v_l}{\tau} \tag{F.5}$$

where v_l is the leaf volume fraction, d is the thickness of the crown layer and τ is the leaf thickness.

F.3 Biomass Parameters

F.3.1 General Definitions

The gravimetric moisture content of a specific plant part is defined as

$$m_g = \frac{M_w}{M_w + M_d} \tag{F.6}$$

where M_w is the mass of the water in the plant part and M_d is its dry mass. The dry mass for a particle with volume $V_p(\text{cm}^3)$ is

$$M_d = \rho_p V_p \qquad \text{(grams)} \tag{F.7}$$

where ρ_p is the dry density of the particle in grams per cubic centimeter. Knowing M_d and m_g, the mass of water in the particle is given by

$$M_w = \frac{m_g}{1 - m_g} M_d \qquad \text{(grams)} \tag{F.8}$$

and the specific water density within such a particle is

$$D^s_{wp} = \frac{M_w}{V_p} \tag{F.9}$$

$$= \frac{m_g}{1 - m_g} \rho_p \qquad \left(\frac{\text{g}}{\text{cm}^3}\right). \tag{F.10}$$

Knowing the density of water in a typical particle, it is of interest to find the total area density of water in the landscape patch that contains the distribution of such particles. For particles distributed with a volume fraction v_p, the total area density of water within the landscape patch is

$$D^t_{wp} = 1000\, D^s_{wp} v_p h_p \tag{F.11}$$

$$= 1000 \frac{m_g}{1 - m_g} \rho_p v_p h_p \qquad \left(\frac{\text{kg}}{\text{m}^2}\right) \tag{F.12}$$

where h_p is the vertical extent (in meters) of the particle distribution.

The specific biomass of a particle is defined in terms of mass per unit volume of the specific plant part. The total biomass is defined in terms of the total mass per unit area over the appropriate landscape patch. Both biomasses may be defined in terms of wet and dry plant material. The specific dry biomass of a particle is equivalent to its dry density. The specific wet biomass of the particle is

$$B^s_{wp} = \rho_p + D^s_{wp} \tag{F.13}$$

$$= \left[\frac{\rho_p}{1 - m_g}\right] \qquad \left(\frac{\mathrm{g}}{\mathrm{cm}^3}\right). \tag{F.14}$$

The total dry biomass of a class of particles is

$$B^t_{dp} = 1000\,\rho_p v_p h_p \qquad \left(\frac{\mathrm{kg}}{\mathrm{m}^2}\right) \tag{F.15}$$

and the total wet biomass of a class of particles is

$$B^t_{wp} = B^t_{dp} + D^t_{wp} \tag{F.16}$$

$$= 1000\,\rho_p v_p h_p \left(\frac{1}{1 - m_g}\right) \tag{F.17}$$

$$= 1000\,v_p B^s_{wp} h_p \qquad \left(\frac{\mathrm{kg}}{\mathrm{m}^2}\right). \tag{F.18}$$

F.3.2 Constituent Biomasses and Water Contents

Table F.1 lists the specific water contents and the specific biomasses for the three canopy constituents. Each of these parameters is given in units of grams per cubic centimeter and represents the density of water or material within the plant part itself. The variable ρ represents the dry density of the vegetation material and the variable m_g represents the gravimetric moisture of the constituent part as defined by (F.6).

Table F.2 lists the total water density and total biomasses of the indicated canopy constituents. These parameters are defined in units of kilograms per square meter and account for the constituent mass per unit area over the appropriate landscape patch. The variable h_c represents the crown the thickness of the crown layer and d represents the thickness of the trunk layer.

The total biomass of leaves is also known as the total foliar biomass and defines the mass of leaves or needles per unit volume of canopy crown. For deciduous trees in temperate climates, this quantity is closely related to the net primary production.

Table F.1.
Specific water content and biomasses of the individual canopy constituents.

Constituent	Specific Water Content ($\frac{\text{g}}{\text{cm}^3}$)	Specific Dry Biomass ($\frac{\text{g}}{\text{cm}^3}$)	Specific Wet Biomass ($\frac{\text{g}}{\text{cm}^3}$)
Leaves	$D^s_{wl} = \frac{m_{gl}}{1-m_{gl}}\rho_l$	$B^s_{dl} = \rho_l$	$B^s_{wl} = \frac{\rho_l}{1-m_{gl}}$
Branches	$D^s_{wb} = \frac{m_{gb}}{1-m_{gb}}\rho_b$	$B^s_{db} = \rho_b$	$B^s_{wb} = \frac{\rho_b}{1-m_{gb}}$
Trunks	$D^s_{wt} = \frac{m_{gt}}{1-m_{gt}}\rho_t$	$B^s_{dt} = \rho_t$	$B^s_{wt} = \frac{\rho_t}{1-m_{gt}}$

Table F.2.
Total water content and biomasses of the canopy constituents.

Constituent	Total Water Density ($\frac{\text{kg}}{\text{m}^2}$)	Total Dry Biomass ($\frac{\text{kg}}{\text{m}^2}$)	Total Wet Biomass ($\frac{\text{kg}}{\text{m}^2}$)
Leaves	$D^t_{wl} = 1000 D^s_{wl} v_l h_c$	$B^t_{dl} = 1000 \rho_l v_l h_c$	$B^t_{wl} = 1000 B^t_{dl} v_l h_c$
Branches	$D^t_{wb} = 1000 D^s_{wb} v_b h_c$	$B^t_{db} = 1000 \rho_b v_b h_c$	$B^t_{wb} = 1000 B^t_{db} v_b h_c$
Trunks	$D^t_{wt} = 1000 D^s_{wt} v_t d$	$B^t_{dt} = 1000 \rho_t v_t d$	$B^t_{wt} = 1000 B^t_{dt} v_t d$
Total Woody Material	$D^t_{ww} = D^t_{wb} + D^t_{wt}$	$B^t_{dw} = B^t_{db} + B^t_{dt}$	$B^t_{ww} = B^t_{wb} + B^t_{wt}$
Total Crown Material	$D^t_{wc} = D^t_{wb} + D^t_{wl}$	$B^t_{dc} = B^t_{db} + B^t_{dl}$	$B^t_{wc} = B^t_{wb} + B^t_{wl}$
Total Canopy Material	$D^t_{w} = D^t_{wl} + D^t_{wb} + D^t_{wt}$	$B^t_{d} = B^t_{dl} + B^t_{db} + B^t_{dt}$	$B^t_{w} = B^t_{wl} + B^t_{wb} + B^t_{wt}$

APPENDIX G WAVE SYNTHESIS

G.1 Point Target

The polarization of an electromagnetic wave may be described in terms of the ellipticity diagram shown in Figure G.1. For a wave travelling in the $\hat{\mathbf{z}}$ direction, the electric field $\mathbf{E}$ has complex $\hat{\mathbf{x}}$ and $\hat{\mathbf{y}}$ components which shall be designated E_h and E_v by choosing the horizontal and vertical polarization unit vectors $\hat{\mathbf{h}} = \hat{\mathbf{x}}$ and $\hat{\mathbf{v}} = \hat{\mathbf{y}}$. Thus,

$$\mathbf{E} = \left(\hat{\mathbf{v}}E_v + \hat{\mathbf{h}}E_h\right) e^{-i(\omega t - kz)}. \tag{G.1}$$

The electric field $\mathbf{E}$ in (G.1) can be written in terms of a normalized polarization vector $\mathbf{A}$; in matrix notation,

$$\mathbf{E} = \mathbf{A}E_0 \quad \text{or} \quad \begin{bmatrix} E_v \\ E_h \end{bmatrix} = E_0 \begin{bmatrix} A_v \\ A_h \end{bmatrix} = E_0 \begin{bmatrix} a_v e^{j\delta_v} \\ a_h e^{j\delta_v} \end{bmatrix} \tag{G.2}$$

where δ_v and δ_h are the phase angles of A_v and A_h, $a_v = |A_v|$, and $a_h = |A_h|$. The factor $e^{-i(\omega t - kz)}$ has been suppressed for convenience. From the relation $a_v^2 + a_h^2 = 1$, the average power carried by the wave is $S_0 = E_0^2$.

The polarization state of the wave may also be expressed in terms of the Stokes vector $\mathbf{F}$ given by

$$\mathbf{F} = \begin{bmatrix} |E_v|^2 + |E_h|^2 \\ |E_v|^2 - |E_h|^2 \\ 2\mathrm{Re}(E_v E_h^*) \\ 2\mathrm{Im}(E_v E_h^*) \end{bmatrix} = \begin{bmatrix} S_0 \\ S_0 \cos 2\psi \cos 2\chi \\ S_0 \sin 2\psi \cos 2\chi \\ S_0 \sin 2\chi \end{bmatrix} \tag{G.3}$$

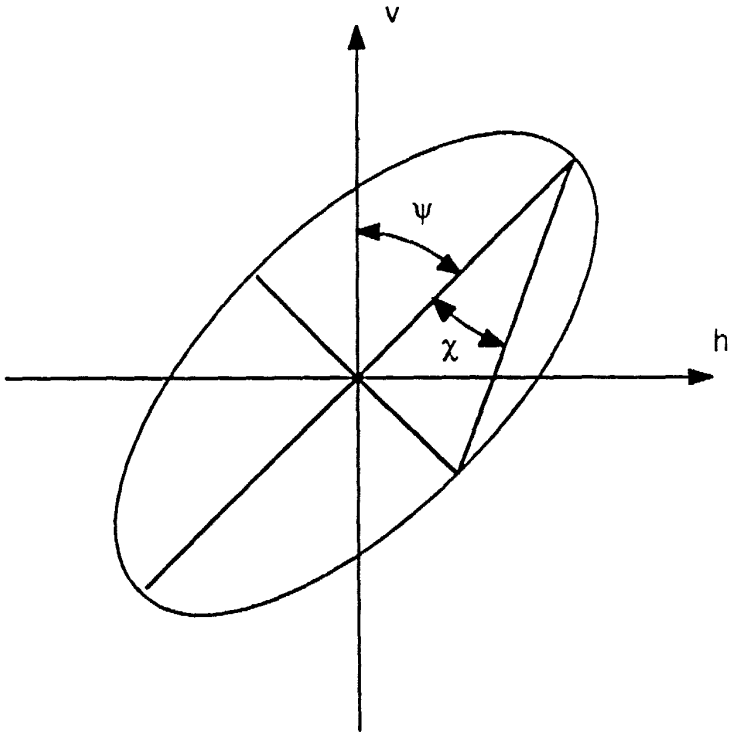


Figure G.1: Polarization of an Electromagnetic Wave.

where ψ and χ are the orientation and ellipticity angles shown in Figure G.1 The angles ψ and χ are sufficient to specify the polarization completely. Notice that we have defined ψ with respect to the vertical Polarization axis instead of the horizontal polarization axis as in van Zyl et al. (1987) and Zebker et al. (1987).

The modified Stokes vector $\mathbf{F}_m$ provides an alternative description of wave polarization. The modified Stokes vector is defined as

$$\mathbf{F}_m = \begin{bmatrix} |E_v|^2 \\ |E_h|^2 \\ 2\mathrm{Re}(E_v E_h^*) \\ 2\mathrm{Im}(E_v E_h^*) \end{bmatrix} = \begin{bmatrix} \frac{1}{2}S_0(1+\cos 2\psi \cos 2\chi) \\ \frac{1}{2}S_0(1-\cos 2\psi \cos 2\chi) \\ S_0 \sin 2\psi \cos 2\chi \\ S_0 \sin 2\chi \end{bmatrix}, \tag{G.4}$$

and it is related to the standard Stokes vector by a simple transformation matrix $\mathbf{U}$;

$$\mathbf{F} = \mathbf{U}\mathbf{F}_m \tag{G.5}$$

where

$$\mathbf{U} = \begin{bmatrix} 1 & 1 & 0 & 0 \\ 1 & -1 & 0 & 0 \\ 0 & 0 & 1 & 0 \\ 0 & 0 & 0 & 1 \end{bmatrix}. \tag{G.6}$$

Consider a scatterer illuminated by an electromagnetic wave with incident electric field $\mathbf{E}^i$. The scattered field $\mathbf{E}^s$ at a distance r from the scatterer is given by

$$\mathbf{E}^s = \frac{e^{ikr}}{r}\mathbf{S}\mathbf{E}^i \quad \text{or} \quad \begin{bmatrix} E_v^s \\ E_h^s \end{bmatrix} = \frac{e^{ikr}}{r}\begin{bmatrix} S_{vv} & S_{vh} \\ S_{hv} & S_{hh} \end{bmatrix}\begin{bmatrix} E_v^i \\ E_h^i \end{bmatrix} \tag{G.7}$$

where

$$\mathbf{S} = \begin{bmatrix} S_{vv} & S_{vh} \\ S_{hv} & S_{hh} \end{bmatrix} \tag{G.8}$$

is the 2×2 complex scattering matrix characterizing the scatterer. The scatterer can also be represented by a corresponding 4×4 real matrix relating the incident and scattered Stokes vectors ($\mathbf{F}^i$ and $\mathbf{F}^s$, respectively). The relation is written explicitly as (van Zyl, et al., 1987; Zebker, et al., 1987)

$$\mathbf{F}^s = \frac{1}{r^2}\mathbf{R}\widetilde{\mathbf{R}}\mathbf{M}\mathbf{F}^i \tag{G.9}$$

where

$$\mathbf{M} = \widetilde{\mathbf{R}}^{-1}\mathbf{W}\mathbf{R}^{-1} \tag{G.10}$$

$$\mathbf{W} = \begin{bmatrix} S_{vv}S_{vv}^* & S_{vh}S_{vh}^* & S_{vv}S_{vh}^* & S_{vh}S_{vv}^* \\ S_{hv}S_{hv}^* & S_{hh}S_{hh}^* & S_{hv}S_{hh}^* & S_{hh}S_{hv}^* \\ S_{vv}S_{hv}^* & S_{vh}S_{hh}^* & S_{vv}S_{hh}^* & S_{vh}S_{hv}^* \\ S_{hv}S_{vv}^* & S_{hh}S_{vh}^* & S_{hv}S_{vh}^* & S_{hh}S_{vv}^* \end{bmatrix} \tag{G.11}$$

$$\mathbf{R} = \begin{bmatrix} 1 & 1 & 0 & 0 \\ 1 & -1 & 0 & 0 \\ 0 & 0 & 1 & 1 \\ 0 & 0 & -j & j \end{bmatrix}. \tag{G.12}$$

The matrix $\mathbf{M}$ is the Mueller matrix, and $\widetilde{\mathbf{R}}$ means $\mathbf{R}$ transpose.

The bistatic scattering cross section of the scatterer is defined as

$$\sigma_{rt} = 4\pi r^2 \frac{|E_r^s|^2}{|E_t^i|^2} \tag{G.13}$$

where the subscripts t and r are the transmit and receive polarizations, respectively. Using (G.13), the bistatic scattering cross section for any combination of transmit and receive polarizations can be written as (van Zyl, et al., 1987; Zebker, et al., 1987)

$$\sigma_{rt}(\psi_r, \chi_r, \psi_t, \chi_t) = 4\pi \widetilde{\mathbf{Y}}^r \mathbf{M} \mathbf{Y}^t \tag{G.14}$$

where $\mathbf{Y}^t$ and $\mathbf{Y}^r$ are the *normalized* Stokes vectors characterizing the transmitter and receiver polarizations. To describe the polarization of the transmit and receive antennas, we adopt the standard convention; the polarization of an antenna is defined as the polarization of the electromagnetic wave produced by the antenna when it is used to transmit. With this definition, a given antenna (either transmitting or receiving) has a corresponding *normalized* Stokes vector. Thus,

$$\mathbf{Y}^t = \begin{bmatrix} 1 \\ \cos 2\psi_t \cos 2\chi_t \\ \sin 2\psi_t \cos 2\chi_t \\ \sin 2\chi_t \end{bmatrix} \quad \text{and} \quad \mathbf{Y}^r = \begin{bmatrix} 1 \\ \cos 2\psi_r \cos 2\chi_r \\ \sin 2\psi_r \cos 2\chi_r \\ \sin 2\chi_r \end{bmatrix} \tag{G.15}$$

where (ψ_t, χ_t) and (ψ_r, χ_r) are the orientation and ellipticity angles for the transmit and receive polarizations.

Relations similar to (G.9) and (G.14) can be derived in terms of modified Stokes vectors $\mathbf{F}_m^i$ and $\mathbf{F}_m^s$ of the form in (G.4). Using (G.5) in (G.9), we obtain

$$\mathbf{F}_m^s = \frac{1}{r^2} \mathbf{V} \widetilde{\mathbf{V}} \mathbf{M}_m \mathbf{F}_m^i \tag{G.16}$$

where

$$\mathbf{M}_m = \widetilde{\mathbf{V}}^{-1} \mathbf{W} \mathbf{V}^{-1} \tag{G.17}$$

$$\mathbf{V} = \mathbf{U}^{-1}\mathbf{R} = \begin{bmatrix} 1 & 0 & 0 & 0 \\ 0 & 1 & 0 & 0 \\ 0 & 0 & 1 & 1 \\ 0 & 0 & -j & j \end{bmatrix}. \tag{G.18}$$

Due to the similarity between (G.9) and (G.16), the matrix $\mathbf{M}_m$ will be called the *modified* Mueller matrix. The matrix $\mathbf{V}\widetilde{\mathbf{V}}\mathbf{M}_m$ is recognized as the modified Stokes matrix. The bistatic scattering cross section is found by using (G.5) in (G.14) resulting in the expression

$$\sigma_{rt}(\psi_r, \chi_r, \psi_t, \chi_t) = 4\pi \widetilde{\mathbf{Y}}^r_m \mathbf{M}_m \mathbf{Y}^t_m \tag{G.19}$$

where the *normalized* modified Stokes vectors $\mathbf{Y}^t_m$ and $\mathbf{Y}^r_m$ are given by

$$\mathbf{Y}^t_m = \begin{bmatrix} \frac{1}{2}(1 + \cos 2\psi_t \cos 2\chi_t) \\ \frac{1}{2}(1 - \cos 2\psi_t \cos 2\chi_t) \\ \sin 2\psi_t \cos 2\chi_t \\ \sin 2\chi_t \end{bmatrix} \text{ and } \mathbf{Y}^r_m = \begin{bmatrix} \frac{1}{2}(1 + \cos 2\psi_r \cos 2\chi_r) \\ \frac{1}{2}(1 - \cos 2\psi_r \cos 2\chi_r) \\ \sin 2\psi_r \cos 2\chi_r \\ \sin 2\chi_r \end{bmatrix}. \tag{G.20}$$

G.2 Distributed Target

The modified Stokes vector $\mathbf{F}_m$ given by (G.4) is defined in a form appropriate for characterizing the polarization state of a wave incident upon or scattered by a point target. For a distributed target, the incident and scattered intensities $\mathbf{I}^i$ and $\mathbf{I}^s$ are used instead. Comparison of (G.4) with (A.2) and (A.3) leads to

$$\mathbf{I}^i = \frac{1}{\eta}\overline{\mathbf{F}}^i_m \tag{G.21}$$

$$\mathbf{I}^s = \frac{r^2}{\eta A \cos\theta_s}\overline{\mathbf{F}}^s_m \tag{G.22}$$

where A is the illuminated area, θ_s is the scattering angle (which is equal to θ_0 for backscatter), and

$$\overline{\mathbf{F}}_m^i = \begin{bmatrix} \langle |E_v^i|^2 \rangle \\ \langle |E_h^i|^2 \rangle \\ 2\mathrm{Re}\langle E_v^i E_h^{i*} \rangle \\ 2\mathrm{Im}\langle E_v^i E_h^{i*} \rangle \end{bmatrix} \quad \text{and} \quad \overline{\mathbf{F}}_m^s = \begin{bmatrix} \langle |E_v^s|^2 \rangle \\ \langle |E_h^s|^2 \rangle \\ 2\mathrm{Re}\langle E_v^s E_h^{s*} \rangle \\ 2\mathrm{Im}\langle E_v^s E_h^{s*} \rangle \end{bmatrix}. \tag{G.23}$$

The notation $\langle \ldots \rangle$ denotes the ensemble average. If the ensemble average of $\mathbf{F}_m^s$ is computed from (G.16), we obtain

$$\overline{\mathbf{F}}_m^s = \frac{1}{r^2} \mathbf{V} \widetilde{\mathbf{V}} \overline{\mathbf{M}}_m \overline{\mathbf{F}}_m^i \tag{G.24}$$

or equivalently,

$$\mathbf{I}^s = \frac{1}{A \cos\theta_s} \mathbf{V} \widetilde{\mathbf{V}} \overline{\mathbf{M}}_m \mathbf{I}^i \tag{G.25}$$

where $\mathbf{V}$ is given by (G.18) and $\overline{\mathbf{M}}_m$ is the average modified Mueller matrix;

$$\overline{\mathbf{M}}_m = \widetilde{\mathbf{V}}^{-1} \overline{\mathbf{W}} \mathbf{V}^{-1} \tag{G.26}$$

with

$$\overline{\mathbf{W}} = \begin{bmatrix} \langle S_{vv} S_{vv}^* \rangle & \langle S_{vh} S_{vh}^* \rangle & \langle S_{vv} S_{vh}^* \rangle & \langle S_{vh} S_{vv}^* \rangle \\ \langle S_{hv} S_{hv}^* \rangle & \langle S_{hh} S_{hh}^* \rangle & \langle S_{hv} S_{hh}^* \rangle & \langle S_{hh} S_{hv}^* \rangle \\ \langle S_{vv} S_{hv}^* \rangle & \langle S_{vh} S_{hh}^* \rangle & \langle S_{vv} S_{hh}^* \rangle & \langle S_{vh} S_{hv}^* \rangle \\ \langle S_{hv} S_{vv}^* \rangle & \langle S_{hh} S_{vh}^* \rangle & \langle S_{hv} S_{vh}^* \rangle & \langle S_{hh} S_{vv}^* \rangle \end{bmatrix}. \tag{G.27}$$

Equation (G.25) for the distributed target is the counterpart of (G.16) for the point target case. By comparing (G.24) with (G.16) we can write an expression

for the bistatic scattering coefficient for the distributed target similar to that for the scattering cross section of a point target in (G.19);

$$\sigma^0_{rt}(\psi_r, \chi_r, \psi_t, \chi_t) = \frac{4\pi}{A}\widetilde{\mathbf{Y}}^r_m \overline{\mathbf{M}}_m \mathbf{Y}^t_m \tag{G.28}$$

where $\mathbf{Y}^t_m$ and $\mathbf{Y}^r_m$ are the normalized modified Stokes vectors for the transmitter and receiver given in (G.20).

G.3 Polarization Coordinate Systems

In the literature, there are basically two conventions for defining the polarization of an electromagnetic wave when considering scattering from an object. One convention defines the vertical and horizontal unit polarization vectors for the incident and scattered waves such that they are equal in the *forward scatter* direction. This convention will be called the FSA (Forward Scatter Alignment) convention. One such representation is given by

$$\hat{\mathbf{n}}_i = \hat{\mathbf{x}}\sin\theta_i\cos\phi_i + \hat{\mathbf{y}}\sin\theta_i\sin\phi_i + \hat{\mathbf{z}}\cos\theta_i \tag{G.29}$$

$$\hat{\mathbf{h}}_i = -\hat{\mathbf{x}}\sin\phi_i + \hat{\mathbf{y}}\cos\phi_i \tag{G.30}$$

$$\hat{\mathbf{v}}_i = \hat{\mathbf{h}}_i \times \hat{\mathbf{n}}_i = \hat{\mathbf{x}}\cos\theta_i\cos\phi_i + \hat{\mathbf{y}}\cos\theta_i\sin\phi_i - \hat{\mathbf{z}}\sin\theta_i \tag{G.31}$$

$$\hat{\mathbf{n}}_s = \hat{\mathbf{x}}\sin\theta_s\cos\phi_s + \hat{\mathbf{y}}\sin\theta_s\sin\phi_s + \hat{\mathbf{z}}\cos\theta_s \tag{G.32}$$

$$\hat{\mathbf{h}}_s = -\hat{\mathbf{x}}\sin\phi_s + \hat{\mathbf{y}}\cos\phi_s \tag{G.33}$$

$$\hat{\mathbf{v}}_s = \hat{\mathbf{h}}_s \times \hat{\mathbf{n}}_s = \hat{\mathbf{x}}\cos\theta_s\cos\phi_s + \hat{\mathbf{y}}\cos\theta_s\sin\phi_s - \hat{\mathbf{z}}\sin\theta_s. \tag{G.34}$$

with the associated geometry shown in Figure G.2. Notice that for forward scatter ($\theta_s = \theta_i$ and $\phi_s = \phi_i$), we have $\hat{\mathbf{n}}_s = \hat{\mathbf{n}}_i$, $\hat{\mathbf{v}}_s = \hat{\mathbf{v}}_i$, and $\hat{\mathbf{h}}_s = \hat{\mathbf{h}}_i$. The FSA convention has been adopted in this document.

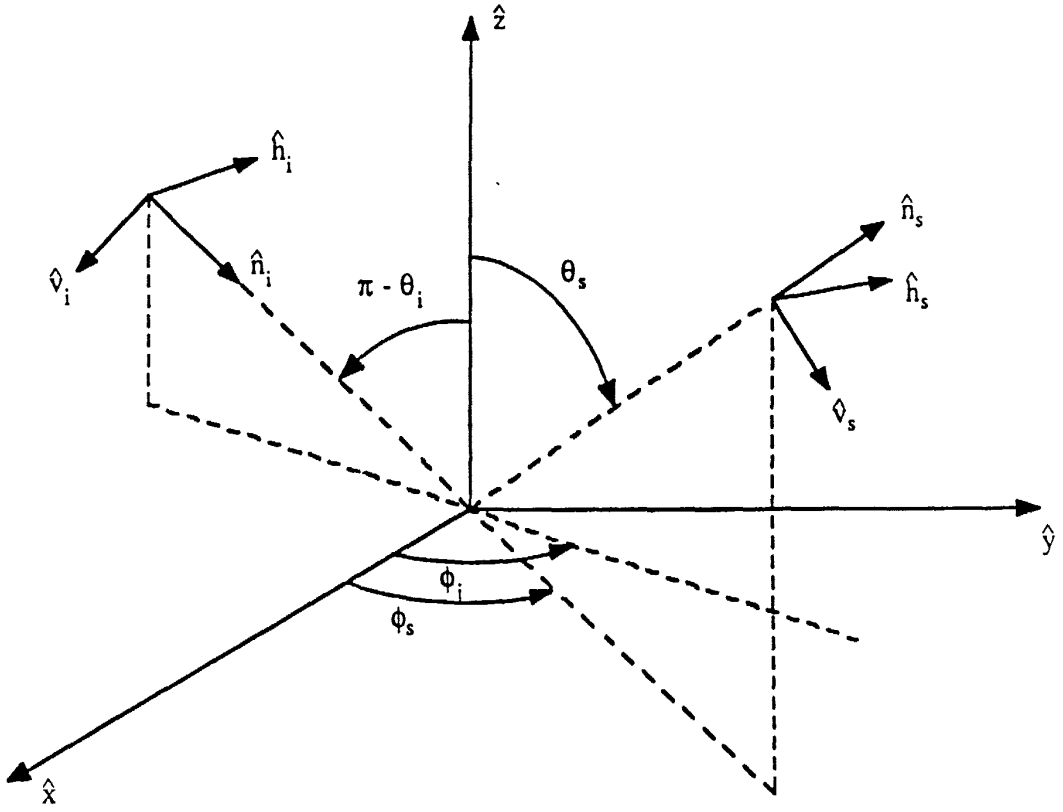


Figure G.2: Geometry for the FSA convention.

The other convention defines the vertical and horizontal unit polarization vectors for the incident and scattered wave such that they are equal in the *backscatter* direction. This convention will be called the BSA (BackScatter Alignment) convention. A corresponding representation for this convention is given by

$$\hat{\mathbf{n}}_i = \hat{\mathbf{x}} \sin\theta_i \cos\phi_i + \hat{\mathbf{y}} \sin\theta_i \sin\phi_i + \hat{\mathbf{z}} \cos\theta_i \tag{G.35}$$

$$\hat{\mathbf{h}}_i = -\hat{\mathbf{x}} \sin\phi_i + \hat{\mathbf{y}} \cos\phi_i \tag{G.36}$$

$$\hat{\mathbf{v}}_i = \hat{\mathbf{h}}_i \times \hat{\mathbf{n}}_i = \hat{\mathbf{x}} \cos\theta_i \cos\phi_i + \hat{\mathbf{y}} \cos\theta_i \sin\phi_i - \hat{\mathbf{z}} \sin\theta_i \tag{G.37}$$

$$\hat{\mathbf{n}}_s = \hat{\mathbf{x}} \sin\theta_s \cos\phi_s + \hat{\mathbf{y}} \sin\theta_s \sin\phi_s + \hat{\mathbf{z}} \cos\theta_s \tag{G.38}$$

$$\hat{\mathbf{h}}_s = \hat{\mathbf{x}} \sin\phi_s - \hat{\mathbf{y}} \cos\phi_s \tag{G.39}$$

$$\hat{\mathbf{v}}_s = -\hat{\mathbf{h}}_s \times \hat{\mathbf{n}}_s = \hat{\mathbf{x}} \cos\theta_s \cos\phi_s + \hat{\mathbf{y}} \cos\theta_s \sin\phi_s - \hat{\mathbf{z}} \sin\theta_s. \tag{G.40}$$

with the associated geometry shown in Figure G.3. Here, when backscatter is considered ($\theta_s = \pi - \theta_i$ and $\phi_s = \pi + \phi_i$), we have $\hat{\mathbf{n}}_s = -\hat{\mathbf{n}}_i$, $\hat{\mathbf{v}}_s = \hat{\mathbf{v}}_i$, and $\hat{\mathbf{h}}_s = \hat{\mathbf{h}}_i$. The only difference between the BSA and FSA conventions is that $\hat{\mathbf{h}}_s$ is replaced with $-\hat{\mathbf{h}}_s$.

The BSA convention has been the standard used in the area of radar polarimetry (van Zyl, et al., 1987; Zebker, et al., 1987). Here, two antennas are said to be identically polarized when upon transmit, the electromagnetic waves produced have identical polarization. Further, the polarization of each antenna is defined to be the polarization of its transmitted wave. Traditionally, the radar cross section σ_{rt} is proportional to the ratio of the scattered power received by an antenna with polarization r to the incident power transmitted by an antenna with polarization t (see equation (G.13)). This definition along with the intuitive notion that identical

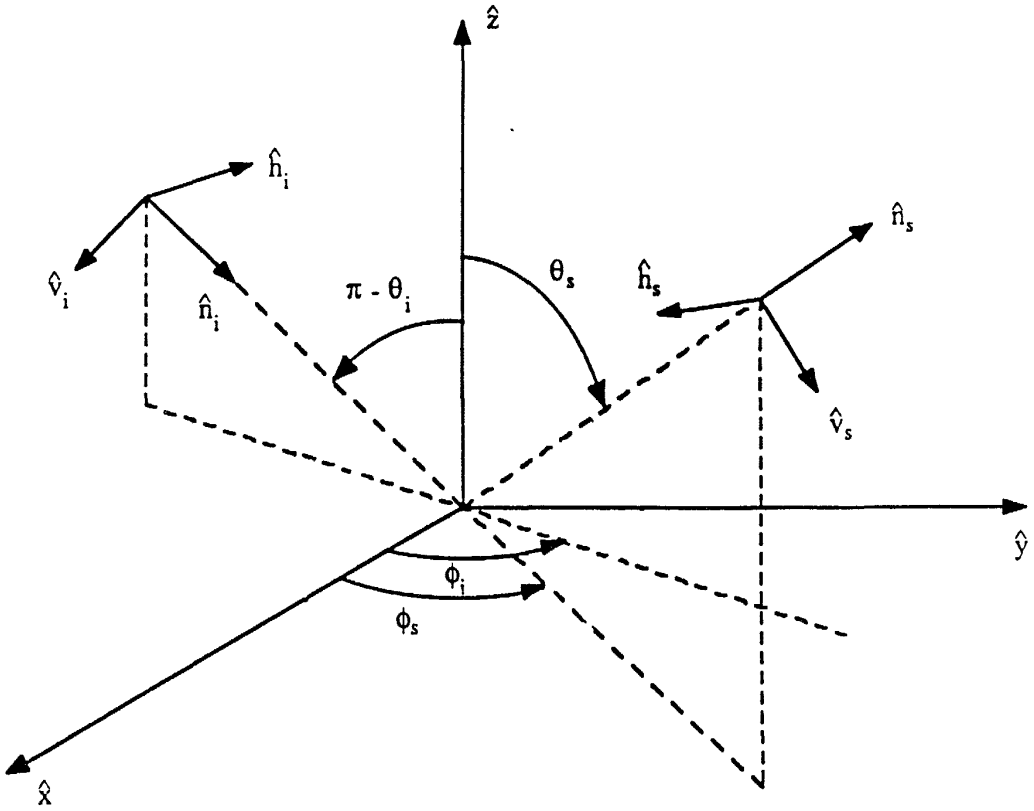


Figure G.3. Geometry for the BSA convention.

antennas have the same polarization is equivalent to using the BSA convention.

Since many scattering formulations use the FSA convention (including this document), we must be able to convert our wave synthesis results between the BSA and FSA conventions. Suppose that the incident and scattered intensities defined with the BSA convention are related by the expression in (G.25) where we let

$$\mathbf{T} = \frac{1}{A\cos\theta_s}\mathbf{V}\widetilde{\mathbf{V}}\overline{\mathbf{M}}_m. \tag{G.41}$$

¿From the definitions of $\mathbf{I}^i$ and $\mathbf{I}^s$ given in (G.21) to (G.23), the incident and scattered intensities defined in the FSA convention are

$$\mathbf{I}^i_F = \mathbf{I}^i \tag{G.42}$$

$$\mathbf{I}^s_F = \mathbf{I}_p\mathbf{I}^s \tag{G.43}$$

where

$$\mathbf{I}_p = \begin{bmatrix} 1 & 0 & 0 & 0 \\ 0 & 1 & 0 & 0 \\ 0 & 0 & -1 & 0 \\ 0 & 0 & 0 & -1 \end{bmatrix}. \tag{G.44}$$

Substituting these relations in (G.25) gives

$$\mathbf{I}^s_F = \frac{1}{A\cos\theta_s}\mathbf{I}_p\mathbf{V}\widetilde{\mathbf{V}}\overline{\mathbf{M}}_m\mathbf{I}^i_F = \frac{1}{A\cos\theta_s}\mathbf{V}\widetilde{\mathbf{V}}\mathbf{I}_p\overline{\mathbf{M}}_m\mathbf{I}^i_F. \tag{G.45}$$

Thus, the corresponding matrices $\mathbf{T}'$ and $\overline{\mathbf{M}}'_m$ defined with the FSA convention are related to $\mathbf{T}$ and $\overline{\mathbf{M}}_m$ defined with the BSP convention by the relations

$$\mathbf{T}' = \mathbf{I}_p\mathbf{T} \tag{G.46}$$

$$\overline{\mathbf{M}}'_m = \mathbf{I}_p\overline{\mathbf{M}}_m. \tag{G.47}$$

Take note that since $\mathbf{I}_p$ is a diagonal matrix whose elements have magnitude equal to one, these expressions can also be written as

$$\mathbf{T} = \mathbf{I}_p \mathbf{T}' \tag{G.48}$$

$$\overline{\mathbf{M}}_m = \mathbf{I}_p \overline{\mathbf{M}}'_m. \tag{G.49}$$

APPENDIX H NUMERICAL SIMULATIONS OF SELECTED CANOPIES

This appendix presents the results of simulations of four tree canopies. The data presented here coincide with the analysis presented in Section 3 of the main report. Relevant canopy parameters are listed in Table H.1.

The parameters of canopies I, II and III were chosen to represent a trembling aspen stand. Canopy I represents a canopy with a leaf-dominated crown layer for which branches are not considered. Canopy II represents an Aspen stand whose crown layer consists of branches only. Canopy III represents a stand whose crown layer consists of both leaves and branches. Except for the presence or absence of leaves and branches, the attributes of canopies I, II and III remain unchanged so that comparisons may be made as to the effect of leaves and branches on the radar backscatter. Canopy IV represents a white spruce stand. Here, the crown layer consists of both needles and branches. A description of branch, leaf, and needle sizes and orientations is given in Section 3 of the main report.

The data presented for each canopy consist of plots of total canopy backscatter as a function of both incidence angle and frequency. Graphs shown as a function of incidence angle were computed for frequencies of 1.62, 4.75 and 10.0 GHz, corresponding to L-, C-, and X-bands, respectively. Graphs shown as a function of frequency were computed using an incidence angle of 30^{o}.

The components of the total backscatter for each canopy are also shown. The total canopy backscatter is shown to consist of 1) a ground-trunk interaction com-

ponent, 2) a total crown backscatter component and 3) a direct ground backscatter component. The total crown backscatter component is shown as consisting of three contributions resulting from 1) the direct backscatter from the crown, 2) the combination of specular scatter from the ground and forward scatter from the crown layer and 3) the combination of specular scatter from the ground that is scattered directly back to the ground from the crown layer and is again scattered in the specular direction by the ground. In all cases, the backscatter is shown for the four polarization configurations HH, VV, VH and HV. Since only azimuthally symmetric canopies are considered in this study, the total cross-polarized backscatter consists only of the cross-polarized crown layer contributions.

TABLE H.1. Test Canopy Parameters

Parameter	Canopy I	Canopy II	Canopy III	Canopy IV
Canopy Density (trees per square meter)	0.11	0.11	0.11	0.20
Trunk Height (meters)	8 m	8 m	8 m	16 m
Trunk Diameter (cm)	24 cm	24 cm	24 cm	20.8 cm
Trunk Moisture (gravimetric)	0.5	0.5	0.5	0.6
Crown Thickness (meters)	2 m	2 m	2 m	11.0 m
Leaf/Needle Density (per cubic meter)	830	0	830	85,000
Leaf/Needle Moisture (gravimetric)	0.8	-	0.8	0.8
LAI (single-sided)	5	0	5	11.9
Branch Density (branches per cubic meter)	0	4.1	4.1	3.4
Branch Length (m)	-	0.75 m	0.75 m	2.0 m
Branch Diameter (cm)	-	0.7 cm	0.7 cm	2.0 cm
Branch Moisture (gravimetric)	-	0.4	0.4	0.6
Soil RMS Height	0.45 cm	0.45 cm	0.45 cm	0.45 cm
Soil Correlation Length	18.75 cm	18.75 cm	18.75 cm	18.75 cm
Soil Volumetric Moisture	0.15	0.15	0.15	0.15
Soil % Sand	10	10	10	20
Soil % Silt	30	30	30	70
Soil % Clay	60	60	60	10

CANOPY I – Leaf-Dominated Crown Layer

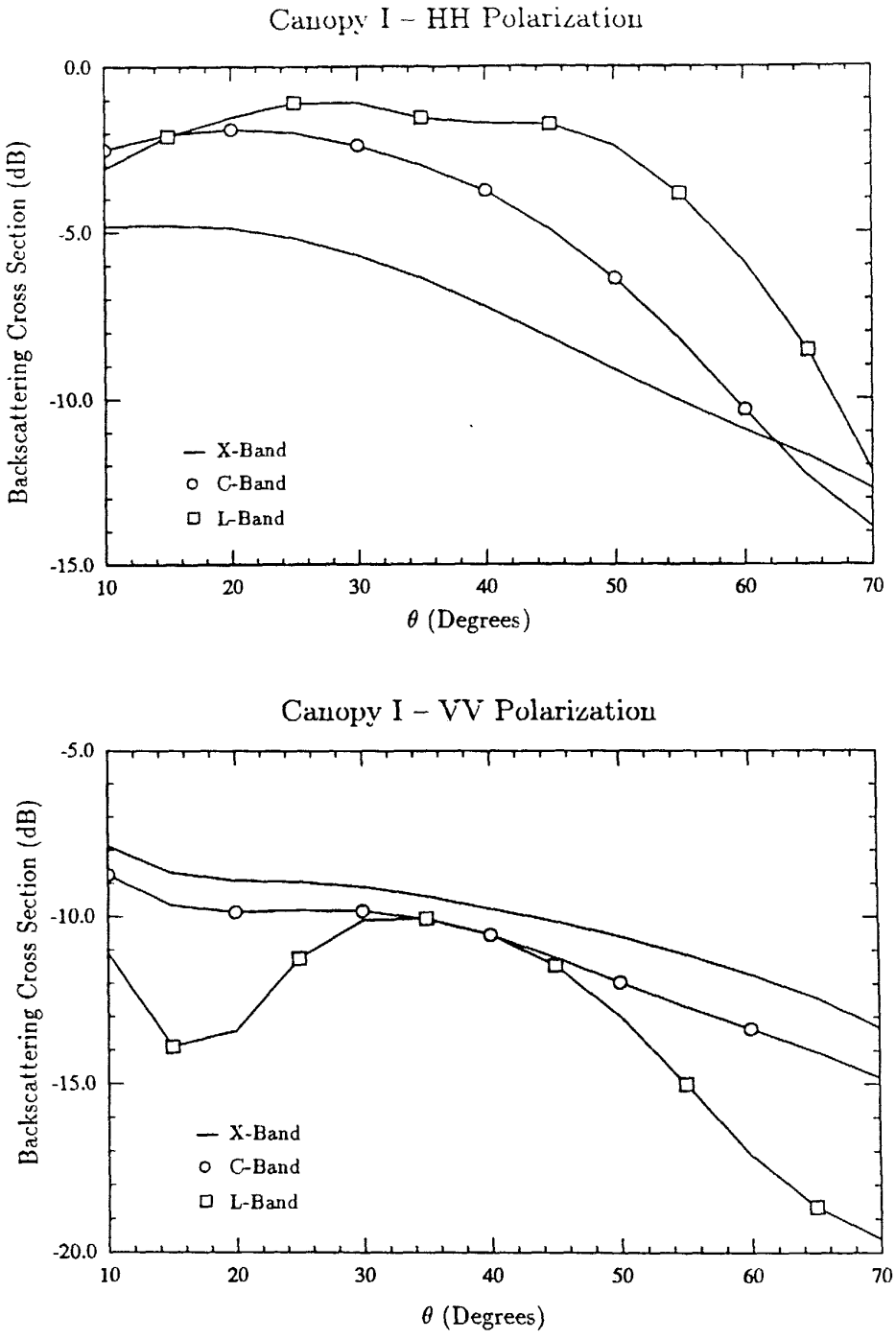


Figure H.1· Total Like-Polarized Canopy Backscatter vs. Incidence Angle

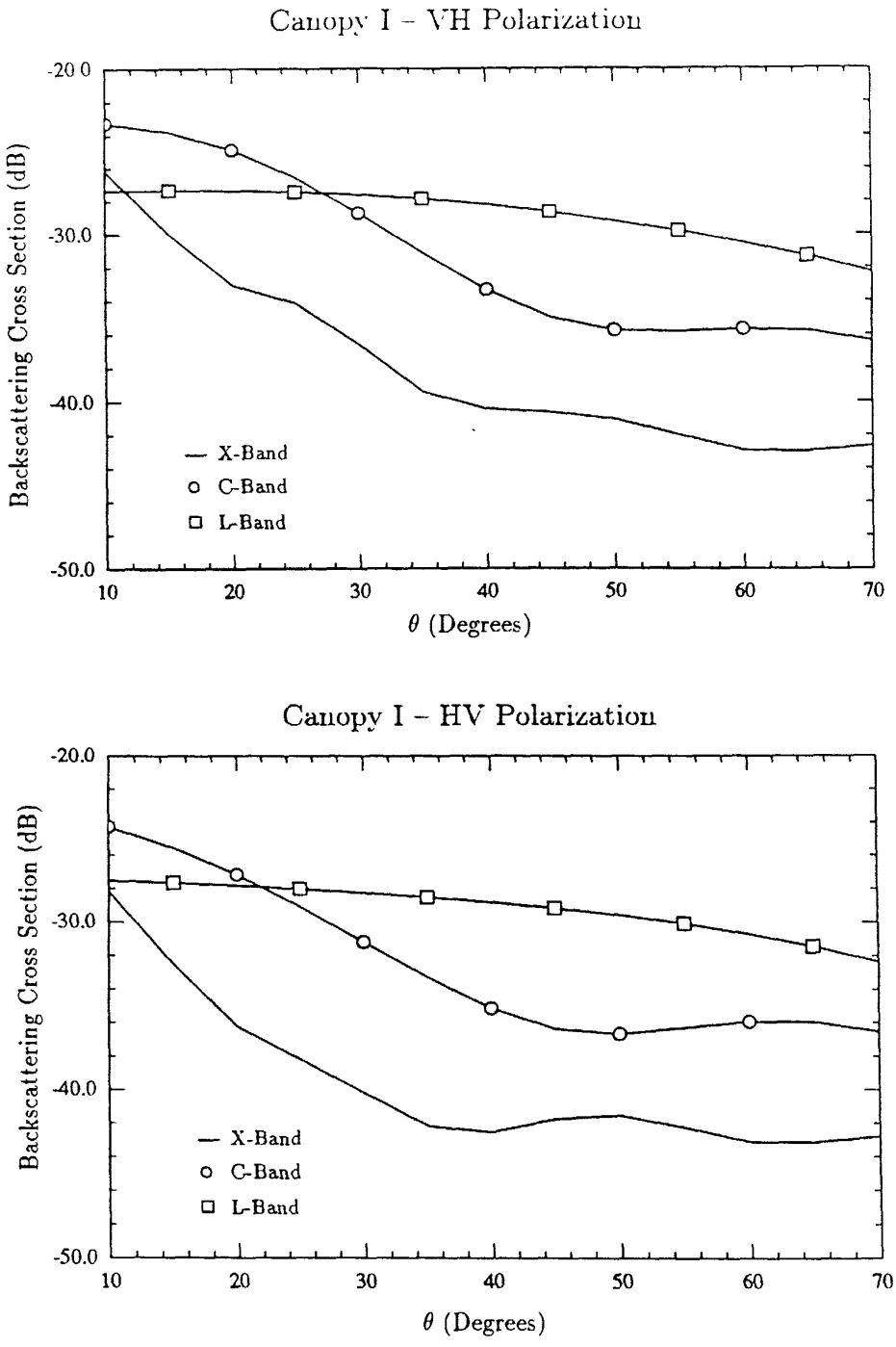


Figure H.2 Total Cross-Polarized Canopy Backscatter vs. Incidence Angle

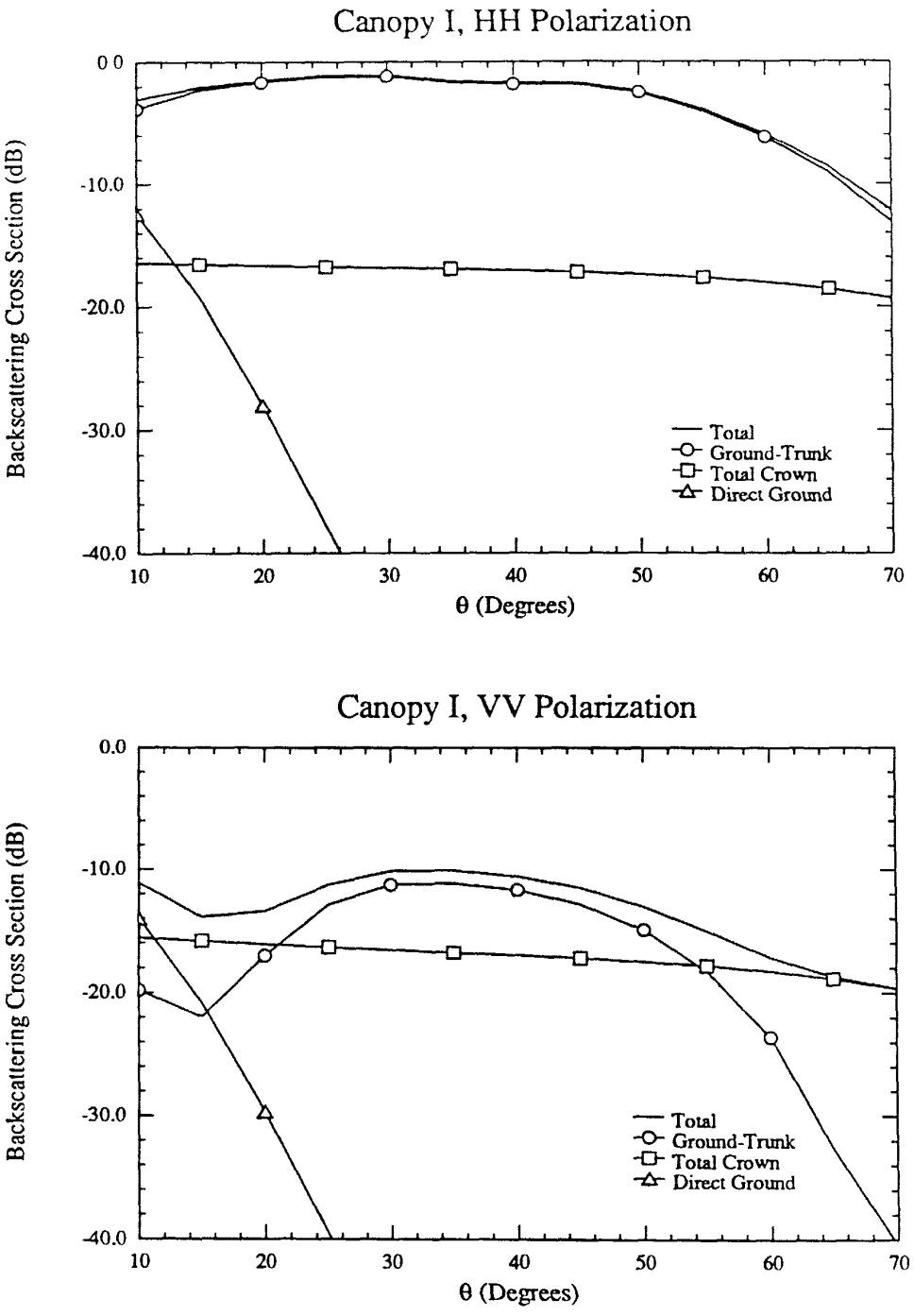


Figure H.3· L-Band Like-Polarized Canopy Backscatter Components vs. Incidence Angle

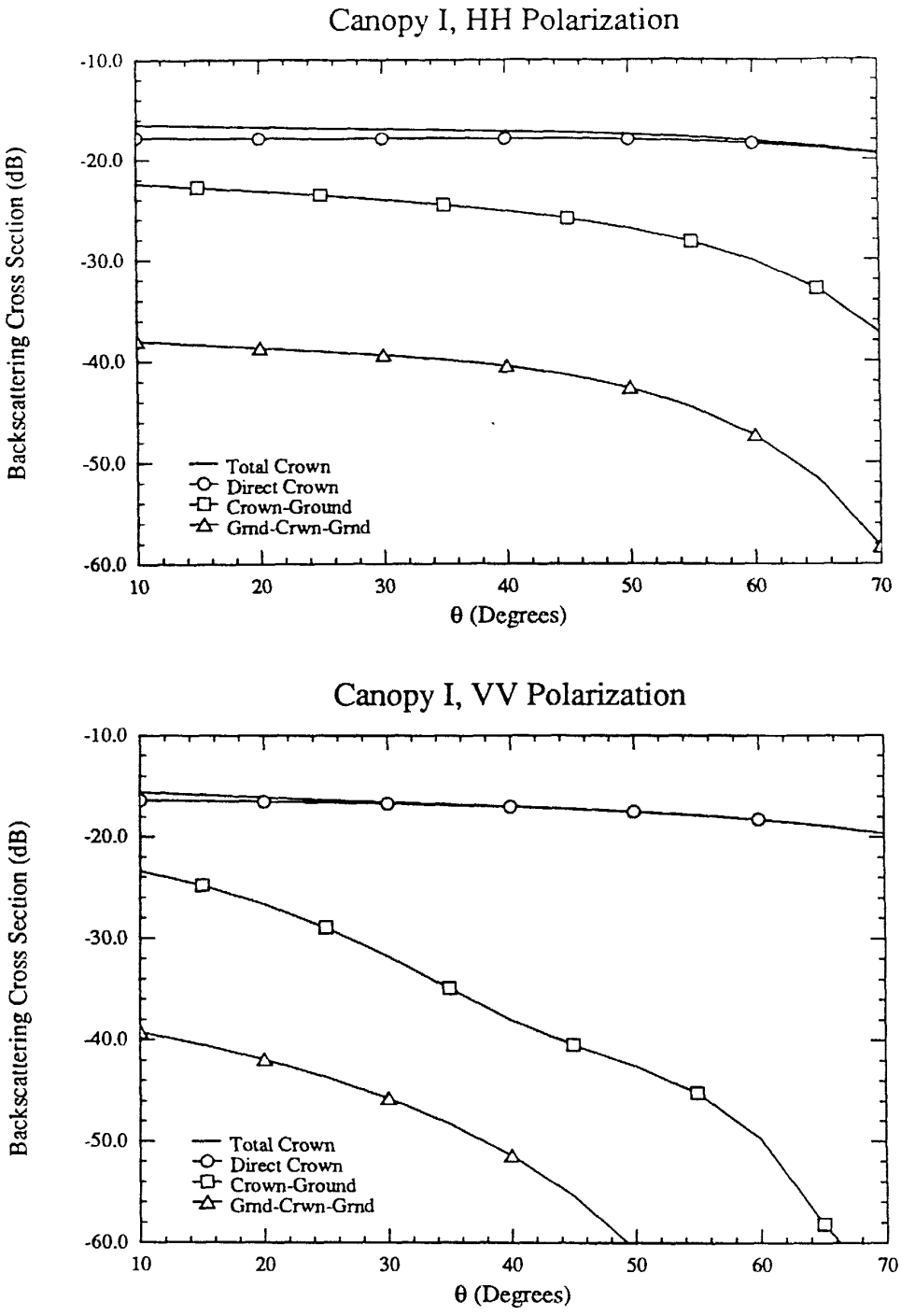


Figure H 4: L-Band Like-Polarized Crown Backscatter Components vs. Incidence Angle

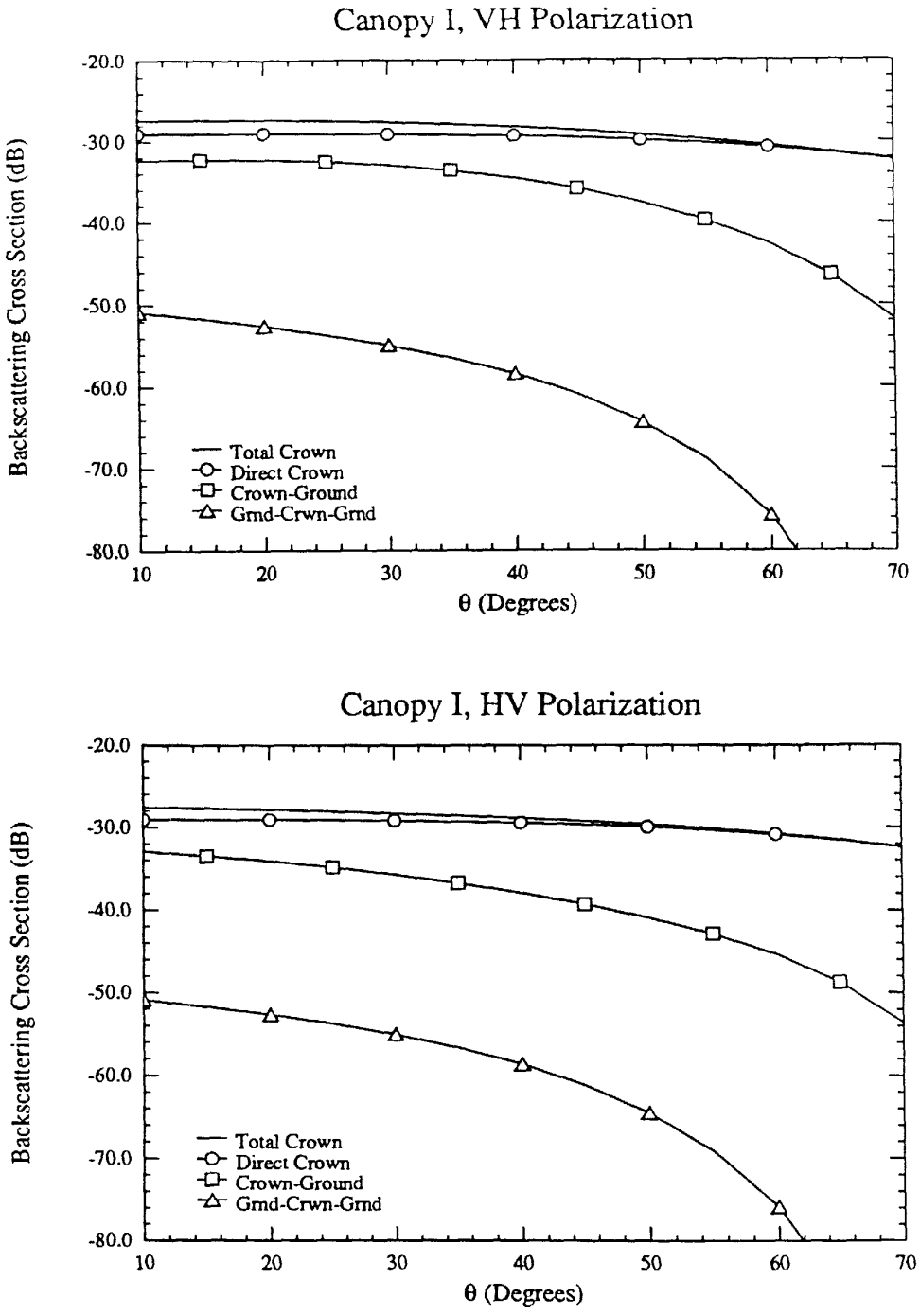


Figure H.5: L-Band Cross-Polarized Crown Backscatter Components vs Incidence Angle

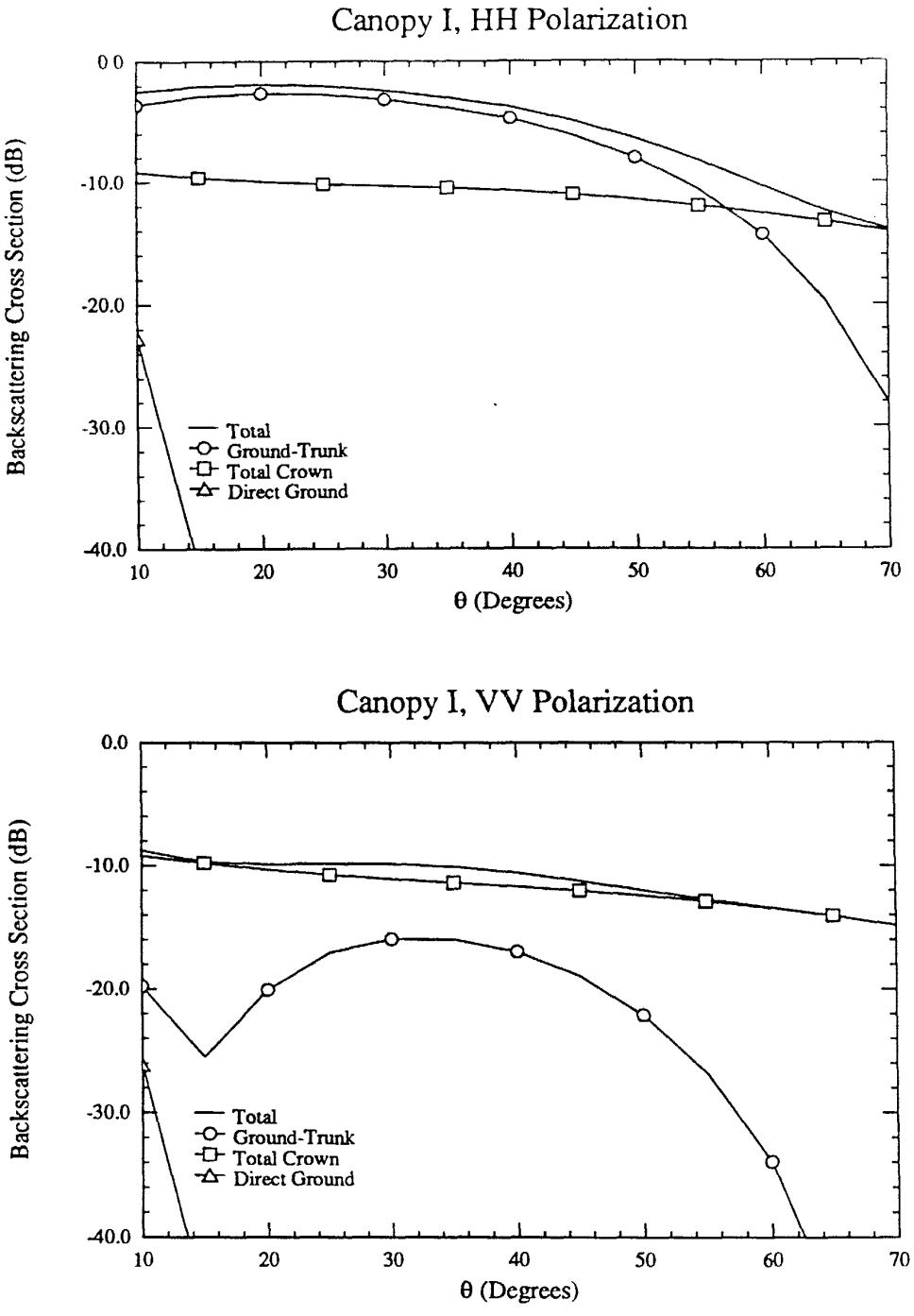


Figure H.6: C-Band Like-Polarized Canopy Backscatter Components vs. Incidence Angle

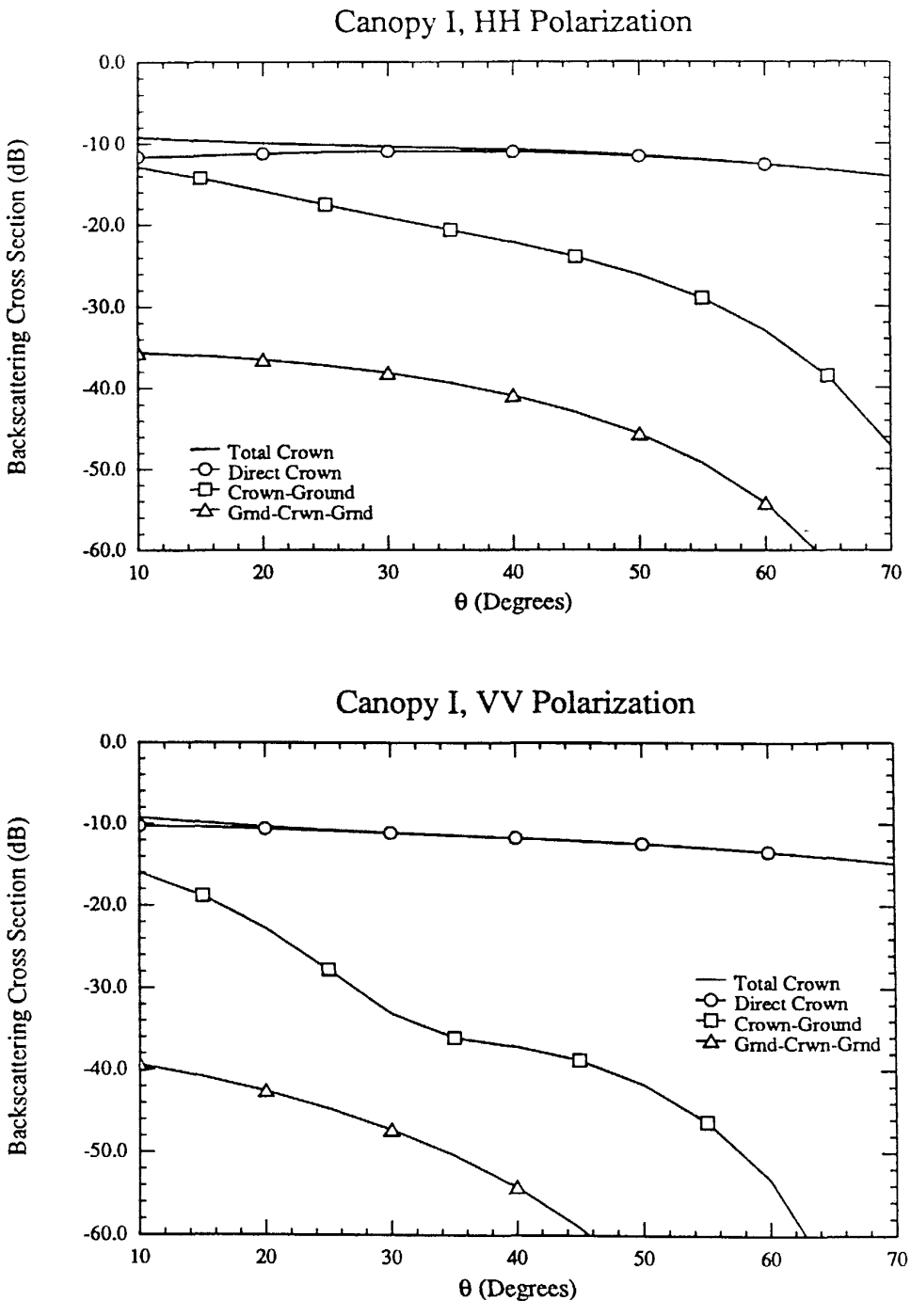


Figure H.7. C-Band Like-Polarized Crown Backscatter Components vs. Incidence Angle

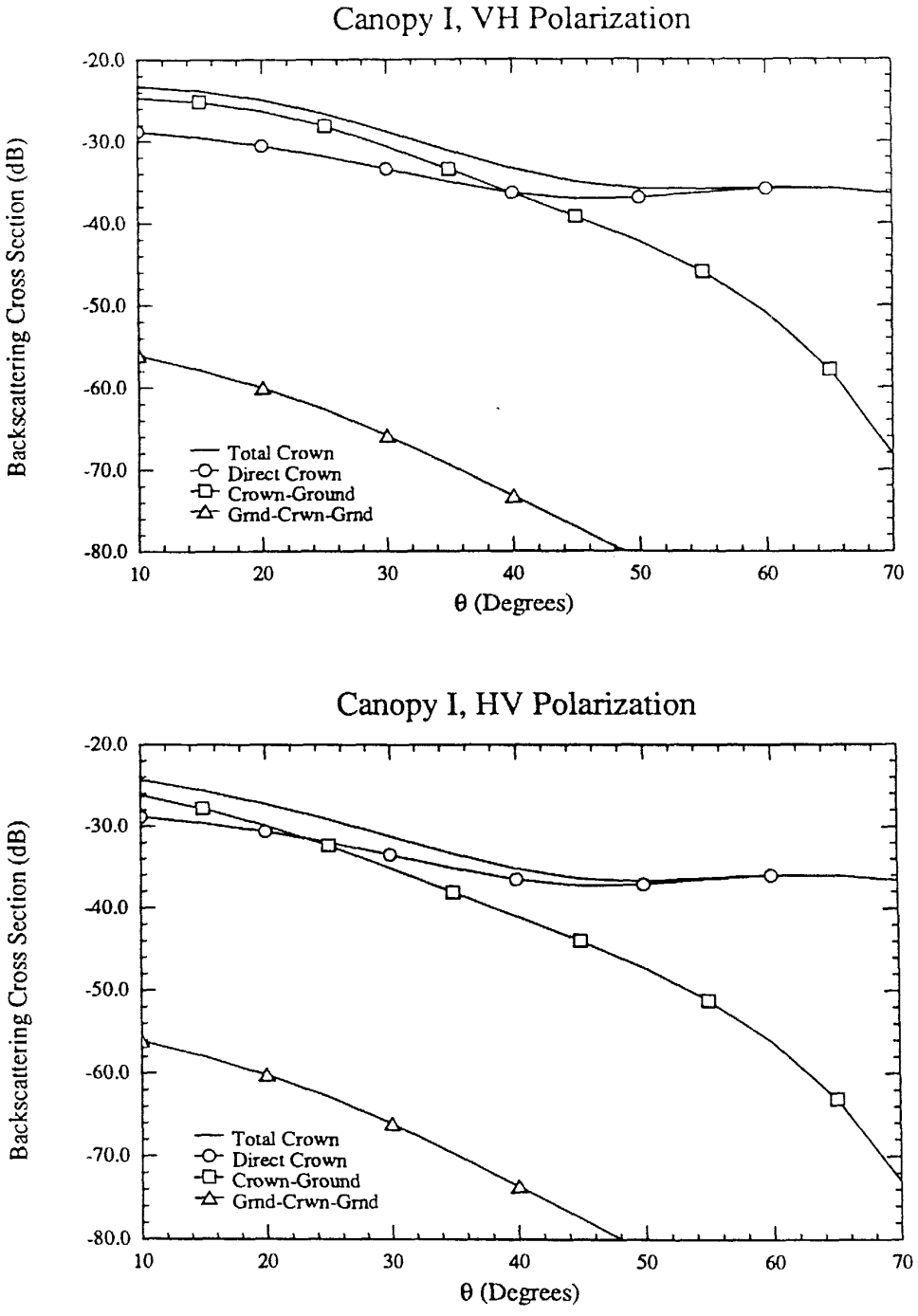


Figure H.8 C-Band Cross-Polarized Crown Backscatter Components vs. Incidence Angle

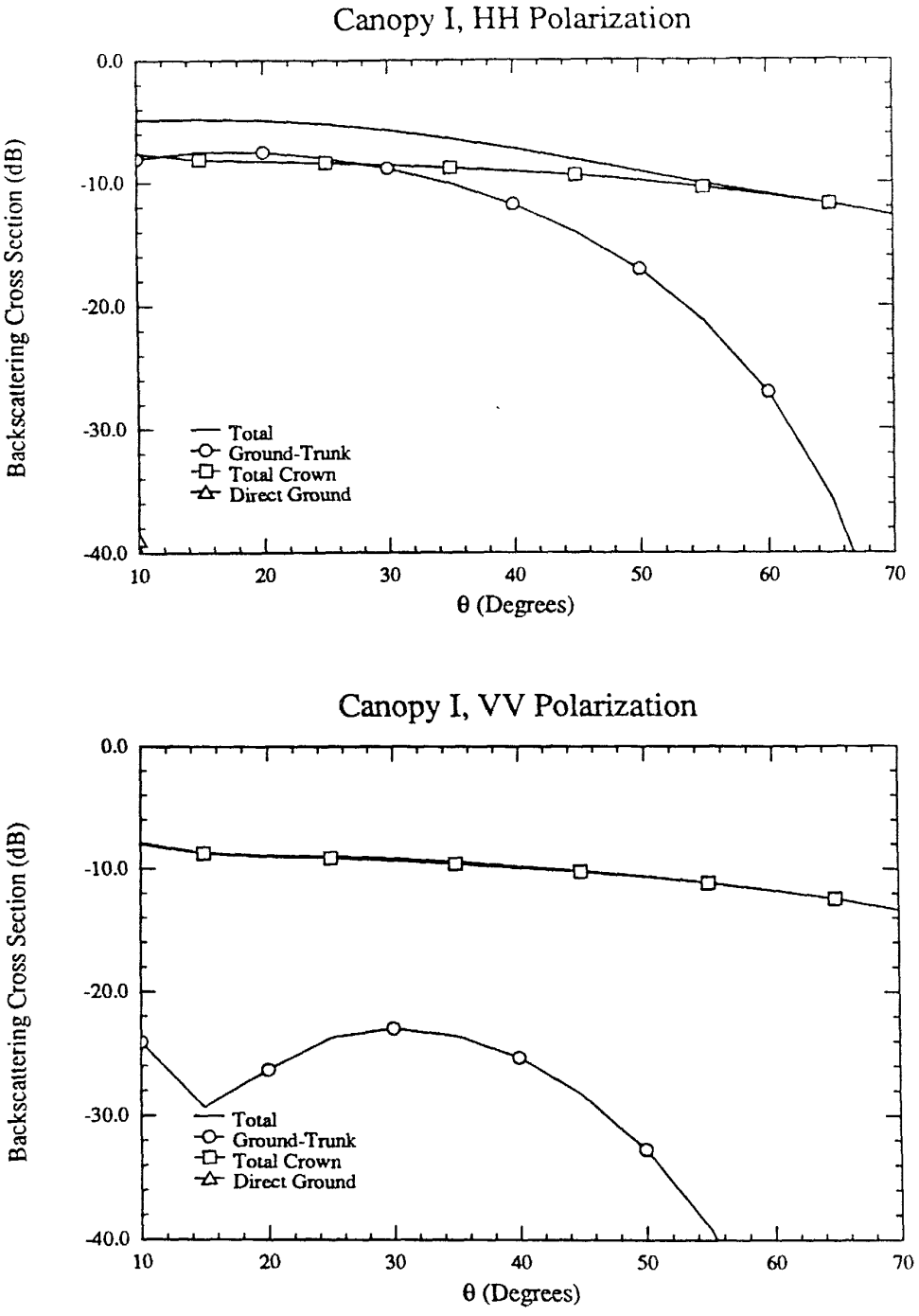


Figure H.9. X-Band Like-Polarized Canopy Backscatter Components vs Incidence Angle

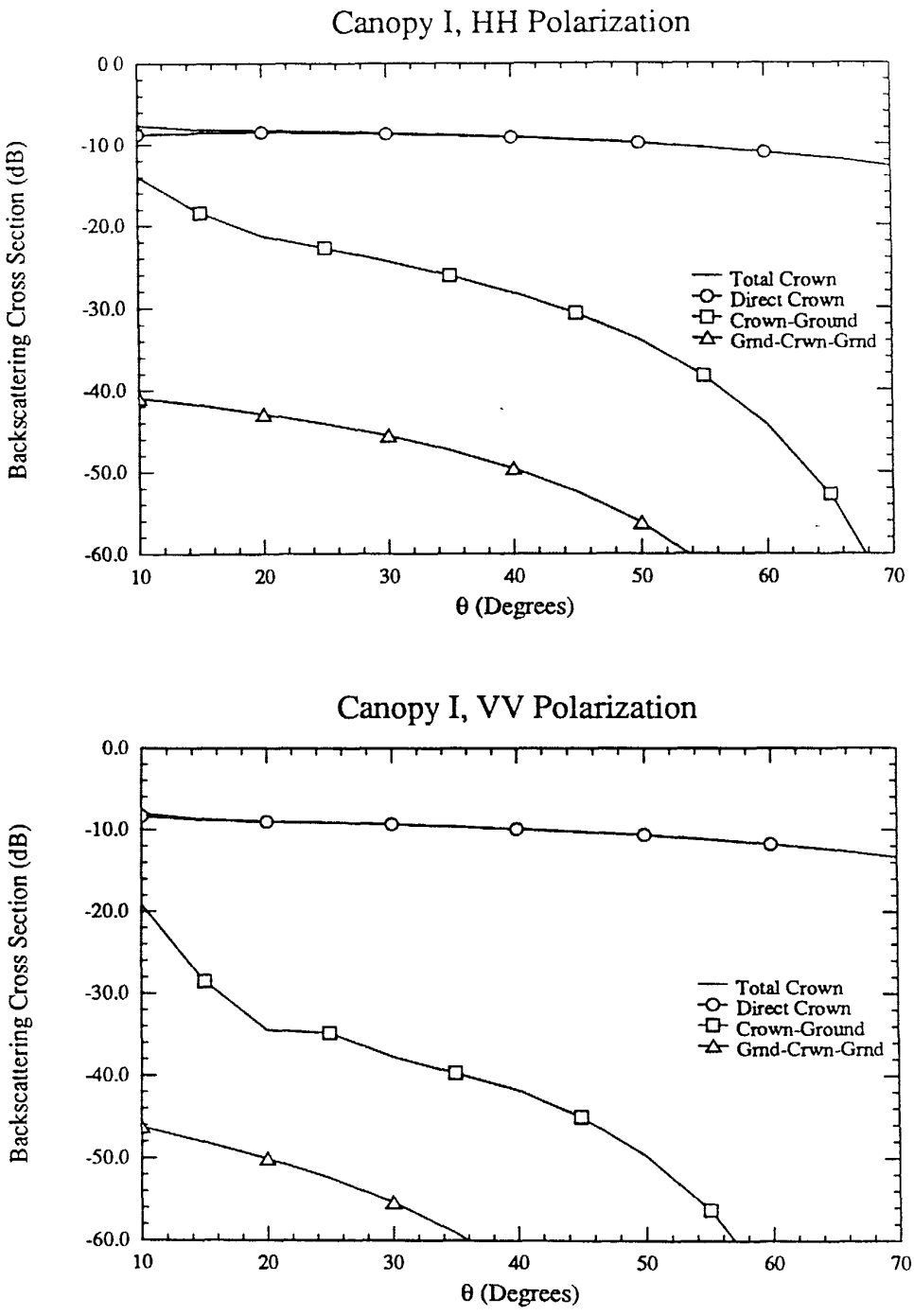


Figure H.10 X-Band Like-Polarized Crown Backscatter Components vs. Incidence Angle

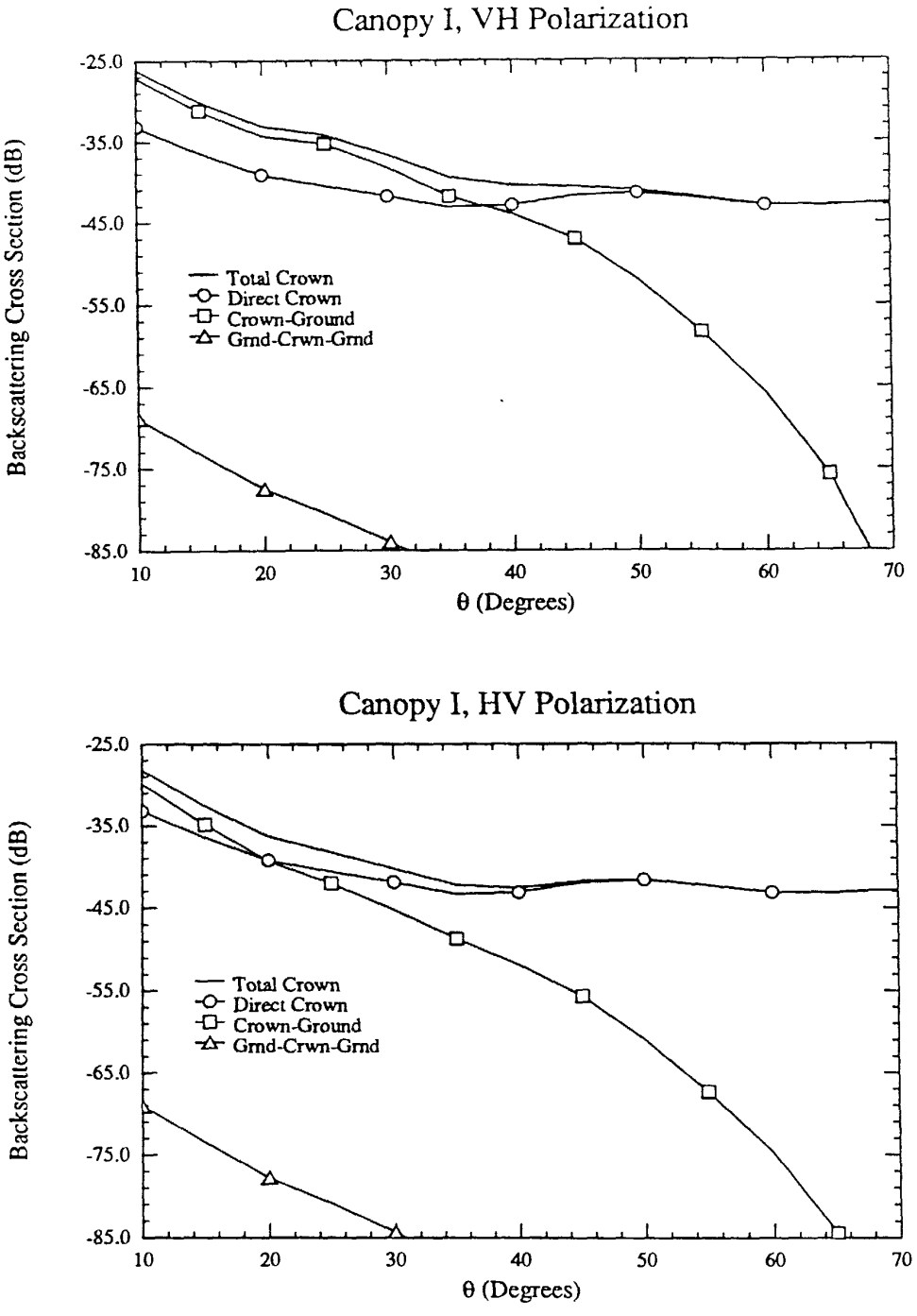


Figure II.11: X-Band Cross-Polarized Crown Backscatter Components vs Incidence Angle

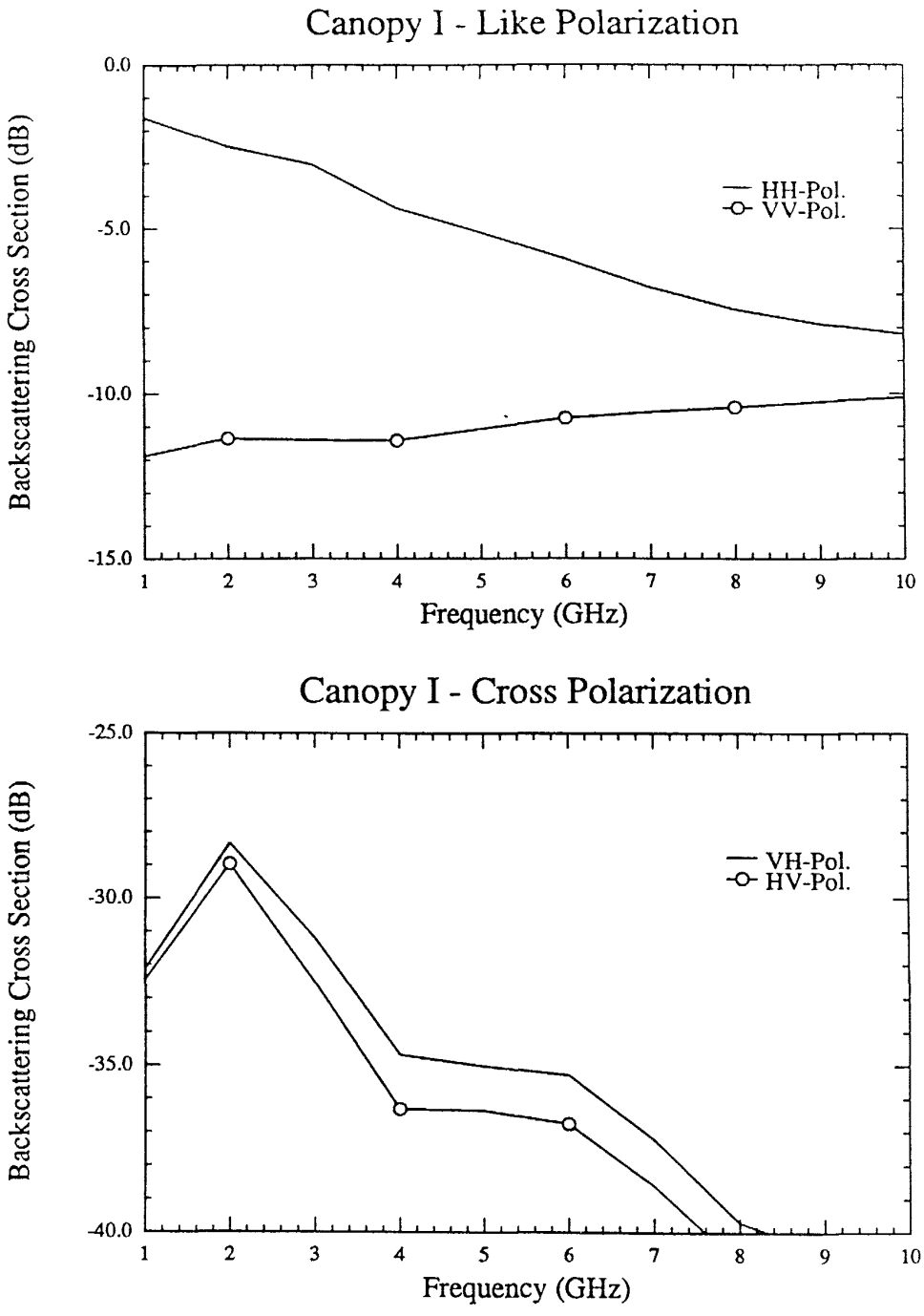


Figure H.12. Total Canopy Backscatter Components vs. Frequency Incidence Angle = 30°

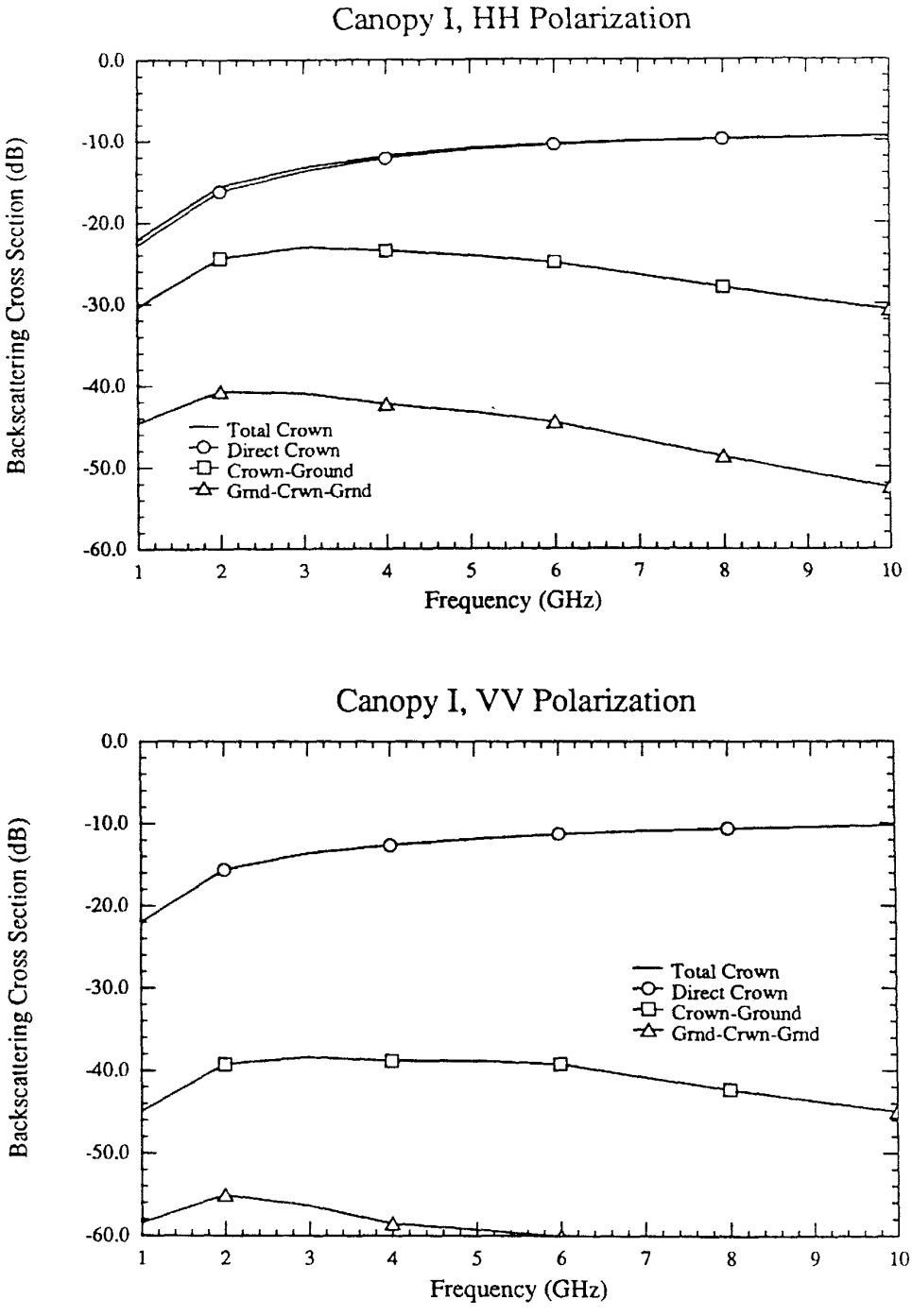


Figure II.13: Like-Polarized Crown Backscatter Components vs Frequency Incidence Angle = 30°

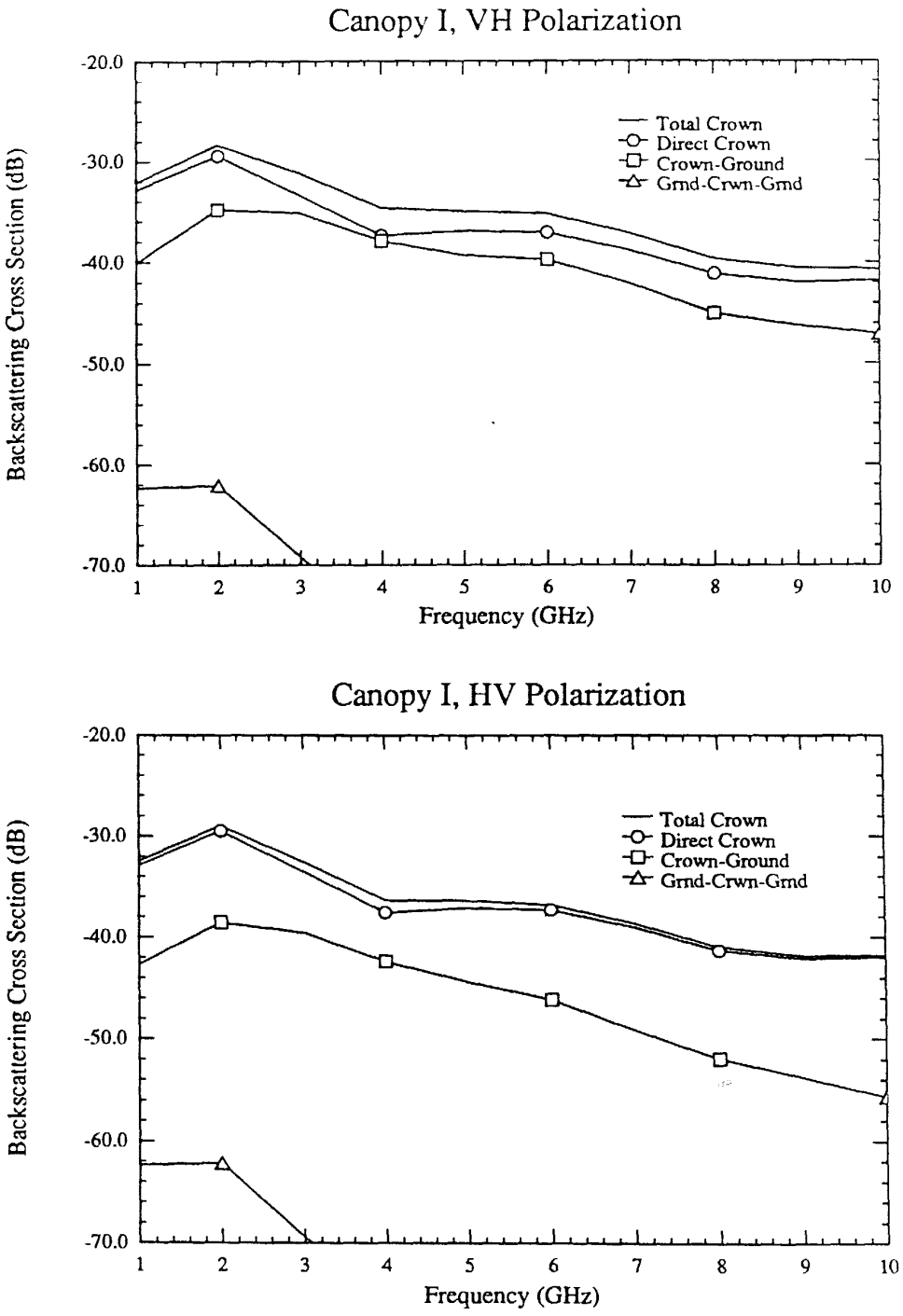


Figure H.14 Cross-Polarized Crown Backscatter Components vs. Frequency. Incidence Angle = 30°

CANOPY II – Branch-Dominated Crown Layer

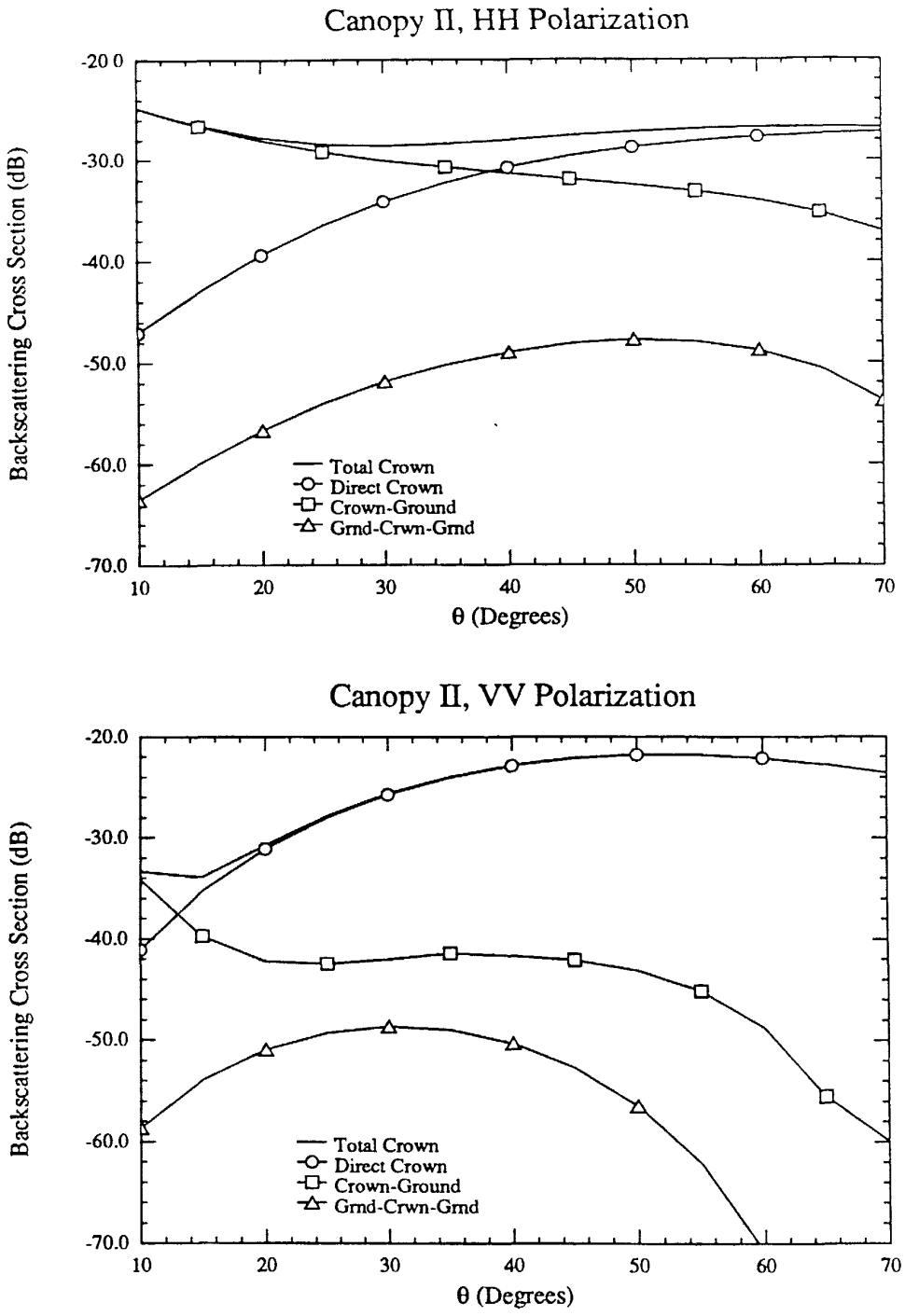


Figure H.18: L-Band Like-Polarized Crown Backscatter Components vs Incidence Angle

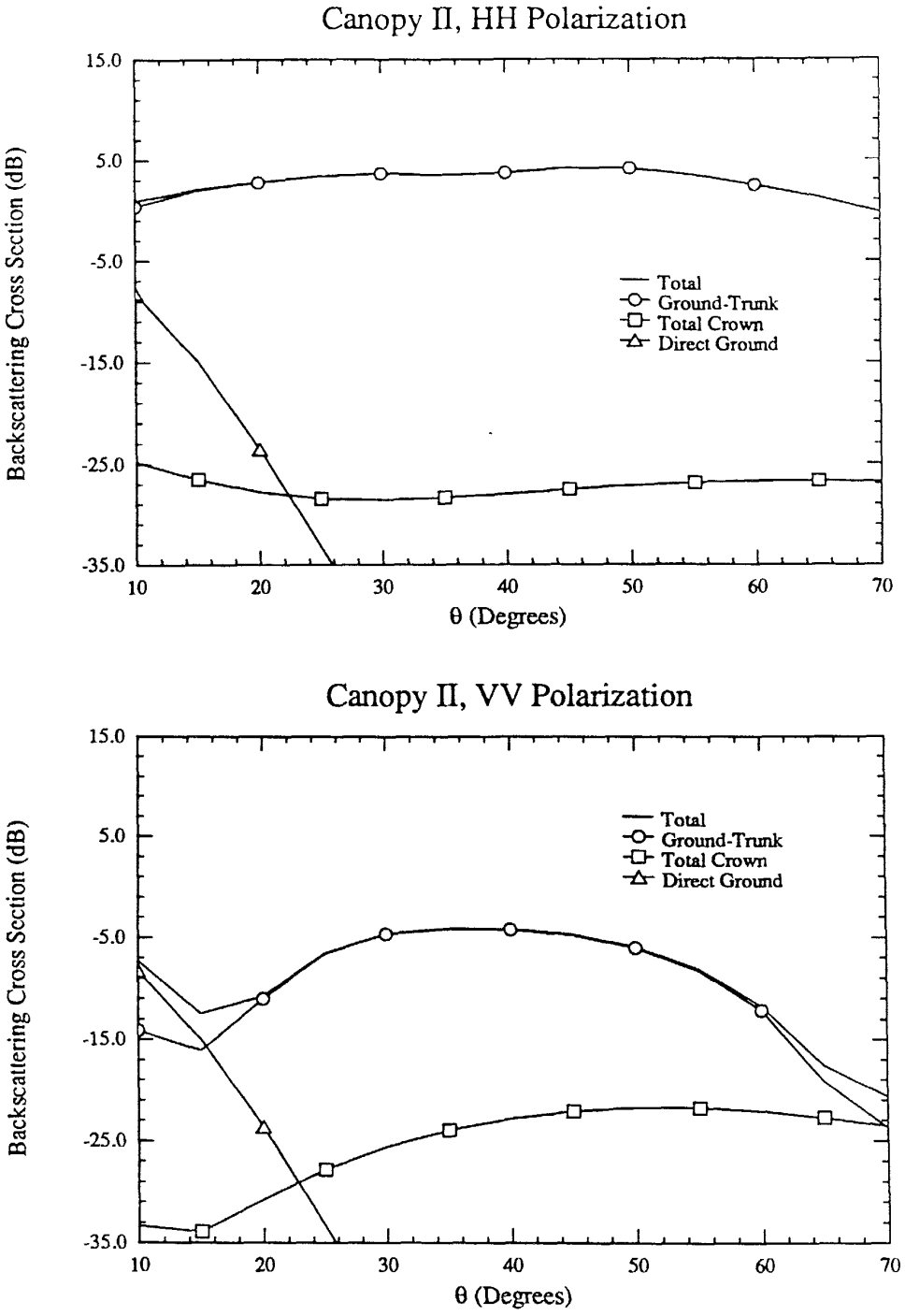


Figure H.17: L-Band Like-Polarized Canopy Backscatter Components vs. Incidence Angle

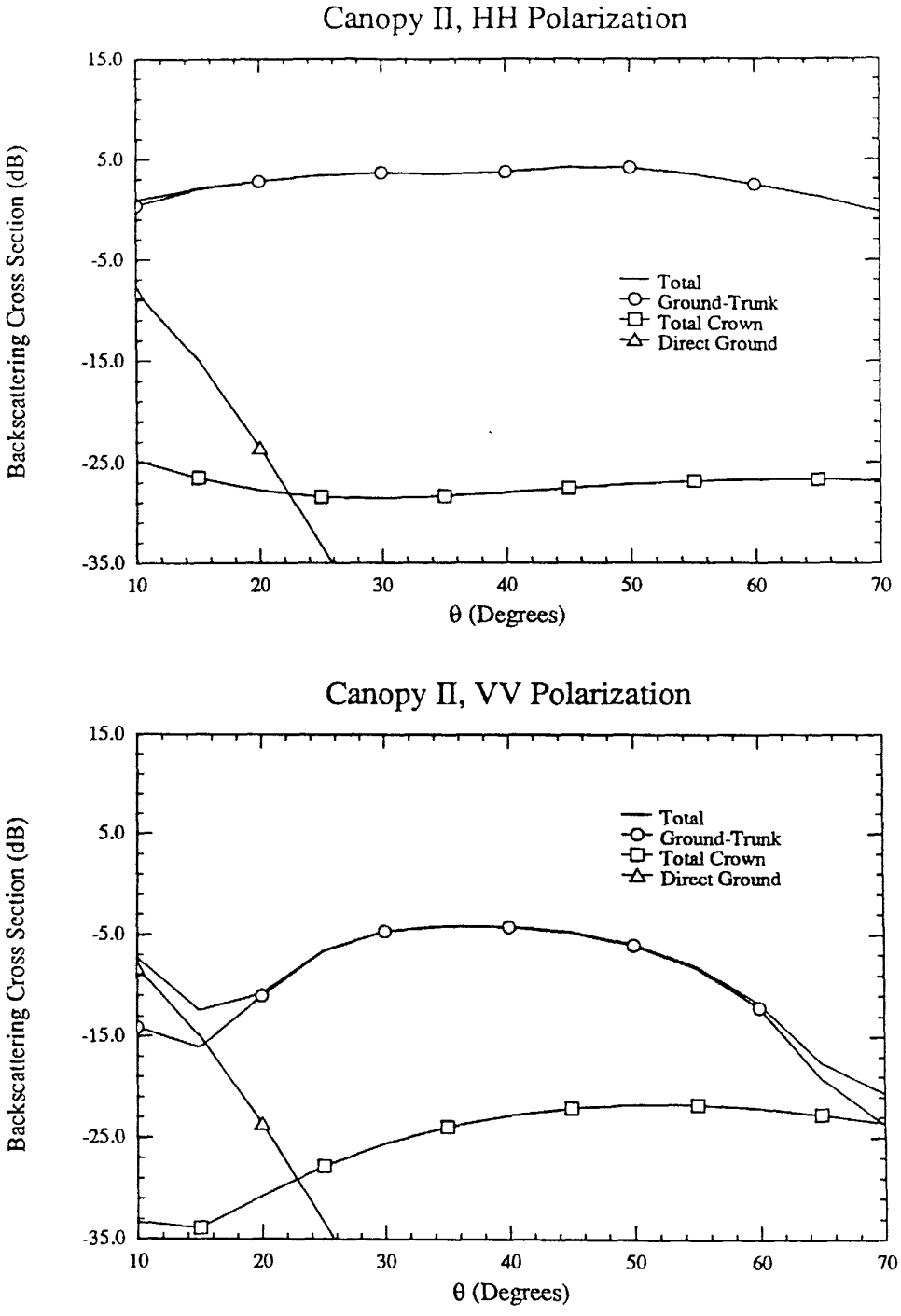


Figure H.17: L-Band Like-Polarized Canopy Backscatter Components vs. Incidence Angle

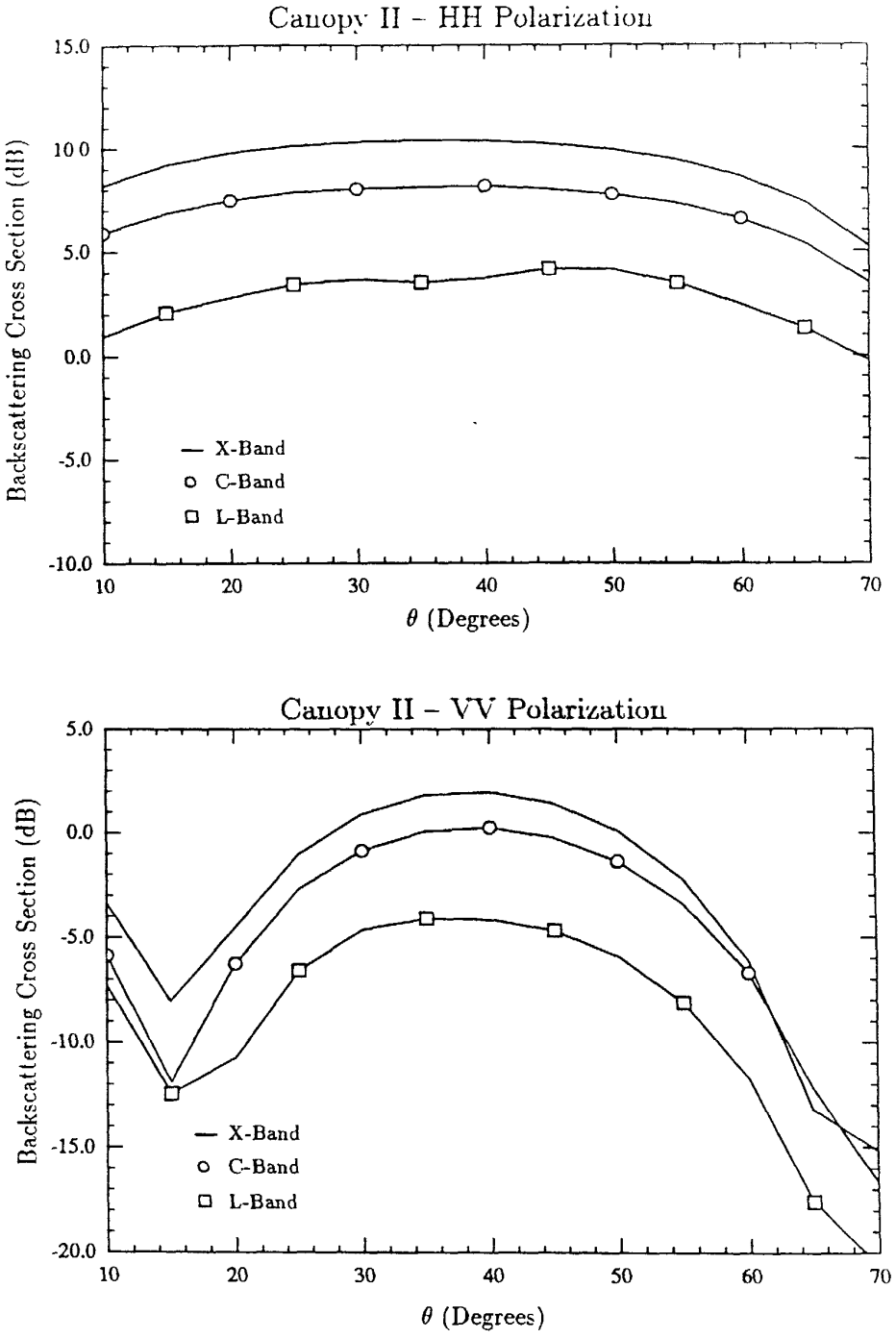


Figure H.15. Total Like-Polarized Canopy Backscatter vs. Incidence Angle

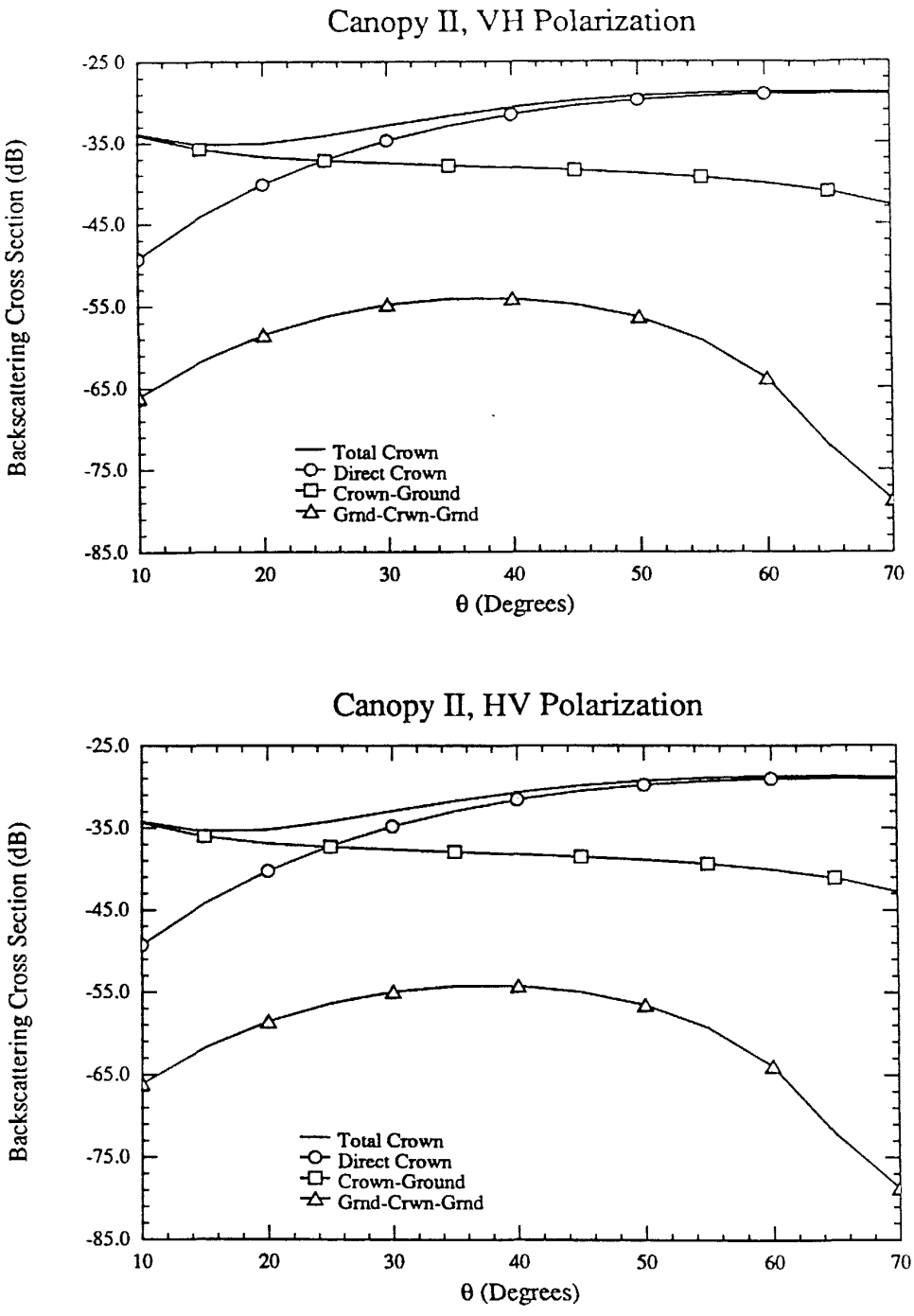


Figure H.19: L-Band Cross-Polarized Crown Backscatter Components vs. Incidence Angle

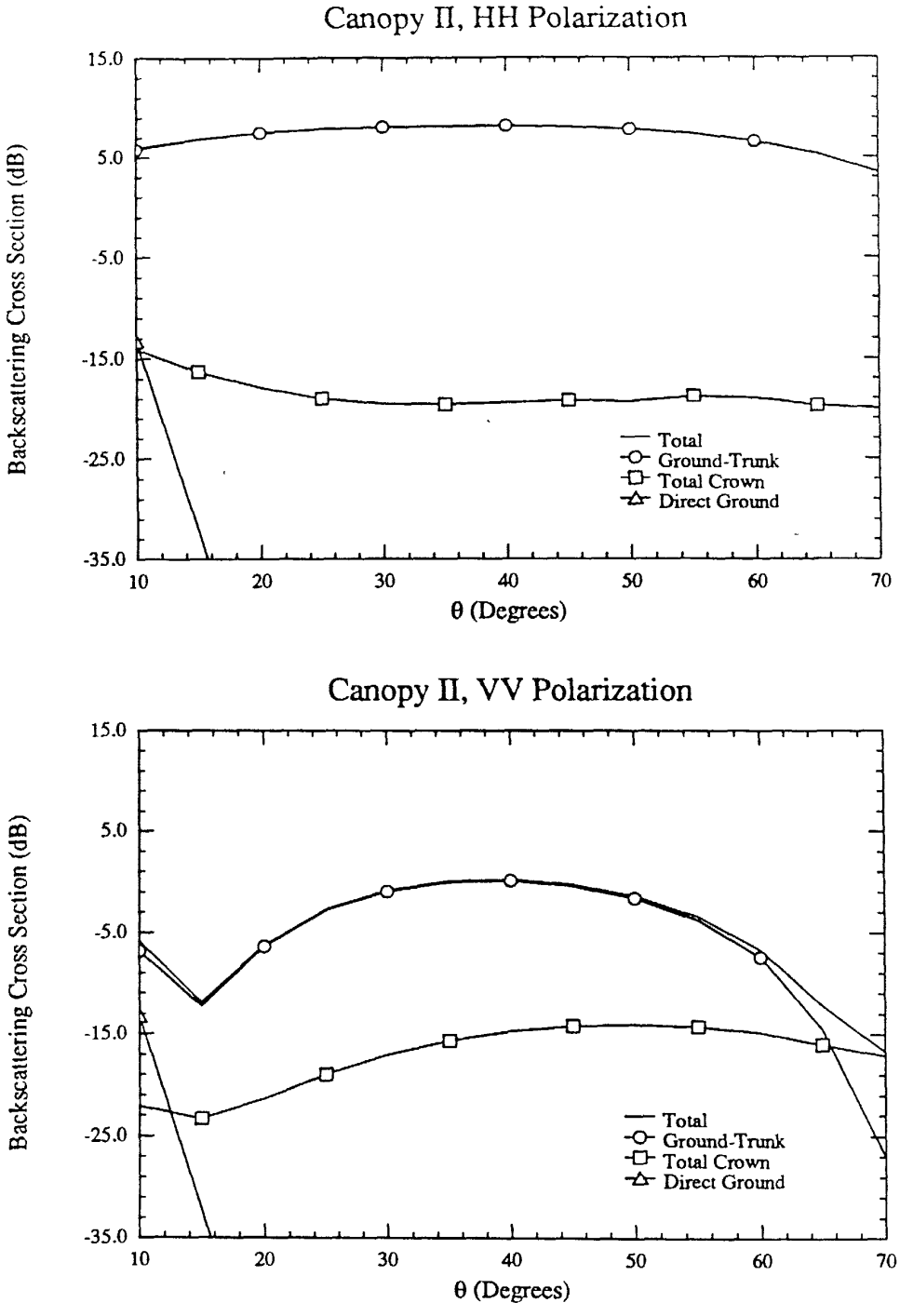


Figure H.20. C-Band Like-Polarized Canopy Backscatter Components vs. Incidence Angle

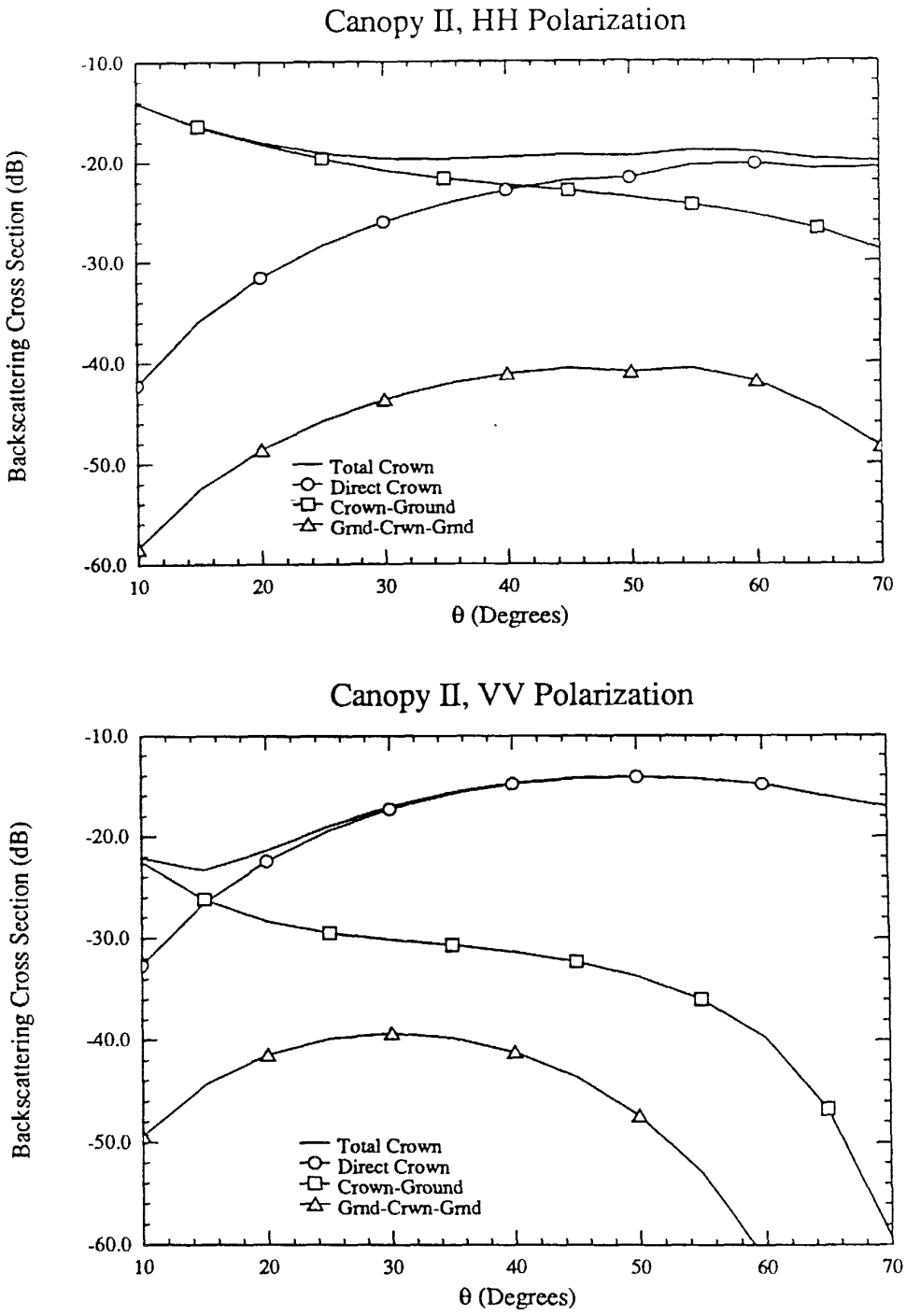


Figure II.21: C-Band Like-Polarized Crown Backscatter Components vs Incidence Angle

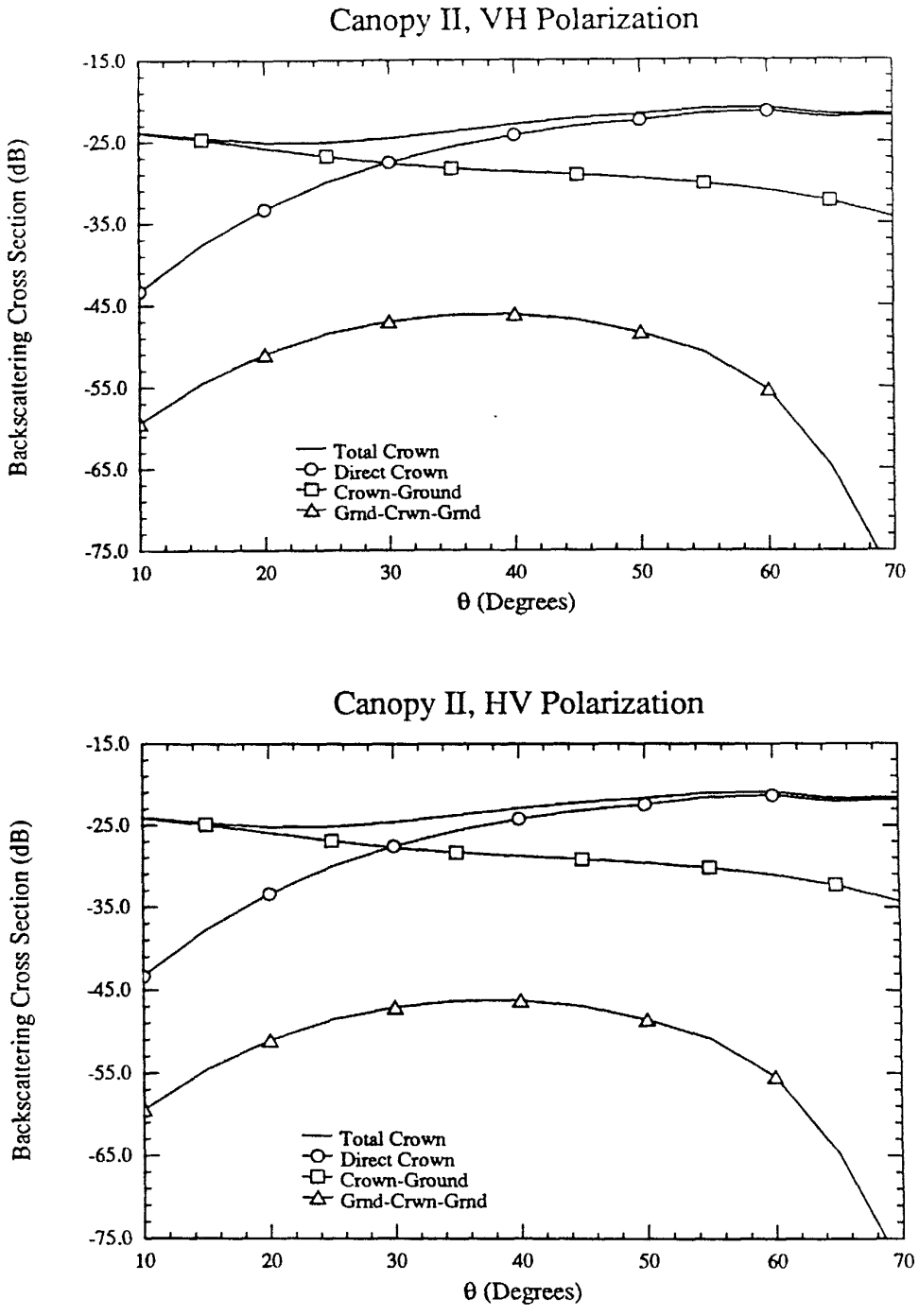


Figure H.22: C-Band Cross-Polarized Crown Backscatter Components vs. Incidence Angle

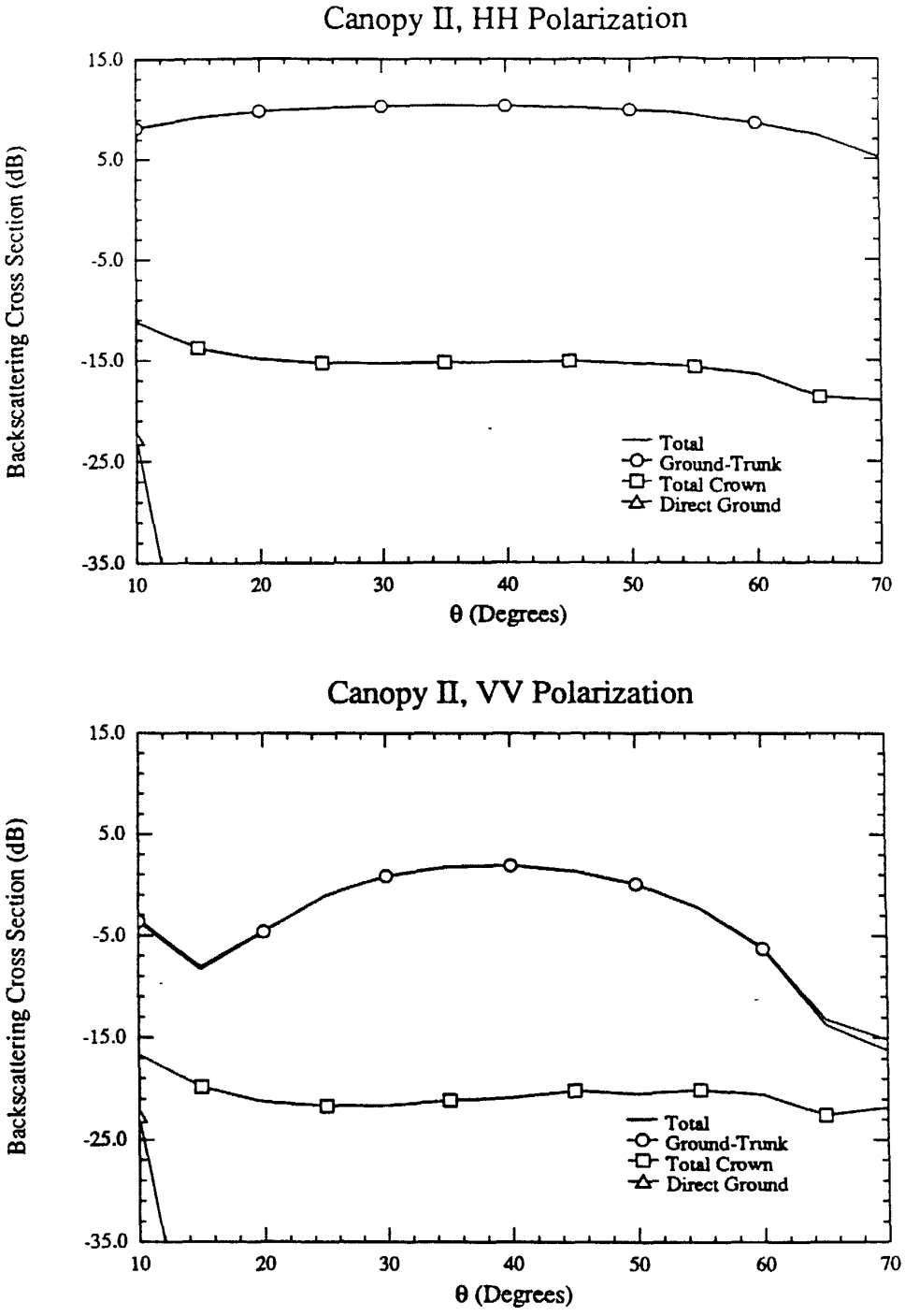


Figure H.23: X-Band Like-Polarized Canopy Backscatter Components vs. Incidence Angle

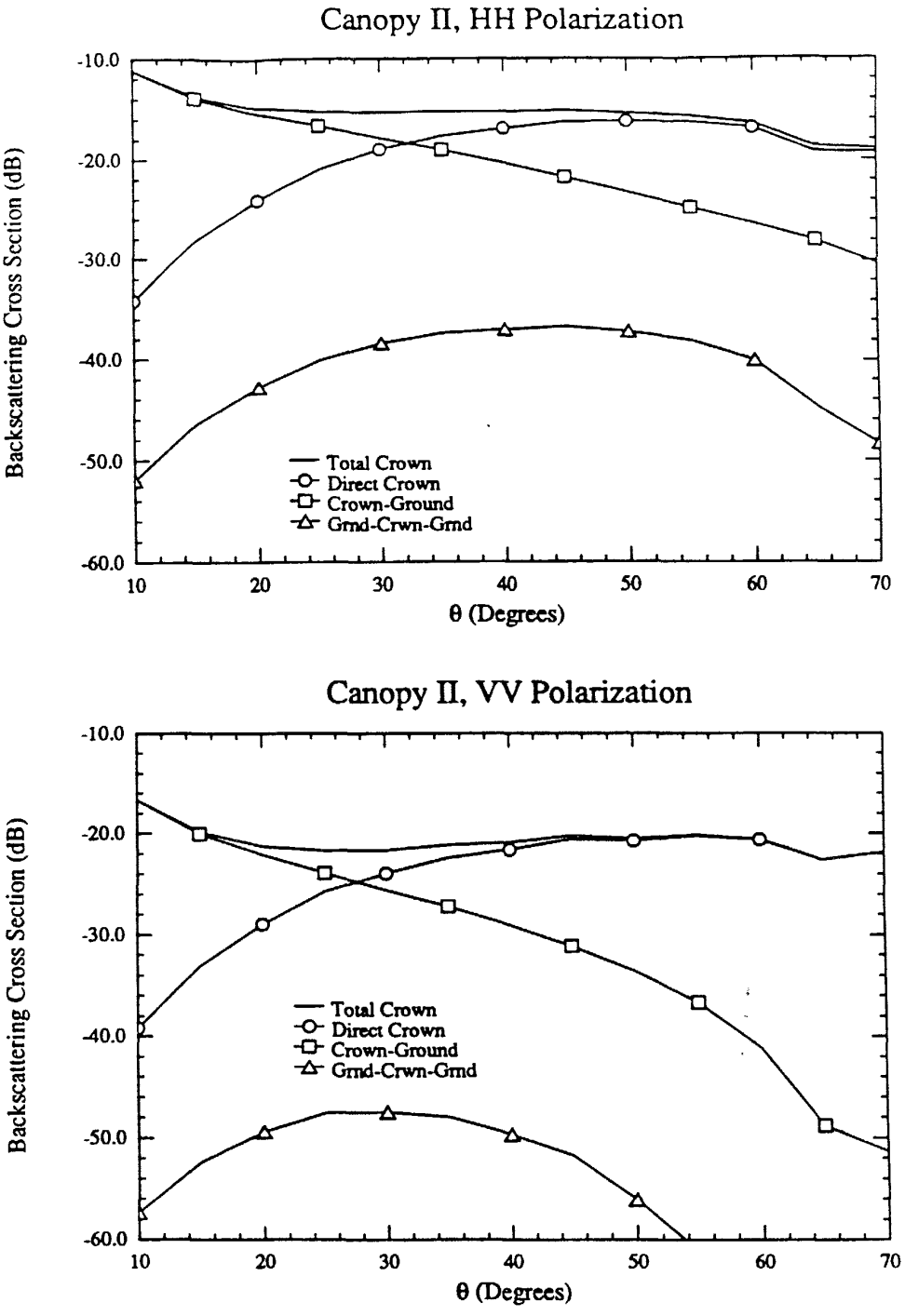


Figure H.24: X-Band Like-Polarized Crown Backscatter Components vs. Incidence Angle

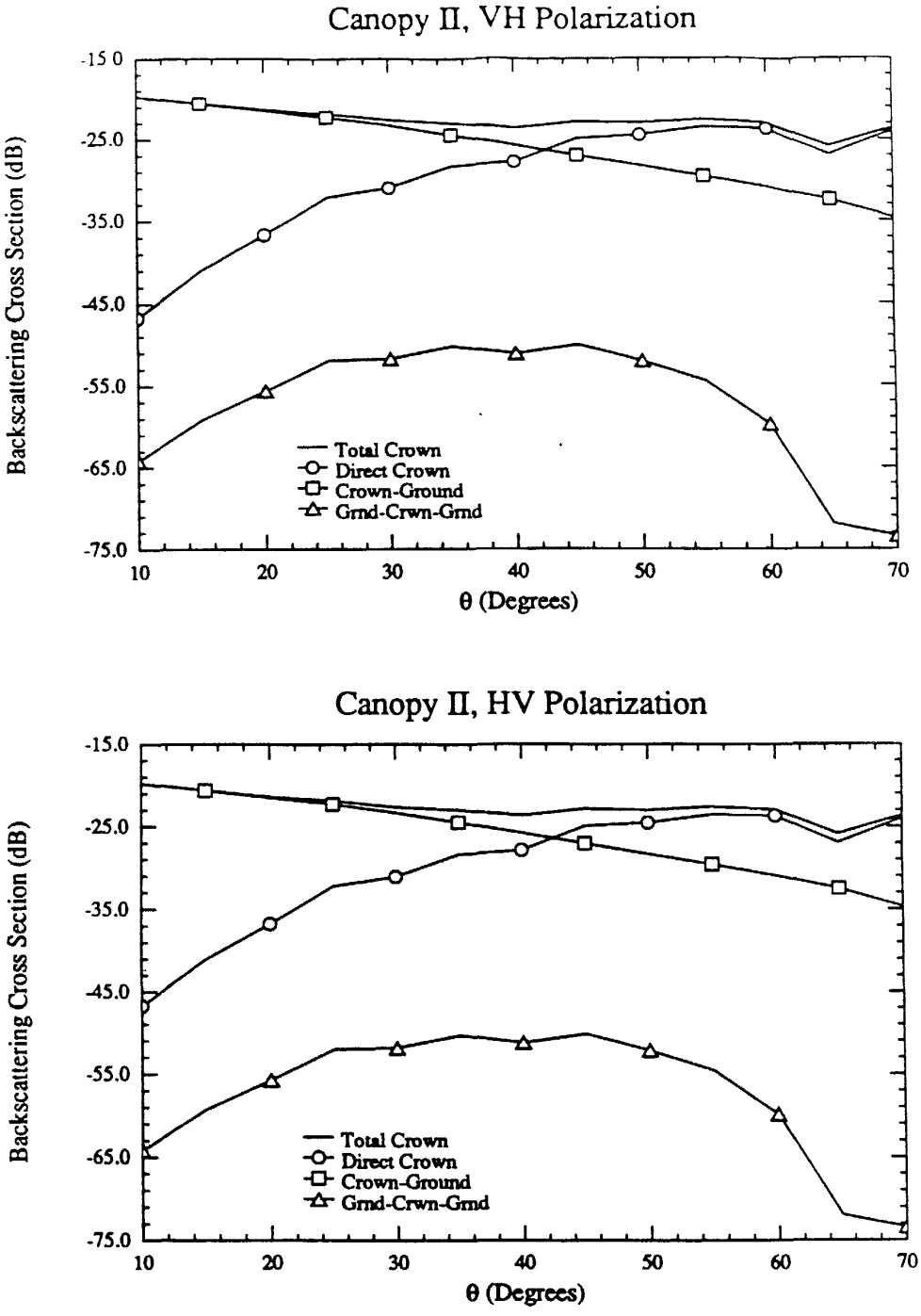


Figure H.25: X-Band Cross-Polarized Crown Backscatter Components vs. Incidence Angle

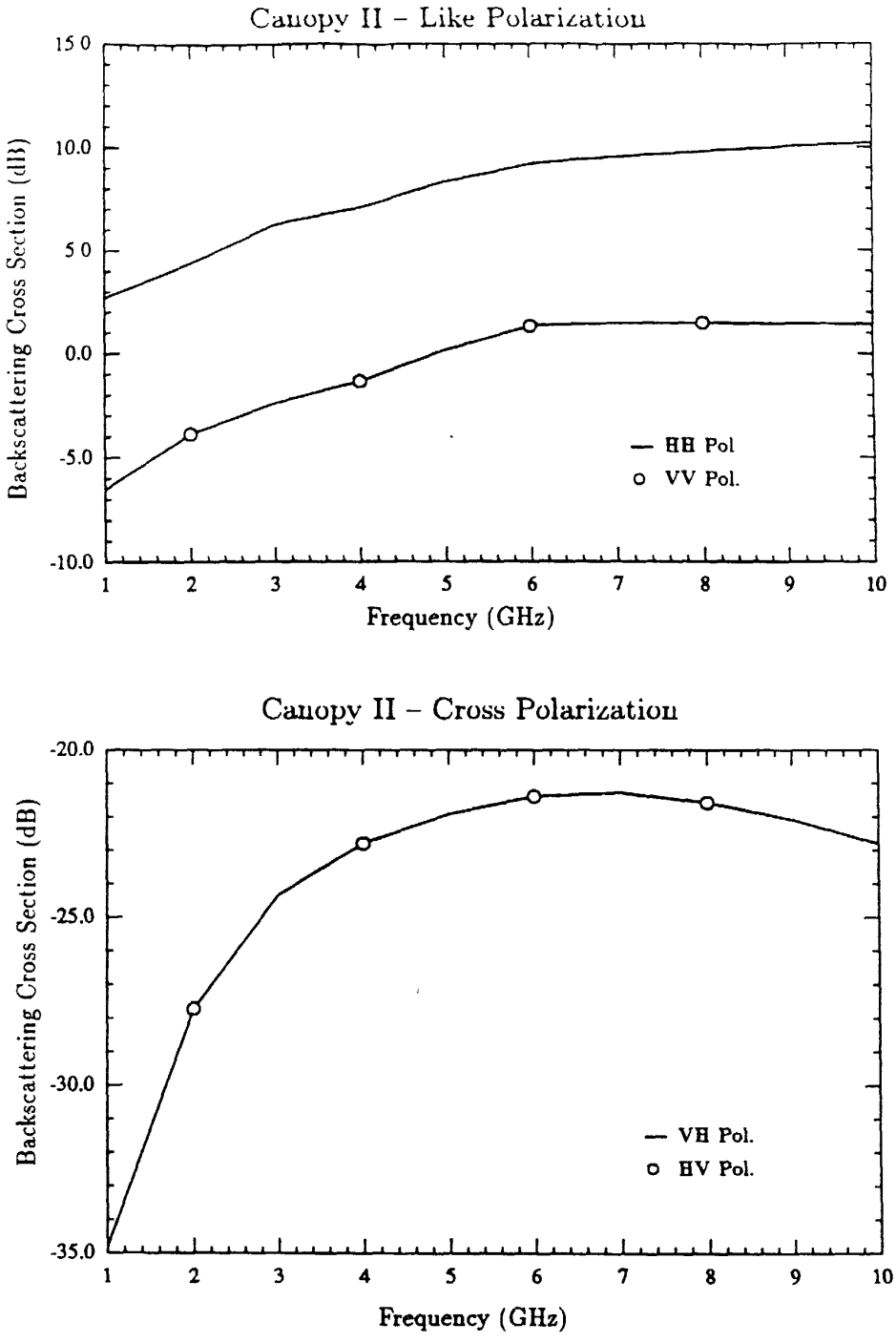


Figure H.26: Total Canopy Backscatter vs. Frequency. Incidence Angle = 30°

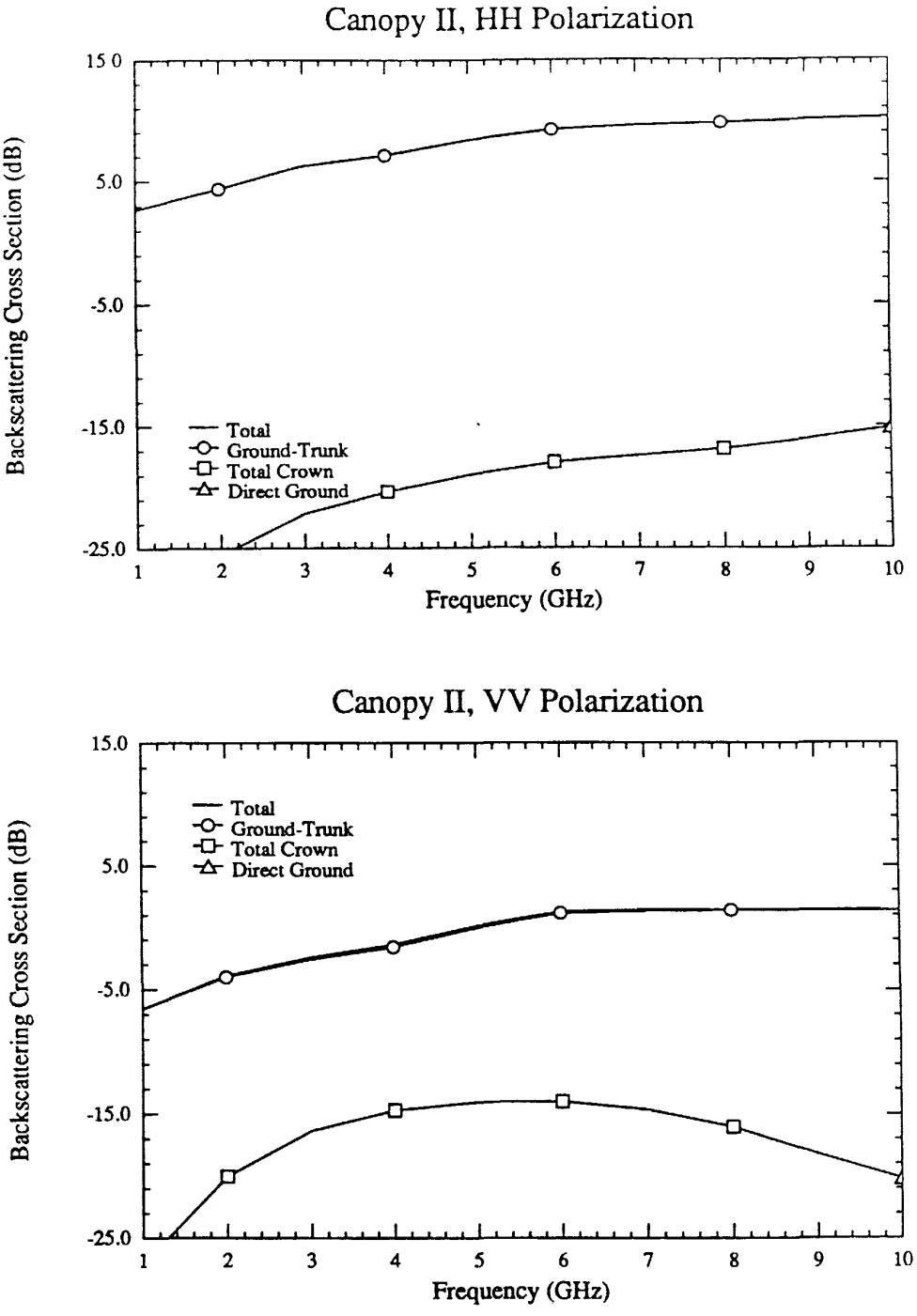


Figure H.27: Like-Polarized Canopy Backscatter Components vs. Frequency. Incidence Angle = 30°

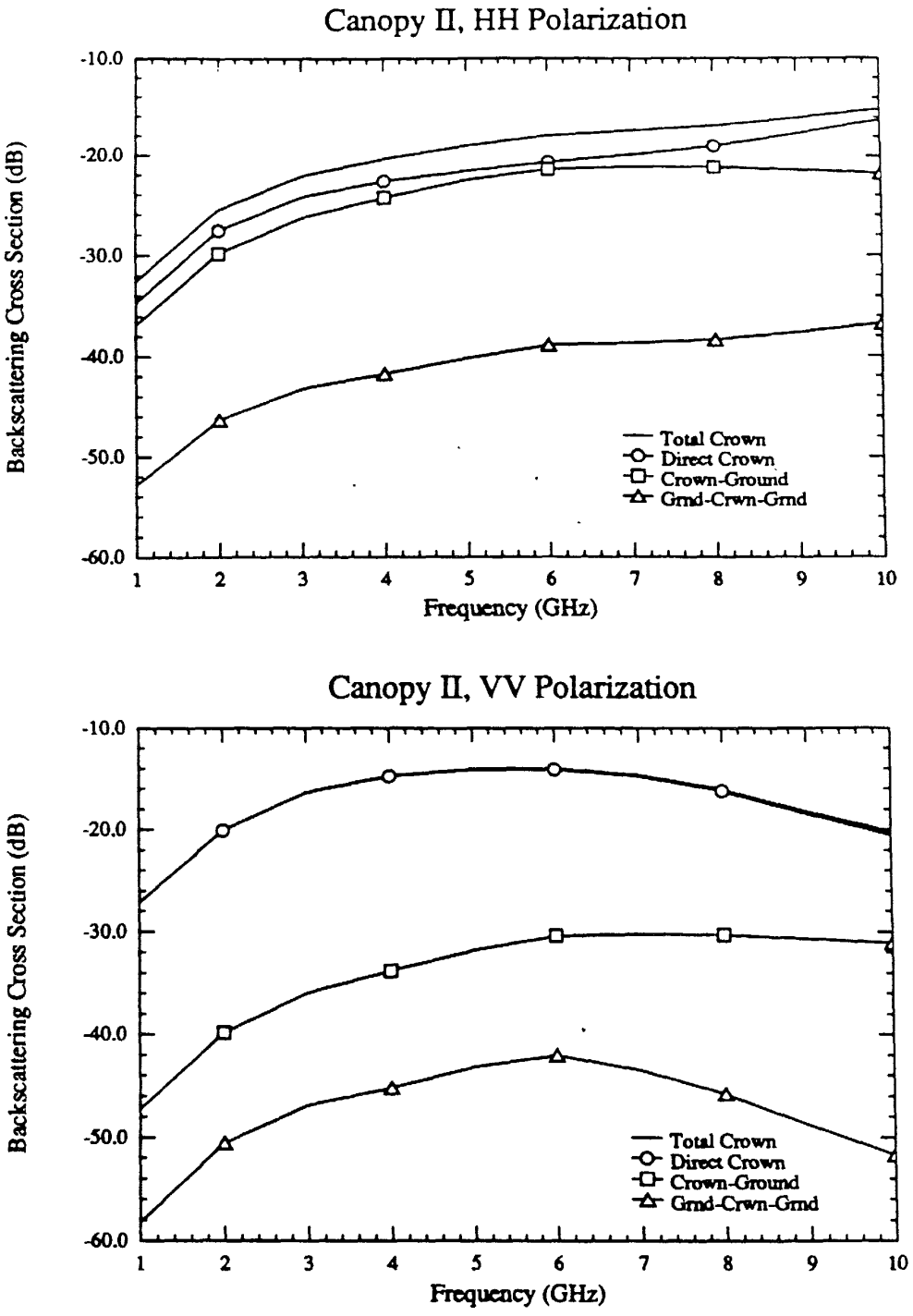


Figure H.28: Like-Polarized Crown Backscatter Components vs. Frequency. Incidence Angle = 30°

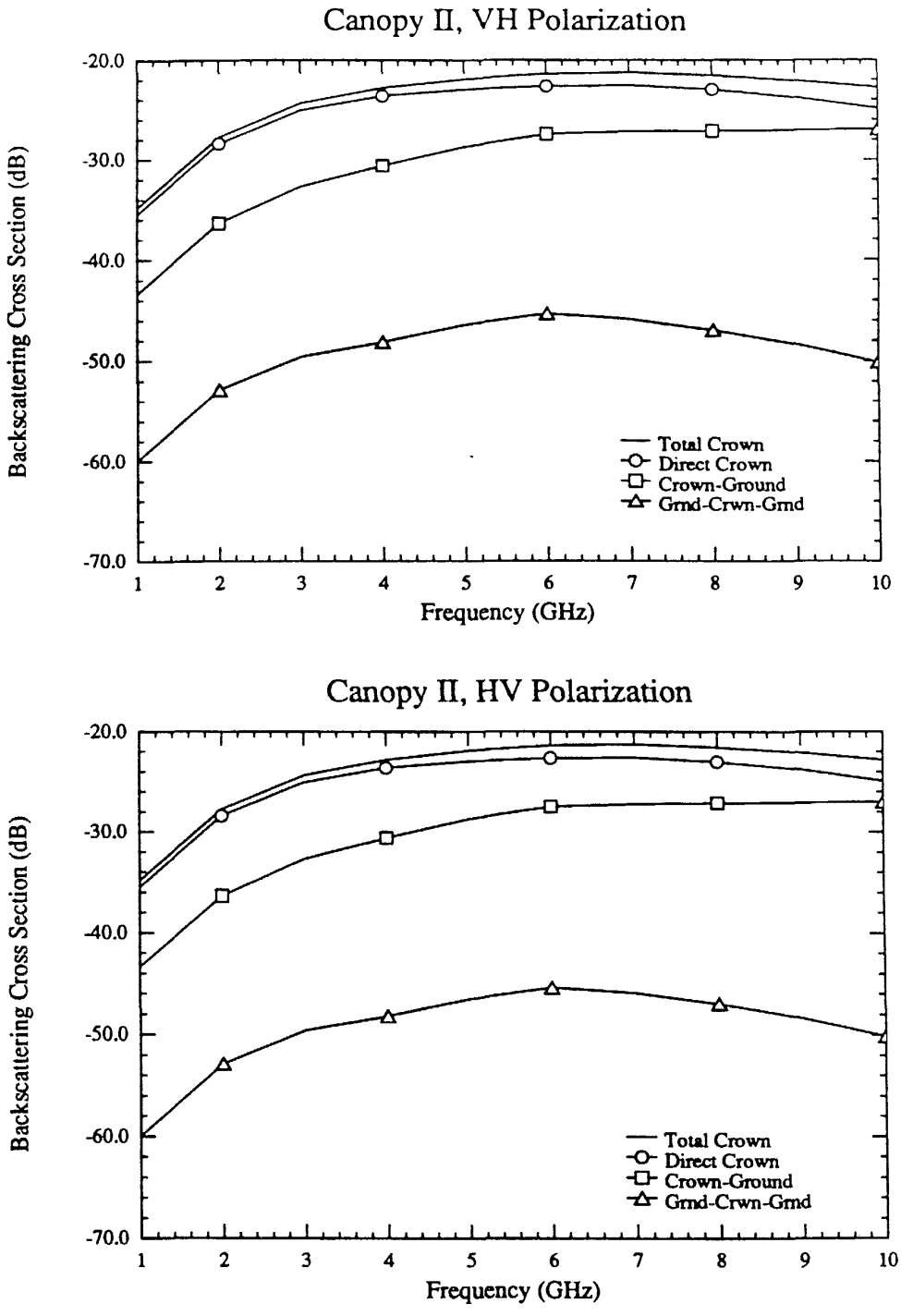


Figure H.29: Cross-Polarized Crown Backscatter Components vs. Frequency. Incidence Angle = 30°

CANOPY III – Crown Layer Consisting of Both Leaves and Branches

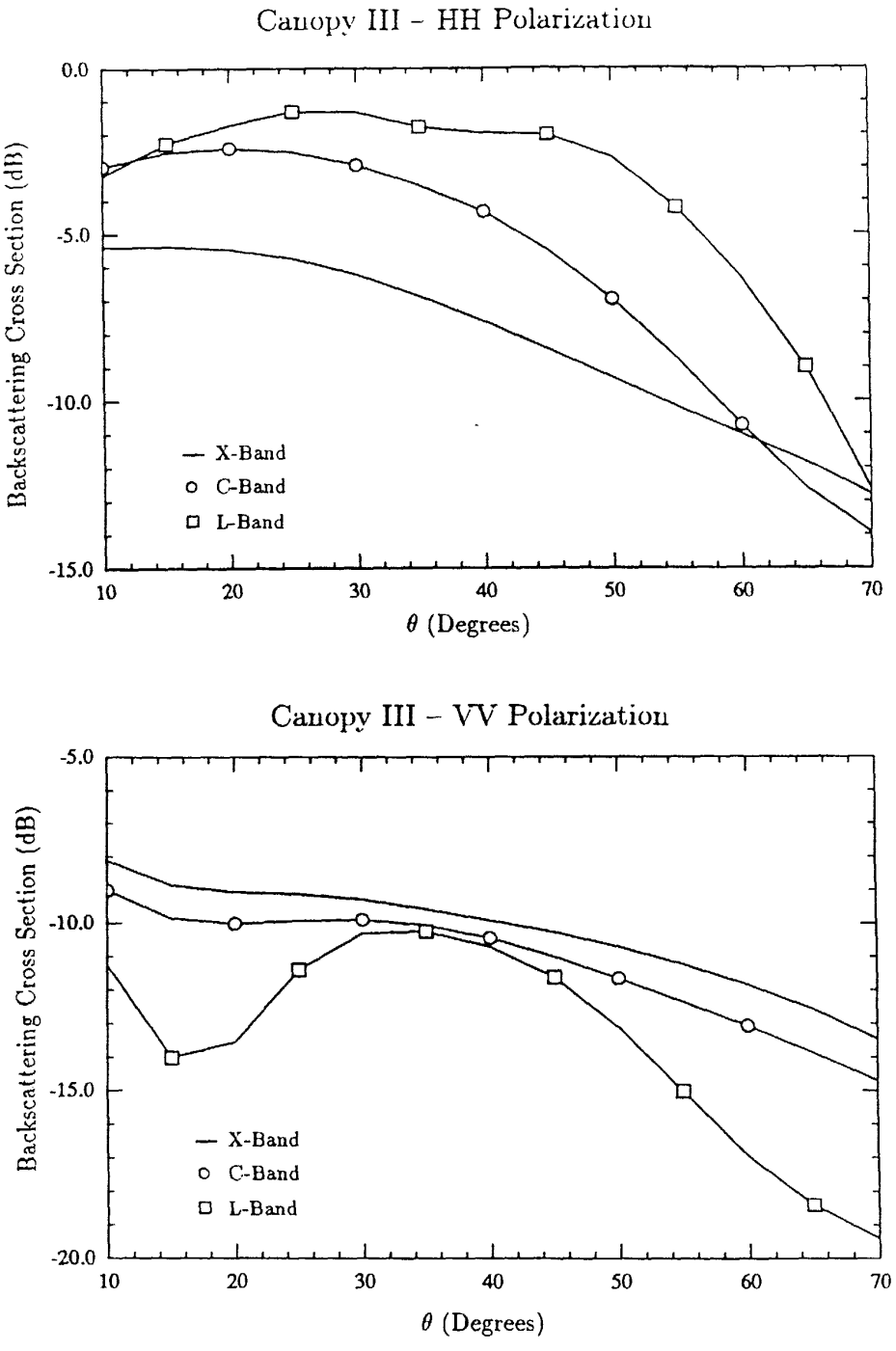


Figure H.30 Total Like-Polarized Canopy Backscatter vs. Incidence Angle

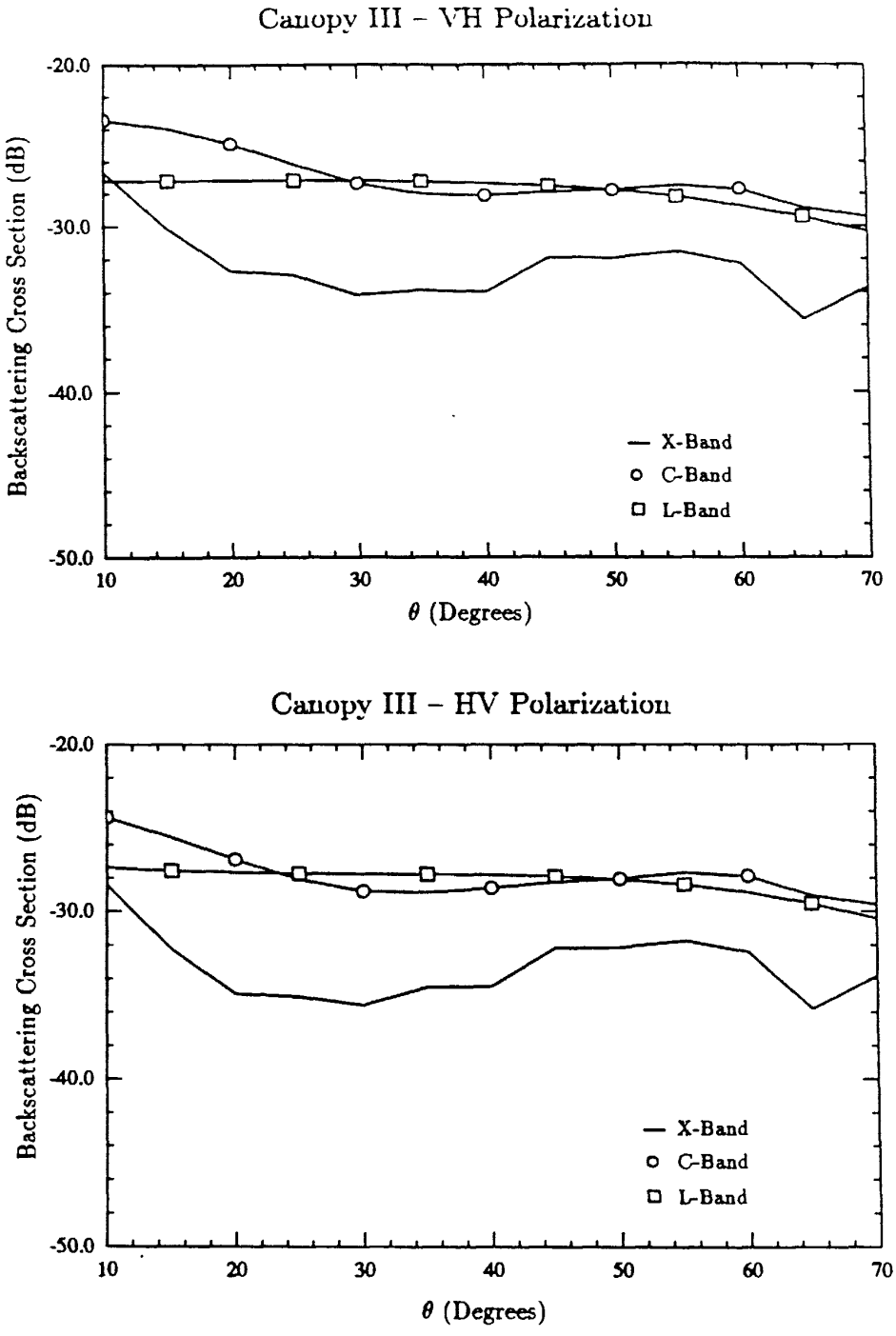


Figure H.31: Total Cross-Polarized Canopy Backscatter vs. Incidence Angle

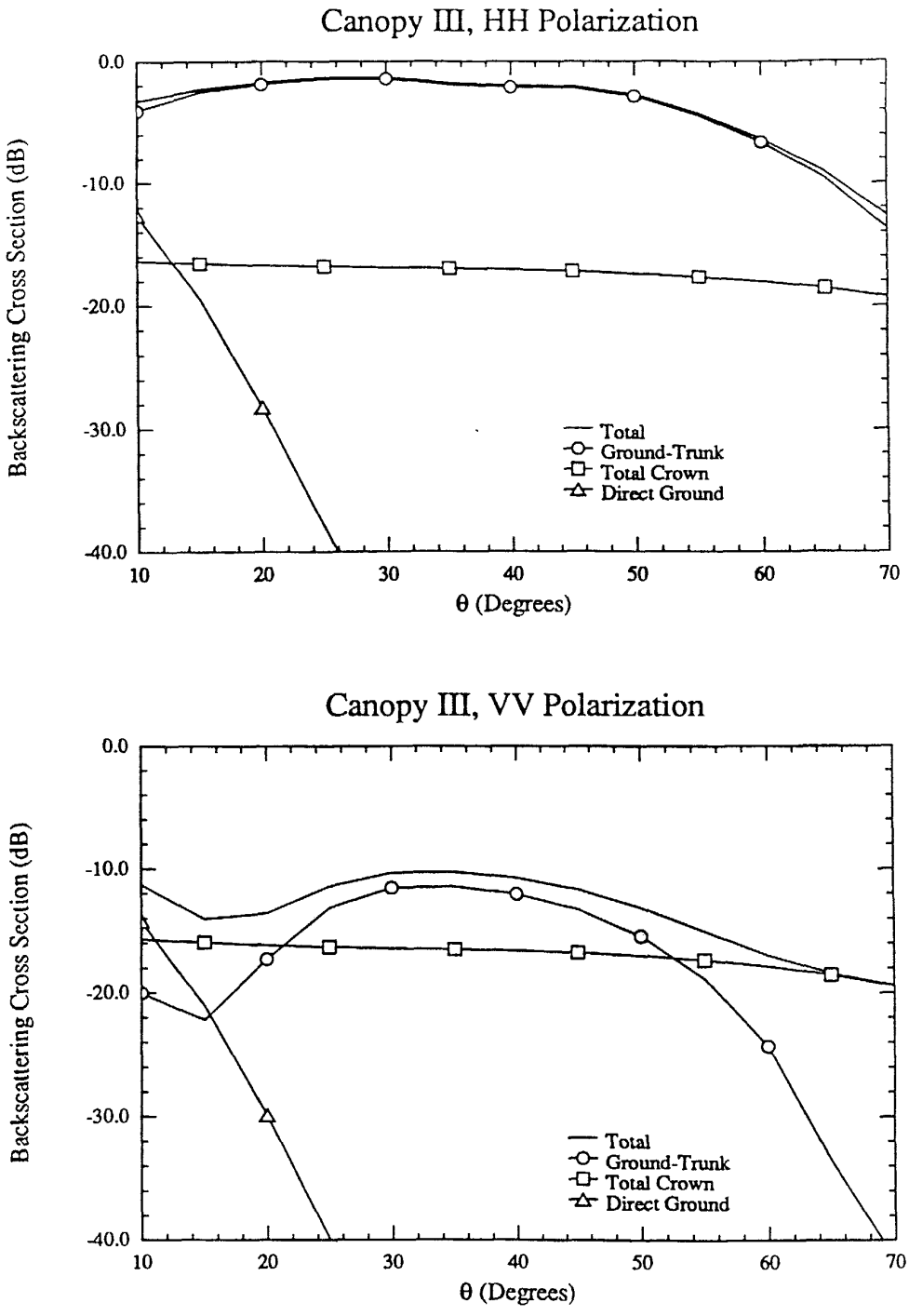


Figure H.32. L-Band Like-Polarized Canopy Backscatter Components vs. Incidence Angle

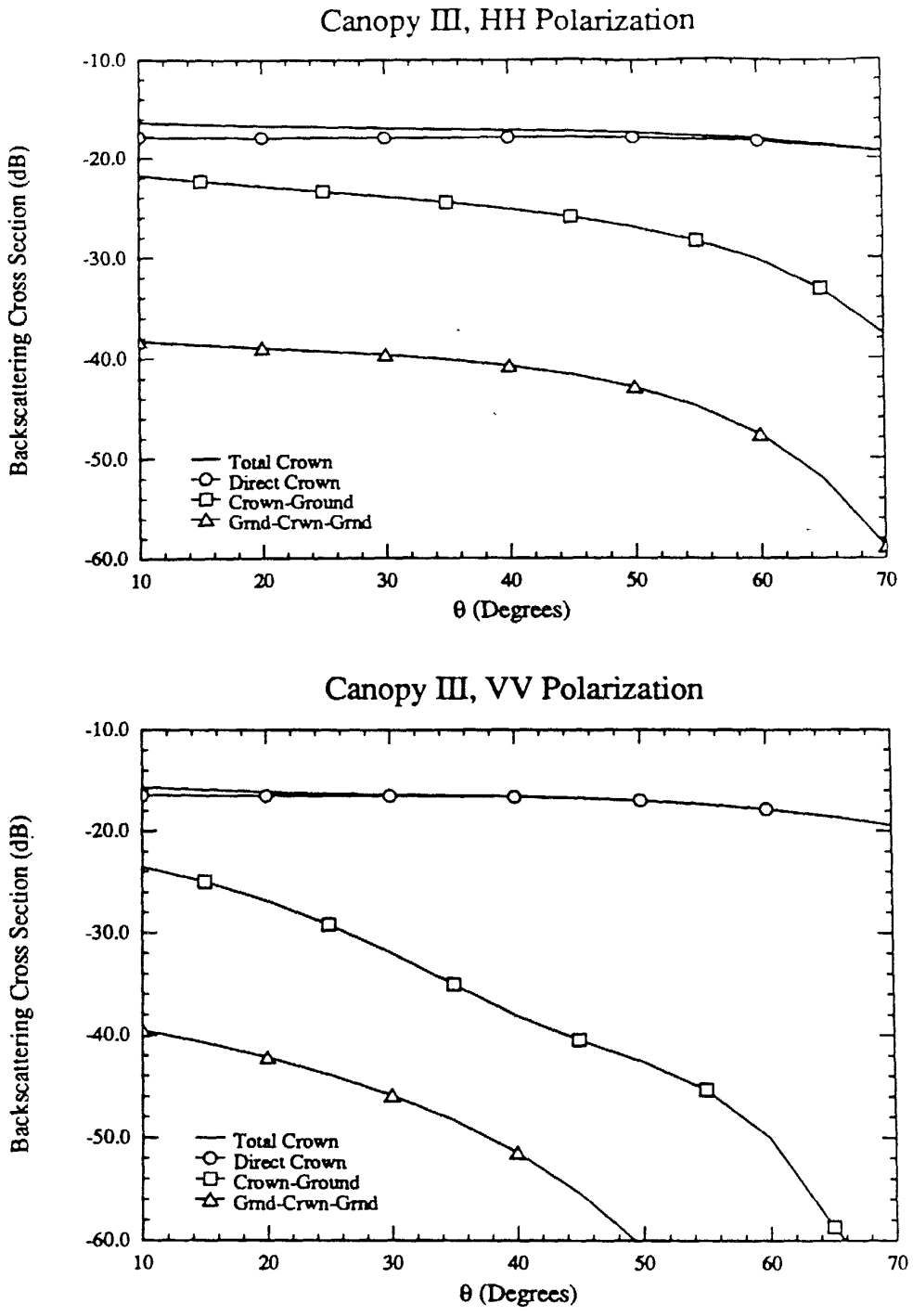


Figure H.33 L-Band Like-Polarized Crown Backscatter Components vs. Incidence Angle

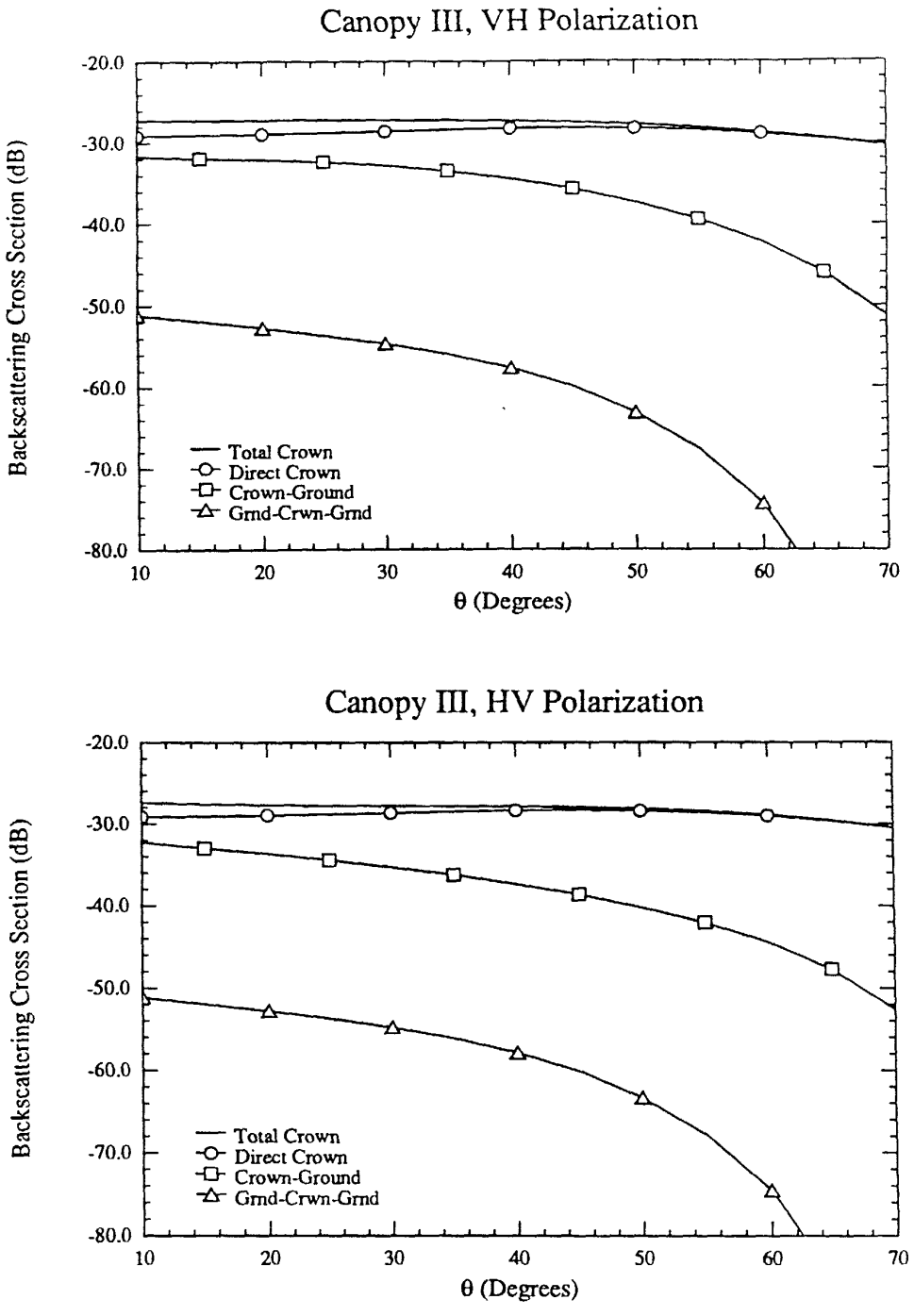


Figure H.34: L-Band Cross-Polarized Crown Backscatter Components vs Incidence Angle

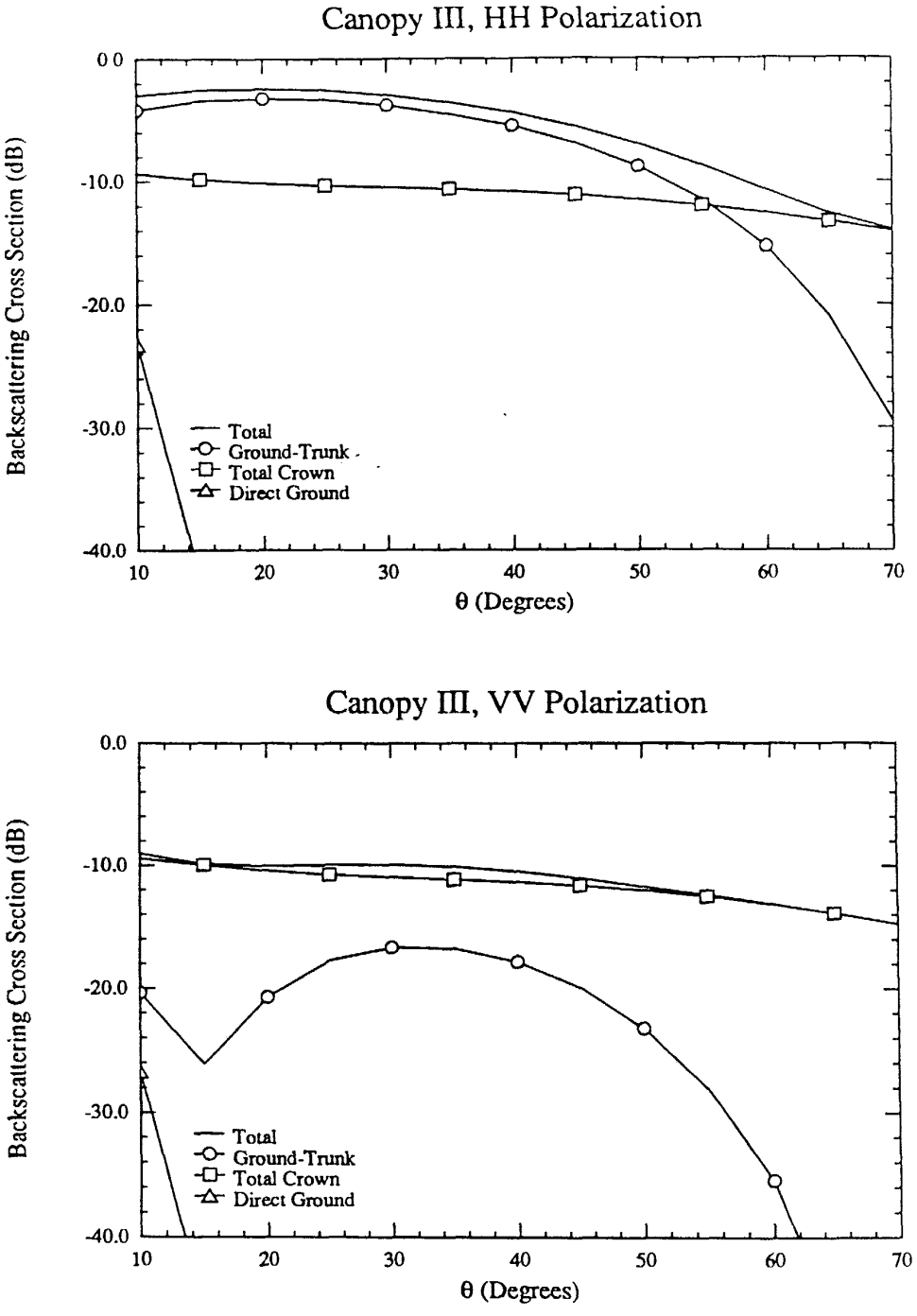


Figure H.35· C-Band Like-Polarized Canopy Backscatter Components vs Incidence Angle

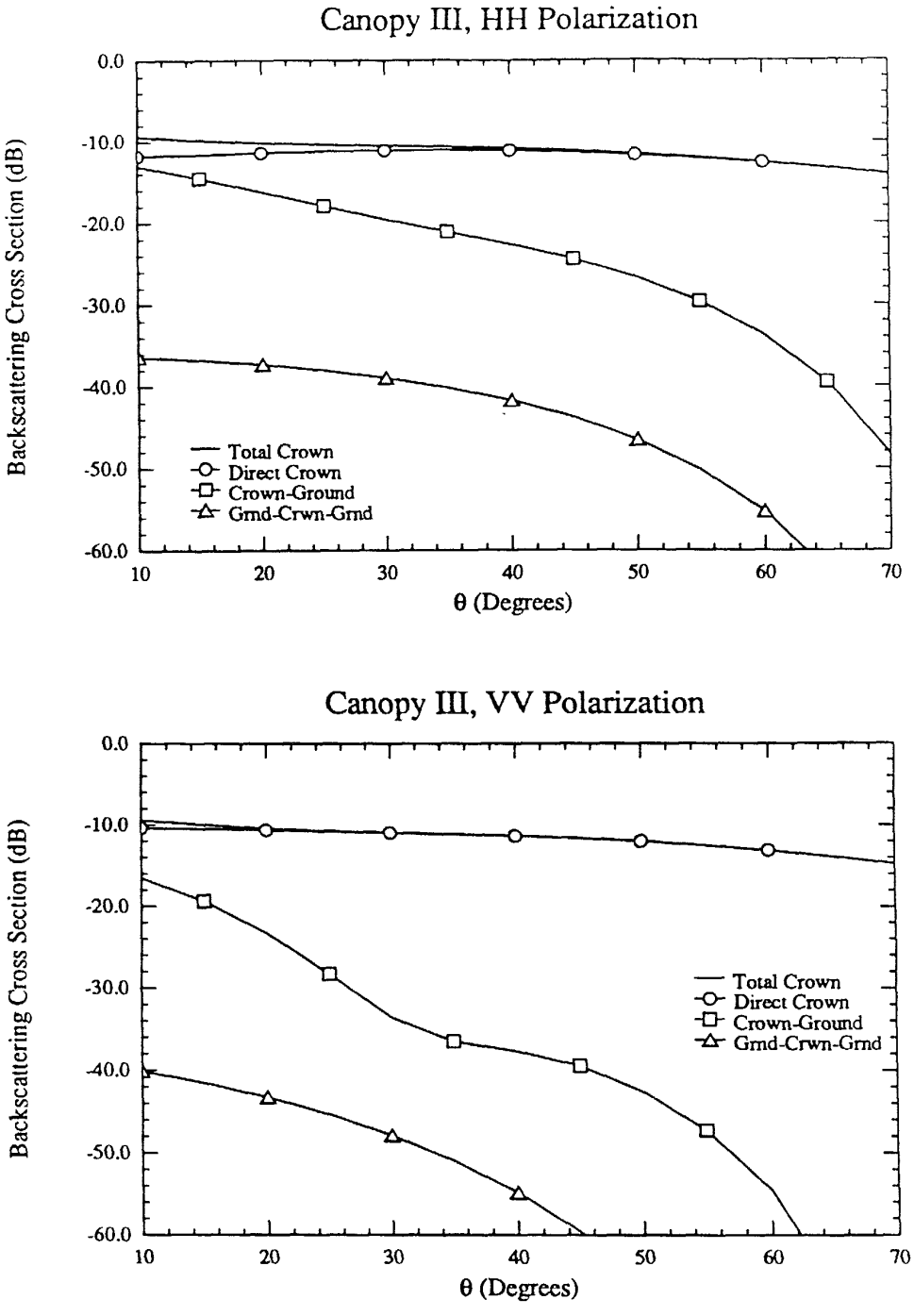


Figure H.36: C-Band Like-Polarized Crown Backscatter Components vs. Incidence Angle

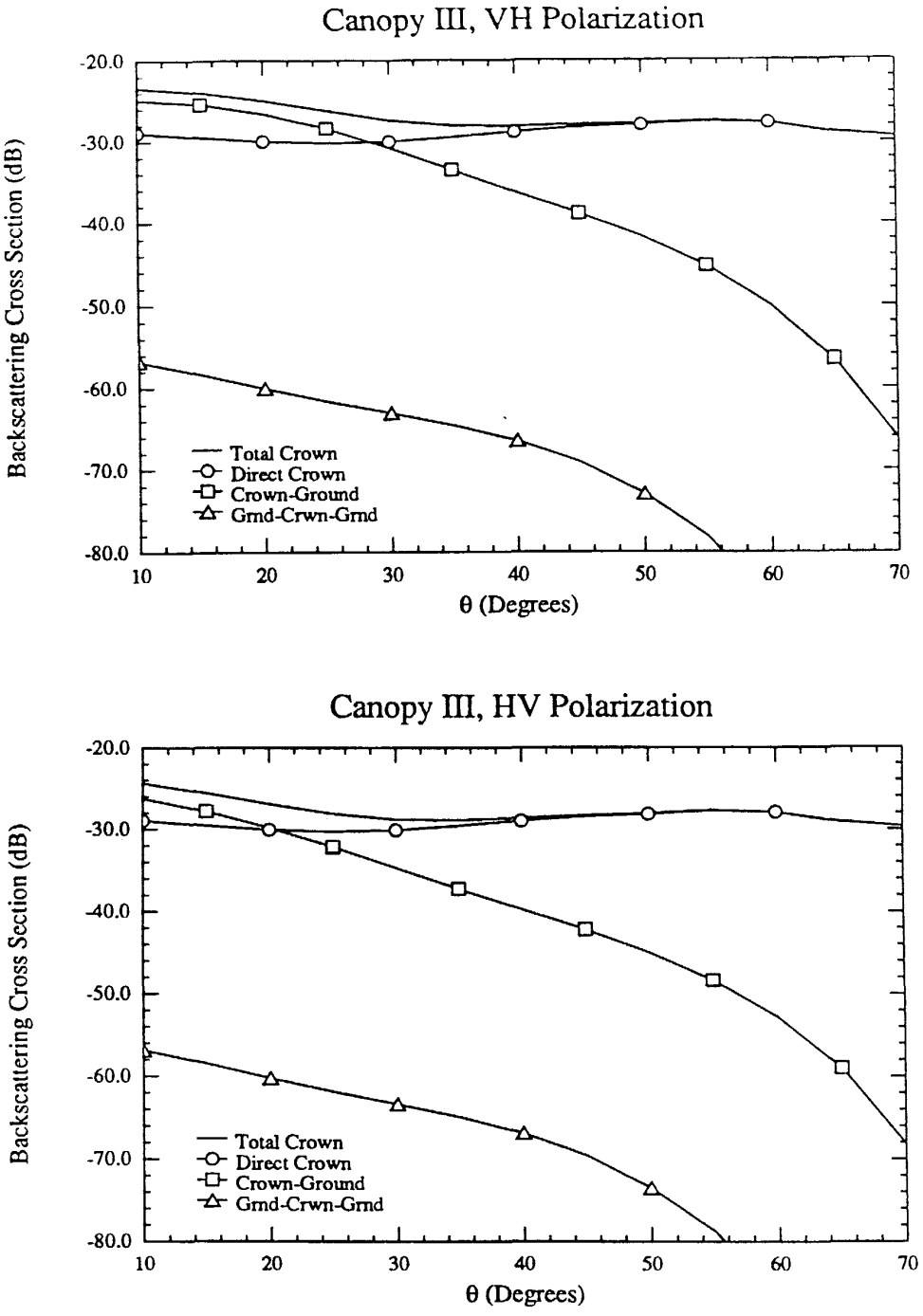


Figure H.37: C-Band Cross-Polarized Crown Backscatter Components vs Incidence Angle

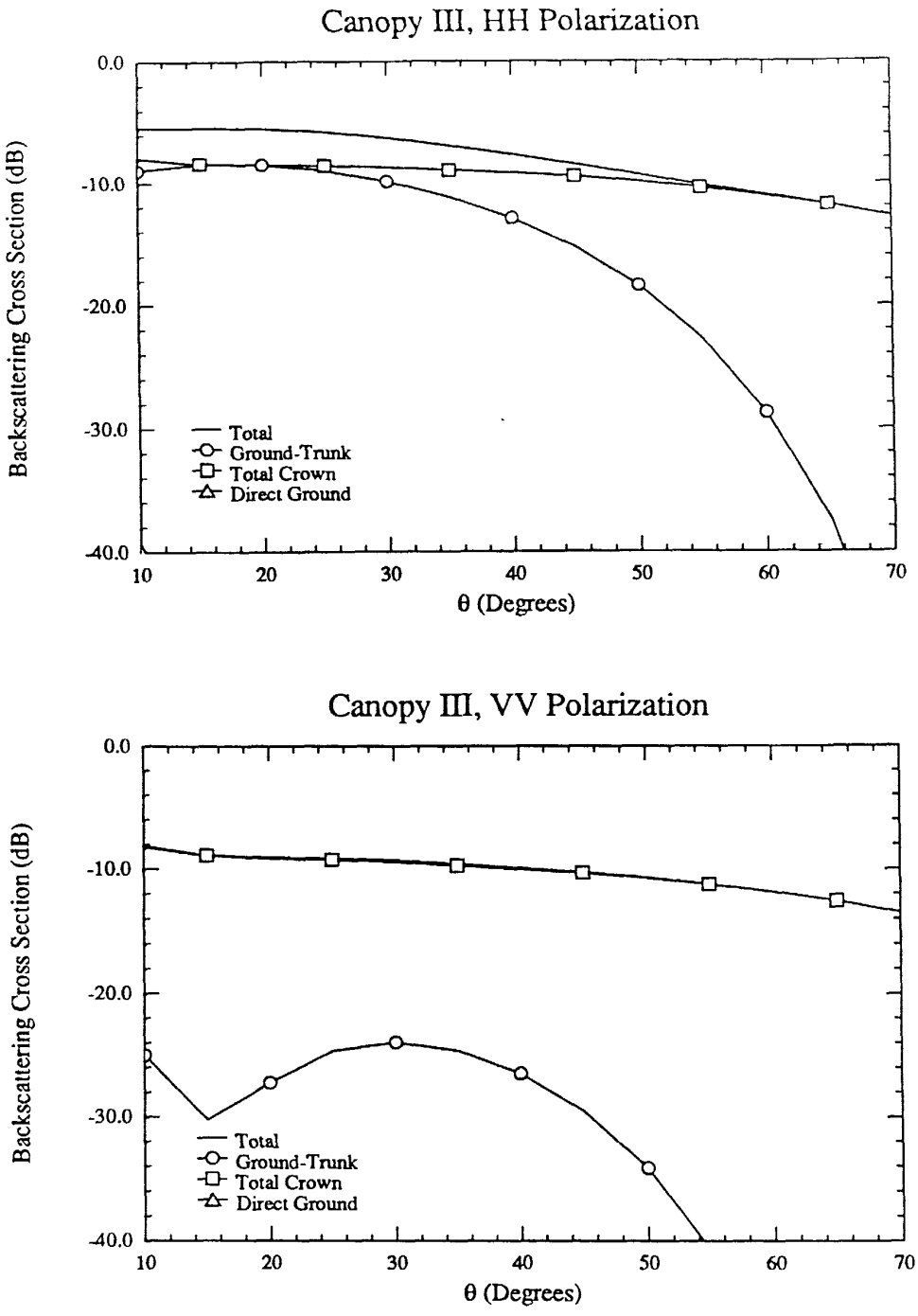


Figure H.38: X-Band Like-Polarized Canopy Backscatter Components vs. Incidence Angle

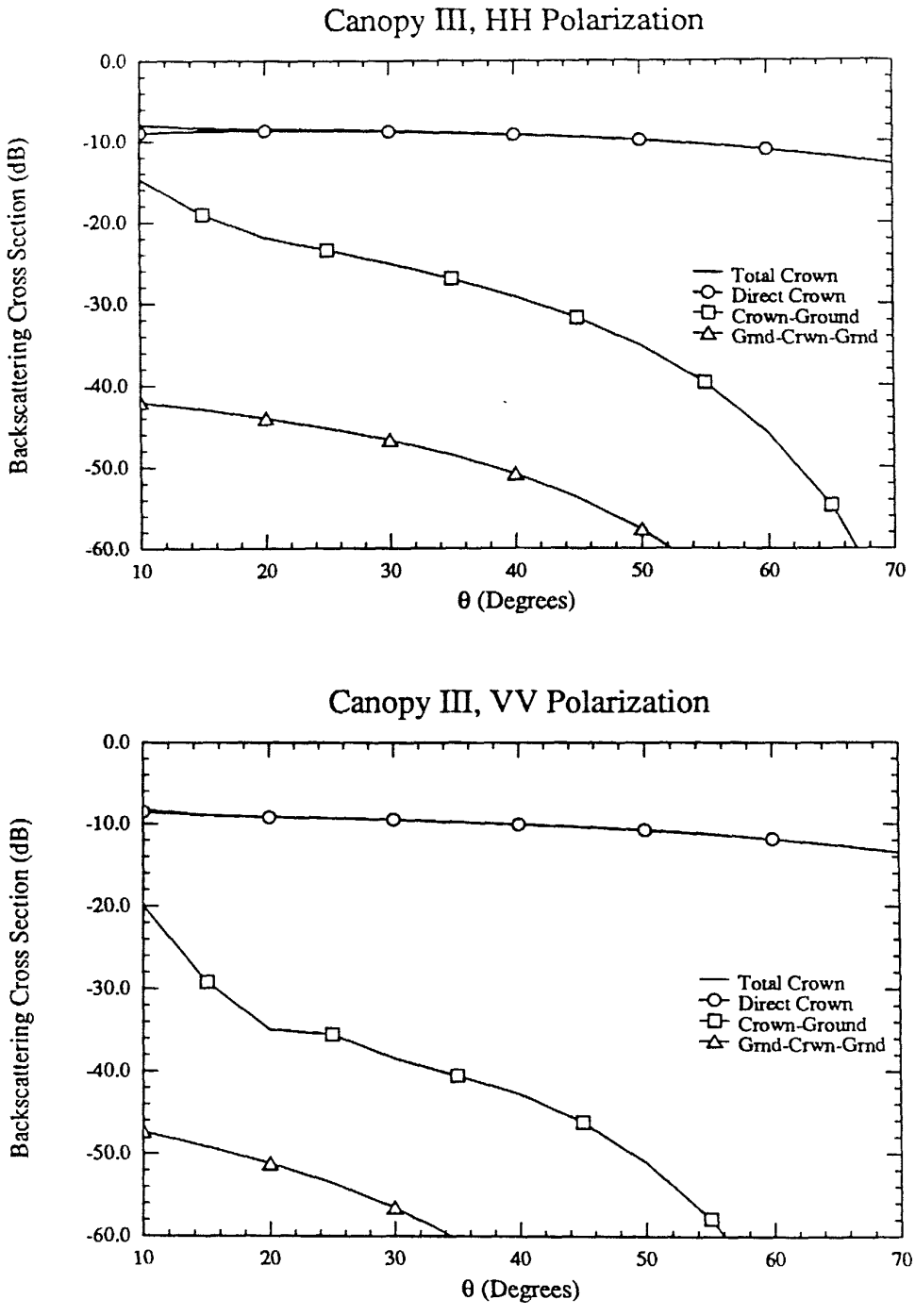


Figure H.39: X-Band Like-Polarized Crown Backscatter Components vs. Incidence Angle

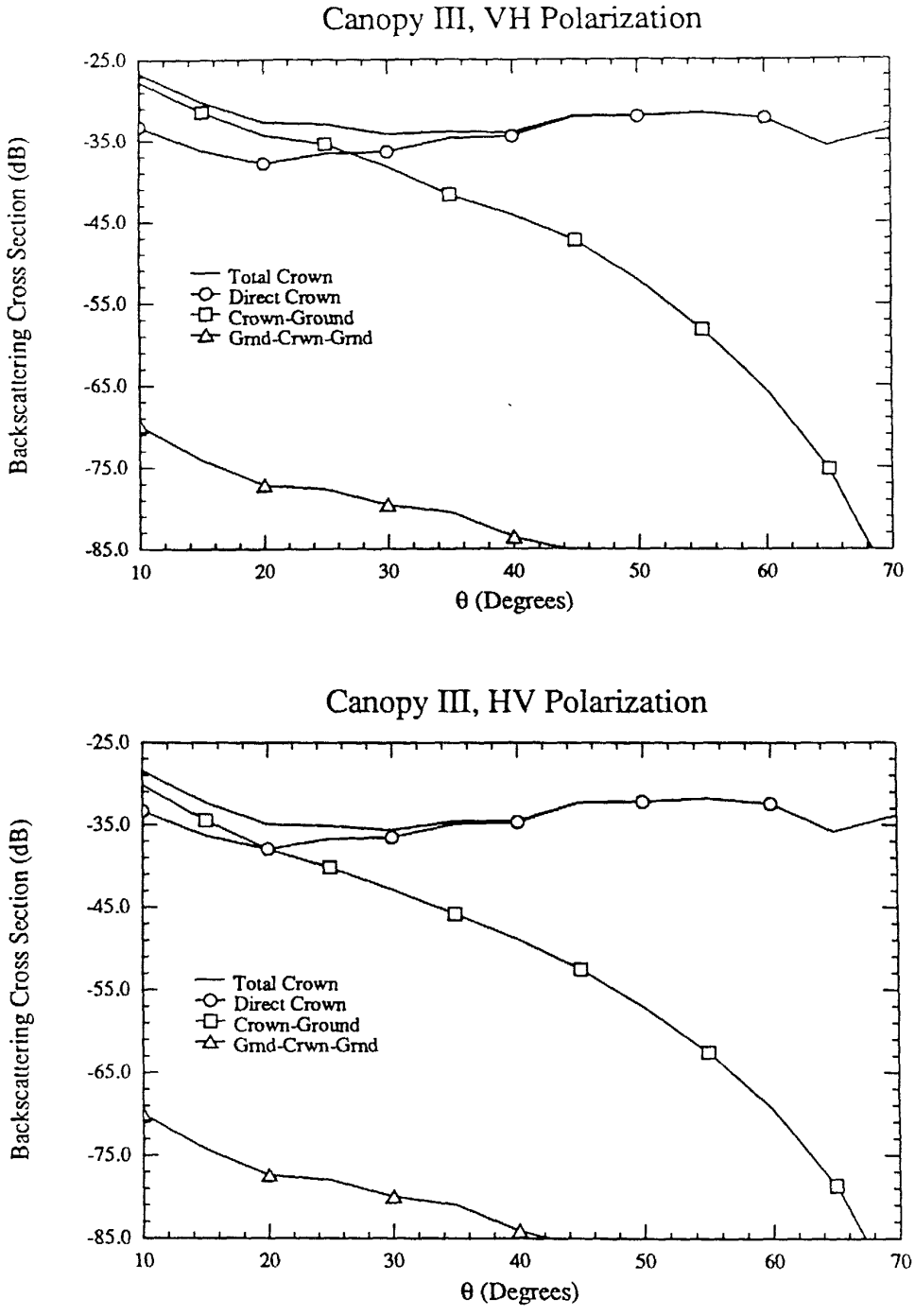


Figure H 40: X-Band Cross-Polarized Crown Backscatter Components vs. Incidence Angle

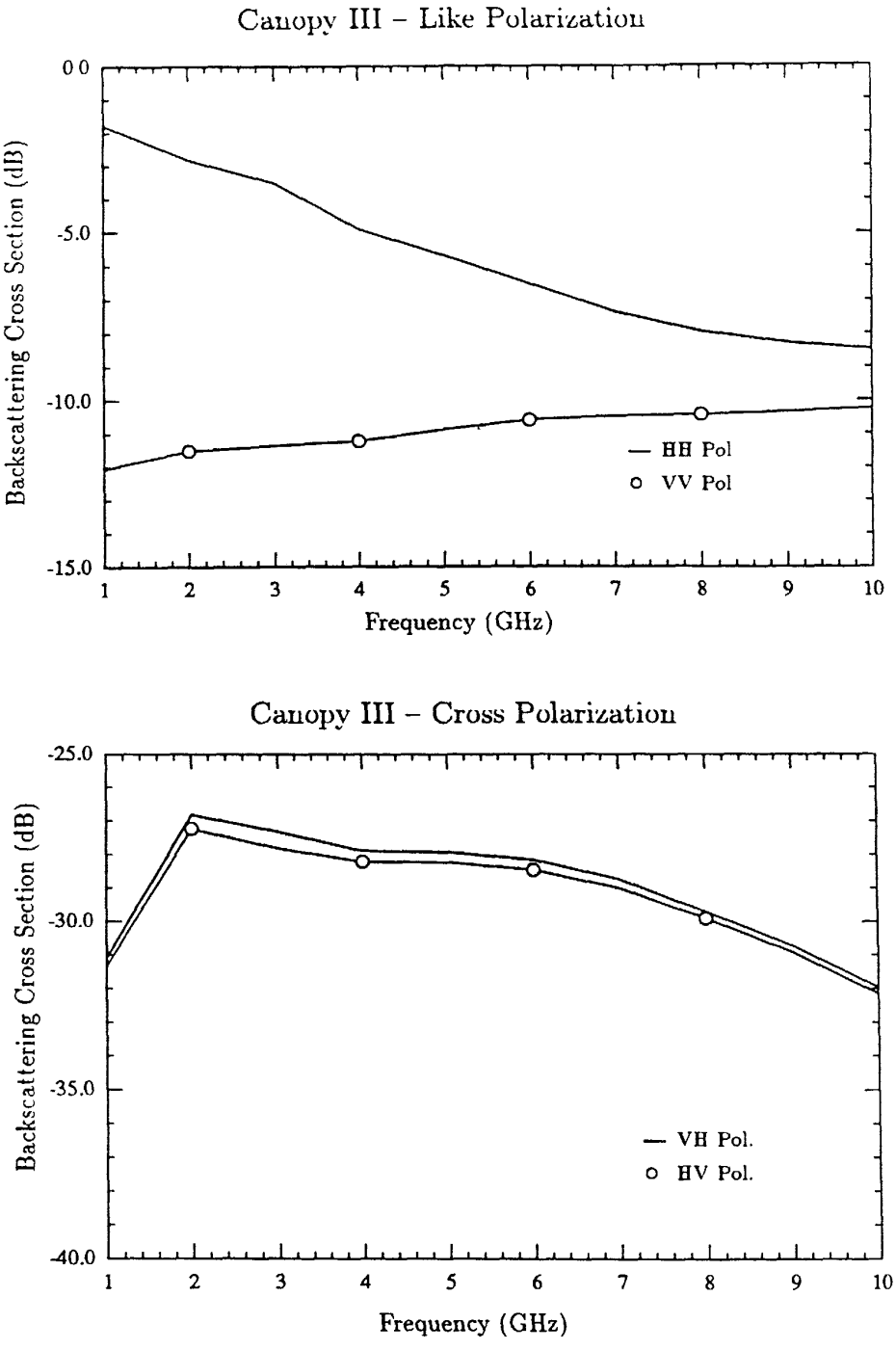


Figure H.41: Total Canopy Backscatter vs Frequency. Incidence Angle = 30^o

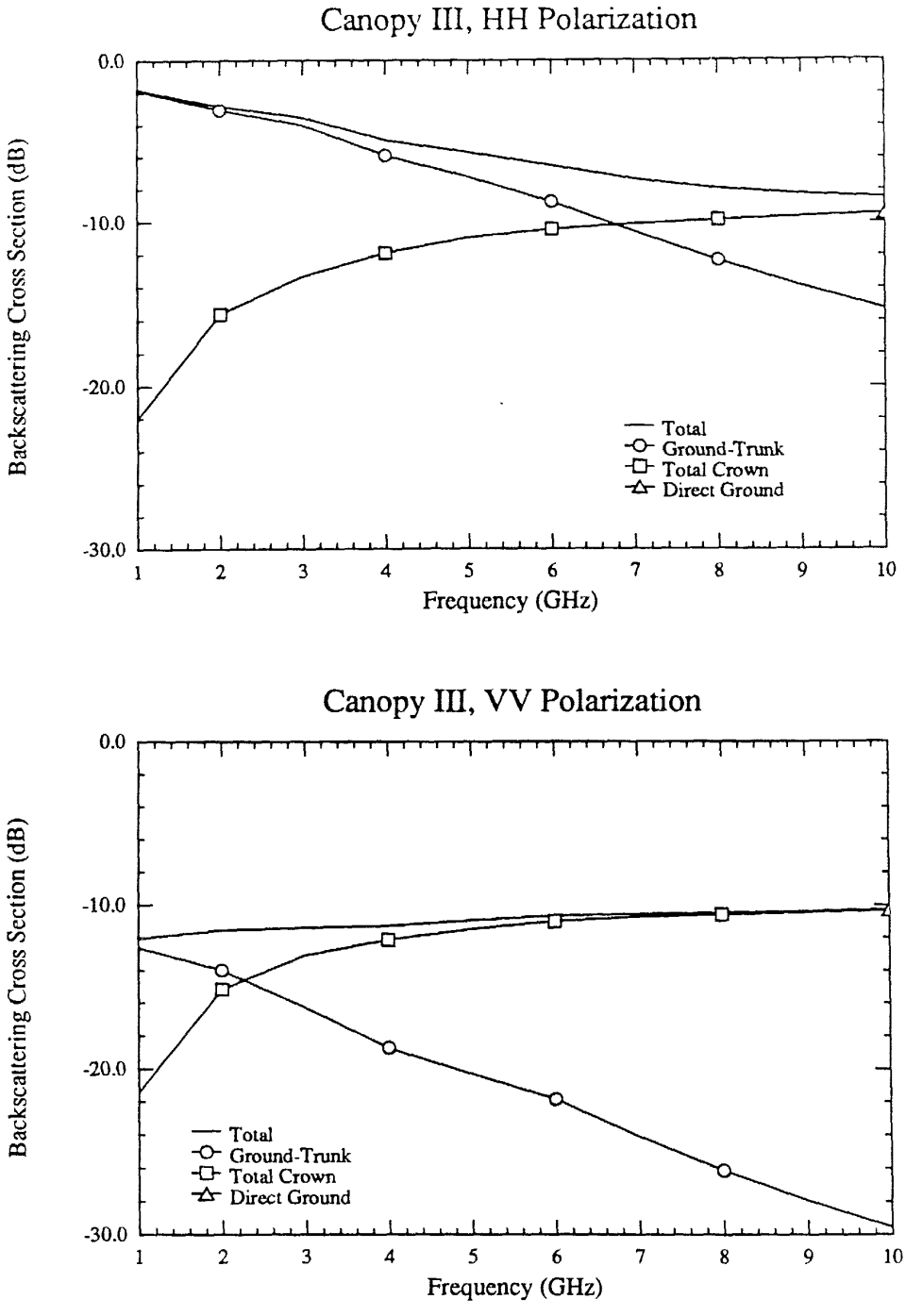


Figure H.42: Like-Polarized Canopy Backscatter Components vs. Frequency. Incidence Angle = 30°

CANOPY IV – Crown Layer Consisting of Needles and Branches

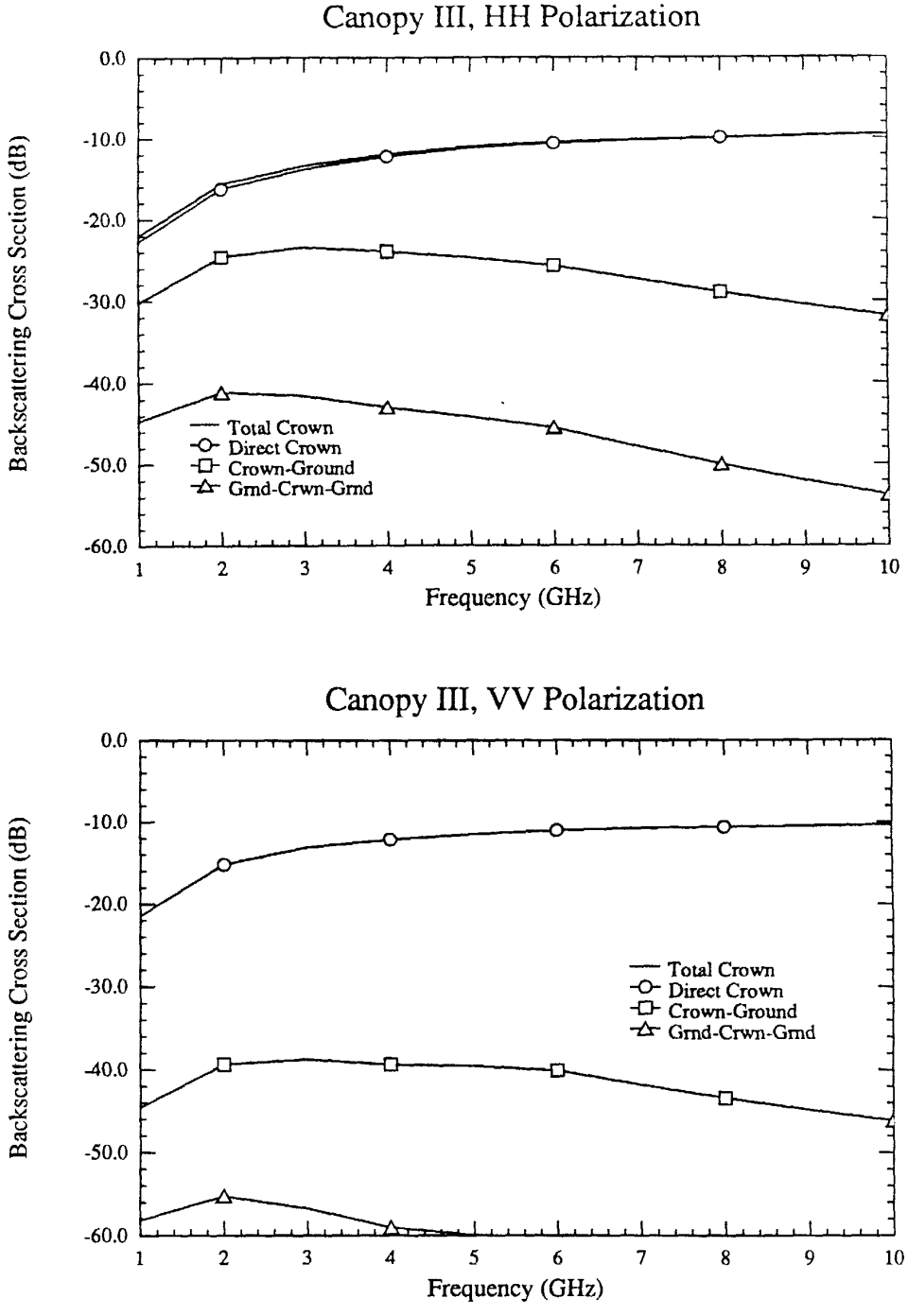


Figure II.43: Like-Polarized Crown Backscatter Components vs Frequency Incidence Angle = 30°

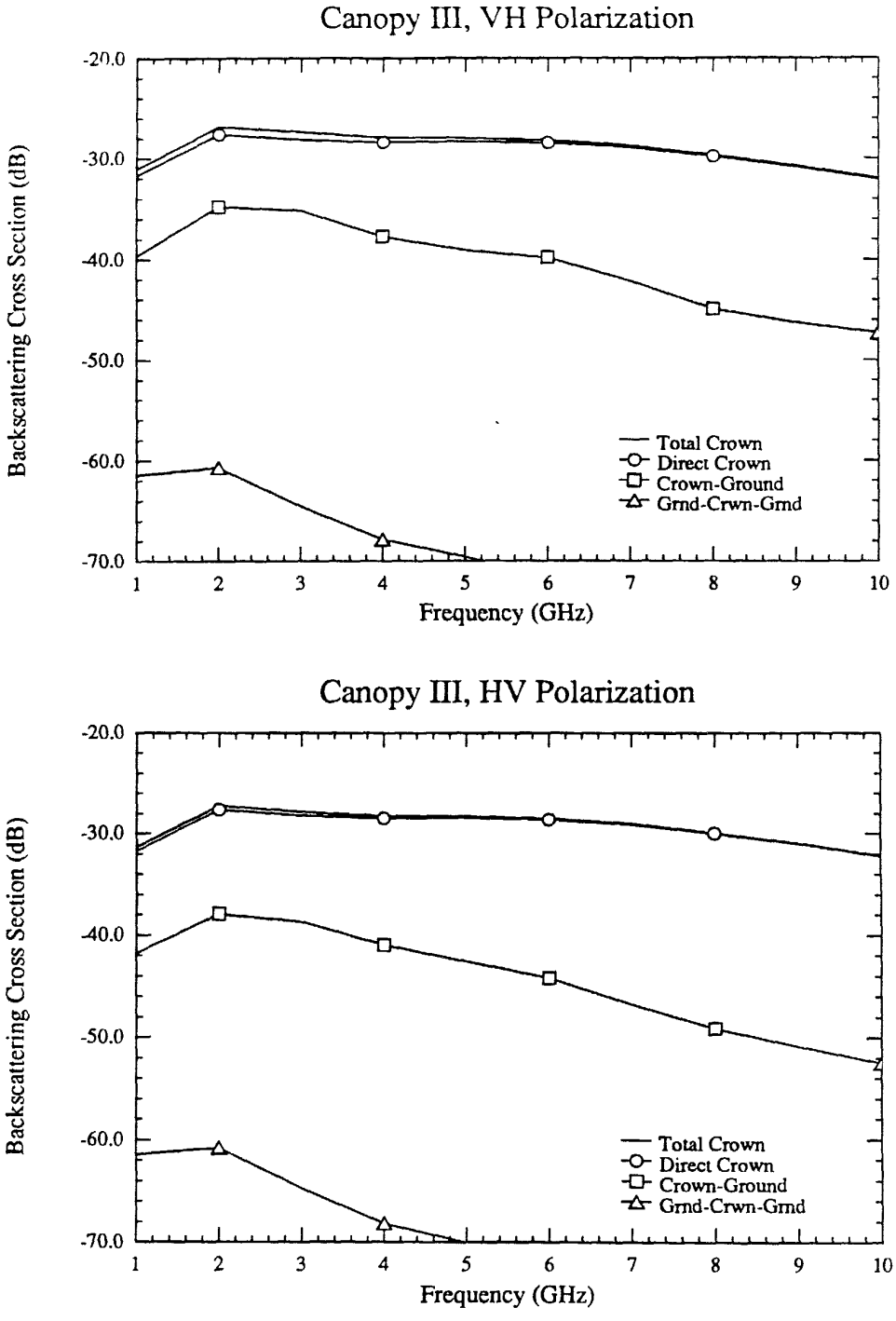


Figure H.44: Cross-Polarized Crown Backscatter Components vs. Frequency. Incidence Angle = 30°

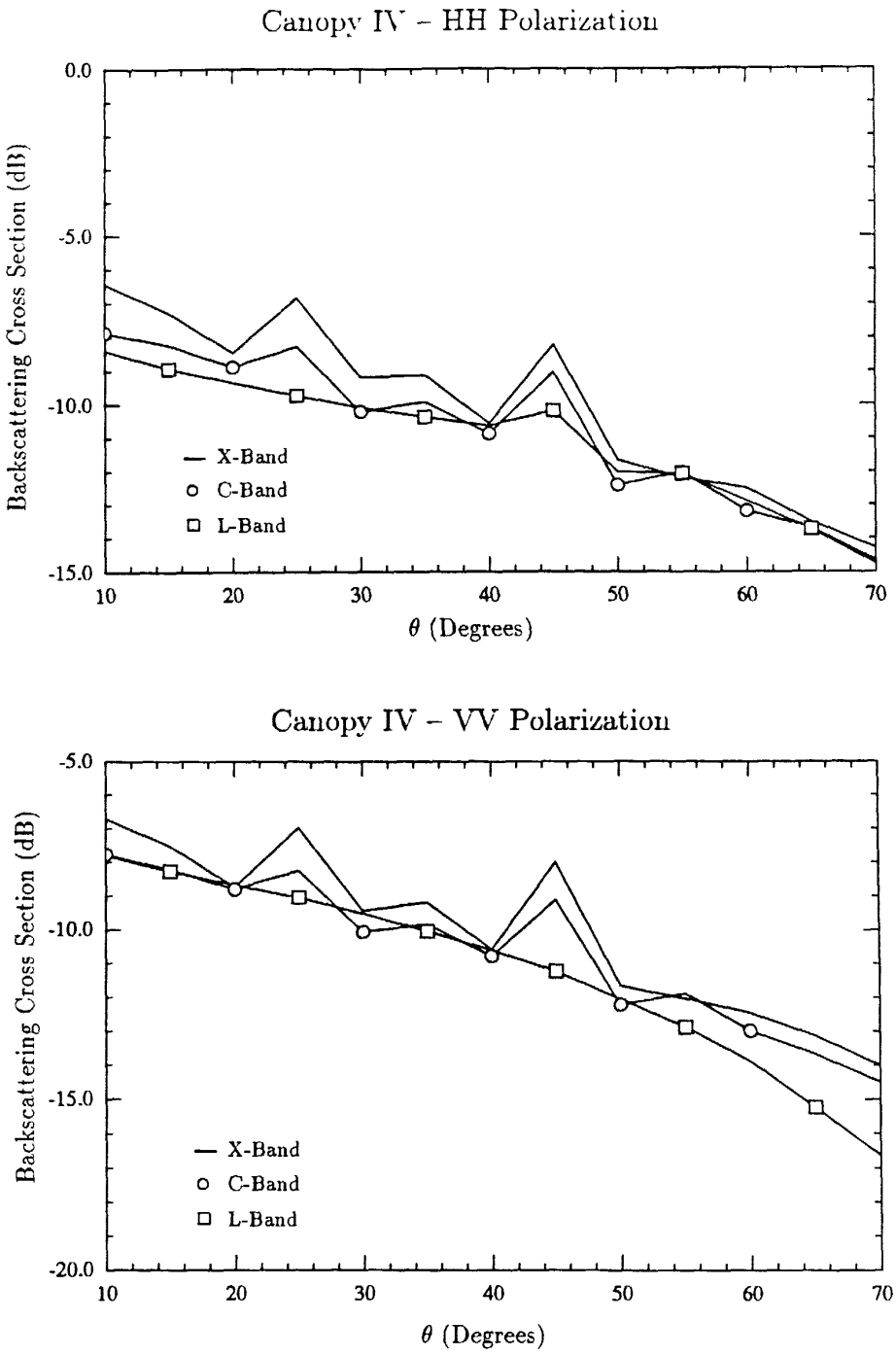


Figure H.45: Total Like-Polarized Canopy Backscatter vs. Incidence Angle

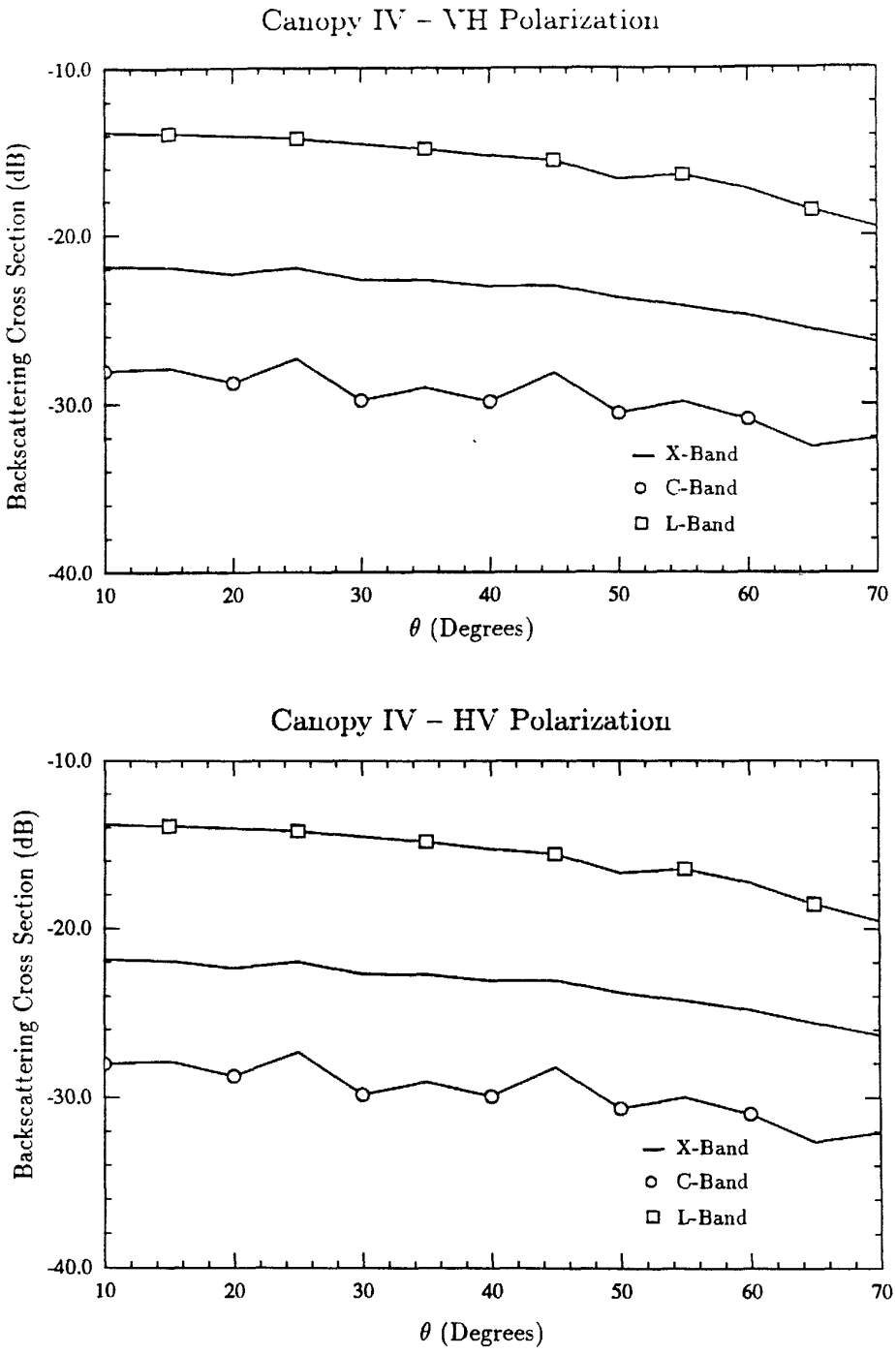


Figure H.46: Total Cross-Polarized Canopy Backscatter vs. Incidence Angle

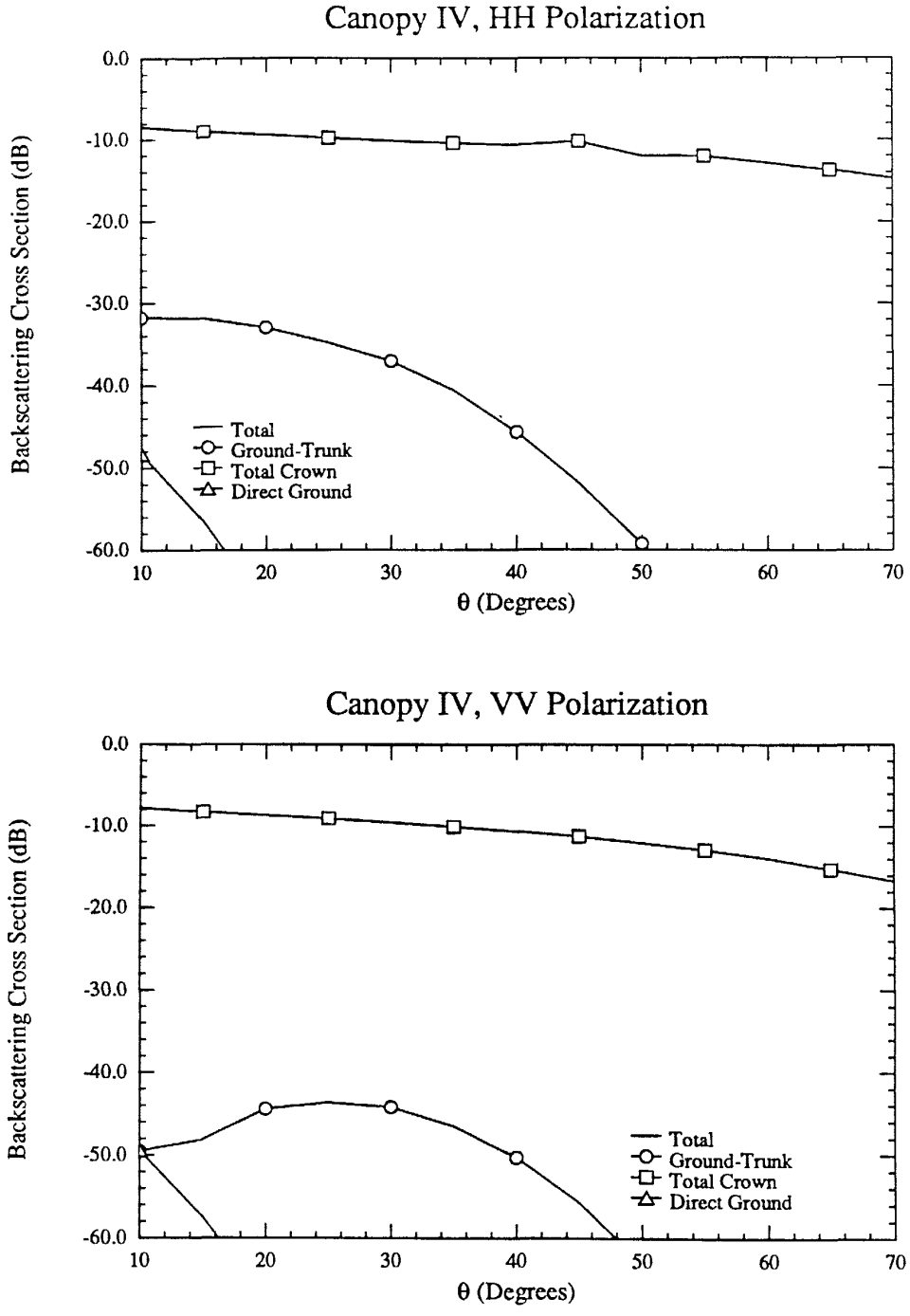


Figure H.47: L-Band Like-Polarized Canopy Backscatter Components vs. Incidence Angle

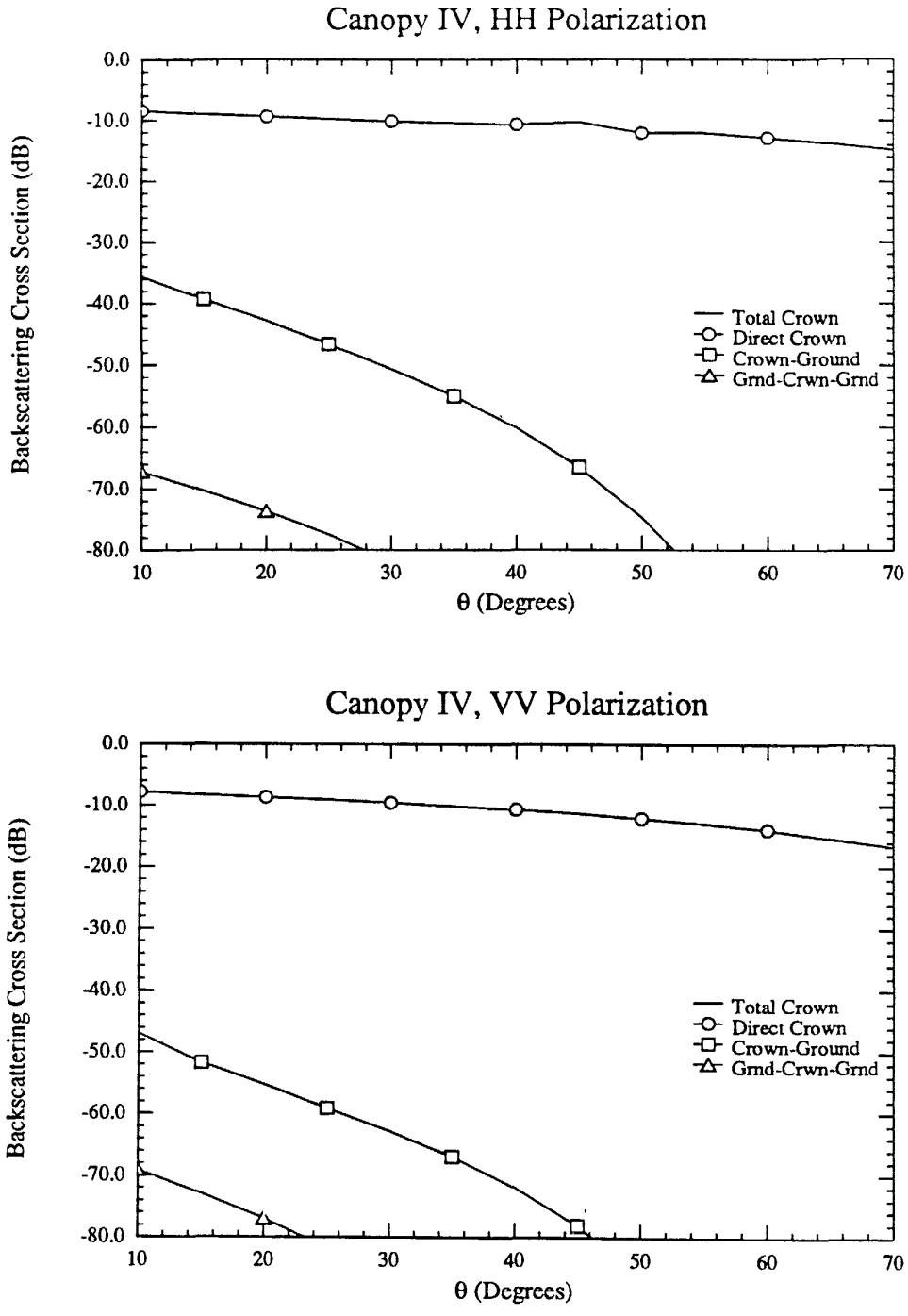


Figure H.48: L-Band Like-Polarized Crown Backscatter Components vs. Incidence Angle

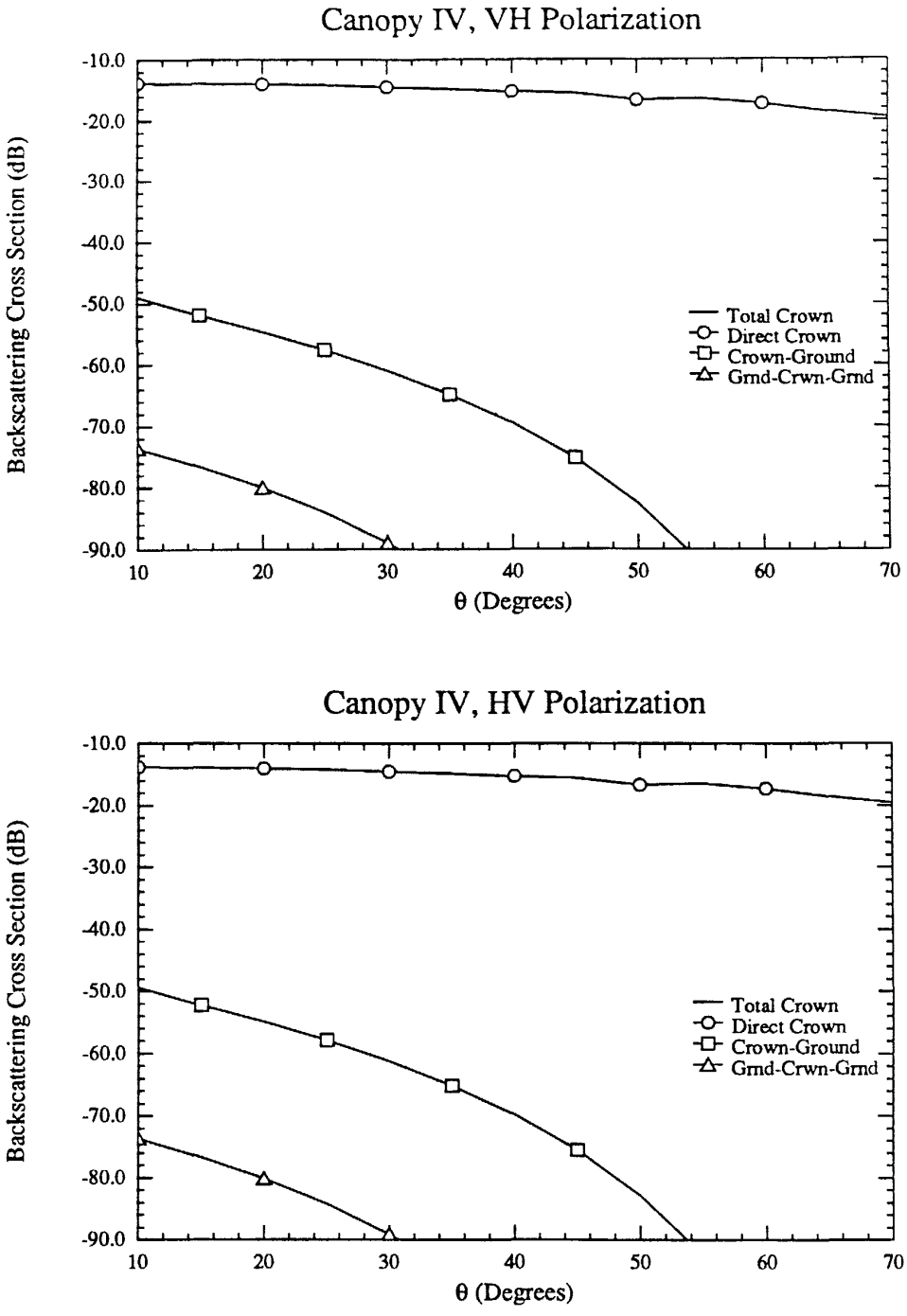


Figure H.49. L-Band Cross-Polarized Crown Backscatter Components vs. Incidence Angle

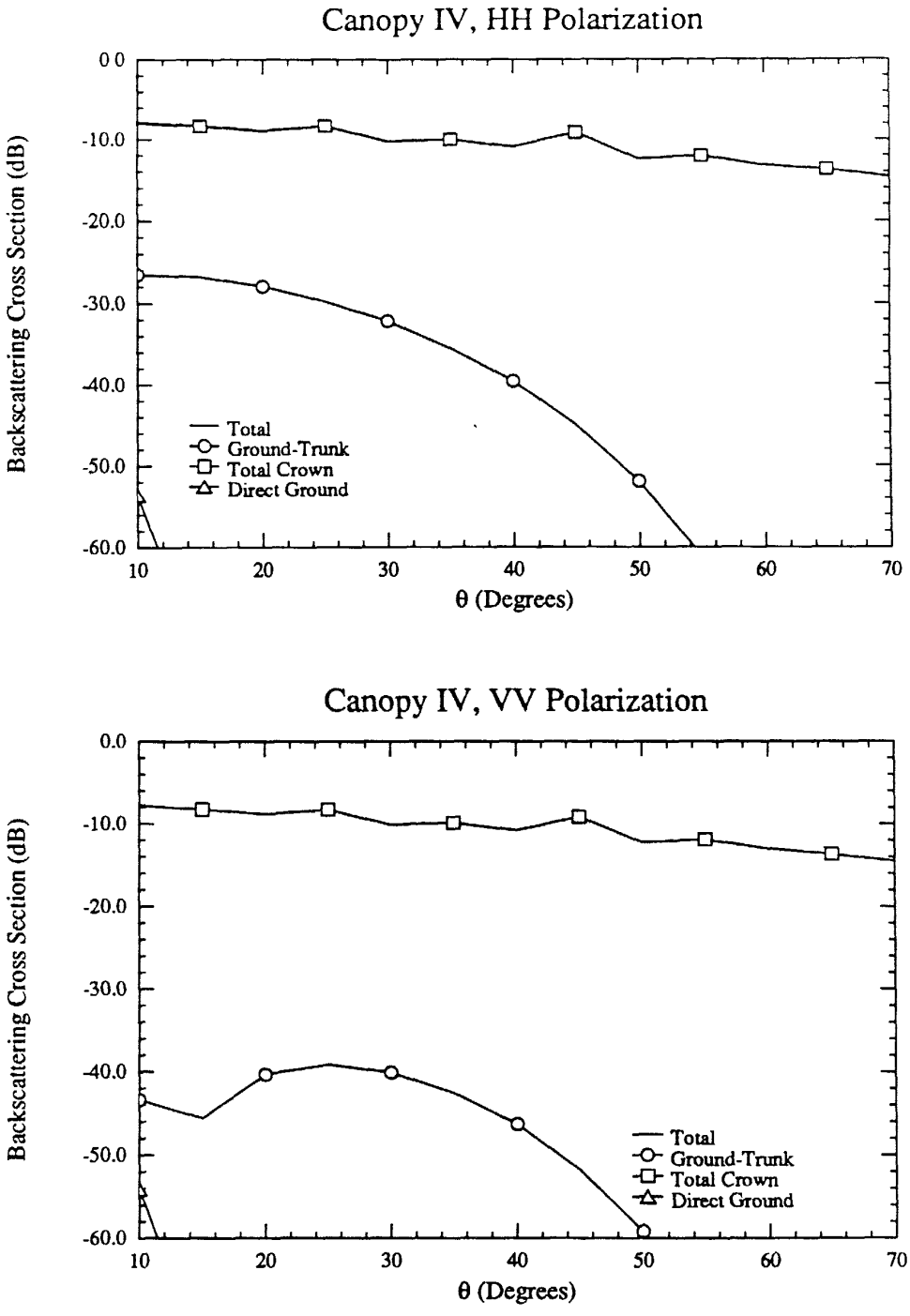


Figure H.50: C-Band Like-Polarized Canopy Backscatter Components vs. Incidence Angle

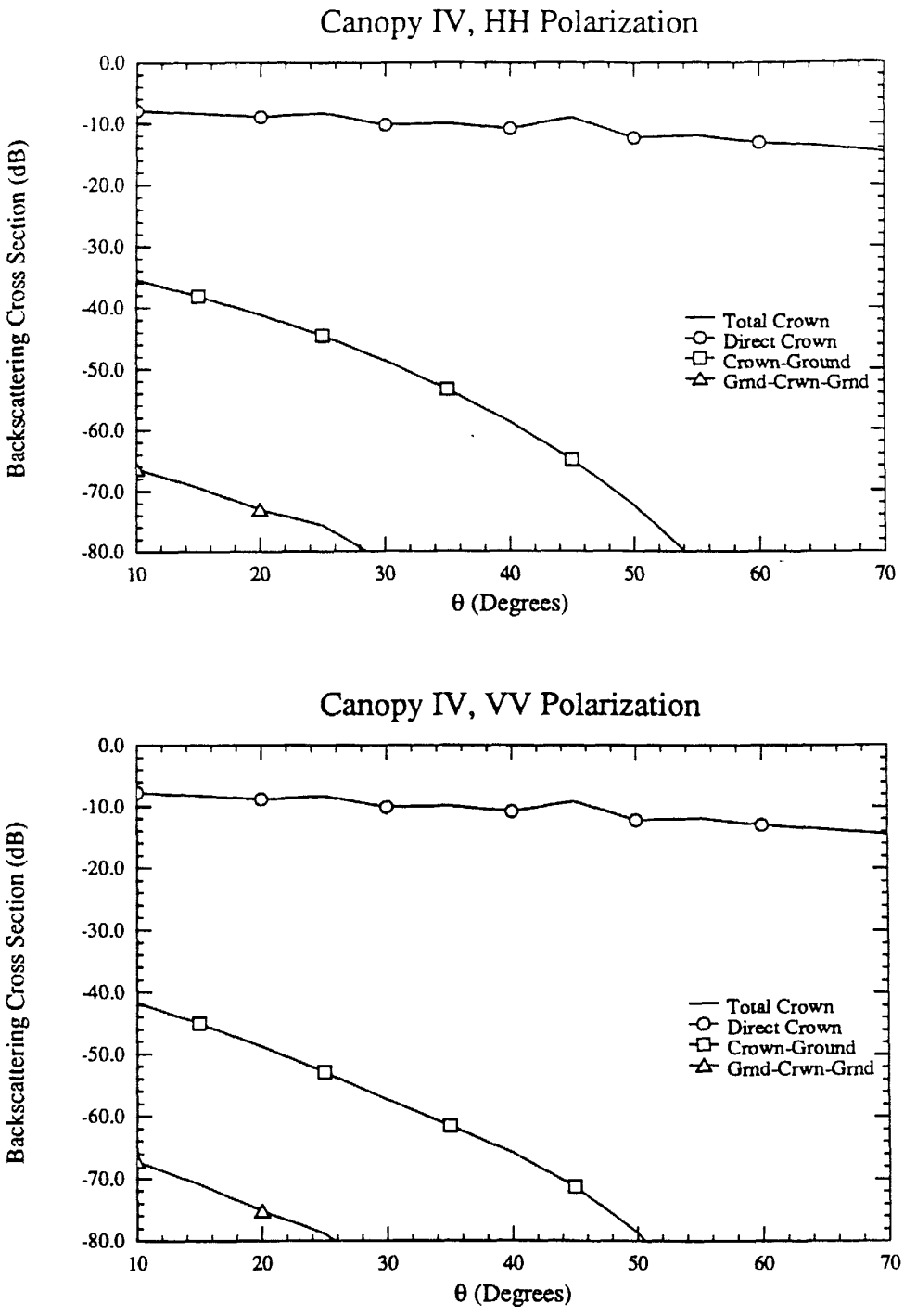


Figure H.51: C-Band Like-Polarized Crown Backscatter Components vs. Incidence Angle

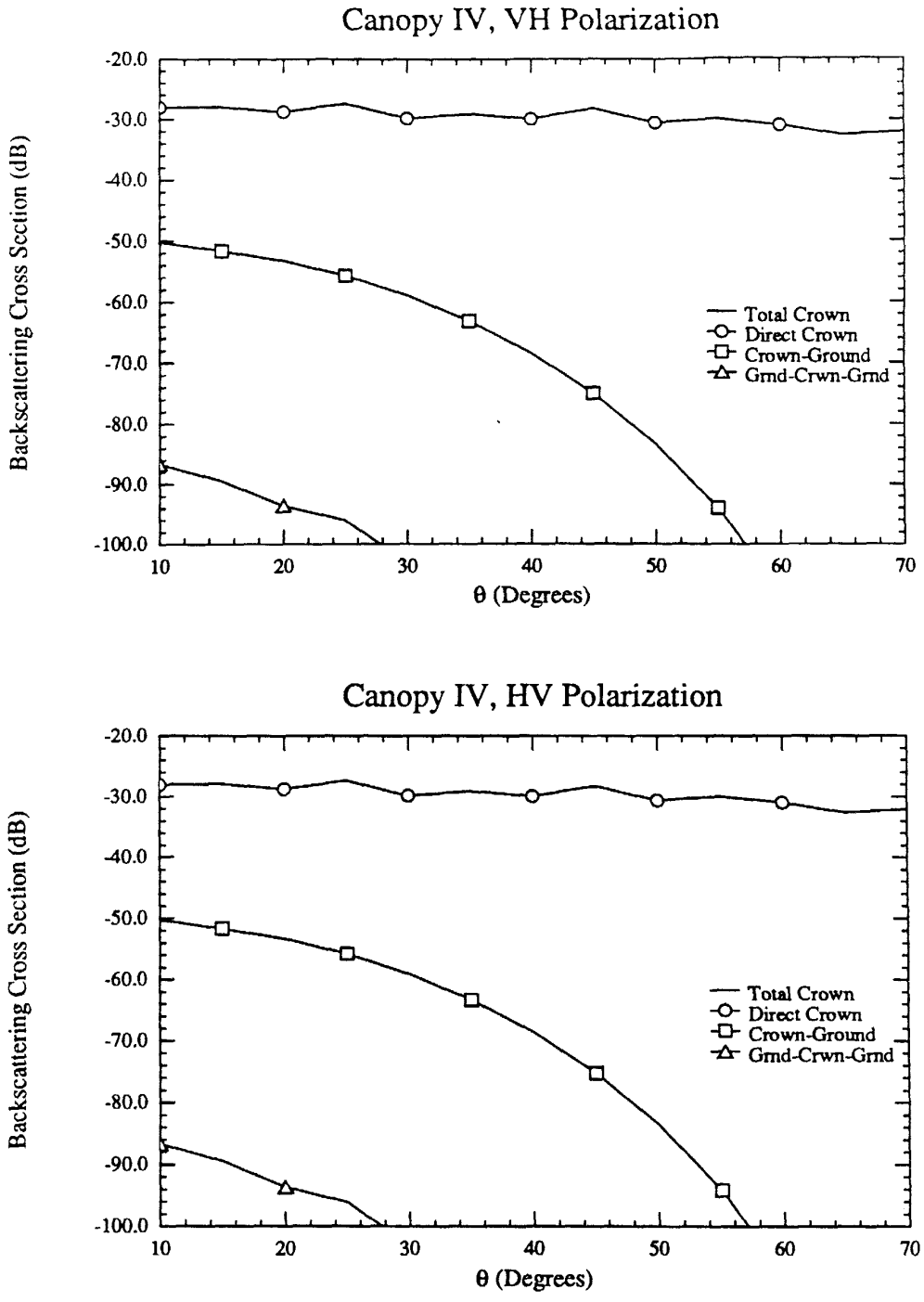


Figure H.52: C-Band Cross-Polarized Crown Backscatter Components vs. Incidence Angle

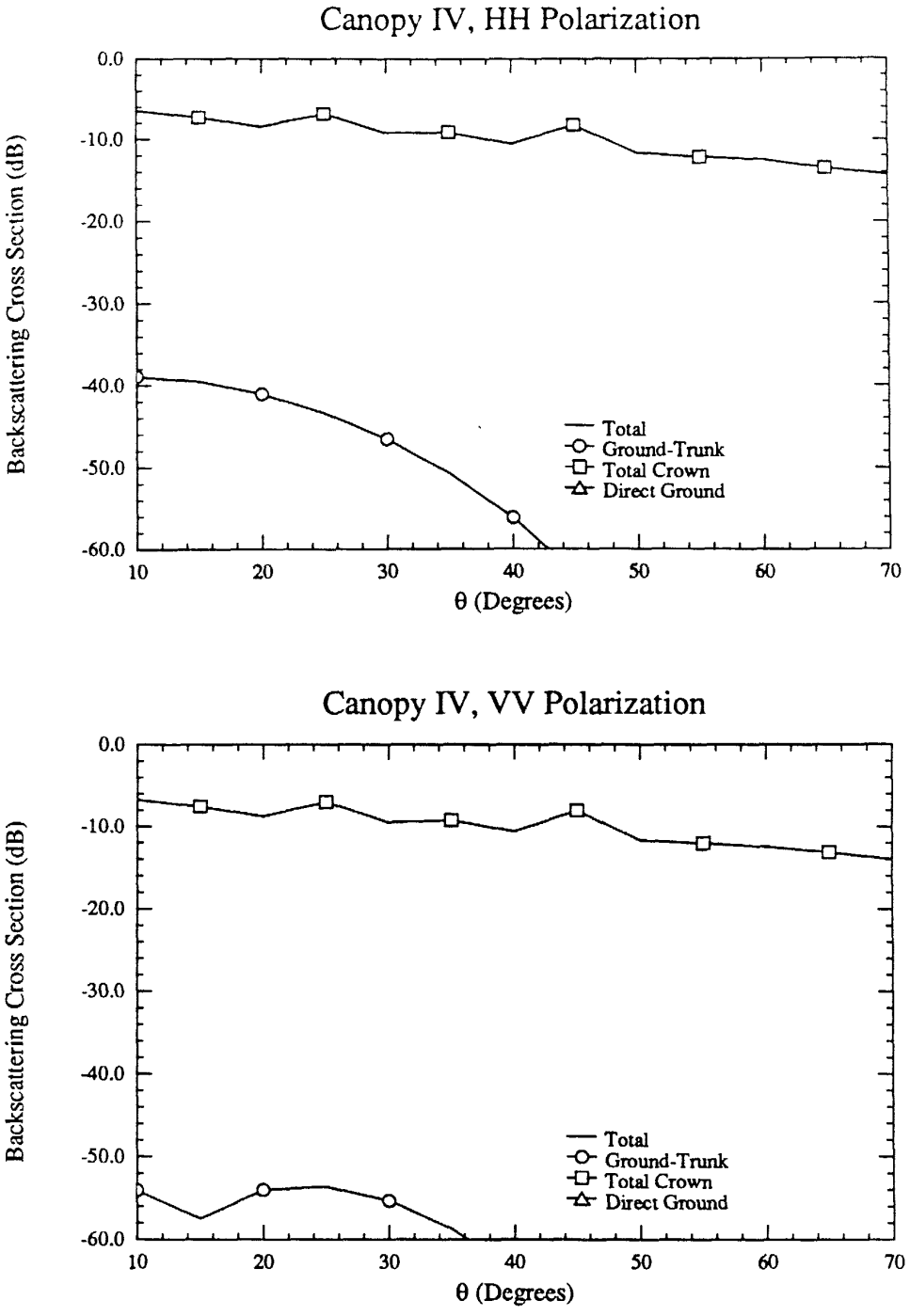


Figure H.53: X-Band Like-Polarized Canopy Backscatter Components vs. Incidence Angle

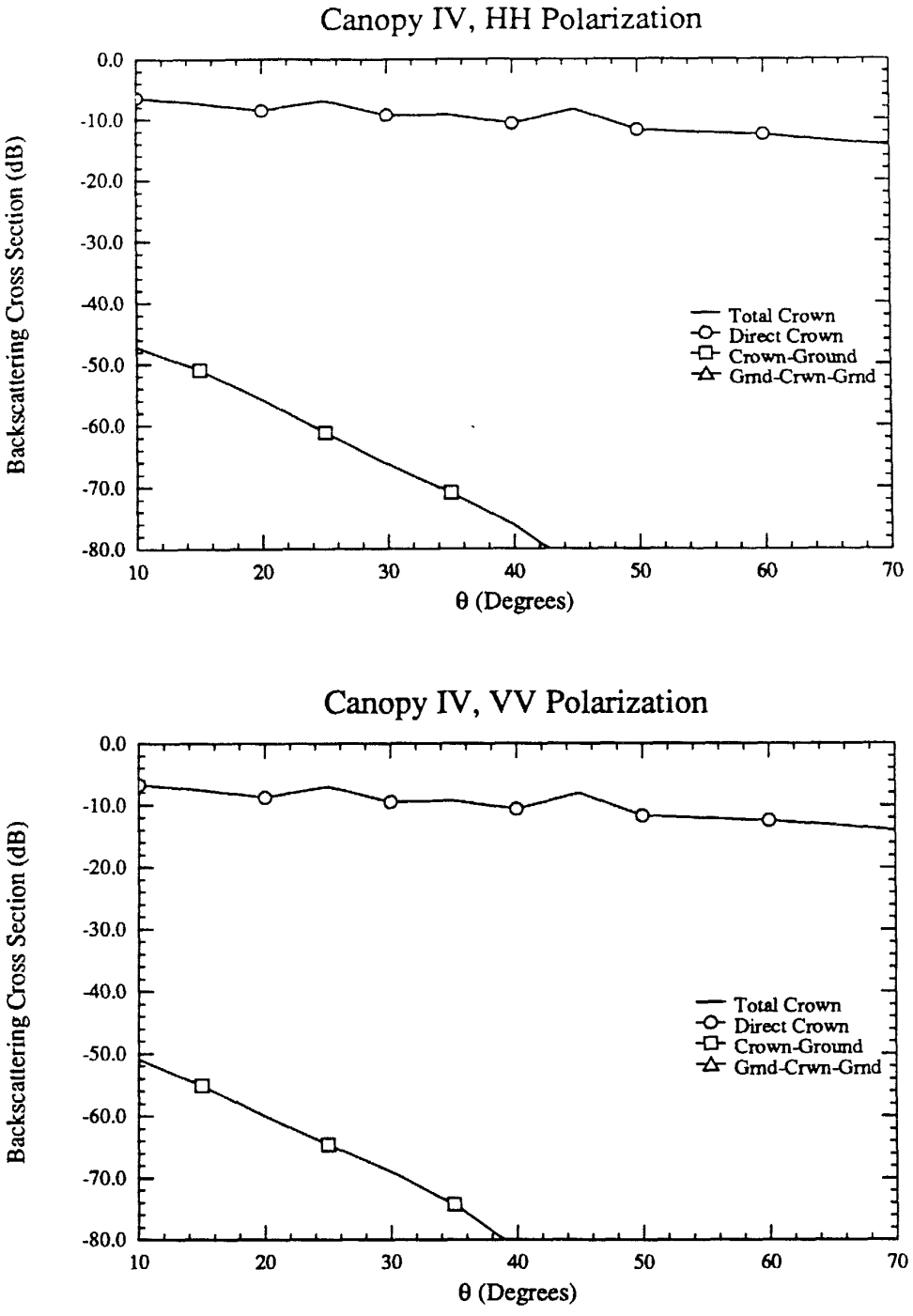
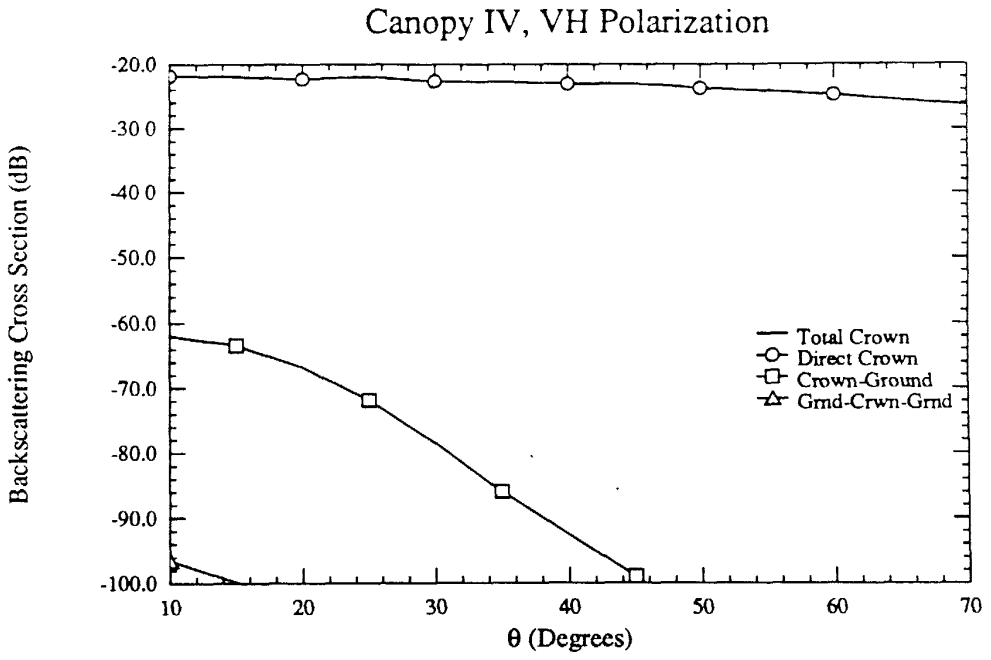


Figure H.54: X-Band Like-Polarized Crown Backscatter Components vs. Incidence Angle



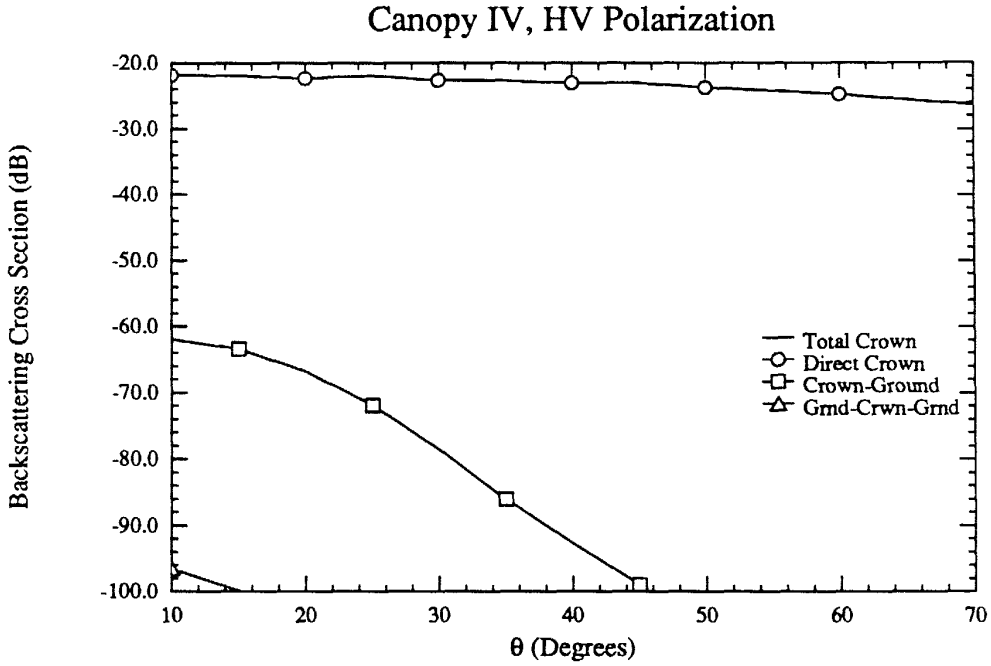


Figure H.55: X-Band Cross-Polarized Crown Backscatter Components vs. Incidence Angle

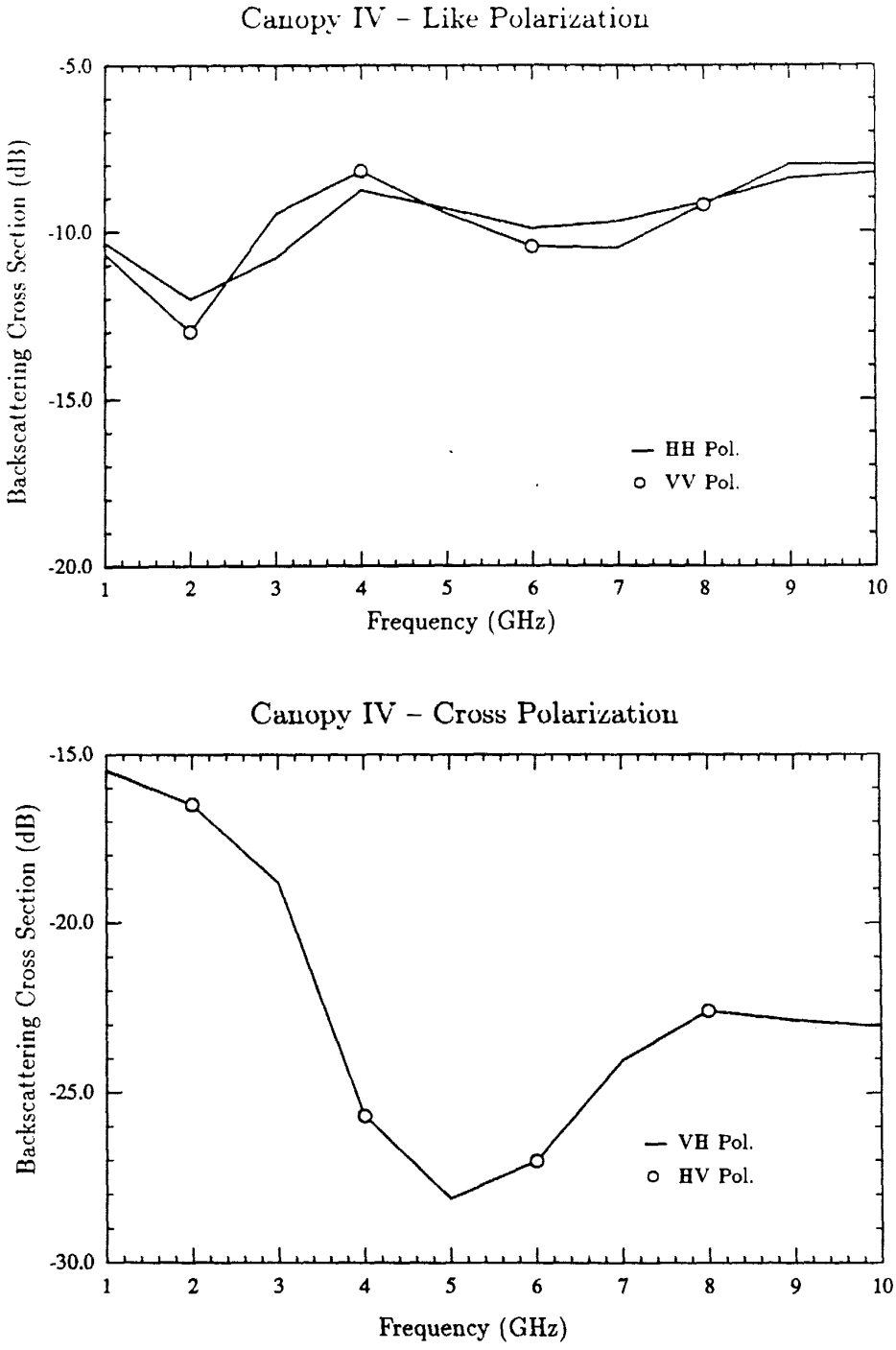


Figure H.56: Total Canopy Backscatter vs. Frequency. Incidence Angle = 30°

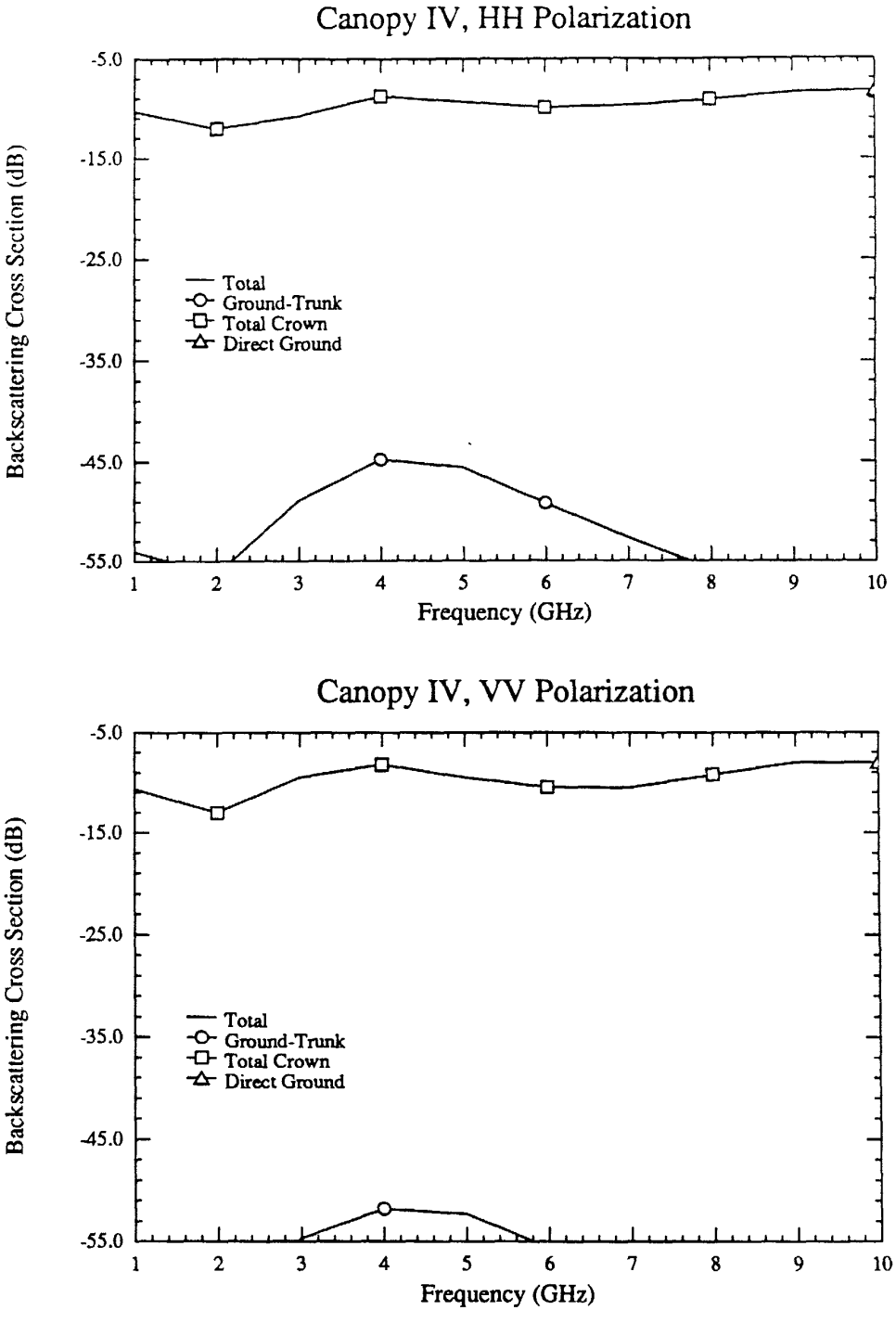


Figure H.57: Like-Polarized Canopy Backscatter Components vs. Frequency. Incidence Angle = 30°

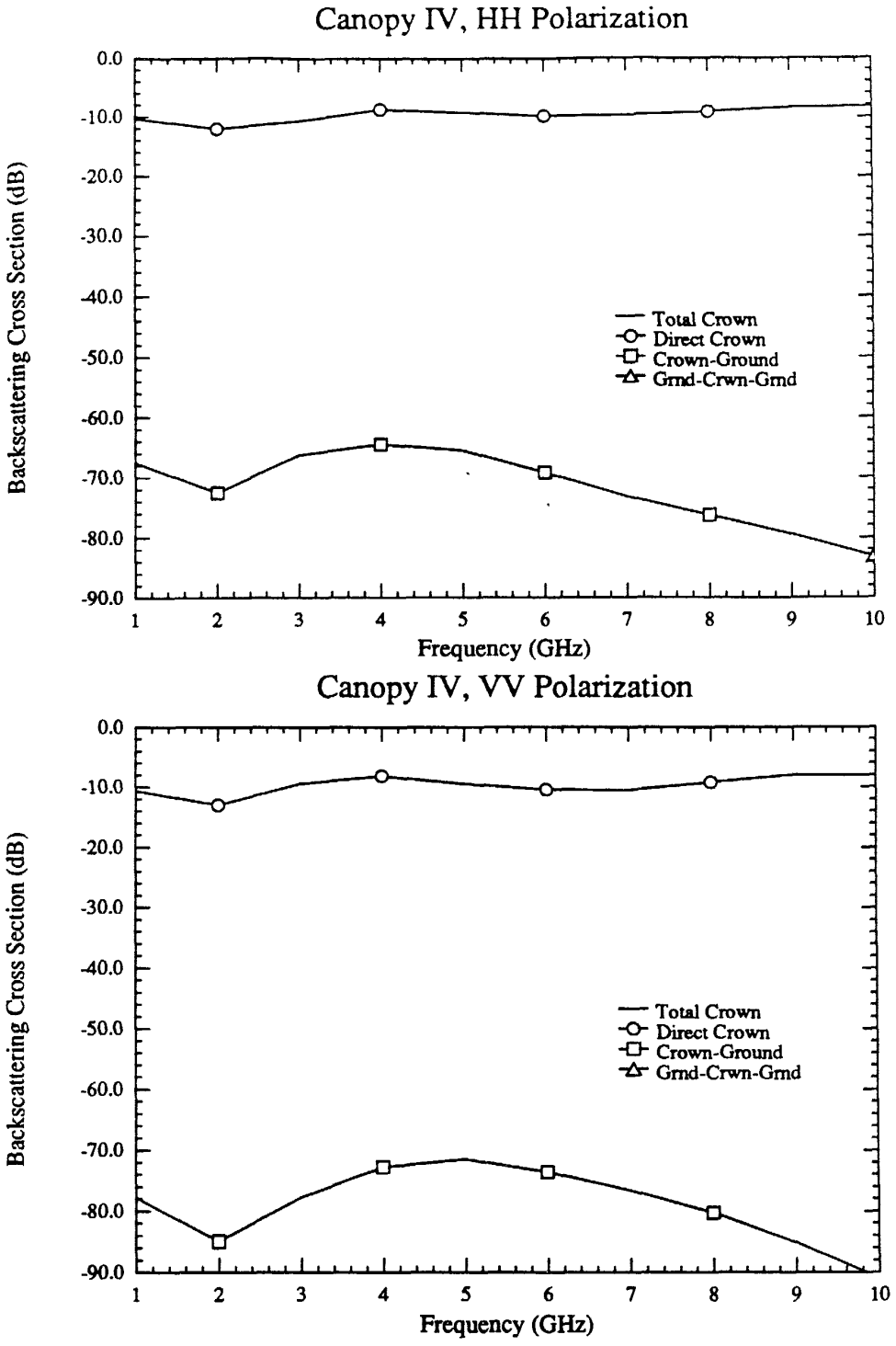


Figure H.58: Like-Polarized Crown Backscatter Components vs. Frequency. Incidence Angle = 30°

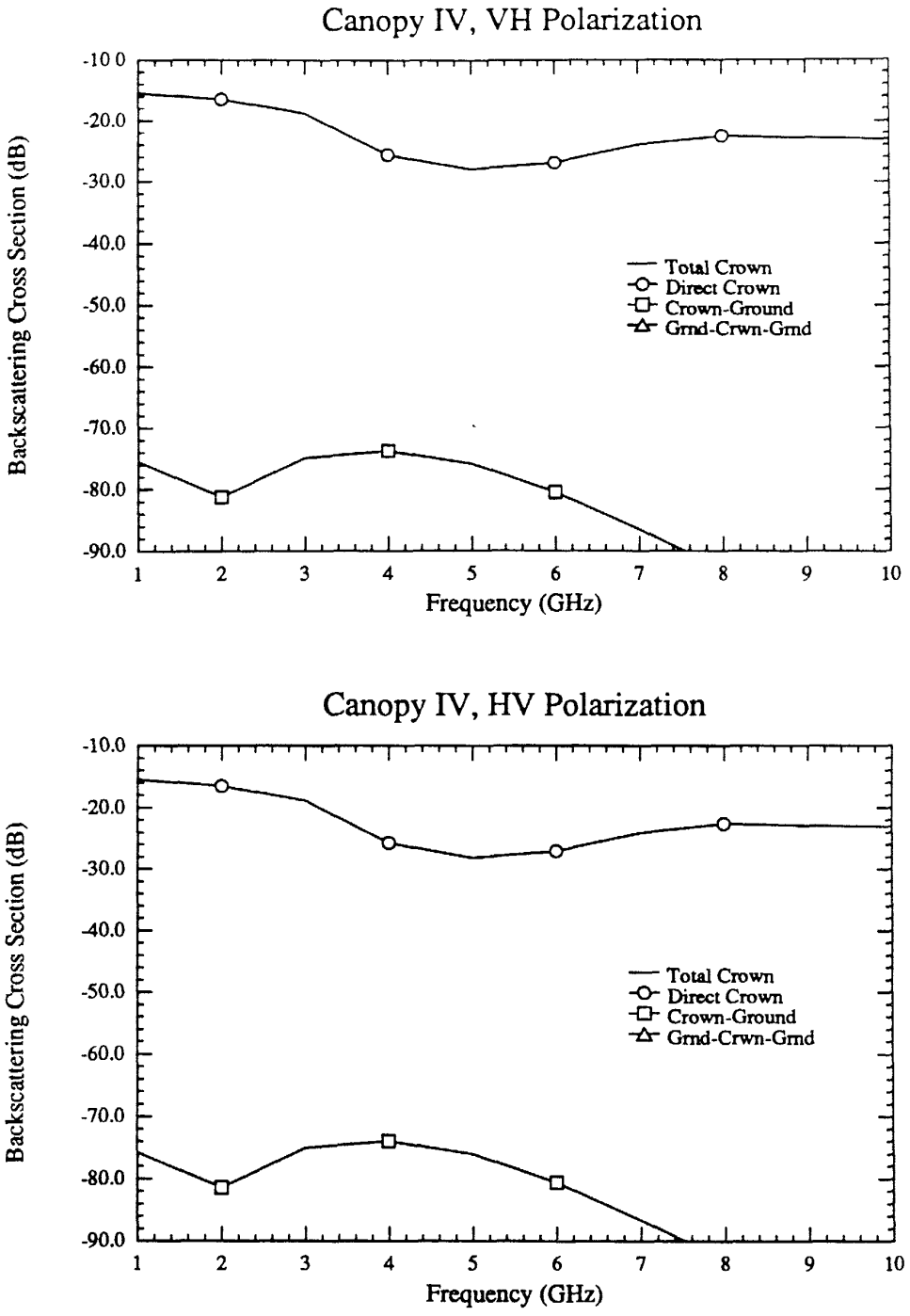
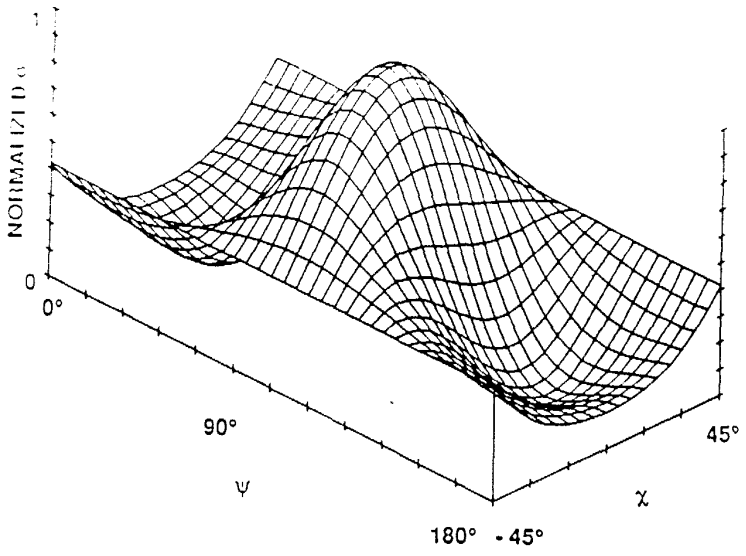


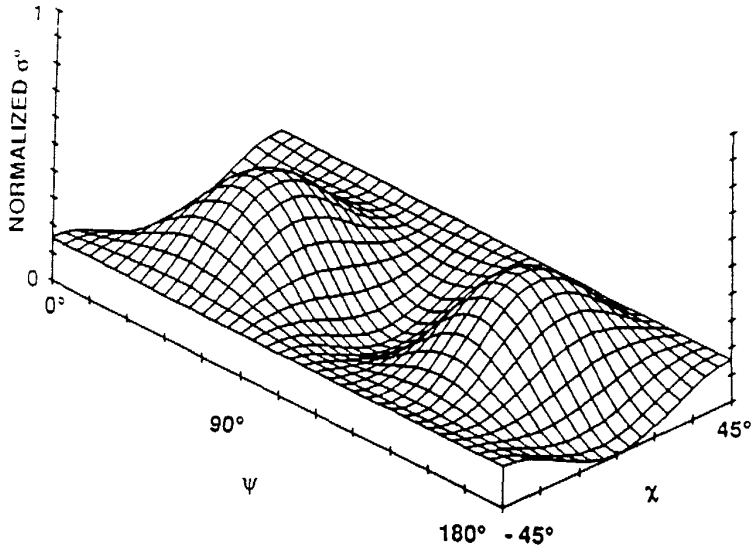
Figure H.59: Cross-Polarized Crown Backscatter Components vs. Frequency. Incidence Angle = 30°

Polarimetric Response Synthesis

Canopy I



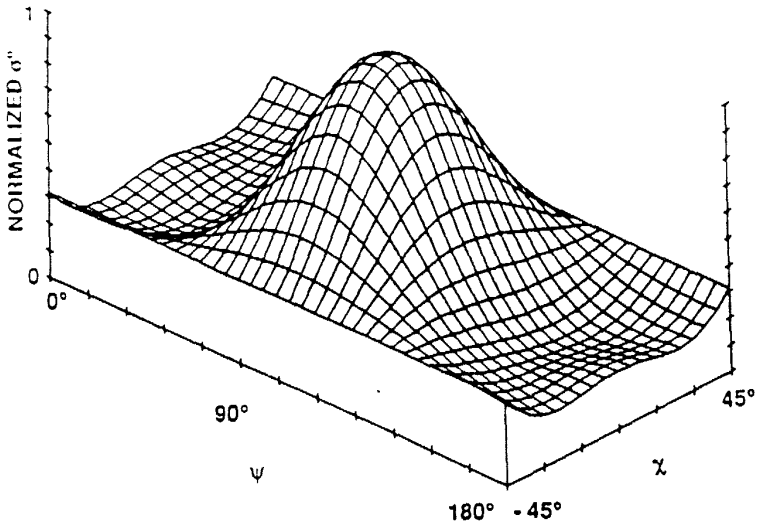
Like Polarized Response.



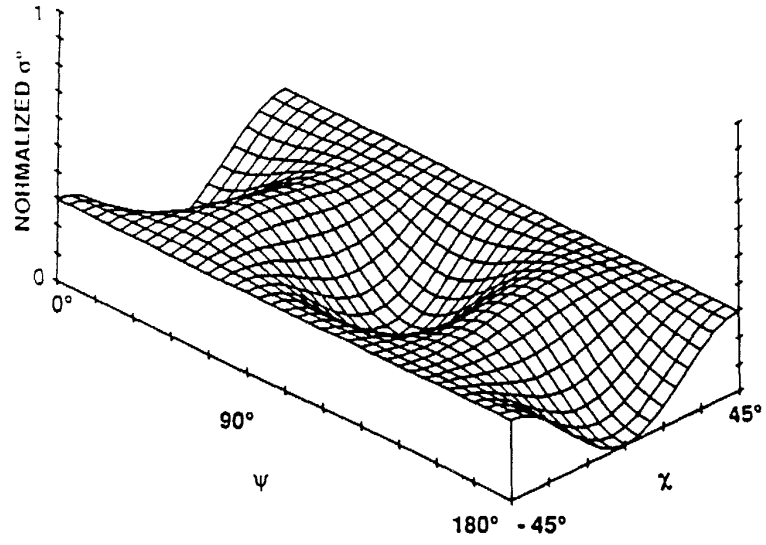
Cross Polarized Response.

Figure H.60: L-Band Polarization Response. Incidence Angle = 40°.

Canopy I



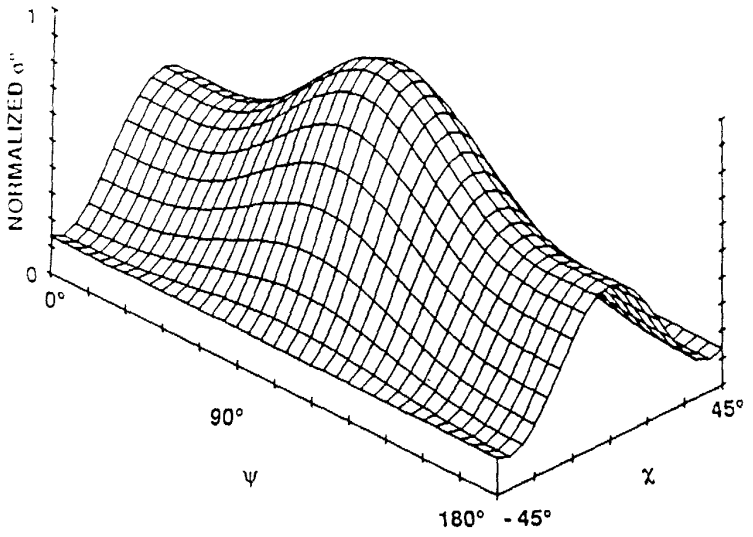
Like Polarized Response.



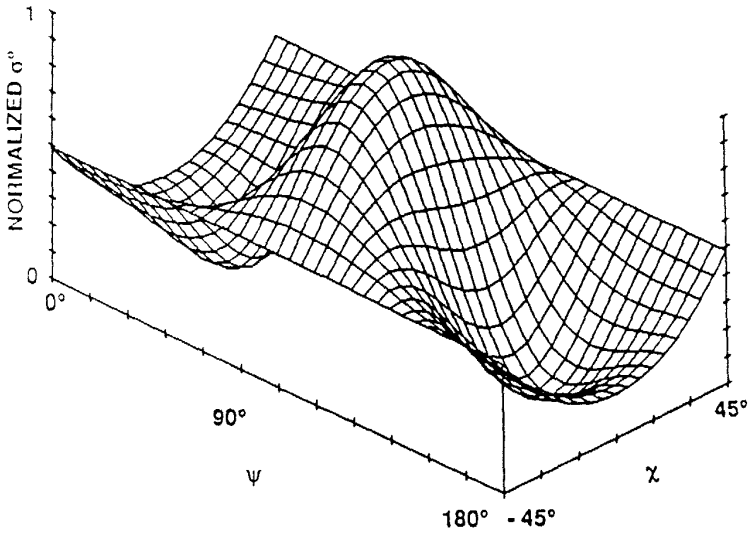
Cross Polarized Response.

Figure H.61: C-Band Polarization Response. Incidence Angle = 40°.

Canopy I



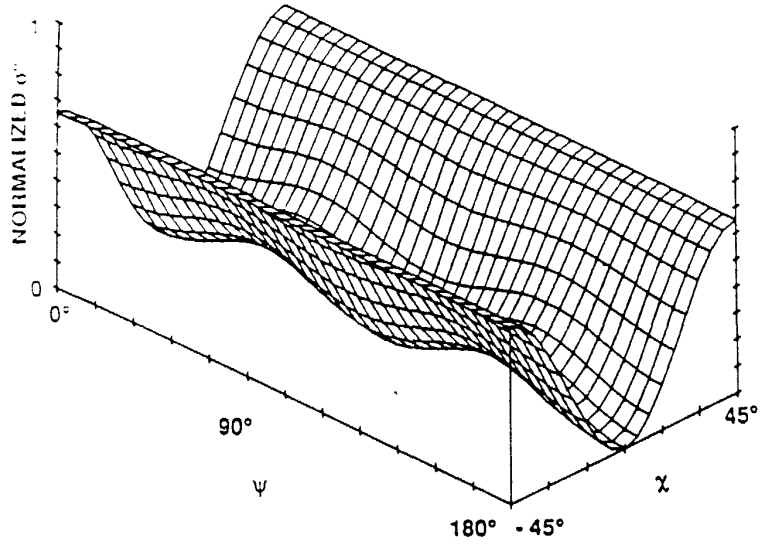
Like Polarized Response.



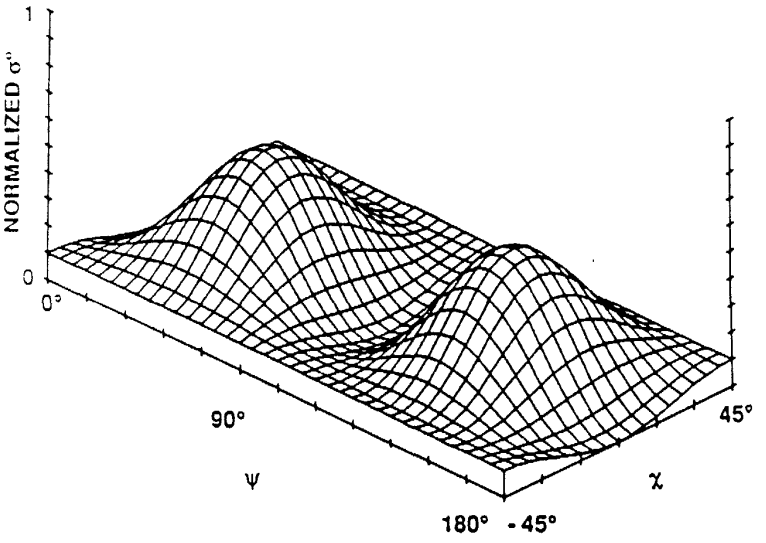
Cross Polarized Response.

Figure H.62: X-Band Polarization Response. Incidence Angle = 40°.

Canopy II



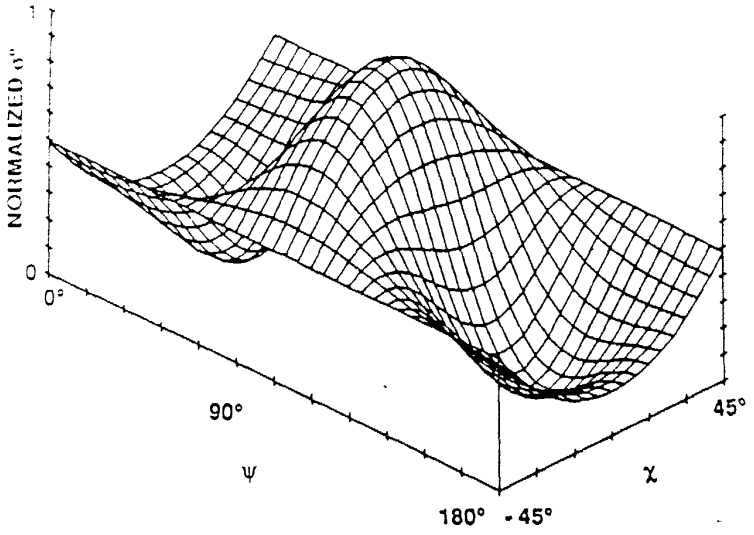
Like Polarized Response.



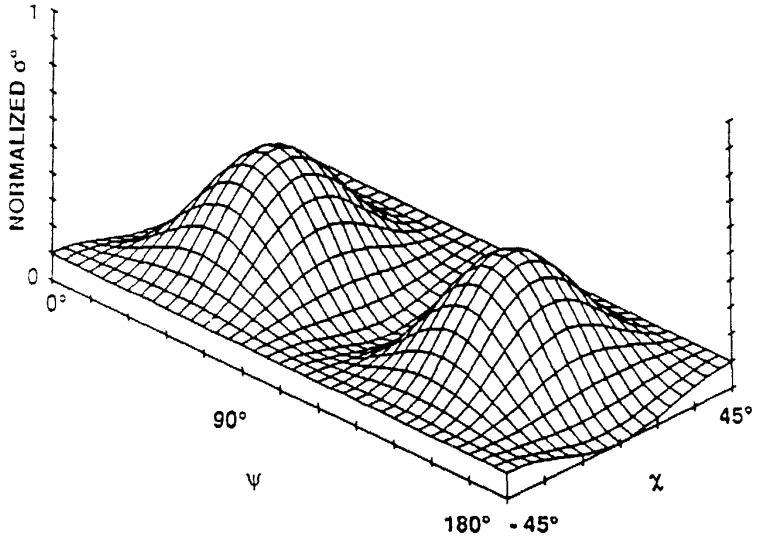
Cross Polarized Response.

Figure H.63: L-Band Polarization Response. Incidence Angle = 40°.

Canopy II



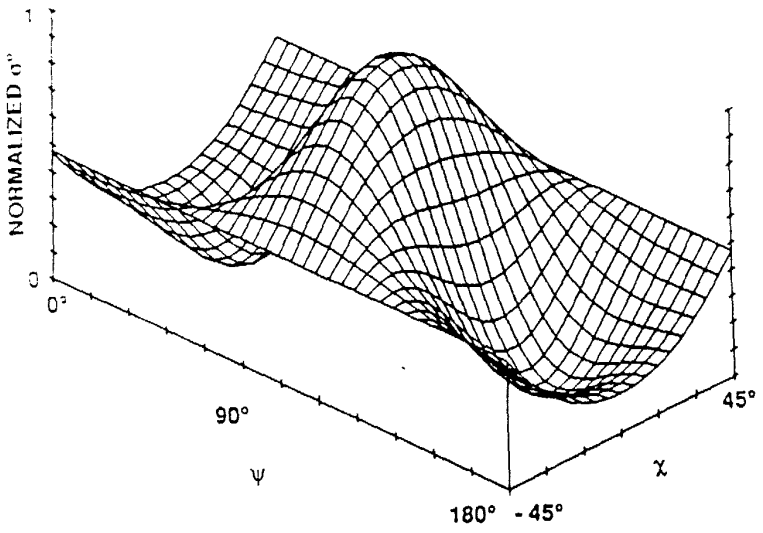
Like Polarized Response.



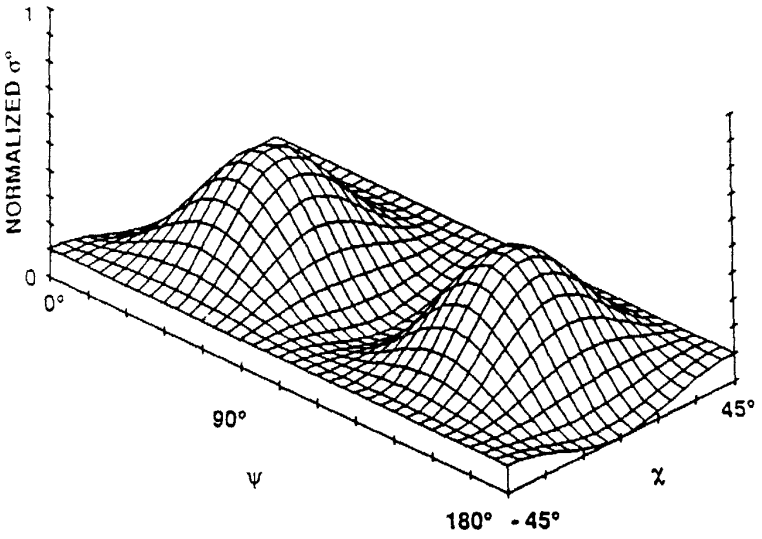
Cross Polarized Response.

Figure H.64: C-Band Polarization Response. Incidence Angle = 40°.

Canopy II



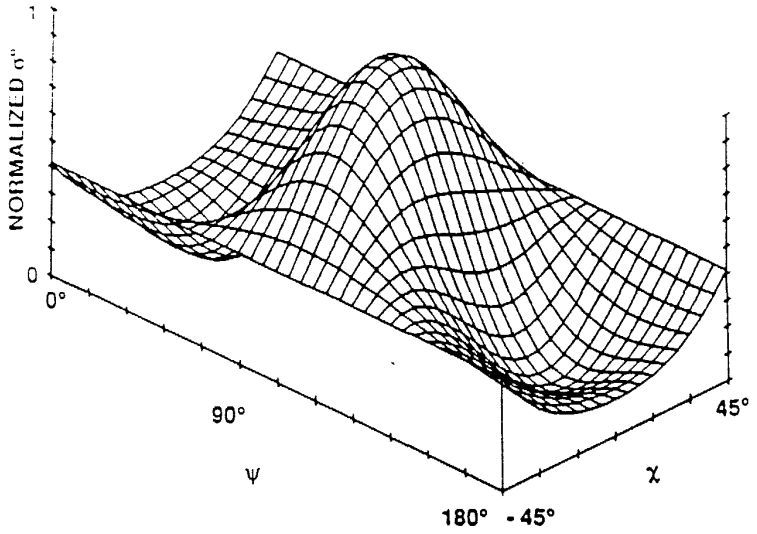
Like Polarized Response.



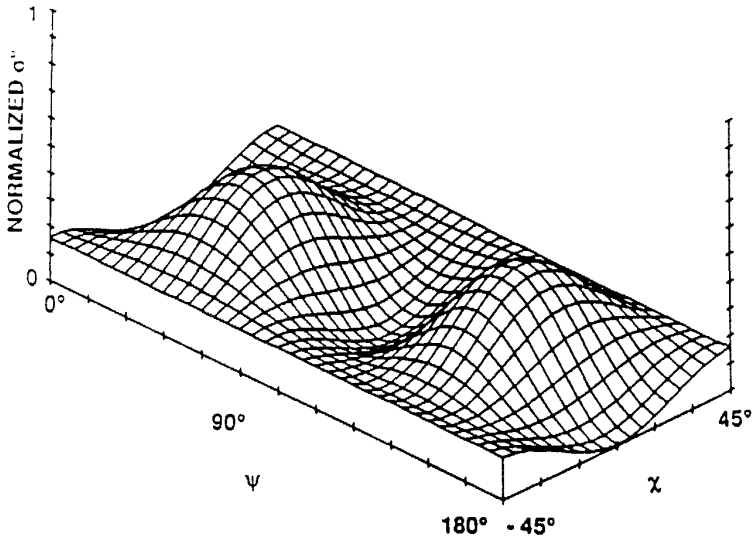
Cross Polarized Response.

Figure H.65: X-Band Polarization Response. Incidence Angle = 40°.

Canopy III



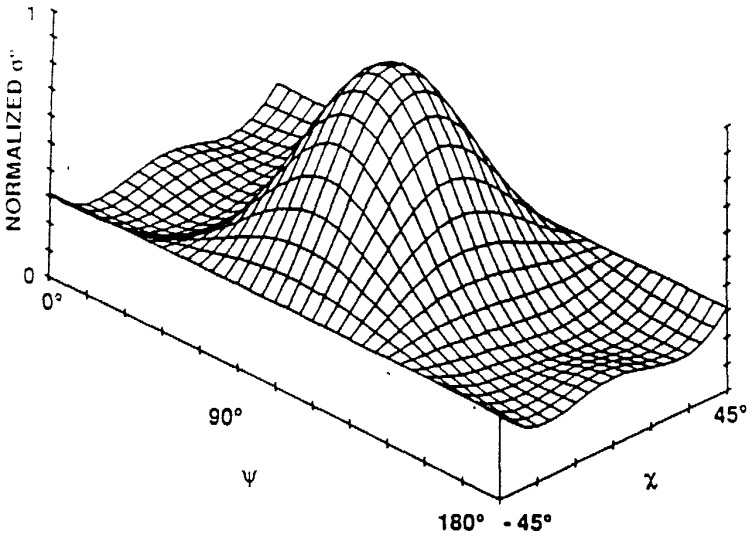
Like Polarized Response.



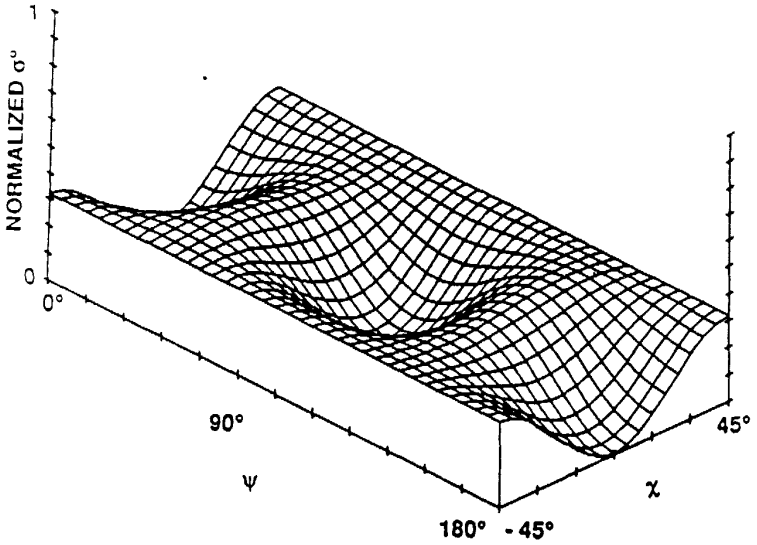
Cross Polarized Response.

Figure H.66: L-Band Polarization Response. Incidence Angle = 40°.

Canopy III



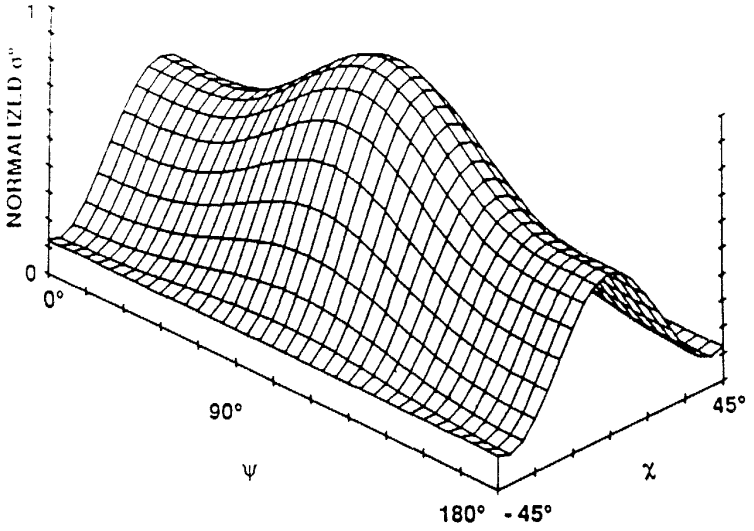
Like Polarized Response.



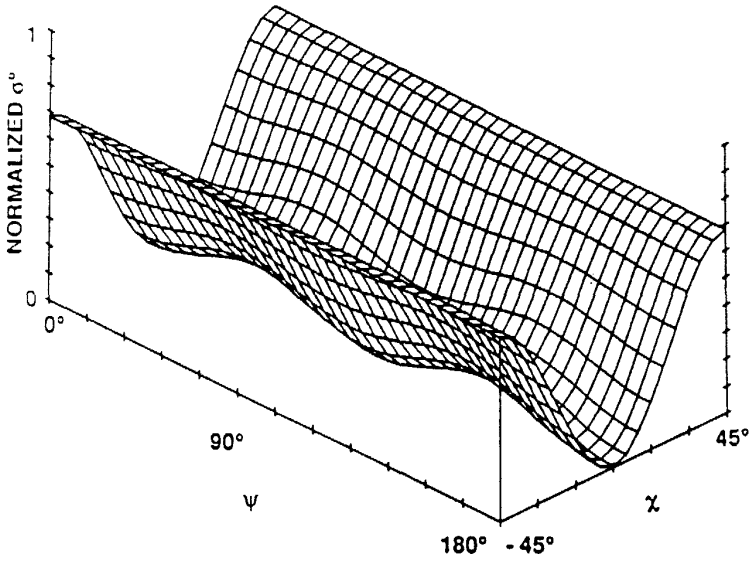
Cross Polarized Response.

Figure H.67: C-Band Polarization Response. Incidence Angle = 40°.

Canopy III



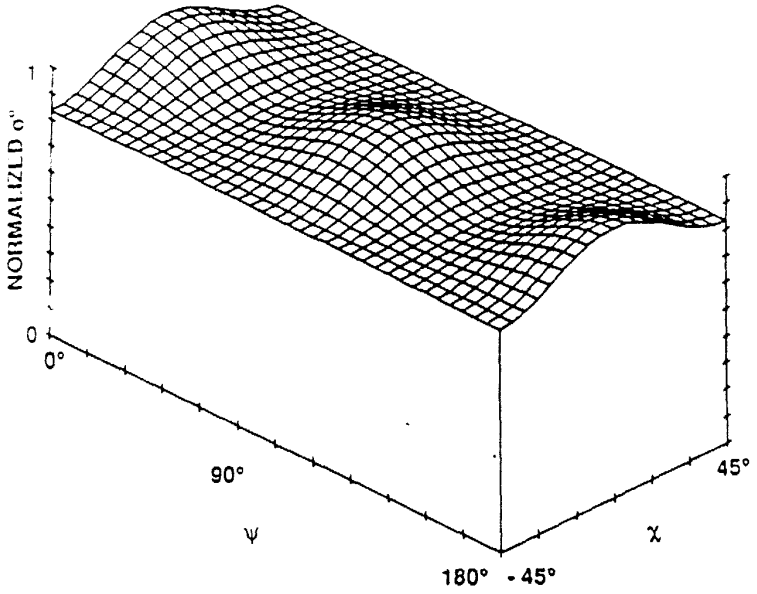
Like Polarized Response.



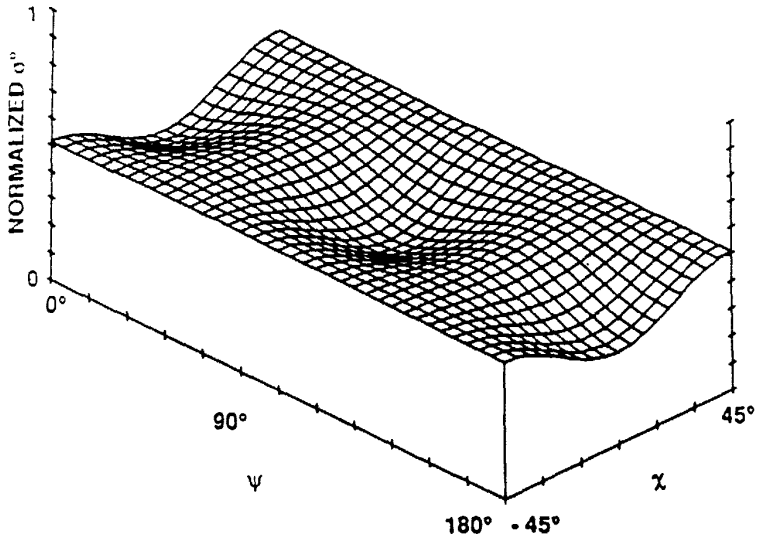
Cross Polarized Response.

Figure H.68: X-Band Polarization Response. Incidence Angle = 40°.

Canopy IV



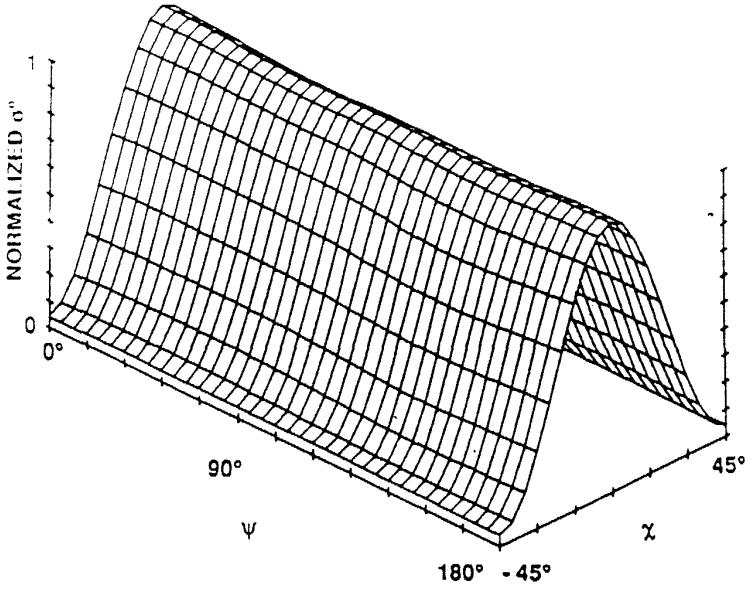
Like Polarized Response.



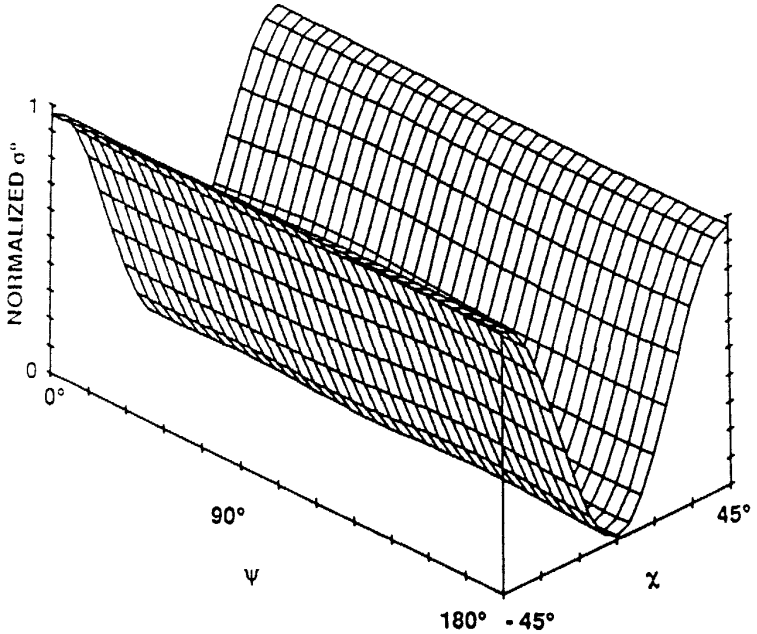
Cross Polarized Response.

Figure H.69: L-Band Polarization Response. Incidence Angle = 40°.

Canopy IV



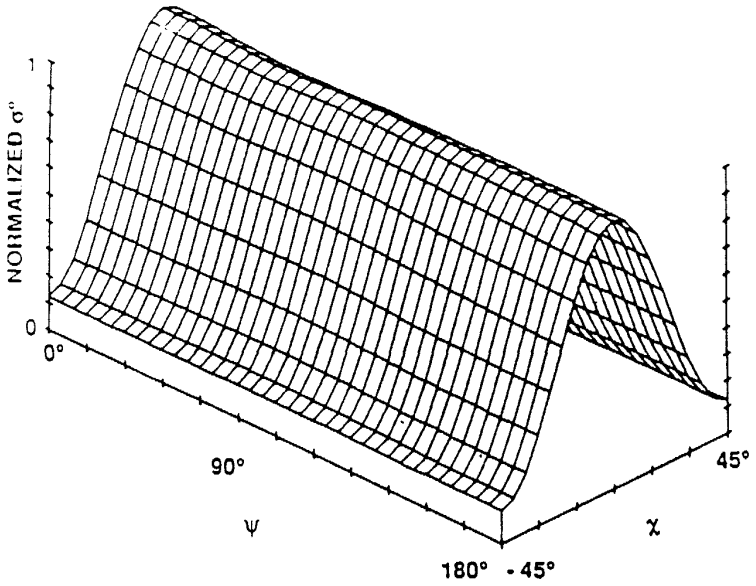
Like Polarized Response.



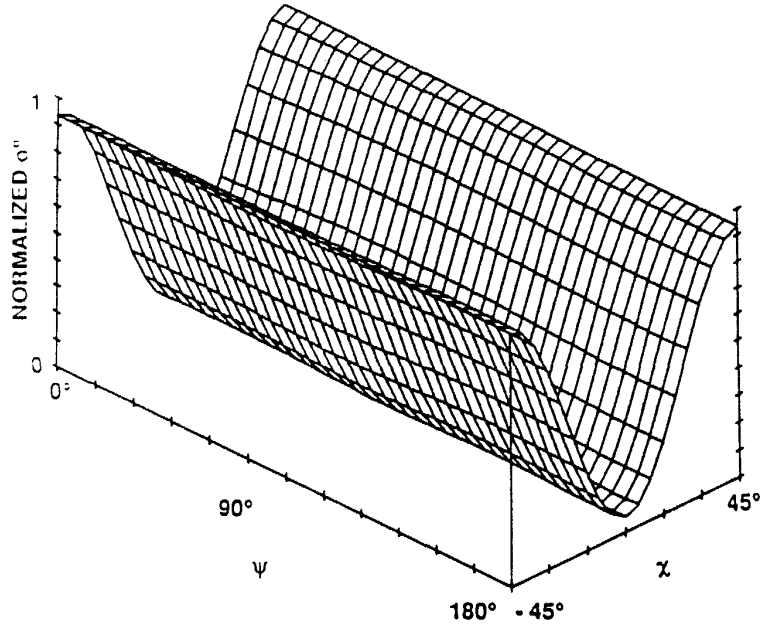
Cross Polarized Response.

Figure H.70: C-Band Polarization Response. Incidence Angle = 40°.

Canopy IV



Like Polarized Response.



Cross Polarized Response.

Figure H.71: X-Band Polarization Response. Incidence Angle = 40°.